Proceedings of the 15th International Students Conference "Modern Analytical Chemistry"

Prague, 19—20 September 2019

Edited by Karel Nesměrák

FACULTY OF SCIENCE
Charles University

Prague 2019

Proceedings of the
15th International Students Conference
"Modern Analytical Chemistry"

Proceedings of the 15th International Students Conference "Modern Analytical Chemistry"

Prague, 19—20 September 2019

Edited by Karel Nesměrák

FACULTY OF SCIENCE
Charles University

Prague 2019

CATALOGUING-IN-PUBLICATION – NATIONAL LIBRARY OF THE CZECH REPUBLIC
KATALOGIZACE V KNIZE – NÁRODNÍ KNIHOVNA ČR

Modern Analytical Chemistry (konference) (15. : 2019 : Praha, Česko)
Proceedings of the 15th International Students Conference "Modern Analytical Chemistry" : Prague, 19–20 September 2019 / edited by Karel Nesměrák. -- 1st edition. -- Prague : Faculty of Science, Charles University, 2019. -- viii, 285 stran
Obsahuje bibliografie a rejstříky

ISBN 978-80-7444-068-7 (brožováno)

543 * (062.534)
▪ analytical chemistry
▪ proceedings of conferences

543 – Analytical chemistry [10]

The electronic version of the Proceedings is available at the conference webpage:
http://www.natur.cuni.cz/isc-mac/

ISBN 978-80-7444-068-7

Preface

These proceedings are brought you forty five contributions, which have been heard at the 15th year of the international student conference "Modern Analytical Chemistry". The conference is traditional meeting of young analytical chemists, Ph.D. students from various universities of European countries, which are coming together to present the results of their research, to master their presentation and language skills and to exchange and discuss ideas and experiences of analytical chemistry.

The contributions presented are assorted by the sequence of their delivery, accompanied with the indexes at the end of the proceedings enabling easy navigation through the pages. The topics of contributions cover all the aspects of modern analytical chemistry from theoretical problems, through development of new analytical methods and improvement of analytical techniques, to the applications involving the solution of medicinal, techanical, or environmental problems. We believe that, like proceedings of previous years of our conference, this one also will be an interesting, beneficial and enjoyable reading. We also hope that the proceeings will give you a guarantee that a new generation of analytical chemists will protect bright and thrilling future of our science.

We are very grateful to the Division of Analytical Chemistry of EuChemS for its long-lasting auspices of our conference. Also, we are thankful to our sponsors, not only for their kind sponsorship making the conference possible, but also for all their cooperation and support in many of our other activities.

EuChemS
European Chemical Society
Division of Analytical Chemistry

Enjoy reading this issue,

doc. RNDr. Karel Nesměrák, Ph.D.
editor

Sponsors

The organizers of 15th International Students Conference "Modern Analytical Chemistry" gratefully acknowledge the generous sponsorship of following companies:

www.ecomsro.com

www.thermofisher.cz

www.lach-ner.com

www.brukeroptics.cz

www.2theta.cz

www.zentiva.cz

Contents

Contributions

Application of the MALDI-TOF MS technique to investigation the molecular profiles of *Escherichia coli* treated with antibiotics and various zinc forms

Agnieszka Rogowska[a, b, *], Viorica Railean-Plugaru[b], Paweł Pomastowski[b], Justyna Walczak[a, b], Bogusław Buszewski[a, b]

[a] *Department of Environmental Chemistry and Bioanalytics, Faculty of Chemistry, Nicolaus Copernicus University, Gagarina 7, 87-100 Torun, Poland* ✉ *bbusz@chem.uni.torun.pl*
[b] *Interdisciplinary Centre of Modern Technology, Nicolaus Copernicus University, Wileńska 4, 87-100 Torun, Poland*

Keywords
flow cytometry
MALDI-TOF MS
metabolism
molecular profile of bacteria
zinc oxide nanoparticles

Abstract
Growing problem of pathogenic bacteria resistance to antibiotics forces the modern science to develop new effective antibacterial substances. One of the proposed strategies is the use of zinc oxide nanoparticles in combination with commercially available antibiotics drugs. However, their mechanism of interaction with microbial cells is still not exactly clear. For this reason the aim of this study was to investigate the effect of zinc ions, zinc oxide nanoparticles, antibiotics (tetracycline and ampicillin) and zinc oxide nanoparticles immobilized with antibiotics on the molecular profile of clinical significance bacteria *Escherichia coli*. For this purpose changes in the lipids and protein profiles of non-treated and treated with a given antibacterial agent bacteria cells was investigated using matrix-assisted laser desorption ionization-time of flight mass spectrometry. Moreover, the antimicrobial properties of tested antibacterial agent were examinated by determination of minimal inhibitory concentration value and flow cytometry analysis.

1. Introduction

One of the most important problems and challenges of modern medicine is the emergence of the phenomenon of antibiotic resistance, which is a threat to public health around the world. For this reason, it is extremely important for modern science to searching for new alternative substances with antibacterial properties. Many of the current research focuses on the use nanoparticles of metals and their oxides as well as their combinations with antibiotics. It has been showed that bactericidal effect of biologically synthesized silver nanoparticle increase when

they are in combination with antibiotics [1, 2]. Tati et al. [3] have proved that zinc oxide nanoparticles show a synergistic effect in combination with penicillin, amoxicillin and amikacin against *Staphylococcus aureus*. However, despite such extensive research into the use of metal nanoparticles and their combinations with antibiotics as an antibacterial agent, their mechanism of interaction with microbial cells is still not exactly clear [4]. It is suggested that the antibacterial effect of such individuals is a complex process in which many mechanisms such as oxidative stress, release metal ions as well as interaction of the nanoparticles with the cell wall are included [4]. Important information on the influence of a given antiseptic agent on cell morphology and metabolism can be provided by analysis of molecular profiles of untreated and treated bacteria using MALDI-TOF MS technique.

The aim of this study was to investigate the impact of the antibiotics and different zinc forms on the bacterial molecular profile. The selected bacterial strains were *Escherichia coli*, one of the most common pathogens. An innovative analytical approach, based on the use of matrix-assisted laser desorption/ionization time-of-flight mass spectrometry, was used for the analysis of non-treated and treated with antimicrobial agents bacteria cells. The selection of appropriate conditions for protein and lipid extraction as well as analytical parameters made it possible to obtain good quality results allowing for tracking changes in lipid and protein profiles of cells exposed to antibacterial substances, and thus identification of mechanisms involved in their antibacterial activity.

2. Experimental

All materials and solvents were purchased from Sigma-Aldrich (Germany). Ultrapure water was purified using the Milli-Q RG system (Bedford, USA).

To obtain immobilized zinc oxide nanoparticles equal volumes of nanoparticles solution (0.45 mg/mL) and antibiotic solution (ampicillin or tetracycline; 0.5 mg/mL) were mixed and incubated for 3 days. Next, solution was dialyzed for three days in MWCO 3500 Spectra/Por dialysis membrane. The kinetic of the antibiotics binding process was examined in batch sorption experiments according to previous methodology [5]. The concentration of antibiotic in supernatant was measured by HPLC (Shimadzu Prominence, Japan) analysis. Obtained zinc oxide-antibiotics nanocomplexes were characterized by zeta potential measurements, FTIR and DLS analysis.

To compare the antibacterial properties of zinc ions, zinc oxide nanoparticles, antibiotics and zinc oxide nanoparticles immobilized with antibiotics minimal inhibitory concentrations was determined as well as flow cytometry analysis was performed.

Further, in order to evaluate the effect of different antiseptics on the molecular profile of *E. coli*, the bacteria was cultured in the presence of a given factor at a concentration of 25% of the MIC value. After 24 hours of incubation at 37 °C, the

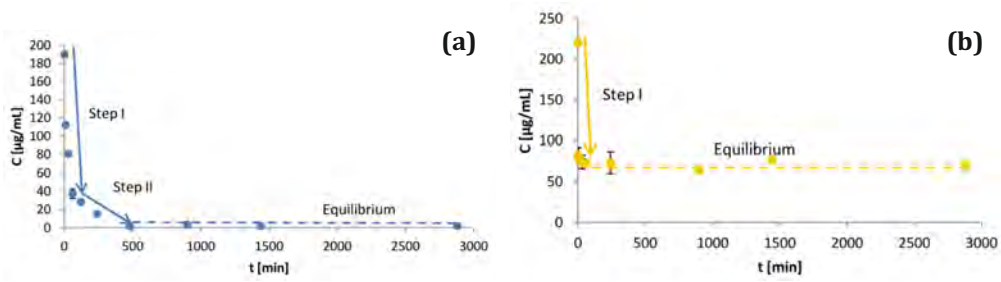

Fig. 1 The kinetic steps of (a) ampicillin, and (b) tetracycline sorption by zinc oxide nanoparticles.

lipids and proteins were extracted using mixture of chloroform/methanol (2:1; v/v) and 70% formic acid/acetonitrile (1:1; v/v), respectively. Next, 1 uL of the obtained extract was spotted on anchor chip target and after drying 1µL of HCCA matrix was applied. The MALDI analysis was performed in both positive and negative ion mode for lipids and in positive mode for proteins in mass range 180–2500 and 2000–20000 *m/z*, respectively.

3. Results and discussion

The kinetic study of antibiotics immobilization on zinc oxide nanoparticles indicates that for both ampicillin and tetracycline it is a complex process but characterized by a slightly different nature. In the case of ampicillin, the sorption process consists of 3 stages, and the maximum efficiency was over 99% here. In turn, for tetracycline only 2 stages can be observed, and the effectiveness of sorption was much lower and amounts about 70% (Fig. 1).

To confirm the antibiotic binding on the zinc oxide nanoparticles surface physico-chemical analysis was performed. The zeta potential measurements indicate that the immobilization do not affect on the zeta potential value and all of tested individuals showed a dispersion stability ($\zeta > |20|$) [6]. In turn, significant changes were observed in the size distribution profile of nanoparticles. It was observed that the functionalization leads to increase of the nanoparticles size uniformity. Moreover, the FT-IR study confirmed the occurrence of zinc oxide nanoparticles immobilization (Fig. 2). On the recorded spectra for nanoparticles immobilized with ampicillin, can be observed many changes compared to the spectrum recorded for unmodified nanoparticles. These changes indicate on the presence of C–C stretching vibrations of aromatic ring as well as N–H, C–O and C–H vibrations present in ampicillin molecules. Similarly, in the case of zinc oxide nanoparticles immobilized with tetracycline, changes in the spectra indicating the presence of tetracycline functional groups.

In order to assess the antibacterial activity of zinc oxide nanoparticles before and after immobilization, as well as the antibiotics and Zn^{2+} themselves, minimal inhibitory concentrations were determined and flow cytometry analysis was performed. The obtained results have shown that use of Zn^{2+} alone was the least

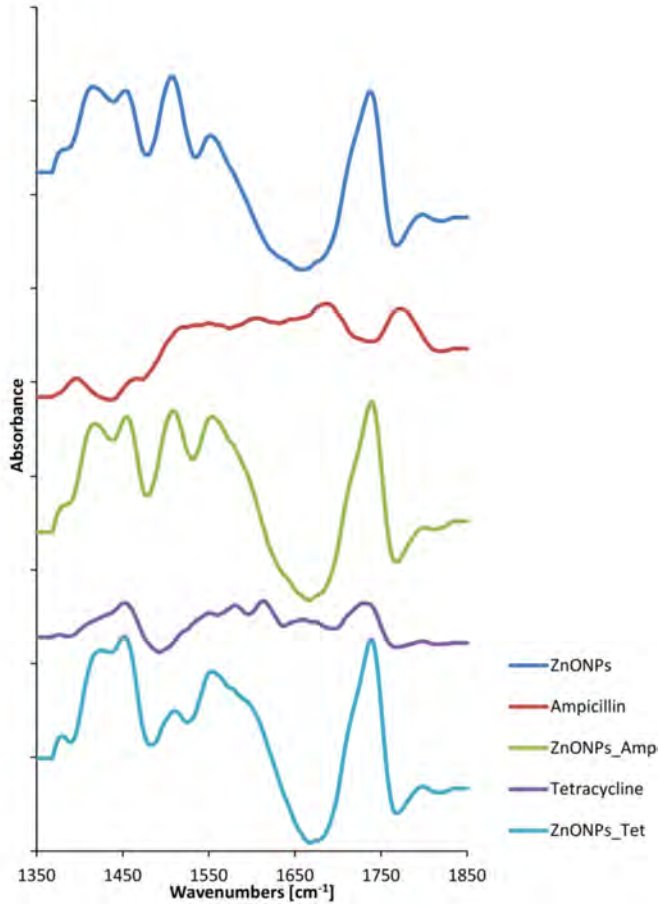

Fig. 2 FTIR spectra of zinc oxide nanoparticles, ampicillin, tetracycline and zinc oxide nanoparticles immobilized with ampicillin and tetracycline.

effective, while zinc oxide nanoparticles effectively inhibited bacterial growth. In addition, flow cytometry analysis indicates that the nature of antibacterial action of nanoparticles after its immobilization with antibiotics is changed. After using nanoparticles in combination with antibiotics, the signals for fragments of disrupted bacterial cells was observed next to the signals from living and dead cells. Moreover, the increase in antibacterial activity of zinc oxide after its combination with tetracycline was observed.

The final step of the work was the comparison of MALDI-TOF mass spectra register for lipids and proteins of non-treated and treated with antibacterial agent bacteria cells. In case of lipids profile it was observed that the incubation of bacteria with antibacterial agents resulted in numerous changes in the recorded spectra such a disappearance of many signals associated with the degradation of lipids building cell membranes as well as the appearance of new signals. Similarly, in the case of protein profile analysis also many changes on the spectra was observed (Fig. 3). The most important changes include loss of signal derived from protein responsible for helicase activity after incubation of cells with both

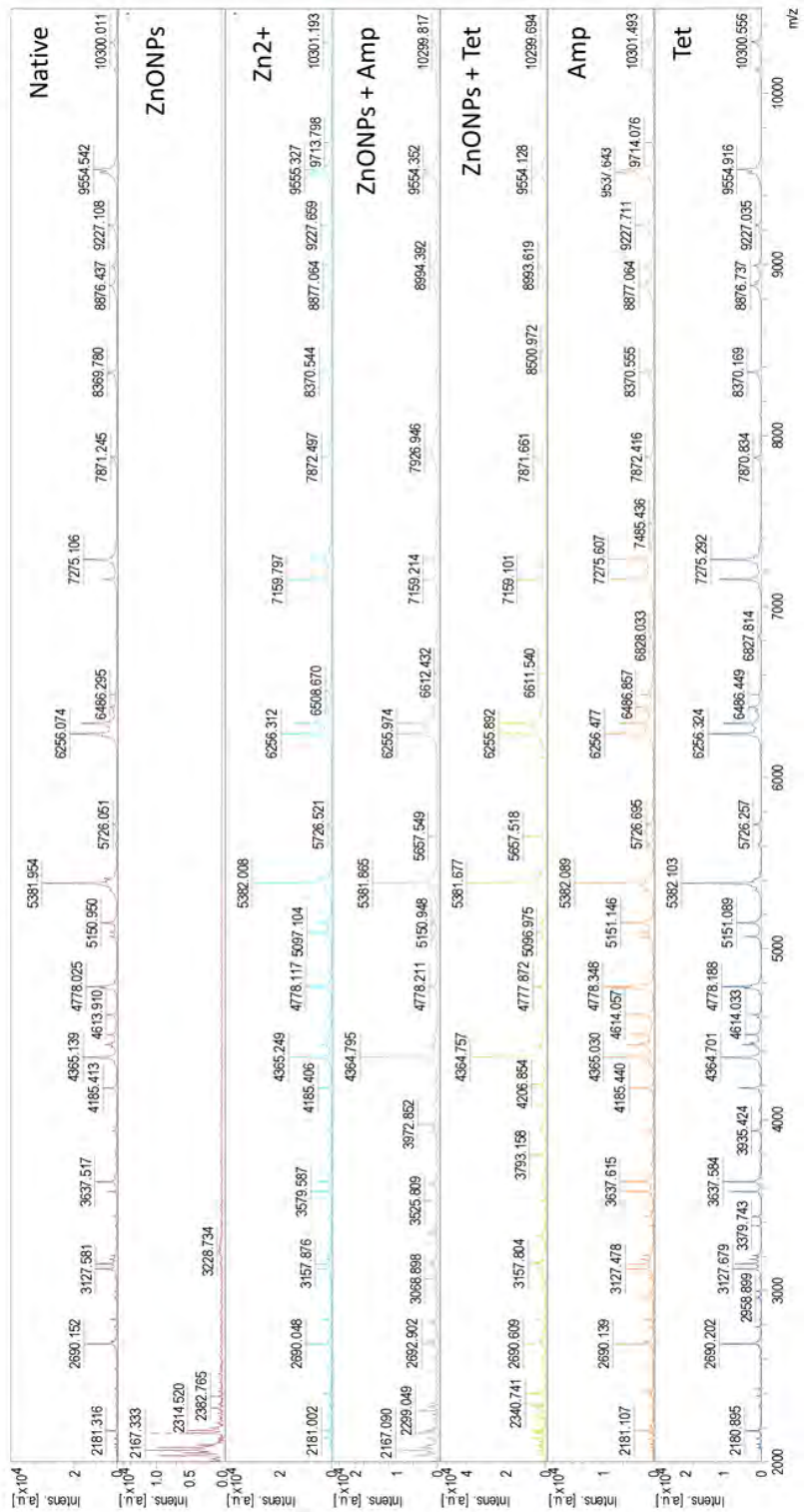

Fig. 3 MALDI-TOF MS spectra of protein from *E. coli* non-incubated and incubated with antibacterial agents.

antibiotics. In addition, after the use of the functionalized zinc oxide nanoparticles, the appearance of signals indicating the presence of protein responds for DNA damage as well as the protein responsible for intermembrane transport. Similarly, another protein responsible for transmembrane transport also appears after the use of antibiotics. After the application of Zn^{2+}, there are also signals from heat shock and acid shock proteins as well as protein responsible for the transport of potassium ions. In addition, after the incubation of cells with tetracycline, the presence of a protein responsible for the loss of cell membrane integrity was observed which confirms the results obtained by flow cytometry and lipid profile analysis.

4. Conclusions

Studies on the kinetics of immobilization of antibiotics on the surface of zinc oxide nanoparticles showed that it is a complex process and its character is dependent on the used antibiotic. Flow cytometry studies have shown that the mechanism of antibacterial activity of nanoparticles after functionalization is different than their non-functionalized counterparts. There was a synergistic effect of nanoparticles in combination with tetracycline. Zinc oxide nanoparticles showed a significantly higher antibacterial activity than zinc ions, suggesting that the mechanism of the antibacterial action of nanoparticles is not only associated with the release of free ions. Studies of molecular profiles of bacteria treated with therapeutic substances showed significant differences compared to untreated cells which was associated with the degradation of proteins and lipids and the activation of defense mechanisms. Studies of lipid and protein profiles as well as flow cytometry have shown that the antibacterial mechanism of tetracycline action is associated with the destruction of the integrity of cell membranes.

Acknowledgments

This work was supported by the Preludium 13 No. 2017/25/N/ST4/01079 (2017-2020) from the National Science Centre, Poland.

References

[1] Buszewski B., Rafińska K., Pomastowski P., Walczak J., Rogowska A.: Novel aspects of functionalized silver nanoparticles. *Colloids Surf. A* **506** (2016), 170–178.

[2] Railean-Plugaru V., Pomastowski P., Rafińska K., Kupczyk W., Jackowski M., Buszewski B.: Antimicrobial properties of biosynthesized silver nanoparticles studied by flow cytometry and related techniques. *Electrophoresis* **37** (2016), 752–761.

[3] Thati V., Roy A.S., Ambika Prasad M.V.N., Shivannavar C.T., Gaddad S.M.: Nanostructured zinc oxide enhances the activity of antibiotics against *Staphylococcus aureus*. *J. Biosci. Tech.* **1** (2010), 64–69.

[4] Baptista P.V., McCusker M.P., Carvalho A., Ferreira D.A., Mohan N.M., Martins M., Fernandes A.R.: Nano-Strategies to Fight Multidrug Resistant Bacteria—"A Battle of the Titans". *Front. Microbiol.* **9** (2018), 1441.

[5] Rogowska A., Rafinska K., Pomastowski P., Walczak J., Railean-Plugaru V., Buszewska-Forajta M., Buszewski B.: Silver nanoparticles functionalized with ampicillin. *Electrophoresis* **38** (2017), 2757–2764.
[6] Kłodzinska E., Szumski M., Dziubakiewicz E., Hrynkiewicz K., Skwarek E., Janusz W., Buszewski B.: Effect of zeta potential value on bacterial behavior during electrophoretic separation. *Electrophoresis* **31** (2010), 1590–1596.

Sensing element based on poly(3,4-(1-azidomethylethylene)dioxythiophene) as electroactive layer of electrochemical DNA sensors

VERA SHAVOKSHINA*, EGOR ANDREEV

Department of Analytical Chemistry, Faculty of Chemistry, Lomonosov Moscow State University, Leninskiye Gory, 119991 Moscow, Russia ✉ *veraleksandrovna@mail.ru*

Keywords
cyclic voltammetry
poly(3,4-(1-azidomethylethylene)dioxythiophene)
poly(3,4-ethylenedioxythiophene)

Abstract
In this work, we demonstrate poly(3,4-(1-azidomethylethylene)-dioxythiophene) modified electrodes as an advanced sensing element for further DNA sensors elaboration. Conducting poly(3,4-(1-azidomethylethylene)-dioxythiophene) combines the advantages of the poly(3,4-ethylenedioxythiophene) and easy surface modification due to azide groups. We have carried out the electrochemical synthesis of poly(3,4-(1-azidomethylethylene)-dioxythiophene) on planar screen-printed electrodes in acidic aqueous solution. Electrochemical activity of poly(3,4-(1-azidomethylethylene)-dioxythiophene) in $K_3[Fe(CN)_6]$ solution investigated by cyclic voltammetry was compared with poly(3,4-ethylenedioxythiophene). Standard heterogeneous rate constant, limit of detection and sensitivity was determined. According to these studies, poly(3,4-(1-azidomethylethylene)dioxythiophene) exhibits better electroactivity than poly(3,4-ethylenedioxythiophene).

1. Introduction

In the past decades, DNA sensors has been drawing particular attention due to great significance of their applications including detection of microorganisms [1], DNA damage [2]. At the same time, one of the most promising areas of research is development of electrochemical sensors based on conducting polymers [3]. The main advantages of these devices are their low cost, sensitivity and selectivity. Conducting polymer-based DNA sensors provide express analysis, since they convert the hybridization event into a direct electrical signal. Poly(3,4-ethylenedioxythiophene) (PEDOT) is one of the most widely used conducting polymer. PEDOT is electroactive in aqueous solutions and exhibits good electrochemical stability and relatively high conductivity [4]. To create an electrochemical DNA-sensor it is necessary to immobilize DNA onto modified electrodes. Unsubstituted PEDOT offers no possibility for covalent bonding of other

molecules, its derivative conducting poly(3,4-(1-azidomethylethylene)dioxythiophene) (azido-PEDOT) combines the advantages of PEDOT with facile functionalization. Azido-PEDOT electrodes can be functionalized with acetylene-terminated DNA probe by Cu(I) catalyzed azide-alkyne cycloaddition ("click chemistry") [5]. Thus, azido-PEDOT can be used as electroactive layer of electrochemical DNA sensors.

Polymers can be synthesized chemically and electrochemically. Electropolymerization is preferable, since deposition can be targeted directly to the electrode surface. Also, the properties of the polymer film can be modulated by varying electrochemical polymerization conditions.

DNA sensors commonly work in aqueous solution, thus it would be better to provide the electropolymerization in the same medium. Azido-PEDOT is synthesized by electrochemical oxidation of the monomer only in an organic medium [5]. PEDOT films are generally synthesized in organic solutions [6], but the electropolymerization of 3,4-ethylenedioxythiophene (EDOT) may also be carried out in aqueous solution even in absence of any surfactants [7].

The properties of the PEDOT films are deeply affected by electropolymerization conditions, such as applied electropolymerization methods, polymerization potential, solvent, supporting electrolyte [6]. Therefore, the purpose of the work was to synthesize and study of the properties of azido-PEDOT for further elaboration of DNA sensors.

2. Experimental

2.1 Reagents and chemicals

Experiments were carried out with Millipore Milli-Q water. The monomer, 3,4-ethylenedioxythiophene (>97%), and potassium ferricyanide were purchased from Sigma-Aldrich (USA). The monomer 3,4-(1-azidomethylethylene)dioxythiophene (azido-EDOT) was purchased from Skolkovo Institute of Science and Technology (Russia). Inorganic salts (chloride, hydrophosphate, and dihydrophosphate of potassium) and perchloric acid were obtained of the highest purity from Reachim (Moscow, Russia).

2.2 Instrumentation

The electrochemical measurements and electropolymerization were carried out by means of a universal potentiostat-galvanostat AutolabPGSTAT 128N (The Netherlands). A Renishaw InVia Raman microscope (Renishaw, UK) was used for recording Raman spectra. The latter were acquired with 514 nm excitation laser source, 20× objective in the range from 900 to 2200 cm^{-1}. Scanning electron microscopy (SEM) was performed on Supra 50 VP LEO (Carl Zeiss, Germany).

2.3 Methods

For electrochemical measurements including electropolymerization of EDOT and azido-EDOT we used the method of cyclic voltammetry. Cyclic voltammetry was conducted in a three-compartment electrochemical cell that contained a glassy carbon counter electrode, Ag | AgCl | 1 M KCl reference electrode, planar screen-printed structures (SPE) (Rusens Ltd., Moscow) with carbon working electrode (diameter 0.9 mm).

Electropolymerization of azido-EDOT was carried out from its 0.01 M solution in 0.1 M perchloric acid in cyclic voltammetric regime. Potential range was from –0.2 to 0.9 V. Sweep rate was 0.04 V s^{-1}.

Electropolymerization of EDOT was carried out from its 0.01 M solution in 0.1 M perchloric acid in cyclic voltammetric regime. Potential range was from –0.2 to 0.9 V. Sweep rate was 0.04 V s^{-1}.

PEDOT SPE and azido-PEDOT SPE with different number of growing cycles were investigated at different concentrations of the $K_3[Fe(CN)_6]$ in 50 mM phosphate buffer (pH = 7.0) containing 0.1 M KCl. The sensitivity was obtained from the slope of the calibration curve (current density vs potassium ferricyanide concentration). Limit of detection was calculated as the ratio of 3 times the standard deviation of the peak currents (10 runs) of the lowest measurable concentration to the sensitivity. To evaluate standard heterogeneous rate constant, cyclic voltammograms were recorded in 5 mM $K_3[Fe(CN)_6]$ (in 50 mM phosphate buffer pH = 7.0, containing 0.1 M KCl) at scan rates ranging from 0.01 to 1.0 V s^{-1}. The experiments were performed at room temperature (24 ± 2 °C).

3. Results and discussion

Electropolymerization of azido-EDOT on screen-printed electrodes (SPE) was performed by cyclic voltammetry. Azido-PEDOT had been electrodeposited from aqueous solutions for the first time. Current increase was observed at around 0.9 V corresponding to the formation of radical cations, current intensity increased with increasing number of cycles (Fig. 1). “Nucleation loop” (current crossover) observed in the first scan indicates the beginning of the nucleation process. After electropolymerization, voltammograms of azido-PEDOT SPE with different number of growing cycles were recorded in an electrolyte solution free of modified monomer. The area of voltammograms increased in step with number of growing cycles.

Also, modified electrodes were studied by Raman spectroscopy. The Raman spectra of the PEDOT and the azido-PEDOT films have common bands corresponding to the main polymer chain. There are bands in the Raman spectra of azido-PEDOT corresponding to stretching vibration of the –N=N=N group: 1310 cm^{-1} (sym.), 2120 cm^{-1}(asym.). Polymer morphology was studied using SEM. Synthesized azido-PEDOT has porous morphology. The thickness of the film obtained during 10 electropolymerization cycles is about 120 nm.

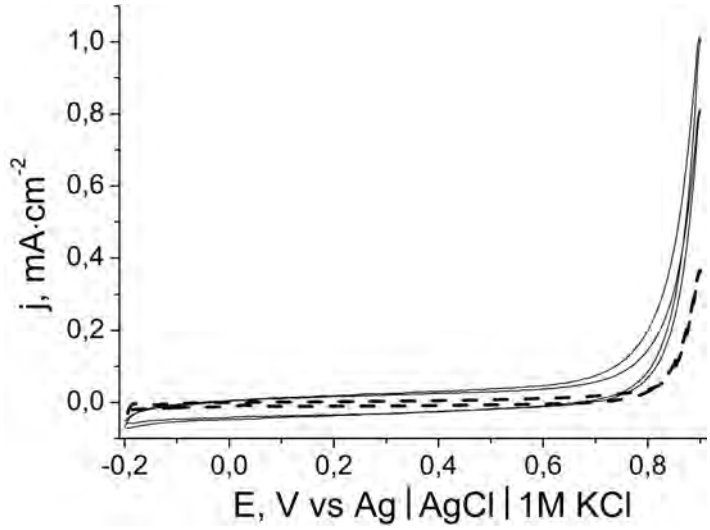

Fig. 1 Potentiodynamic electrodeposition of azido-PEDOT on screen-printed electrode from a solution of 0.01 M EDOT in 0.1 M $HClO_4$ in the potential range of−0.2 to 0.9 V during 10 cycles (scan rate 0.04 V s^{-1}). Dashed line represents the first electropolymerization cycle.

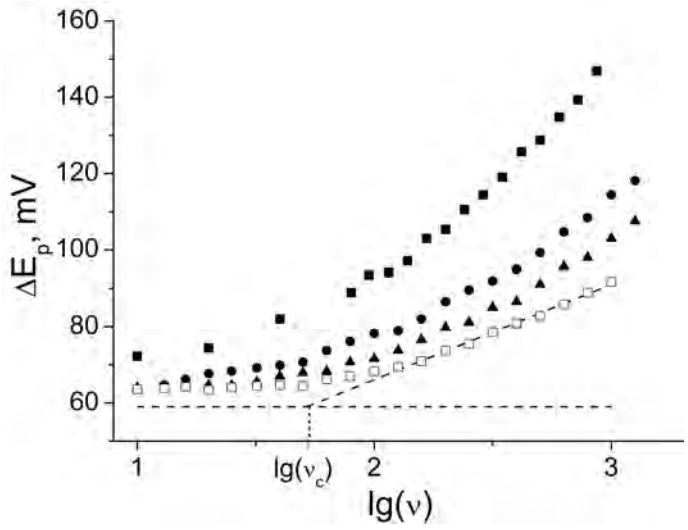

Fig. 2 Plot between the difference of the anodic and cathodic peak potentials (ΔE_p) versus logarithm of scan rate (lg v) for screen-printed electrodes (in 5 mM $K_3[Fe(CN)_6]$) modified azido-PEDOT during different numbers of growing cycles: 1 (■), 5(●), 10(▲), 20(□). The dashed line shows the definition of the critical scan rate (v_c) for 20 cycles.

Table 1
Standard heterogeneous rate constant calculated from Eq. (1) for polymer-modified screen-printed electrodes with different polymer amount in 5 mM $K_3[Fe(CN)_6]$ solution.

Number of growing cycles	k_s° / 10^{-3} cm s^{-1}	
	Azido-PEDOT	PEDOT
1	3.1	4.3
5	3.3	3.4
10	3.7	3.2
20	3.8	–
average	3.5±0.3	3.6±0.4

Electrochemical DNA sensors based on indirect methods require the use of labels or electroactive indicators, such as ferri-/ferrocyanide redox couple (mediators shuttle the electrons between the double-stranded DNA and the electrode). The study of processes between modified electrodes and a redox couple in the solution is essential for sensors elaboration.

Kinetics of electron transfer between $[Fe(CN)_6]^{3-/4-}$ and azido-PEDOT in aqueous solution was studied by cyclic voltammetry. The standard electrochemical rate constant was evaluated from the difference of the anodic and cathodic peak potentials ($\Delta E_p = E_{pa} - E_{pc}$) measured from the cyclic voltammograms (Fig. 2). This method is based upon the determination of critical scan rate at which the electrode reaction changes from reversible to quasireversible and Matsuda Ayabe parameter Λ is 1 (ref. [8]). Then following equation is used to calculate the value of k_s°

$$k_s^0 = \Lambda \sqrt{\frac{FDv}{RT}} \tag{1}$$

Diffusion coefficient values, required to evaluate k_s° by the methods described above, was 7.6×10^{-6} $cm^2\,s^{-1}$. The value of k_s° for PEDOT-modified electrodes was calculated similarly.

According to calculated k_s° (Table 1) PEDOT SPE and azido-PEDOT SPE exhibit a similar electrochemical activity in $K_3[Fe(CN)_6]$ solution. However, PEDOT SPE does not have analytical characteristics similar to that of the azido-PEDOT modified electrodes. Azido-PEDOT SPE has shown the higher faradaic/capacitive current ratio (I_f/I_c) (Fig. 3). For example, at scan rate 150 mV s^{-1} I_f/I_c for azido-PEDOT is 6 and for PEDOT –4. The sensitivity of the azido-PEDOT SPE is 3.7 mA cm^{-2} M^{-1}, PEDOT SPE –3.4 mA cm^{-2} M^{-1}. For the azido-PEDOT SPE a limit of detection of 0.4 mM was obtained while for the PEDOT SPE a limit of detection of 0.8 mM was achieved.

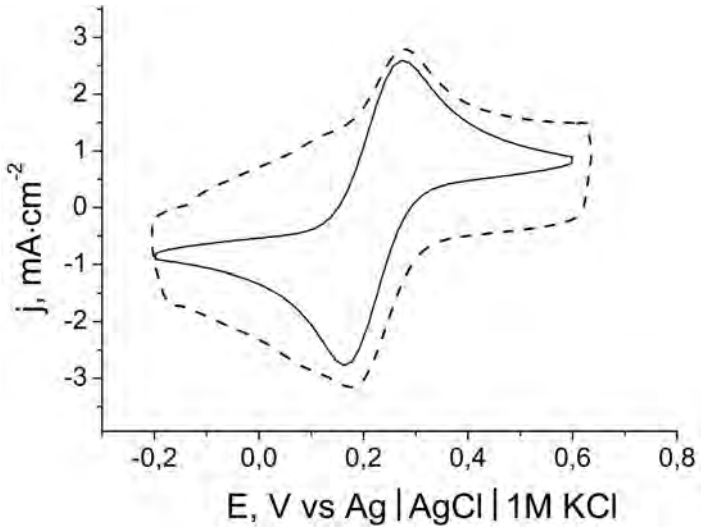

Fig. 3 Azido-PEDOT modified electrode (solid line) and PEDOT modified electrode (dashed line) in 5 mM $K_3[Fe(CN)_6]$. Conditions: 5 electropolymerization cycles, scan rate 1 V s^{-1}.

4. Conclusions

Conducting polymer azido-PEDOT has been electrochemically synthesized from aqueous solution. Azido-PEDOT has porous morphology, that provides anion exchange in polymer film. Nonfaradaic processes at PEDOT modified electrodes contributes significantly to currents. The result is that the analytical characteristics (limit of detection, sensitivity) of azido-PEDOT modified electrodes are better than for PEDOT-modified ones. Thus, azido-PEDOT modified electrode is proper sensing element for further elaboration of DNA sensors.

Acknowledgments

Financial support through Russian Science Foundation grant # 19-13-00131 is greatly acknowledged.

References

[1] Datta M., Desai D., Kumar A.: Gene Specific DNA Sensors for Diagnosis of Pathogenic Infections. *Indian J. Microbiol.* **57** (2017), 139–147.
[2] Sohrabi N., Valizadeh A., Farkhani M., Akbarzadeh A.: Basics of DNA biosensors and cancer diagnosis. *Artif. Cells, Nanomed., Biotechnol.* **44** (2016), 654–663.
[3] Evtugyn G., Hianik T.: Electrochemical DNA sensors and aptasensors based on electropolymerized materials and polyelectrolyte complexes. *TrAC, Trends Anal. Chem* **79** (2016), 168–178.
[4] Melato A., Mendonça M., Abrantes L.: Effect of the electropolymerisation conditions on the electrochemical, morphological and structural properties of PEDOTh films. *J. Solid State Electrochem.* **13** (2009), 417–426.
[5] Galán T., Prieto-Simón B., Alvira M., Eritja R.: Label-free electrochemical DNA sensor using 'click'-functionalized PEDOT electrodes. *Biosens. Bioelectron.* **74** (2015), 751–756.

[6] Poverenov E., Li M., Bitler A., Bendikov M.: Major effect of electropolymerization solvent on morphology and electrochromic properties of PEDOT films. *Chem. Mater.* **22** (2010), 4019–4025.
[7] Bobacka J., Lewenstam A., Ivaska A.: Electrochemical impedance spectroscopy of oxidized poly(3,4-ethylenedioxythiophene) film electrodes in aqueous solutions. *J. Electroanal. Chem.* **489** (2000), 17–27.
[8] Compton R., Banks C.: *Understanding Voltammetry.* 2nd ed. London, Imperial College Press 2007, p. 107–153.

New sorbent based on silica gel modified with eremomycin-stabilized gold nanoparticles for enantioseparation by liquid chromatography

A. D. Golubova, E. N. Shapovalova, I. A. Ananieva

Department of Chemistry, Lomonosov Moscow State University, Leninskie gory 1/3, 119991 Moscow, Russian Federation ✉ *nasgolubova@gmail.com*

Keywords
chromatography
enantioseparation
gold nanoparticles
macrocyclic antibiotics

Abstract
Synthesis of new sorbent and its application for separation of enantiomers of some biologically active compounds were suggested. It has been shown that macrocyclic antibiotic eremomycin is able to stabilize gold nanoparticles and these eremomycin-stabilized gold nanoparticles can be effectively adsorbed on the sorbent surface. Such sorbent has a number of advantages including simple and cheap way of obtaining and small selector consumption. Hydrophilic and acid-base properties of new sorbent were explored to understand its best using. It was found that the sorbent demonstrates a high enantioselectivity to amino acid in the enantioseparation by liquid chromatography.

1. Introduction

Nowadays one of the topical tasks is the synthesis and study of properties of new hydrophilic sorbents for separation of wide range of compounds, including enantiomers. Nanoparticles can be effectively used in making of new stationary phases, particularly chiral phases, for liquid chromatography due to their unique properties. For example, in some cases they allow obtain sorbents with homogeneous surface of large area, change the mechanical and chemical stability of sorbents and increase their selectivity [1, 2]. Silica gels modified with gold nanoparticles stabilized with various organic ligands are one of the modern perspective classes of stationary phases. It has been already obtained silica gel modified with citrate-stabilized gold nanoparticles [1], cysteine-stabilized gold nanoparticles [3] and chitosan-stabilized gold nanoparticles [4]. These sorbents were used for enantioseparation and for separations of mixtures of some polar substances.

In the last decade, it has been found that various organic nitrogen-containing compounds (for example, amines, polymers and proteins) act as reducing agents for $[AuCl_4]^-$ and stabilize formed nanoparticles [5–6]. One of these compounds are macrocyclic glycopeptide antibiotics. They are able to stabilize gold nanoparticles and at the same time they are universal chiral selectors, thus complexes of gold nanoparticles and macrocyclic antibiotics can be applied for separation of enantiomers. It is interesting both from theoretical and practical aspects explore the ability to identify enantiomers of gold nanoparticles stabilized with only macrocyclic antibiotics without using other additional reagents.

Eremomycin is the macrocyclic antibiotic which similar in structure to vancomycin. It became use as a chiral selector relatively recently and it is successfully used for the separation of enantiomers in HPLC [7–11]. It was obtained the silica gel modified with gold nanoparticles and eremomycin chemically bonded through the mercaptopropionic acid residue, which was used for enantioseparation of some organic compounds [12].

The aim of this work was to obtain the sorbent based on the silica gel adsorption-modified with gold nanoparticle, stabilized with eremomycin and to explore its hydrophilic, acid-base and enantioselective properties.

2. Experimental

2.1 Reagents and chemicals

Acetonitrile (for chromatography; Panreac, Spain), methanol (for chromatography; J. T. Baker, The Netherlands), ammonium acetate (pur.), triethylamine (Sigma-Aldrich) were used to prepare the mobile phases.

In the work solutions of the following substances were used: uridine, 5-methyluridine, 2-deoxyuridine, caffeine, theophylline, theobromine, tryptophane, phenylalanine, alanine, 4-chlorophenylalanine, methionine, serine, aspartic acid, 3,4-dihydroxyphenylalanine, phenoprophen, flurbiprophen, indoprophen (Sigma-Aldrich). These solutions were prepared by accurate weighting (500 μg ml^{-1}) in acetonitrile-water mixture.

To obtain a new sorbent following chemicals were used: silica gel Kromasil, 10 nm, 5 micrometers (Ekachemicals, Sweden), eremomycin hydrochloride provided by Staroverov S.M. (BioHimMak ST, Moscow, Russia), gold(III) chloride tetra hydrate (puris).

Nanoparticles were synthesized by prolonged heating of a mixture of $HAuCl_4$ (100 μg ml^{-1}) and eremomycin (1 mg ml^{-1}) in a 0.05 M borate buffer solution. Formation of gold nanoparticles was proved by the appearance of a ruby-colored solution. The obtained gold nanoparticles were immobilized on the surface of silica gel by physical adsorption, by means of saturating the surface of silica gel.

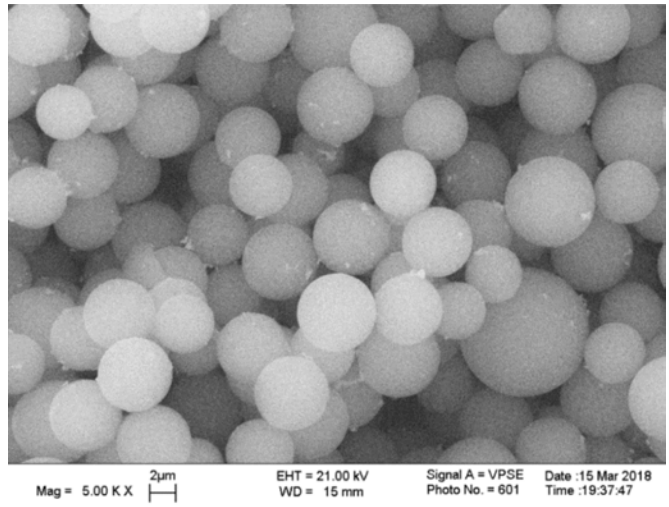

Fig. 1 The microphotograph of the sorbent.

2.2 Instrumentation

The work was performed on a liquid chromatograph LC-10AT VP (Shimadzu, USA) with diode array detector SPD-10AV VP (Shimadzu, USA). The mobile phase was degassed before use on the ultrasonic bath Sapphire 6580 (operating frequency 35 kHz, power 60 W; Sapphire, Russia) for 10 minutes. To obtain micrographs of the sorbents, a JEOL JSM-6390LA scanning electron microscope (accelerating voltage of 20 kV; JEOL, Japan) was used. The diffuse reflectance spectra of the synthesized sorbents were recorded on a CS-9001PC Dual-Wavelength Flying Spot Scanner (Shimadzu; Japan).

3. Results and discussion

3.1 Synthesis of the sorbent

After modifying the silica gel with eremomycin-stabilized gold nanoparticles, sorbent was examined by methods of scanning electron microscopy and diffuse reflection. The microphotograph of the sorbent is presented in Fig. 1. It can be noticed, that stabilized gold nanoparticles almost uniformly adsorbed on the surface of spherical silica gel particles. From the microanalysis it was obtained the percentage of elements in the sorbent. The eremomycin content on the surface, calculated from the chlorine content, was 0.017 mmol g^{-1}, which is significantly less than in the case of chemical fixing of eremomycin on epoxy silica gel (0.07 mmol g^{-1}) [12]. Presence of the absorption maximum in the region of 540 nm in the diffuse reflection spectrum proves the presence of gold nanoparticles in a non-aggregated state on the sorbent surface, absorption maximum of aggregated gold nanoparticles is in the region of 750 nm [13] (Fig. 2). These data confirm the modification of silica gel.

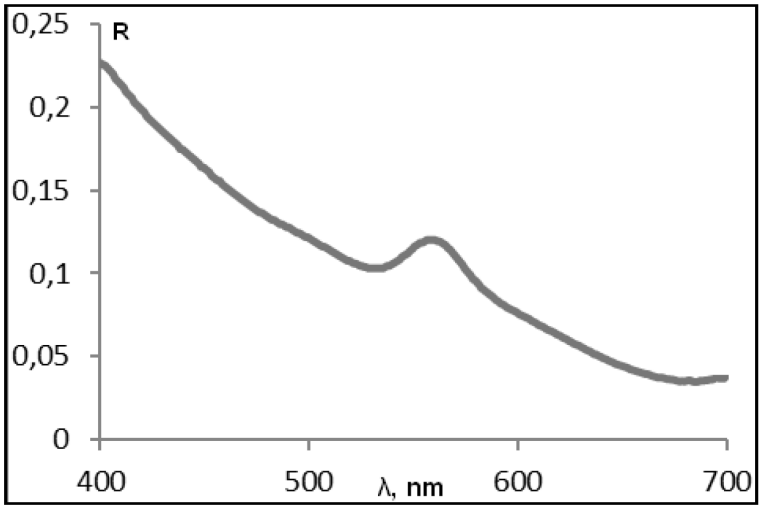

Fig. 2 The diffuse reflection spectrum of the sorbent (*R* is the diffuse reflection coefficient).

Table 1
The values of the methylene (hydrophobic) selectivity factor ($\alpha(CH_2) = k_{5\text{-methyluridine}}/k_{\text{uridine}}$), the selectivity for the hydroxyl group ($\alpha(OH) = k_{\text{uridine}}/k_{2\text{-deoxyuridine}}$) and the retention factors k_{caf}/k_{theoph} and k_{caf}/k_{theobr} of the studied sorbent. Mobile phase: acetonitrile:ammonium acetate buffer (20 mM, pH = 4.7) = 90:10. The flow rate of the mobile phase is 0.5 mL min^{-1}.

$\alpha(CH_2)$	0.88
$\alpha(OH)$	1.21
k_{caf}/k_{theobr}	0.89
k_{caf}/k_{theoph}	0.70

3.2 Hydrophilic-hydrophobic and acid-base properties of the new sorbent

To explore hydrophilic properties of the sorbent mixtures of following substances were used: uridine, 5-methyluridine and 2-deoxyuridine. As the non-retained component toluene was used. These compounds and their mixtures were selected on the basis of literature data [14]. For quantitative estimation of hydrophobic interactions between analytes and stationary phase the methylene (hydrophobic) selectivity α (CH_2) was used, since the additional methylene group of 5-methyluridine contributes to the hydrophobic interactions. Hydroxy group of urudine affects the hydrophilic interactions with the sorbent. Similarly, selectivity factor α (OH) can be used for evaluation of hydrophilic interactions. The uridine is eluted after 5-methyluridine and 2-deoxyuridine, which suggests more contribution of hydrophilic interactions to retention. As it was calculated (Table 1), α (OH) is more than α (CH_2), thus the sorbent demonstrates more hydrophilic properties, however it has also weak hydrophobic properties.

For investigation of acid-base properties of the sorbent mixtures of caffeine, theophylline and theobromine were used. Theophylline (pK_a = 8.77) and theobromine (pK_a = 10.55) are weak acids, in contrast to caffeine (pK_a = 14.00) [15]. The ratio of the retention factors of these compounds was calculated:

Table 2
Influence of the mobile phase composition on the chromatographic parameters of amino acids: k_1 and k_2 are retention factors of the first and the second enantiomer respectively, α is the selective coefficient and R_s is the resolution of enantiomers.

Mobile phase	Substance	k_1	k_2	α	R_s
Acetonitrile-water (20:80)	Tryptophane	0.82	1.44	1.76	2.62
	Alanine	0.40	0.55	1.38	1.05
	Phenylalanine	0.54	1.10	2.04	3.15
	4-Chlorphenylalanine	0.53	0.84	1.58	2.45
	Methionine	0.48	0.55	1.15	0.48
Methanol-water (20:80)	Tryptophane	2.21	3.59	1.62	2.06
	Phenylalanine	2.02	3.24	1.60	1.87
	4-Chlorphenylalanine	1.63	2.48	1.52	2.26
Acetonitrile-water (80:20)	Tryptophane	12.27	16.41	1.28	1.47
	Phenylalanine	17.42	22.33	1.28	1.22
	Flurbiprophen	0.97	1.03	1.60	0.60
	Indoprophen	1.94	2.13	1.09	0.50
	Phenoprophen	0.47	0.64	1.36	0.20

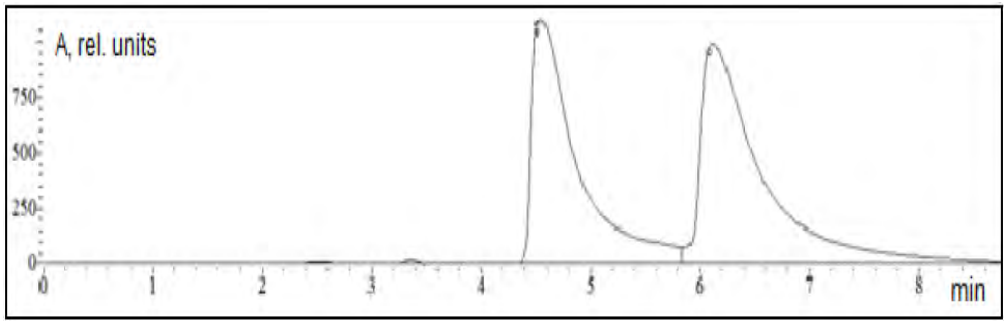

Fig. 3 The chromatogram of racemic tryptophan mixture. Mobile phase: acetonitrile:water = 20: 80, the flow rate of the mobile phase is 0.5 mL min^{-1}, detection wavelength is 220 nm.

k_{caf}/k_{theoph} and k_{caf}/k_{theobr}. If the resulting selectivity factor is less than 1, then the phase is basic, if it is equal to 1, the phase is neutral, and if it is more than 1, then the phase is acidic [14]. It was found (Table 1), that both k_{caf}/k_{theoph} and k_{caf}/k_{theobr} are less than 1, the new sorbent has primarily basic properties.

3.3 Enantioselective properties of the new sorbent

Tryptophan, phenylalanine, 4-chlorophenylalanine, alanine, methionine, serine, aspartic acid, 3,4-dihydroxyphenylalanine, flurbiprofen, indoprofen and phenoprofen were chosen for studying enantioselective properties.

The analysis has begun in the reversed-phase mode with using the following mobile phase: acetonitrile:water as 20:80. It can be seen (Table 2) that the enantioseparation of almost all studied compounds was obtained (one of the chromatogram is presented in the Fig. 3) except the separation of enantiomers of

serine and aspartic acid, which can be related to the possible interactions between SH-group (for serine) or carboxy group (for aspartic acid) and gold atoms. It was also no enantioseparation for profens. While varying the nature and content of the organic solvent in the mobile phase the retention changed dramatically. Replacing acetonitrile with methanol increases the retention of amino acids, but decreases the selectivity and resolution of the peaks of enantiomers. The same effect can be seen when water or acetonitrile content increases. In the polar-organic mode, using mobile phases with a high content of organic solvent (usually acetonitrile) with polar additives (acetic acid, triethylamine, water), where the acetonitrile content was 80% good enantioseparations were obtained for tryptophan and phenylalanine and partial separation of enantiomers for flubiprophen, indoprophen and phenoprophen.

4. Conclusions

The new sorbent based on silica gel adsorption-modified with eremomycin-stabilized gold nanoparticles was obtained. Modification of the sorbent surface was confirmed by methods of scanning electron microscopy, microanalysis and diffuses reflection. It was established that the sorbent is mainly hydrophilic with basic properties. The sorbent has a high enantioselectivity in respect to some amino acids, particularly to tryptophan, phenylalanine and 4-chlorphenylalanine in both reversed-phase and polar-organic phase and weak enantioselectivity in respect to prophens in the polar-organic phase.

Acknowledgments

This work was supported by Russian Foundation for Fundamental Research, number 18-03-00742.

References

[1] Ananieva I.A., Polyakova Y.A., Shapovalova E.N., Shpigun O.A.: Using adsorbents modified by gold nanoparticles in chromatography. *J. Anal. Chem.* **72** (2017), 714–726.
[2] Nesterenko E.P., Nesterenko P.N., Connoly D., He X Floris P., Duffyc E., Paull B. Nano-particle modified stationary phases for high-perfomance liquid chromatography. *Analyst* **138** (2013), 4229–4254.
[3] Polyakova Y.A., Ananieva I.A., Shapovalova E.N., Mazhouga A.G.: Separation of water soluble vitamins with L-cysteine-stabilized gold nanoparticles using HPLC. *Mosc. Univ. Chem. Bull.* **71** (2016), 54–59.
[4] Shapovalova E.N., Ananieva I.A., Elfimova Y.A., Grineva L.A., Mazhouga A.G., Shpigun O.A.: HPLC separation of nitrogen-containing compounds on silica gel modified with gold nanoparticles stabilized by chitosan. *Mosc. Univ. Chem. Bull.* **67** (2012), 72–77.
[5] Maruyama T., Fujimoto Y., Maekawa T.: Synthesis of gold nanoparticles using various amino acids. *J. Colloid Interface Sci.* **447** (2015), 254–257.
[6] Majzik A., Fülöp L.: Functionalization of gold nanoparticles with amino acids, β-amyloid peptides and fragment. *Colloids Surf. B* **81** (2010), 235–241.
[7] Staroverov S.M., Kuznetsov M.A., Nesterenko P.N., Vasiarov G.G., Katrukha G. S., Fedorova G.B.: New chiral stationary phase with macrocyclic antibiotic eremomycin chemically bonded to silica. *J. Chromatogr. A* **1108** (2006), 263–267.

[8] Kuznetsov M.A., Nesterenko P.N., Vasiarov G.G., Staroverov S.M.: High-perfomance liquid chromatography of α-amino acids enantiomers on eremomycin-modified silica. *J. Anal. Chem.* **63** (2008), 57–64.
[9] Kuznetsov M.A., Nesterenko P.N., Vasiarov G.G., Staroverov S.M.: Sorbents with immobilizes glycopeptides antibiotics for separating optical isomers by high-perfomance liquid chromatography. *Appl. Biochem. Microbiol.* **42** (2006), 536–544.
[10] Решетова Е.Н., Аснин Л.Д.: Хроматографическое поведение и термодинамика адсорбции энантиомеров профенов на силикагеле с привитым антибиотиком эремомицином. *Журнал физической химии* **83** (2009), 643–648.
[11] Prokhorova A.F., Shapovalova E.N., Shpak A.V., Staroverov S.M., Shpigun O.A.: Enantiorecognition of profens by capillary electrophoresis using a novel chiral selector eremomycin. *J. Chromatogr. A* **1216** (2009), 3674–3677.
[12] Федорова И. А.: *Диссертация кандидата химических наук*. Москва 2017.
[13] Apyari V.V., Arkhipova V.V., Dmitrienko S.G., Zolotov Yu.A.: Using gold nanoparticles in spectrophotometry. *J. Anal. Chem.* **69** (2014), 1–11.
[14] M. Dolci: Chromatographic characterization of stationary phases for hydrophilic interaction liquid chromatography. *Thermo Fisher Scientific: Technical Note* 2013.
[15] www.drugfuture.com/chemdata

Analytical investigations of fusing und detailing agents used in the context of the multi jet fusion process in 3D printing

Beate Scherer[a, b, *], Frank-Michael Matysik[a]

[a] *Institute of Analytical Chemistry, Chemo- and Biosensors, Faculty of Chemistry and Pharmacy, University of Regensburg, Universitätsstraße 31, 93053, Regensburg, Germany*
✉ *beate.scherer@ur.de*
[b] *BMW Group, Landshuter Straße 56, 84130, Dingolfing, Germany*

Keywords
detailing agent
fusing agent
high-resolution mass spectrometry
2-pyrrolidone
triethylene glycol

Abstract
The 2016 newly introduced powder bed based 3D printing process called Multi Jet Fusion from the company HP is used in various industries for different applications. It convinces by speed compared to the selective laser sintering process. Thus, the so-called fusing and detailing agents and an infrared radiation source are needed. The agents mainly contain water and organic cosolvents. In the fusing agent also carbon black is very important because it is able to absorb infrared radiation. These novel materials offer some challenges for analytical characterization. In order to obtain more information of the raw materials qualitative and quantitative analytical investigations of the materials are important. The substances 2-pyrrolidone and triethylene glycol were identified as organic solvents in the agents by means of highresolution mass spectrometry in combination with a data base search. Based on the distinct isotopic patterns of 2-pyrrolidone and triethylene glycol the identification of both compounds was confirmed. Furthermore, the amount of organic solvents in the agents was quantified by means of gas chromatography with flame ionization detection.

1. Introduction

The field of additive manufacturing alias 3D printing is gaining more and more importance with applications in automobile, aerospace, and medical industry [1]. Over the years, a bunch of different technologies has been evolved to satisfy the needs of the different application areas. Powder-based techniques are categorized as one of the most important ones in additive manufacturing [2]. Consequently, powder is just fused were actually needed. In 2016, the new technology named Multi Jet Fusion was introduced by the company HP [3]. The process starts with a controlled deposition of a thin layer of powder. Then, an agent system comes into play which is applied by an inkjet head. Firstly, black

fusing agent is distributed selectively where the powder needs to be molten. The fusing agent remains on the polymer powder. In a second step, the detailing agent is deposited on the borderline between particles that need to be fused and the surrounding powder. The detailing agent helps to improve the accuracy and surface quality of the component. Infrared radiation is applied to the powder bed by means of an infrared lamp that is moved across the powder surface. Infrared radiation melts the powder material covered with fusing agent as solely the fusing agent is able to absorb infrared radiation. These steps are repeated layer by layer until the printing process is completed [3]. So far, in literature only little information about the analytical characterization of these agents is reported. However, the determination of the organic solvents 2-pyrrolidone and triethylene glycol included in solvents has been described in the context of other applications. For example, 2-pyrrolidone was detected in pyrolyzed sewage sludge by gas chromatography (GC) combined with a single quadrupole detector [4]. In the work of Lehtonen [5] amines were extracted out of wine. The extracts were measured via high performance liquid chromatography and a fluorescence detector. Thus, the substances had to be derivatized with dansyl chloride.

Triethylene glycol is reported to be analyzed by ion chromatography and a pulsed amperometric detector [6]. Furthermore, GC and electron ionization together with selective ion monitoring mode was used for the quantification of glycols in human plasma and urine. For this purpose also derivatization was necessary [7].

Scope of the work was to investigate the agents used in the Multi Jet Fusion process as these materials offer novel analytical challenges. Characterization was achieved by means of high-resolution time-of-flight mass spectrometry and gas chromatography with flame ionization detection.

2. Experimental

2.1 Reagents and chemicals

Ethanol and methanol were of HPLC grade. Acetonitrile and non-stabilized tetrahydrofuran were LC-MS quality. All solvents were purchased from Merck (Darmstadt, Germany) and used without further purification. Furthermore, ultrapure water (18.2 MΩ cm) generated from a Sartorius Stedim Biotech system was used. The Karl-Fischer reagent for water content determination was Hydronal^{TM}-Coulomat AG-Oven from Fluka (Seelze, Germany). 2-Pyrrolidone for synthesis was purchased from Merck. The internal standard diethylene glycol monobutyl ether also for synthesis was obtained from Merck-Schuchardt (Hohenbrunn, Germany). Triethylene glycol (99%) was purchased from Thermo Fisher (Karlsruhe, Germany).

The 3D agents (fusing and detailing agent) 3D700 were obtained from HP (Palo Alto, USA). For LC-MS measurements 250 mg of each agent were dissolved in 5 mL methanol and stored in the ultrasonic bath for 10 min.

For GC and LC-MS measurements all fusing agent samples were filtrated with an MS Syringe Filter (0.2 µm WWPTFE) from Acrodise (Westborough, USA).

For GC-flame ionization detection (FID) measurements standard stock solutions of 100 mg L^{-1} of reference materials and the internal standard were prepared. Solutions from 1 mg L^{-1} up to 10 mg L^{-1} for external calibration were prepared by diluting the stock solution.

2.2 Instrumentation

2.2.1 Determination of water content

The coulometric determination of water content of the agents was achieved by Karl Fischer titration using the 774 Oven Sample Processor from Metrohm (Herisau, Schweiz) according DIN EN ISO 12937.

2.2.2 High performance liquid chromatography-electrospray ionization-quadruopole time-of-flight (HPLC-ESI-QTOF) device

HPLC-MS was carried out using a 1260 Infinity LC system in combination with an electrospray ionization source and a 6530 Accurate-Mass QTOF detector from Agilent Technologies. 1 µL of sample solution was injected into the system and separated on a reversed-phase SB-C18, RRHD column (150×2.1 mm; 1.8 µm) from Agilent Technologies. Chromatographic separation was realized using gradient elution containing 0.02% formic acid in water as solvent A and acetonitrile:tetrahyrofuran (70:30, v/v) as solvent B. The flow rate was set to 0.45 mL min^{-1}. LC gradient was : 0 min: 95% of solvent A + 5% solvent B, 1 min: 95% A + 5% B, 15 min: 100% B until 20 min, followed by reconditioning of the system back to initial conditions. Column oven temperature was set to 45 °C. UV spectra were recorded in the range of 200–640 nm. The ESI source was operated in positive ion mode. Source parameters were 250 °C gas temperature, 8 L min^{-1} drying gas flow, 35 psi nebulizer pressure, 350 °C sheath gas temperature, and 11 L min^{-1} sheath gas flow (nitrogen). As a capillary voltage 3000 V were applied and a fragmentor voltage of 80 V was used. The skimmer voltage was set to 65 V. MS data were received in the range of 20–1500 *m/z* with an acquisition rate of 2 spectra/s and an acquisition time of 500 ms/spectrum.

2.2.3 GC-FID

Quantitative analyses for triethylene glycol and 2-pyrrolidone were performed using a GC-FID 7890A system (Agilent Technologies, Waldbronn, Germany). The injector temperature was set to 280 °C. Injection volume was 1 µL in split mode (25:1). Helium was used as a carrier gas at a constant flow of 1.688 mL min^{-1}. Chromatographic separation was carried out on a HP-5MS 5% phenyl methyl

Table 1
Water content of fusing agent and detailing agent. The water content of the samples was determined coulometrically according DIN EN ISO 12937.

	Water content / %		
	1st measurement	2nd measurement	mean value
Fusing Agent	64.9	64.3	65
Detailing Agent	83.1	82.9	83

polysiloxane (30 m × 250 µm × 0.25 µm) capillary column from Agilent Technologies. The oven temperature was set to 40 °C for 4 min followed by a temperature increase up to 300 °C at a rate of 10 °C min^{-1}. The temperature was held for 10 min. Total analysis time was 40 min. FID parameters were 320 °C heater temperature, 30 mL min^{-1} H_2 flow, 400 mL min^{-1} air flow and 25 mL min^{-1} makeup gasflow.

3. Results and discussion

3.1 Determination of water content of the agents

The water content of fusing and detailing agents was determined according to DIN EN ISO 12937 in order to know the rough amount of water in the samples regarding further measurements. The results of the double determination are given in Table 1. The water content of the detailing agent is higher and has a local cooling effect on the powder material based on water evaporation. Consequently, contours become sharper and the surface quality is increased. Additionally, detailing agent can be applied on the same area as the fusing agent to obtain better controlling of heat generation [8]. The water content of fusing agent is lower since its aim is to obtain proper infrared absorption at the fused powder. Therefore, fusing agent contains carbon black. For a homogeneous distribution of carbon black in the liquid surfactants and organic solvents are required.

3.2 Qualitative investigations on agents

For qualitative investigations on the agents high performance liquid chromatography measurements in combination with ESI high-resolution mass spectrometry (HPLC-ESI-QTOF) were conducted. The total ion chromatograms (TIC) for both agents are illustrated in Fig. 1 A and B. Up to 2.5 min the shape of the TICs looks similar. However, after 2.5 min the chromatograms differ from each other. The first peak (1.1 min) was integrated for both agents and two mass traces identified which occurred in both agents. The MS spectra of the peak at 1.1 min of fusing and detailing agents are shown in Fig. 2 A and B. Fig. 2 C and D show the zoom in at a m/z 150–154 g mol^{-1}. Here the isotopic pattern becomes visible which is needed for the assignment of mass traces to distinct compounds. Applying a

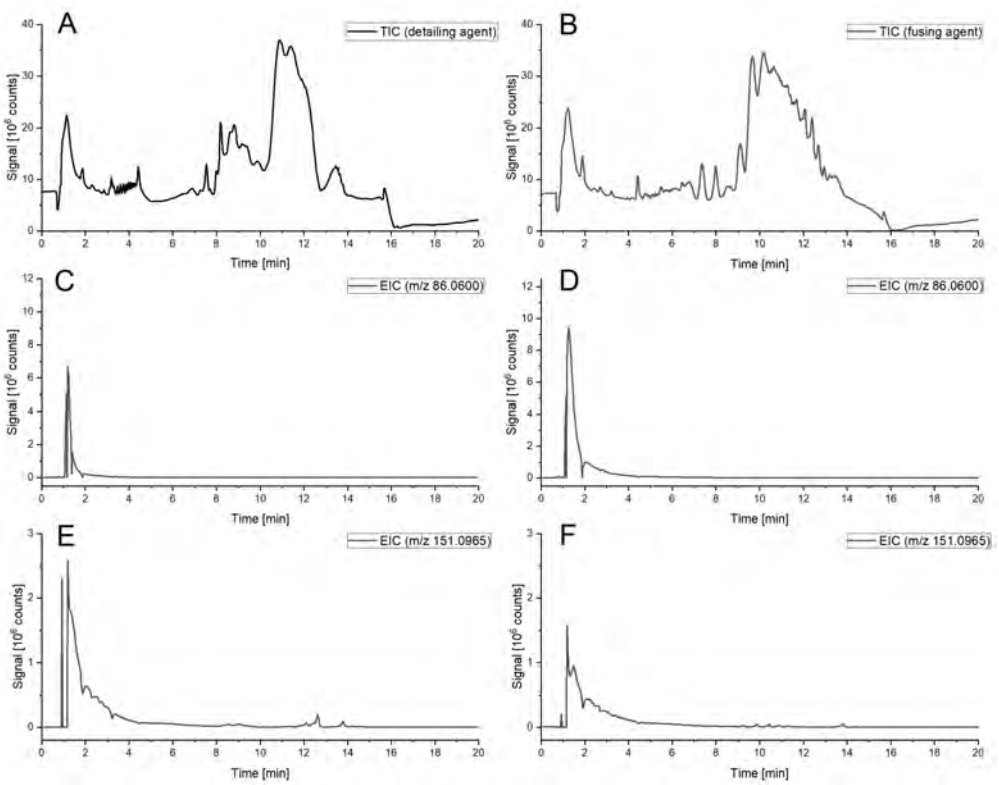

Fig. 1 (A) shows the total ion chromatogram (TIC) of detailing agent, and (B) of fusing agent. In (C)–(F) extracted ion chromatogtrams (EIC) of m/z = 86.0600 and m/z = 151.0965 are depicted. The extracted ion chromatograms are taken from the total ion chromatograms above, respectively. 86.0600 is the $[M+H]^+$ ion of 2-pyrrolidone and 151.0965 is the $[M+H]^+$ ion of triethylene glycol. The chromato-grams were extracted with a mass range interval of ±20 ppm.

software tool for calculation of molecular formulas based on the isotopic pattern of the mass traces and additional database research helped to proof the identity of 2-pyrrolidone and triethylene glycol in both agents. The calculated $[M+H]^+$ values for both substances (2-pyrrolidone: m/z = 86.0600, triethylene glycol: m/z = 151.0965) were extracted from the TIC with a mass range interval of ±20 ppm. The corresponding extracted ion chromatograms (EIC) for both agents are shown in Fig. 1 C–F. The intensities of the EICs differ for both substances and both agents.

3.3 Quantitative determination of 2-pyrrolidone and triethylene glycol in fusing and detailing agent

In order to obtain quantitative results for the amount of 2-pyrrolidone and triethylene glycol in the agents GC-FID measurements were conducted. For quantitative determination of 2-pyrrolidone and triethylene glycol in the agents

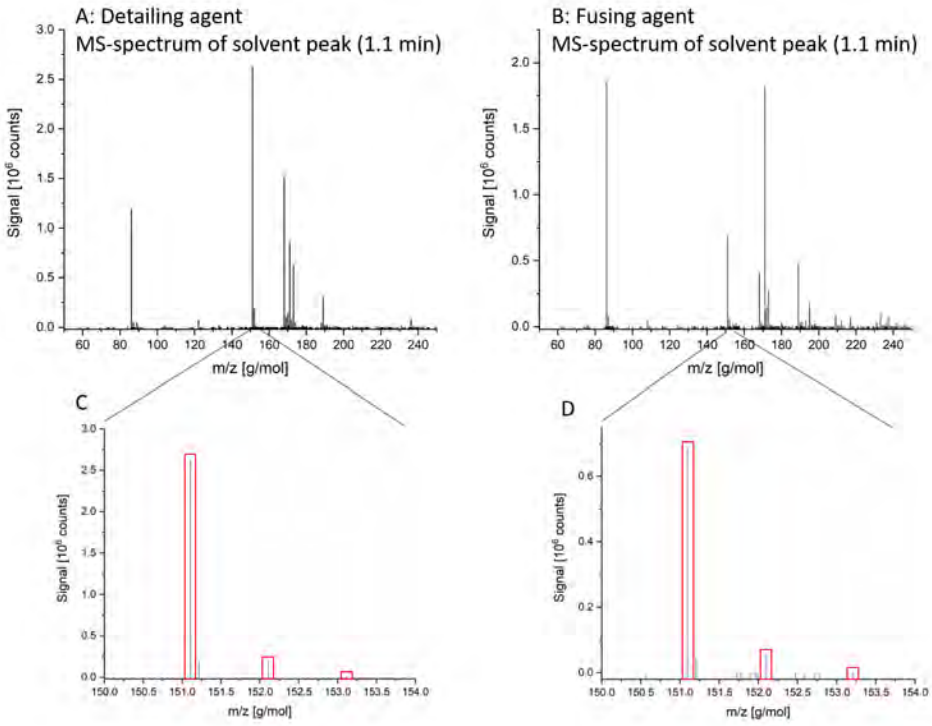

Fig. 2 (A) shows the MS spectrum of detailing agent of the peak at a retention time of 1.1 min. (B) shows the MS spectrum of the solvent peak for fusing agent. (C) shows a zoom into the range of *m/z* 150–154. The isotopic pattern of triethylene glycol becomes visible which is mandatory to identify substances like 2-pyrrolidone and triethylene glycol. (D) also shows the isotopic pattern of triethylene glycol identified in fusing agent by means of the unique isotopic pattern and a data base search.

Table 2
Overview of the results of the quantitative determination of 2-pyrrolidone and triethylene glycol by means of GC-FID. R^2 of external calibration with and without internal standard is given for 2-pyrrolidone and triethylene glycol. Furthermore, the slope of the calibration curves, the recovery of a test sample, and the calculated amounts of 2-pyrrolidone and triethylene glycol in detailing and fusing agent are shown.

Substance	Calibration type	R^2 / slope	recovery of test sample / %	amount in detailing agent / %	amount in fusing agent / %
2-pyrrolidone	external calibration	0.99999/202114	96.99 ± 0.13	3.80 ± 0.01	18.94 ± 0.12
	external with ISTD	0.99996/0.8871	97.98 ± 0.20	3.67 ± 0.01	18.74 ± 0.02
triethylene glycol	external calibration	0.99983/135538	99.91 ± 0.26	11.56 ± 0.06	8.50 ± 0.06
	external with ISTD	0.99998/0.60466	100.24 ± 0.02	11.08 ± 0.03	8.36 ± 0.02

GC was chosen since the substances can be transferred to the gas phase quite easily. Furthermore, the FID offers a linear signal in the range of 10^7 for hydrocarbon containing substances. External calibration was possible with and without internal standard for 2-pyrrolidone and triethylene glycol. As an internal standard diethylene glycol monobutyl ether was used. All calibration curves show a strictly linear behavior. The slopes of the different calibration curves, R^2 values, recovery of a test sample, and the calculated amounts of detailing and fusing agents are given in Table 2. Quantification is confirmed by the calculation of the recovery of the test sample. A recovery of 99.9% was achieved for triethylene glycol with external calibration, 100.2% using the additional internal standard. The detailing agent contained 11% triethylene glyol and 4% 2-pyrrolidone. The fusing agent contained 19% 2-pyrrolidone and 8% triethylene glycol (calculated with internal standard). Consequently, both substances can be determined with and without internal standard.

4. Conclusions

Fusing and detailing agent of the Multi Jet Fusion process were analytically investigated regarding their water and organic solvent content. Based on the agents different functionalities the water content of detailing agent is 18% higher compared to fusing agent. The identity of two organic solvents in the agents was determined by LC-ESI-QTOF measurements with the help of a data base and the distinct isotopic pattern. They were 2-pyrrolidone and triethylene glycol. An external calibration applying GC-FID for both solvents with and without internal standard was established. The results for both quantification methods were in good agreement. For 2-pyrrolidone the recovery was in the range of 97-98%. For triethylene glycol the recovery rate was 100%. The detailing agent contained 4% of 2-pyrrolidone and 11% triethylene glycol. The fusing agent contained 19% of 2-pyrrolidone and 8% of triethylene glycol.

References

[1] Yuan S., Shen F., Chua C.K., Zhou K.: Polymeric composites for powder-based additive manufacturing: Materials and applications. *Prog. Polym. Sci.* **91** (2019), 141–168.

[2] Sillani F., Kleijnen R.G., Vetterli M., Schmid M., Wegener K.: Selective laser sintering and multi jet fusion: Process-induced modification of the raw materials and analyses of parts performance. *Addit. Manuf.* **27** (2019), 32–41.

[3] Ligon S.C., Liska R., Stampfl J., Gurr M., Mülhaupt R.: Polymers for 3D printing and customized additive manufacturing. *Chem. Rev*. **117** (2017), 10212–10290.

[4] Cao J.P., Zhao X.Y., Morishita K., Li L.Y., Xiao X.B., Obara R., Wei X.Y., Takarada T.: Triacetonamine formation in a bio-oil from fast pyrolysis of sewage sludge using acetone as the absorption solvent. *Bioresour. Technol.* **101** (2010), 4242–4245.

[5] Lehtonen P.: Isolation and HPLC determination of amines in wine. *Z. Lebensm. Unters. Forsch.* **183** (1986), 177–181.

[6] Mrklas O., Chu A., Lunn S.: Determination of ethanolamine, ethylene glycol and triethylene glycol by ion chromatography for laboratory and field biodegradation studies. *J. Environ. Monit.* **5** (2003), 336–340.
[7] Meyer M.R., Weber A.A., Maurer H.H.: A validated GC-MS procedure for fast, simple, and cost-effective quantification of glycols and GHB in human plasma and their identification in urine and plasma developed for emergency toxicology. *Anal. Bioanal. Chem.* **400** (2011), 411–414.
[8] Riedelbauch J., Rietzel D., Witt G.: Analysis of material aging and the influence on the mechanical properties of polyamide 12 in the Multi Jet Fusion process. *Addit. Manuf.* **27** (2019), 259–266.

The influence of process parameters of the supercritical carbon dioxide extraction on the antioxidant activity in extracts from *Medicago sativa* L. and *Solidago gigantea* Ait.

Olga Wrona[a, c, *], Katarzyna Rafińska[b, c], Cezary Możeński[a], Bogusław Buszewski[b, c]

[a] *Łukasiewicz Research Network New Chemical Syntheses Institute, Al. Tysiąclecia Państwa Polskiego 13A, 24-110 Puławy, Poland* ✉ *olga.wrona@ins.pulawy.pl*
[b] *Interdisciplinary Centre of Modern Technologies, Nicolaus Copernicus University, Wilenska 4, 87-100 Toruń, Poland*
[c] *Department of Environmental Chemistry and Bioanalytics, Faculty of Chemistry, Nicolaus Copernicus, Gagarina 7, 87-100 Toruń, Poland*

Keywords
antioxidant activity
Medicago sativa L.
Solidago gigantea Ait.,
response surface methodology
supercritical fluid extraction

Abstract
The aim of this study was to conduct and improve the separation of bioactive compounds from two different plant materials: *Medicago sativa* L. and *Solidago gigantea* Ait. by optimization of parameters of non-polar supercritical carbon dioxide extraction simultaneously providing the highest antioxidant activity. The assumed goal fits into the "green analytical chemistry concept". The influence of three process parameters on the chosen criterion was investigated and results for two different plant materials were compared. For the optimization purpose the Box-Benkhen design, response surface methodology and analysis of variance were used. The obtained results have proved that it is possible to manipulate the separation of bioactive compounds by optimization of pressure, temperature and solvent flow rate of extraction and provide the highest antioxidant activity of the obtained product. High diversity in obtained optimal parameters imposes the necessity for optimization of parameters for individual plant material.

1. Introduction

According to the definition of traditional analytical chemistry, one of the main subjects of its interest is studies and application of instruments and methods used to separate sample, identify, and quantify their constituents. In a laboratory practice, separation is a first step and it should be focused to improve isolation of

analytes. The proper separation is a crucial and it can improve the further analysis. Nowadays a new dimension has been added to analytical chemistry: "green analytical chemistry concept". It involves the development of analytical methodologies with respect to environmental issues; embrace the application of direct analysis to avoid sample preparation that involves energy and solvent consumption which generates wastes. In line with the requirements of green analytical chemistry, supercritical fluid extraction as a separation methods allow to obtain pure samples without any solvent contamination [1, 6].

One of the most difficult materials for separation of samples is natural plant material. The extraction of plant materials is a crucial step in the isolation of bioactive compounds. The proper separation plays an important role in pretreatment of sample for further analysis. The type of extraction has a huge impact on the composition of the final extract which has an impact on the sample's properties. One of the main aims of the extraction is to obtain the highest amount of the pure extract, which is enriched in desired groups of compounds exhibiting certain properties. This is possible by choosing the suitable extraction method and optimizing the proper process parameters [6–8].

The supercritical carbon dioxide extraction is very suitable for the separation of bioactive compounds from plant materials according to "green analytical chemistry" standards. The popularity of this technique is related to the nature of carbon dioxide and specificity of the obtained product. Carbon dioxide has a lot of advantages i.e. it is inexpensive, easily available and generally regarded as safe (GRAS) [9–11]. It has interesting physicochemical properties: it is an inert gas, non-polar, tasteless, and odorless and therefore, it does not contaminate the final product. Carbon dioxide reaches critical state at low values of parameters, at 304.4 K (31.1 °C) and the pressure of 7.4 MPa (73.8 bar). Supercritical fluid extraction with pure supercritical carbon dioxide may seem to be a great separation technique for bioactive compounds. Additionally, after the process, carbon dioxide change into gasses and automatically leaves the process environment. There is no waste either after the process or in the sample.

Medicago sativa L. (lucerne, alfalfa) is a plant species widely spread in Poland and it is rich in bioactive compounds including phenols, lipids, saponins, essential amino acids, chlorophylls or vitamins. Due to the high content of the bioactive constituents and antifungal, antibacterial, insecticidal as well as nematicidal properties, the product from *Medicago sativa* L. has been used as food and feed additives and as a supplement in traditional medicine [2–5]. In Europe, *Solidago gigantea* Ait. (goldenrod) is considered among the most aggressive plant [6–8]. On the one hand, this is an advantage because this species is rich in bioactive secondary metabolites like flavonoids, terpenes and different nitrogen-containing compounds. The preparations from *Solidago gigantea* Ait. have health-promoting effects.

Table 1
Antioxidant activity of *Medicago sativa* L. and *Solidago gigantea* Ait. extracts.

Experiment	Box-Behnken design			DPPH/μmol TEAC g^{-1} of dry mass	
	T/K	*P*/MPa	*S*/kg h^{-1}	*Medicago sativa* L.	*Solidago gigantea* Ait.
E1	333.15 (0)	80.00 (1)	7.00 (1)	0.36	13.16
E2	353.15 (1)	80.00 (1)	5.00 (0)	8.90	11.42
E3	353.15 (1)	20.00 (–1)	5.00 (0)	5.90	0.00
E4	313.15 (–1)	50.00 (0)	3.00 (–1)	8.36	2.11
E5	333.15 (0)	50.00 (0)	5.00 (0)	2.88	8.96
E6	353.15 (1)	50.00 (0)	3.00 (–1)	8.75	7.13
E7	333.15 (0)	50.00 (0)	5.00 (0)	2.69	8.37
E8	333.15 (0)	50.00 (0)	5.00 (0)	5.13	11.19
E9	313.15 (–1)	80.00 (1)	5.00 (0)	3.08	0.32
E10	333.15 (0)	20.00 (–1)	3.00 (–1)	5.70	0.36
E11	313.15 (–1)	20.00 (–1)	5.00 (0)	11.17	8.96
E12	313.15 (–1)	50.00 (0)	7.00 (1)	3.36	12.15
E13	333.15 (0)	80.00 (1)	3.00 (–1)	4.48	3.41
E14	333.15 (0)	20.00 (–1)	7.00 (1)	3.36	0.36
E15	353.15 (1)	50.00 (0)	7.00 (1)	6.67	10.86

2. Experimental

2.1 Reagents and chemicals

Liquid carbon dioxide was produced in Grupa Azoty Zakłady Azotowe "Puławy" PLC. All others chemicals and reagents were purchased from Sigma Aldrich (Germany) and were of analytical grade.

2.2 Plant material

Medicago sativa L. was harvested in Zalesie, Poland. The plants were dried and ground into powder with moisture content about 12.1 % (w/w). *Solidago gigantea* Ait. was harvested in Choceń, Poland and dried and ground into 1–2 cm pieces. The content of *Solidago gigantea* Ait. moisture was 10.3% (w/w).

2.3 Extractions plan according to Box-Behnken design

Box-Behnken design was used to verify the effects of various factors:
1. temperature *T* (coded *A*) in the range of 313.15–353.15 K (40–80°C),
2. pressure *P* (coded *B*) in the range of 20–80 MPa), and
3. flow rate of carbon dioxide *S* (coded *C*) in the range of 3–7 kg h^{-1},
on the selected criteria [12]. The different process conditions that comprise the complete design are summarized in Table 1. To evaluate the effect of those variables the antioxidant activity was determined. All the results and statistical

analysis were accomplished using Design Expert 11.0 (Stat-Ease, USA). Supercritical fluid extraction was performed using quarter-technical plant (SITEC-Sieber Engineering, Switzerland) placed in Łukasiewicz Research Network New Chemical Syntheses Institute in Puławy, Poland.

2.4 DPPH-radical scavenging assay

The free radical scavenging activity in extracts was studied by 2,2-diphenyl-1-picrylhydrazyl (DPPH) radical scavenging method. 1.2 mL of a 0.1 mM ethanol solution of DPPH was added to 300 μL sample of diluted extract. Mixtures were vigorously mixed and incubated for 30 min in the dark. The absorbance was measured at 517 nm. Results were expressed as 6-hydroxy-2,5,7,8-tetramethylchroman-2-carboxylic acid (Trolox) equivalent antioxidant capacity (TEAC) using a calibration curve from Trolox solutions in 96% ethanol.

3. Results and discussion

Extractions with supercritical carbon dioxide of *Medicago sativa* L. and *Solidago gigantea* Ait. were performed. The new approach of this study was to induce the changes in the solubility or diffusivity of bioactive compounds by maintain the wide range of process parameters, particularly pressure and temperature and observe the difference of antioxidant activity in obtained products. The diversity of obtained results for *Medicago sativa* L. and *Solidago gigantea* Ait. extracts was also investigated. All of the obtained data are summarized in the Table 1. The process parameters are presented in both: coded and uncoded forms.

The antioxidant activity expressed as a Trolox equivalents showed a distinct diversity for both plant materials. The highest antioxidant activity for *Solidago gigantea* Ait. extract was obtained under temperature 333.15 K, pressure 80.00 MPa and solvent flow rate 7.0 kg h^{-1}. But at the same process parameter's, the lowest antioxidant activity was obtained for *Medicago sativa* L. extract. Despite the similarity in external structure of both analyzed plant materials, the obtained extracts have the different composition of bioactive components which finally had an impact on the determined values of antioxidant activity. This allowed concluding, that it is a necessity to optimize of supercritical fluid extraction parameters separate for individual plant material.

The obtained regression equations for both plant materials and the values of the most important statistical parameters are summarized in Table 2. Those crucial statistical values have to exhibit a proper correlation between output and input values in analyzed range of process parameters which indicate the proper model fitting. Coefficients of determination provide information about proper fitting between process parameters and DPPH results. Coefficient of determination for DPPH data for both *Medicago sativa* L. and *Solidago gigantea* Ait. were 0.96 and 0.92, respectively. The high values coefficient of determination has proven the

Table 2
Polynominal quadratic equations for DPPH (μmol TEAC g^{-1} of dry mass) as a result of the studies on the extracts of *Medicago sativa* L., *Solidago gigantea* Ait., resp. (R^2 – coefficient of determination, LOF – lack of fit *F*-value, p-value of the model).

Plant	Type	Regression equation	R^2	*LOF*	*p*-value
Medicago sativa L.	coded	DPPH = 3.56 + 0.5312 *A*– – 1.16 *B* – 1.69 *C* + 2.77 *AB* + + 0.7300 *AC* – 0.445 *BC* + + 3.50 A^2 + 0.1946 B^2 – 0.2829 C^2	0.96	0.25	0.006
	uncoded	DPPH = 1077.5992 – 6.13349 *T* – – 1.56276 *P* – 5.8481 *S* + + 0.00462 *TP* + 0.0043 *TS* – – 0.00741 *PS* + 0.008761 T^2 + + 0.00021 P^2 – 0.07072 S^2			
Solidago gigantea Ait.	coded	DPPH = 9.51 + 0.7337 *A* + + 2.33 *B* + 2.94 *C* + 5.02 *AB* – – 1.58 *AC* + 2.44 *BC* – 2.958 A^2 – – 4.04 B^2 – 1.15 C^2	0.92	0.23	0.029
	uncoded	DPPH = –30.7281 + 0.3087 *T* – – 2.46165 *P* + 15.44819 *S* + + 0.008658 *TP* – 0.0394 *TS* + + 0.0406 *PS* – 0.0007 T^2 – 0.00448 P^2 – 0.28708 S^2			

$R^2 > 0.8$: statistically important
LOF > 0.05: statistically important
$p < 0.0001$: very highly significant, $p < 0.01$: very significant, $p < 0.05$ significant, $p > 0.1$: not statistically significant

correctness of the adopted model. Non-statistically significant lack of fit *F*-value (0.25 and 0.23 > 0.05) and statistically significant *p*-value (0.006 and 0.029 < 0.05) for *Medicago sativa* L. and *Solidago gigantea* Ait. respectively, indicate that the adopted model describes adequately the dependence of respon-ses and process parameters.

The influence of three investigated process parameters: temperature (*T*, coded *A*), pressure (p, coded *B*) and solvent flow rate (*S*, coded *C*) on DPPH results and their interactions were determined and presented as a response surface plots in Fig. 1. The bigger slope indicates faster increases of the evaluation index which showed stronger dependence between input variables. It is observed especially for extracts obtained from *Solidago gigantea* Ait. where the diversity in obtained response surface is more clearly to see. Based on the obtained response surface plots, it can be concluded that all variables have effect on the all responses.

The optimal conditions, obtained as a result of extraction of *Medicago sativa* L. and *Solidago gigantea* Ait. and analysed data by response surface methodology and ANOVA were determined and summarized in the Table 3. The main criterion

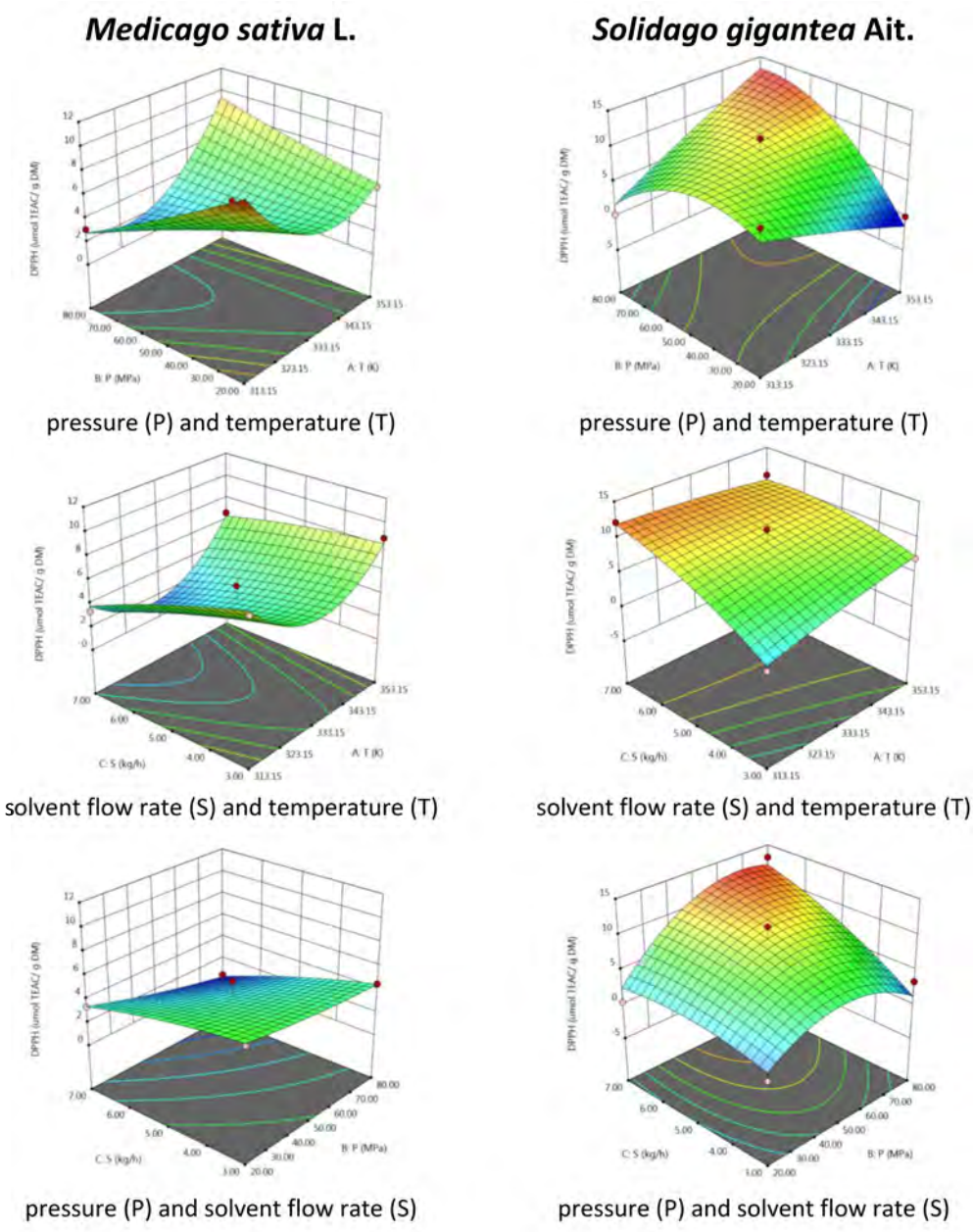

Fig. 1 Response surface plots for both plant materials as a function of the antioxidant activity and the main process parameters.

Table 3
Results of analysis of variance of obtained values and the comparison of predicted and experimental values of each evaluation index.

	Medicago sativa L.	*Solidago gigantea* Ait.
Optimal conditions (desirability – 1.0)		
T/K (°C)	313.28 (40.13)	345.98 (72.83)
P/MPa	20.14	74.86
S/kg h^{-1}	4.11	6.98
DPPH/μmol TEAC g^{-1} of dry mass		
Predicted value	11.42	14.47
Actual value	11.06	13.88
Confidence interval (± 5%)	10.85–11.99	13.75–15.19

was to achieve the highest value of DPPH for both plant materials. It is interesting to see how process parameters can change the composition of the final product by giving the difference in antioxidant activity despite the similarity in external structure for both plant materials (they are non-oily plant materials). Different values of DPPH results indicated the different composition of the product. This diversity can be also observed in the values of optimal conditions:

- For *Medicago sativa* L. the highest antioxidant activity was obtain under lower range of investigated parameters: 313.28 K (40.13 °C), 20.14 MPa and 4.11 kg h^{-1}.
- For *Solidago gigantea* Ait. the highest antioxidant activity was obtain under higher range of temperature, pressure and solvent flow rate: 345.98 K (72.83 °C), 74.86 MPa and 6.98 kg h^{-1}.

In order to verify the accuracy of the process modeling, extractions in optimal parameters for both plant materials were carried out. The antioxidant activity in the obtained products was in the range within the confidence interval. The results are very interesting, because for quite similar plant materials we obtained completely different optimal conditions which providing the highest value of DPPH result. The antioxidant properties of both extracts are the result of the action of various biologically active compounds isolated from the tested plants. This allowed concluding that, the proper optimization is a crucial step in sample preparation and it has to be carried out for individual plant material.

4. Conclusions

The goal of this study was to optimize parameters for supercritical carbon dioxide extraction of *Medicago sativa* L. and *Solidago gigantea* Ait. providing the highest antioxidant activity by stimulation of proper separation of bioactive constituents.

Box-Benkhen design, response surface methodology and analysis of variance (ANOVA) were used for the optimization of temperature, pressure and solvent flow rate. Based on obtained results, all of the investigated extraction parameters had an influence on antioxidant activity. Despite of the similarity of the external structure of both plant materials, the optimal conditions were in different range of process parameters: 313.28 K (40.13 °C), 20.14 MPa and 4.11 kg h^{-1} for *Medicago sativa* L. and 345.98 K (72.83 °C), 74.86 MPa and 6.98 kg h^{-1} for *Solidago gigantea* Ait.. These results revealed that pure supercritical carbon dioxide can be efficient in separation of bioactive compounds providing great antioxidant activity. However, the difference of optimal conditions indicates the necessity of the optimization of separation process for individual plant materials. Finally, at the stage of plant materials extraction, it is possible to prepare sample for analysis by purification due to specific solvent properties and concentrating the desired groups of compounds. According to the green analytical chemistry concept, supercritical fluid extraction as a separation method allows to obtain pure samples without any solvent contamination. Due to the proper optimization the sample shows desired properties.

Acknowledgments

This study was supported by PRELUDIUM 15 project No. 2018/29/N/ST4/01464 from National Science Centre, Poland.

References

[1] Armenta S., Garrigues S., Esteve-Turrillas F., Guardia M.: Green extraction techniques in green analytical chemistry. *TrAC, Trends Anal. Chem.* **116** (2019) 248–253.

[2] Rafińska K., Pomastowski P., Wrona O., Górecki R., Buszewski B.: *Medicago sativa* as a source of secondary metabolites for agriculture and pharmaceutical industry. *Phytochem.* **20** (2017), 520–539.

[3] Gatouillat G., Alabdul M.A., Bertin E., Okiemy-Akelia M.G., Morjani H., Lavaud C., Madoulet C.: Cytotoxicity and apoptosis induced by alfalfa (*Medicago sativa*) leaf extracts in sensitive and multidrug-resistant tumor cells. *Nutr. Cancer.* **66** (2014), 483–491.

[4] Goławska S., Łukasik I., Leszczyński B., Effect of alfalfa saponins and flavonoids on pea aphid. *Entomol. Exp. Appl.* **128** (2008), 147–153.

[5] Stochmal A., Oleszek W.: Seasonal and structural changes of flavones in alfalfa (*Medicago sativa*) aerial parts. *J. Food Agric. Environ.* **5** (2007), 170–174.

[6] Wrona O., Rafińska K., Możeński C., Buszewski B. : Supercritical fluid extraction of bioactive compounds from plant materials. *J. AOAC Int.* **100** (2017), 1624–1635.

[7] Wrona O., Rafińska K., Możeński C., Buszewski B.: Supercritical fluid extraction as a technique for isolation of biologically active compounds from plant material of industrial importance. *Przem. Chem.* **97** (2018), 1246–1252. (In Polish.)

[8] Wrona O., Rafińska K., Możeński C., Buszewski B.: Supercritical carbon dioxide extraction of *Solidago gigantea* Ait.: optimization at quarter-technical scale and scale up the process to half-technical plant. *Ind. Crop. Prod.* **130** (2019), 316–324.

[9] Oniuszuk A., Podgórski R.: Influence of different extraction methods on the quantification of selected flavonoids and phenolic acids from *Tilia cordata* inflorescence. *Ind. Crop. Prod.* **76** (2015), 509–514.

[10] Liu J., Ji F., Chen F., Guo W., Yang M., Huang S., Zhang F., Liu Y.: Determination of garlic phenolic compounds using supercritical fluid extraction coupled to supercritical fluid chromatography/tandem mass spectrometry. *J. Pharm. Biomed. Anal.* **159** (2018), 513–523.
[11] Mukhopadhyay, M.: *Natural Extract Using Supercritical Carbon Dioxide.* CRC Press 2000.
[12] Maran J.P., Manikandan S., Priya B., Gurumoorthi P.: Box-Behnken design based multi-response analysis and optimization of supercritical carbon dioxide extraction of bioactive flavonoid compounds from tea (*Camellia sinensis* L.) leaves. *J. Food Sci. Tech. Mys.* **52** (2015), 92–104.

Determination of low-molecular-mass heparin using affinity capillary electrophoresis

Katarína Molnárová*, Tomáš Křížek

Department of Analytical Chemistry, Faculty of Science, Charles University, Hlavova 8, 128 43, Prague, Czech Republic ✉ *molnark1@natur.cuni.cz*

Keywords
affinity interactions
capillary electrophoresis
Fraxiparine
low-molecular-mass heparin

Abstract
This work is dedicated to determination of low-molecular-mass heparin, namely Fraxiparine, using affinity capillary electrophoresis. Fraxiparine was detected indirectly by using tetraarginine, which forms a stable complex with Fraxiparine. The developed method used 50 μm i.d. fused silica capillary (length was optimized). Phosphoric acid (9 mM) with addition of 0.1% w/v hydroxyethylcellulose was used as a background electrolyte. The samples were injected hydrodynamically into the capillary by a pressure of 5 kPa. After that, voltage was applied for a certain period of time. During this time the zones migrate through each other, which enables formation of the complex. Fraxiparine was determined from the amount of remaining free tetraarginine. The injection time of Fraxiparine was subject to optimization. After the optimization, different experiments were performed for the determination of Fraxiparine in blood plasma. Acetonitrile, acetone and trifluoroacetic acid were tested for deproteination of the samples.

1. Introduction

Heparin is widely used an anticoagulant agent. It is a heterogeneous mixture of highly sulfated polysaccharide chains whose molecular weight ranges from 5 000 to 30 000 Da. Unfractionated heparin has several limitations such as poor bioavailability at low doses, short half-life, differential molecular weight-based clearance [1]. Due to its varying structure it is difficult to determine the exact dose which is used in the therapy. It can lead to an overdose, with hemorrhagic complications. To overcome some of heparin limitations, low-molecular-weight species have been developed [2]. They are produced by depolymerization of unfractionated ones. The depolymerization can be either chemical or enzymatic [3]. There are different types of low-molecular-weight species, in this work Fraxiparine was used. The active substance of Fraxiparine is calcium salt of nadroparin (Fig. 1). Although laboratory monitoring of low-molecular-weight species level in

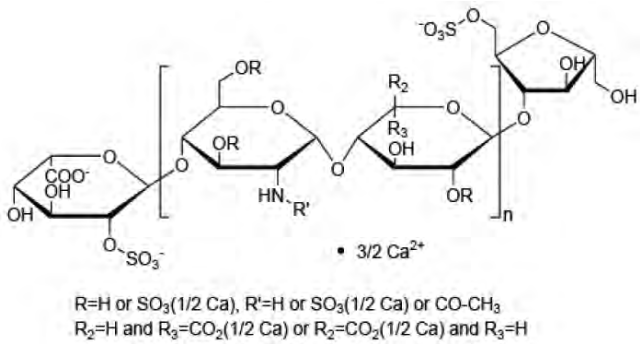

Fig. 1 Chemical structure of nadroparin calcium.

blood is not common, it is recommended in some cases, especially when patients are at age or weight extreme and during pregnancy. For monitoring of low-molecular-mass heparin levels, anti-factor Xa assay is used, which has some significant drawbacks [4]. In case of heparin overdose, protamine sulfate may be used as an antidote. Protamine is a highly positively charged peptide consisting of about 32 amino acids, and neutralizes the effect of heparin through electrostatic binding between the cationic arginine groups of protamine and the anionic heparin [5]. Because protamine has a complex, not precisely defined structure, it was replaced by well-defined tetraarginine in our study.

The aim of this work was to develop and to optimize a method for the determination of Fraxiparine by affinity capillary electrophoresis. The injection time of Fraxiparine and the total length of the capillary were subject to optimization.

2. Experimental

2.1 Reagents and chemicals

Orthophosphoric acid (85%, p.a.), acetonitrile (p.a.), acetone (p.a.) were purchased from Lach–Ner (Czech Republic). The injection solutions of Fraxiparine (3 800 IU anti–Xa in 0.4 ml) and Fraxiparine Forte (11 400 IU anti–Xa in 0.6 ml) were purchased from Glaxo Wellcome Production (France). The stock solutions were prepared by diluting the injection solutions with the background electrolyte and stored in the refrigerator. Tetraarginine was purchased from Bachem AG (Switzerland). The solution of tetraarginine was prepared by dissolving solid tetraarginine in water and was stored at temperature –18°C. Hydroxyethycellulose was purchased from Ashland (USA), the solution was prepared by dissolving solid hydroxyethycellulose in water. The water used for preparation of the solutions and BGEs was purified with Premier MFG' D System (USA).

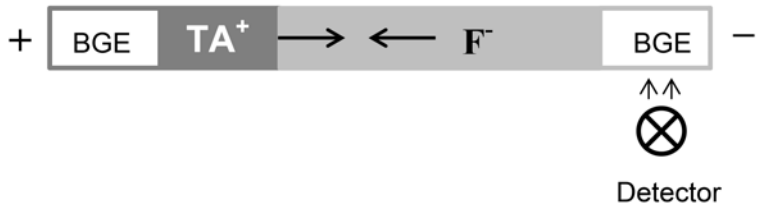

Fig. 2 Design of the experiment. TA^+ is the zone of tetraarginine; F^- is the zone of Fraxiparine.

2.2 Instrumentation

An Agilent CE 1600 capillary electrophoresis instrument (Agilent Technologies, Waldbronn, Germany) equipped with a built-in photometric diode-array detector (DAD) was used for all experiments. A fused silica capillary of 50 μm i.d. and 50.0 cm total length (unless stated otherwise) was used for the experiments. The capillary was thermostated at 25 °C. The samples were injected hydrodynamically into the capillary by a pressure of 5 kPa. The optimal method used a capillary of 40.0 cm total length (effective length was 31.5 cm). Fraxiparine was injected for 120 s, tetraarginine for 5 s. Then, separation voltage of 20 kV was applied for 30 s. Data acquisition and instrument control were carried out using Agilent OpenLAB ChemStation software.

3. Results and discussion

During the first experiments the basic design of the experiment had to be verified. Both Fraxiparine and tetraarginine were injected as zones hydrodynamically by pressure of 5 kPa. First, the zone of Fraxiparine was injected into the capillary for certain period of time. Then, the zone of tetraarginine was injected into the capillary. After that, 30 kV voltage was applied for 30 s (Fig. 2). During this time the zones migrate through each other, which enables formation of the complex. After the application of the voltage the zones were mobilized by pressure of 5 kPa towards the detector. Fraxiparine was determined from the amount of remaining free tetraarginine detected at a wavelength of 200 nm. The concentration range of Fraxiparine was selected from 0.00 to 4.75 anti–Xa IU ml^{-1}. Tetraarginine was injected with concentration of 1 mg ml^{-1}. In case of Fraxiparine the basic design of the experiment did not work because no free tetraarginine was detected, so it was necessary to optimize the conditions. First the injection time of tetraarginine was increased to 5 s while the injection time of Fraxiparine was not changed (120 s). As a result of this change we were able to detect the peak of tetraarginine in the whole concentration range of Fraxiparine (Fig. 3). The basic principle of the determination is that with the increasing concentration of Fraxiparine the peak of tetraarginine is decreasing. That is the reason why the calibration curve has a negative slope. Under these conditions the determination is finished within 17 minutes (including the preconditioning and zone injection steps) which is not a

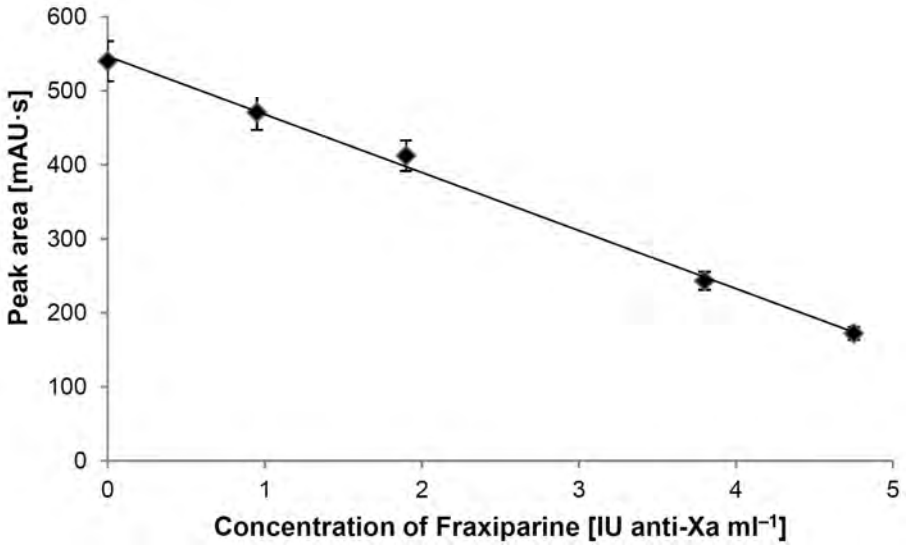

Fig. 3 Calibration graph for Fraxiparine obtained under optimized conditions, $y = -78.513\,x + 546.71$ ($R^2 = 0.9969$).

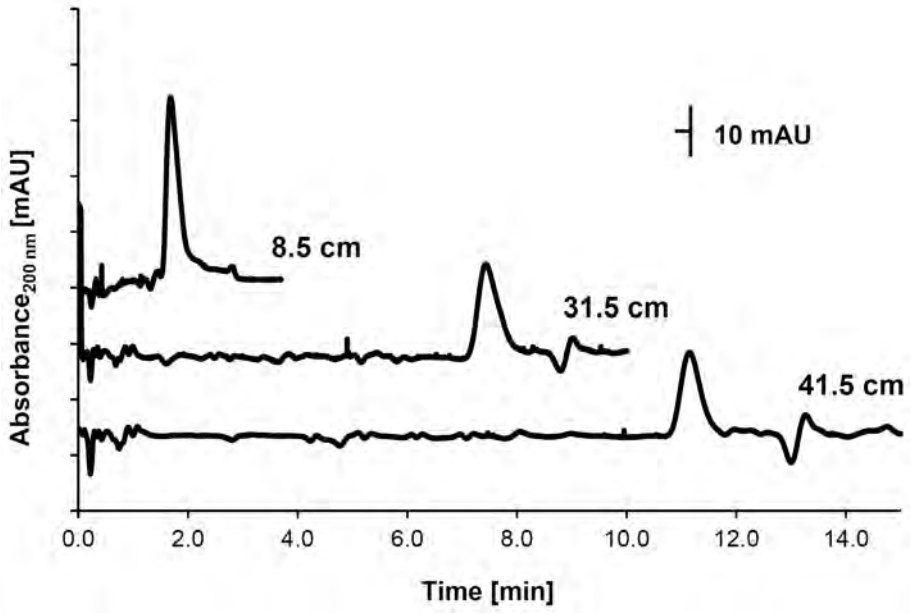

Fig. 4 Electropherograms comparing different effective lengths of the capillaries and duration of the analysis.

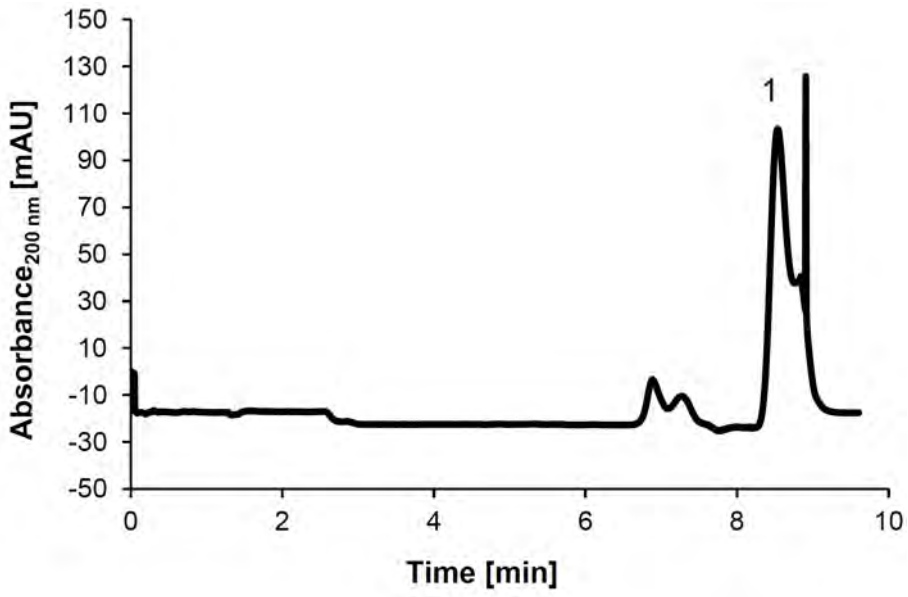

Fig. 5 Determination of Fraxiparine in plasma sample which was deproteinized after the addition of Fraxiparine. Peak (1) belongs to tetraarginine.

satisfactory time in routine analysis. There are some possibilities which can lead to reduction of the analysis time. One of these is using a method so-called "short-end injection". During these experiments the solutions are injected on the opposite side of the capillary, closer to the detector, while the polarity is reversed. The effective length of the capillary is 8.5 cm. Experiments performed under these conditions lead to peak and baseline distortion so the short-end injection was not applicable for our purpose despite the fact that analysis time was shortened to 5 minutes. The other option is to shorten the capillary. In our case the capillary was shortened to 40.0 cm (effective length was 31.5 cm). To make sure that the solutions will not overheat in the capillary the voltage was decreased to 20 kV and applied for 30 s. Total time of one analysis is 11 min. Electropherograms comparing different effective lengths of the capillaries and duration of the analysis are shown in Fig. 4. Performance of the optimized method was tested on a sample of Fraxiparine Forte injection. First the solution was diluted 8000× by BGE. Then the solution was measured 3 times. Results obtained using this method indicated that the sample contained 20 911 ± 934 IU anti–Xa ml^{-1} (*RSD* = 2.0 %) of Fraxiparine. The concentration declared by the manufacturer is 19 000 IU anti–Xa ml^{-1}, which is in a good agreement with our determined value.

The next step was to optimize the method for the determination of Fraxiparine in blood plasma. Different deproteinization agents were tested. The best one was acetonitrile, which was used in 1:3 = plasma: acetonitrile volume ratio. During the first experiments Fraxiparine was added to the deproteinized plasma. 50 µl of

plasma was mixed with 150 µl of acetonitrile, then BGE was added to the solution in 1:1 ratio. Fraxiparine was added to this solution with final concentration of 3.8 IU anti–Xa ml^{-1}. The aim of this experiment was to make sure that the components of the blood plasma does not affect the basic principle of the determination. Addition of Fraxiparine after deproteinization lead to decrease of tetraarginine peak area. Components of deproteinized sample thus did not interfere with the measurement. After that, Fraxiparine was added to the plasma which was deproteinized after the addition of Fraxiparine. Resulting electropherogram can be seen in Fig. 5. It is obvious that the peak of tetraarginine is distorted. Then 5 µl (26.6 IU anti–Xa ml^{-1}) of standard of Fraxiparine was added to the sample. After this addition the peak of tetraarginine should decrease which was not observed. It is supposed that these unfavourable results are caused because by addition of Fraxiparine to plasma that inhibits the precipitation of some of the components which affect the determination. Studying these interferences will be subject to following research.

4. Conclusions

Method of affinity capillary electrophoresis was optimized for determination of Fraxiparine. The time of analysis was successfully reduced to 12 minutes. The performance of the method was tested on Fraxiparine Forte. Since these experiments showed acceptable results, the method can be used for determination of nadroparin in pharmaceutical products. The optimized method was tested on plasma samples. Unfortunately, these experiments did not provide satisfactory results.

References

[1] Hirsh J., Warkentin T.E., Shaughnessy S.G., Anand S.S., Halperin J.L., Raschke R., Granger C., Ohman E.M., Dalen J.E.: Heparin and low-molecular-weight heparin mechanisms of action, pharmacokinetics, dosing, monitoring, efficacy, and safety. *Chest* **119** (2001), 64–94.
[2] Cosmi B., Palareti G.: Old and new heparins. *Thromb. Res.* **129** (2012), 388–391.
[3] Patel R.P., Narkowicz C., Hutchinson J.P., Hilder E.F., Jacobson G.A.: A simple capillary electrophoresis method for the rapid separation and determination of intact low molecular weight and unfractionated heparins. *J. Pharm. Biomed. Anal.* **46** (2008), 30–35.
[4] Thomas O., Lybeck E., Strandberg K., Tynngård N., Schött U.: Monitoring low molecular weight heparins at therapeutic levels: dose-responses of, and correlations and differences between aPTT, anti-factor Xa and thrombin generation assays. *PLoS One* **10** (2015), e0116835.
[5] Boer C., Meesters M.I., Veerhoek D., Vonk A.B.A.: Anticoagulant and side-effects of protamine in cardiac surgery: a narrative review. *Br. J. Anaesth.* **120** (2018),914–927.

Selection of experimental conditions for the identification of bacteria by MALDI-TOF MS

Oleksandra Pryshchepa[a, b, *], Michał Złoch[b], Katarzyna Pauter[a, b], Małgorzata Szultka-Młyńska[a, b], Paweł Pomastowski[b], Bogusław Buszewski[a, b]

[a] *Department of Environmental Chemistry and Bioanalysis, Faculty of Chemistry, Nicolaus Copernicus University, Gagarina 7, 87-100 Torun, Poland* ✉ *pryshchepa.alexie@gmail.com*
[b] *Interdisciplinary Centre of Modern Technology, Nicolaus Copernicus University, Wileńska 4, 87-100 Torun, Poland*

Keywords
bacteria
identification
MALDI-TOF MS
PCR
urine

Abstract
The work presents the identification study of uropathogens by MALDI-TOF MS (Matrix-assisted laser desorption/ionization time-of-flight mass spectrometry). The standard method supplied by Bruker Daltonik, that utilize α-cyano-4-hydroxycinnamic acid as a matrix have been optimized to improve the identification rate and accuracy. The optimized technique have been used to identify bacteria isolated from urine, which have been also identified by sequencing of 16S rDNA genes. Sequencing of 16S rDNA technique actually is considered to be a "gold standard" in microorganisms identification. Moreover, the influence of some other matrices such as 2,5-dihydroxybenzoic acid (DHB) and super-DHB on MALDI-TOF MS spectra of bacterial proteins profiles is shown.

1. Introduction

Urine is reported as one of the most popular biological matrix in clinical microbiology. At least 40% of hospital acquired infections and 20% of non-hospital infections are accounted for urinary tract infections. It is reported that the most often urinary tract infections are caused by *Escherichia coli* (75–95% of uncomplicated and nearly 50% of complicated urinary tract infections). To other bacteria that can cause urinary tract infections include *Staphylococcus saprophyticus*, *Proteus mirabilis*, *Klebsiella* spp., *Enterococci* and *Streptococci*, *Enterobacteriaceae*, *Pseudomonas aeruginos*, *Candida albicans* [1].

Nowadays conventional techniques are still widely used for identification of microorganisms. Conventional techniques are based on investigation of phenotypic characteristics of microorganisms such as morphology of bacterial cells or biochemical profiles [2]. However due to high similarities in phenotypic characteristics of microorganisms such methods often lead to misidentification and therefore to improper treatment [3, 4]. To disadvantages of conventional methods also include its time- and work-consuming character [2].

In the most complicated cases the PCR and sequencing of 16S rDNA are utilized [3, 4]. However, these techniques are work- and money-consuming, which is a reason of searching for new methods in microbiology. MALDI-TOF MS is a relatively new and cost-effective technique that offers the same secure as identification based on sequencing of 16S rDNA [2]. Moreover, the analysis along with sample preparation by MALDI-TOF MS for single sample is not exceed 15 minutes and consumables cost not much. Therefore the main goal of this work was to elaborate MALDI-TOF MS technique for identification of microorganisms isolated from urine.

2. Experimental

2.1 16S rDNA identification of bacterial isolates

Total bacterial DNA was isolated from 24h cultures (TSA, CLED, Schaedler Agar, TSB, 37 °C) using the Extractme DNA Bacteria Kit (Blirt S.A., Poland). Regions of 16S rDNA were amplified using universal primers for bacteria: 27F (5-AGAGTTTGATCMTGGCTCAG-3) and 1492R (5-GGTTACCTTGTTACGACTT-3), thermostable Taq DNA polymerase (Qiagen, Hilden, Germany), Mastercycler® pro S thermocycler (Eppendorf AG, Hamburg, Germany), and following PCR program: (1) 95 °C, 1 min. (initialization); (2) 95 °C, 15 s (denaturation); (3) 55 °C, 15 s (annealing); (4) 72 °C, 90 s (elongation): (2)–(4) repeated 30×; (5) 72 °C, 7 min (final elongation); (6) 10 °C (cooling for final hold). PCR products were then purified using Extractme Genomic DNA kit (Blirt S.A., Poland) followed by direct DNA sequencing via Sanger dideoxy method using the same 27F and 1492R primers. Quality of obtained chromatograms of 16S rDNA sequences were checked using Chromas ver. 2.6.2 software(Technelysium Pty Ltd, Australia). Contigs were assembled via BioEdit Sequences Alignment Editor ver. 7.2.5 (Tom Hall, USA), and finally, consensus sequences were compared with known16S rDNA genes present in the The National Center for Biotechnology Information BLAST database. Evolutionary relationships of investigated bacterial strains were presented on a phylogenetic tree created using the Neighbor-Joining method with computing the evolutionary distances by the Maximum Composite Likelihood method via MEGA7 ver. 7.0.21 software.

2.2 MALDI-TOF MS bacteria analysis

For selection of conditions of protein extraction two batches for each chosen microorganism (*Proteus mirabilis*, *Pseudomonas aeruginosa*, *Klebsiella pneumoniae*, *Escherichia* spp., *Streptococcus agalactiae*, *Enterococcus faecalis*, *Staphylococcus aureus*, *Staphylococcus haemolyticus*, *Candida albicans*) were used for analysis. α-cyano-4-hydroxycinnamic acid solution in standard solvent (acetonitrile 50%, water 47.5% and trifluoroacetic acid 2.5%) at final concentration:

10 mg/mL was used as matrix. For sample preparation, ethanol/formic acid extraction procedure was performed according to Bruker's guideline with small modifications and using different amounts (2, 5, 10, 20 and 30 μL) of 70% formic acid and acetonitrile. Biological material was transferred by 1 μL calibrated disposable inoculation loop into 5 Eppendorf tubes containing 300 μL of deionizated water and mixed thoroughly. Subsequently, 900 μL of absolute ethanol were added and thoroughly vortexed, then centrifuged at max speed for 5 min. The supernatant was discarded, and the remaining cell pellet was dried by evaporation of ethanol residue at 37 °C for 20 minutes to increase the extraction efficiency. To each of the five tubes containing cell pellets 2, 5, 10, 20 and 30 μL of 70% formic acid respectively was added and mixed by pipetting. Then an equal volume of acetonitrile was added, mixed by pipetting. The mixture was centrifuged for 2 min at 13000 rpm, 1 μL of supernatant in two repeats was transferred onto a MALDI MTP ground steel target sample spot (Bruker Daltonik GmbH, Germany). Next, the dried sample spots were overlaid with 1 μL of α-cyano-4-hydroxycinnamic acid matrix solution and air dried. For calibration Bruker Bacterial Test Standard was utilized, mass spectra were processed with the use of software provided by the manufacturer – flexControl and flexAnalysis, and subsequently used for bacterial identification via MALDI Biotyper Compass platform (Bruker Daltonik GmbH, Germany).

For bacteria identification isolated from urine the above mentioned method was used, in which 20 μL of 70% formic acid and acetonitrile for bacterial proteome extraction were utilized.

To investigate the influence of different matrices on MALDI-TOF MS spectra the same method as for bacteria identification was utilized. 10 mg/ml α-cyano-4-hydroxycinnamic acid and 50 mg/ml 2,5-dihydroxybenzoic acid/sDHB (i.e., mixture 9:1 of 2,5-dihydroxybenzoic acid and 2-hydroxy-5-methoxybenzoic acid) in standard solvent solutions were used.

3. Results and discussion

The probability of correct identification in the MALDI Biotyper Compass platform expressed in the form of number indicator named "score value". The identification is more reliable in case of higher score value. Choosing the extraction conditions of bacterial proteins we took into account the frequency of occurrence of the highest score value depending on the amount of used solvents. The most often the highest score value was observed in case of usage of 20 μL of formic acid and equal volume of acetonitrile 16 times. In case of usage of 10 μL of solvents the highest score value was observed 10 times, for 5 μL and 30 μL it was 6 times and for 2 μL no times. Small amounts of solvents (2–10 μL) used for extraction cannot ensure extraction of proteins with high efficiency, so the quality of obtained spectra cannot allow to identify microorganisms with high reliability. The increase of amount leads to improvement in quality of obtained spectra as it was for 20 μL of formic acid and

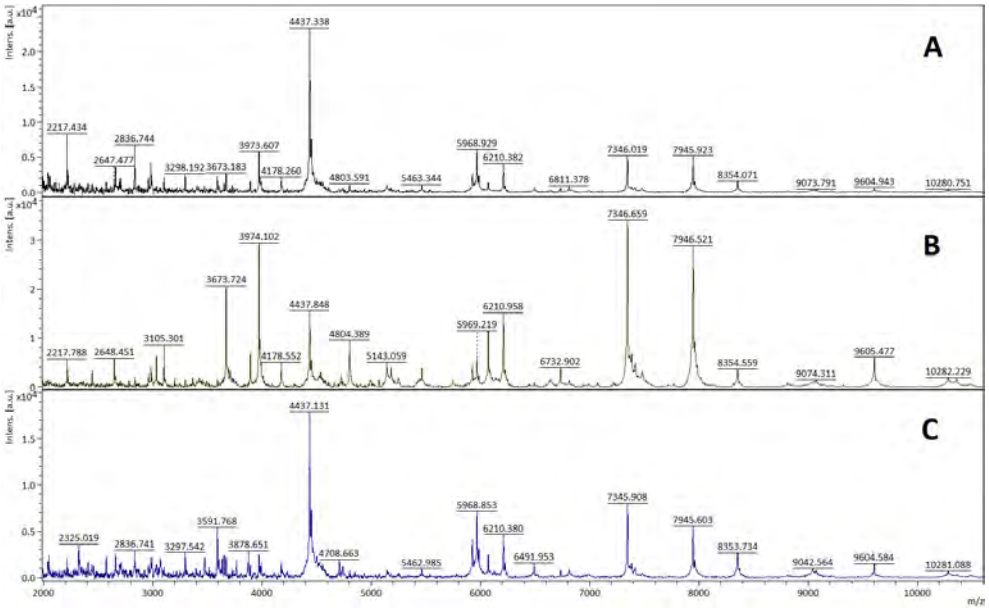

Fig. 1 Spectra for protein extracts of *Escherichia* spp. cells obtained with usage of different amount of solvents: (A) 2 µl, (B) 20 µl, and (C) 30 µl of 70% formic acid and equal amount of acetonitrile.

acetonitrile. Further volume increase cause the reduction of solutions concentration and therefore to impossibility to ionize a sufficient number of proteins (Fig. 1).Subsequent investigations were performed with usage of 20 µL of formic acid and equal amount of acetonitrile for protein extraction from bacterial cells. Nevertheless, the distributions of the best score value indicates that the more data should be gathered.

Based on sequencing of 16S rDNA region of bacterial genome it was identified 48 strains of bacteria isolated from urine. Almost 92% of isolates belonged to gram-positive bacteria, among which *Staphylococcaceae*, *Streptococcaceae*, *Enterococcaceae*, *Enterobacteriaceae* and *Bacillaceae* families are present. Even though sequencing of 16S rDNA is considered to be a "gold standard" in microorganisms identification, it was impossible to discriminate some closely related bacteria due to small differences in 16S rDNA (< 0.5%) [6]. For example, it was impossible to differentiate *Shigella* and *Escherichia* genus.

Used procedure for protein extraction allows obtaining MS spectra of high quality (Fig. 2). 94.1% and 78.4% of isolated bacteria were identified on species level in RAW and MSP mode respectively by MALDI-TOF MS technique. MALDI-TOF MS identification of bacterial isolates corresponds to results obtained by sequencing of 16S rDNA. 34 from 48 bacteria were identified on species level by both techniques. Moreover MALDI-TOF MS technique was able to discriminate some bacteria from *Streptococci* and *Staphylococci* families, which was impossible in case of sequencing of 16S rDNA. However, it was impossible to identify bacteria

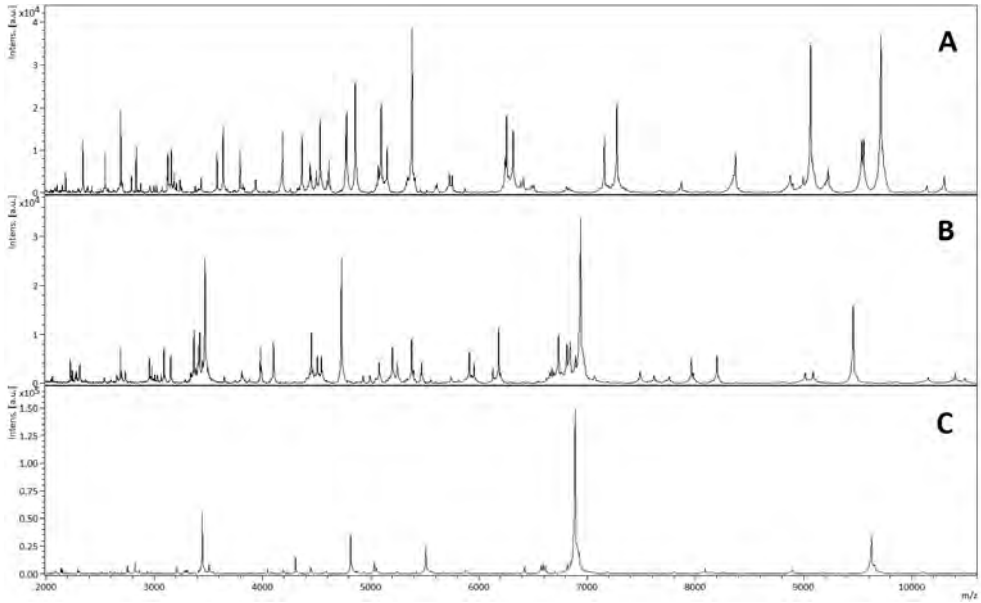

Fig. 2 Spectra obtained for different species of microorganisms: (A) *Escherichia* spp., (B) *Streptococcus agalactiae*, (C) *Streptococcus aureus*.

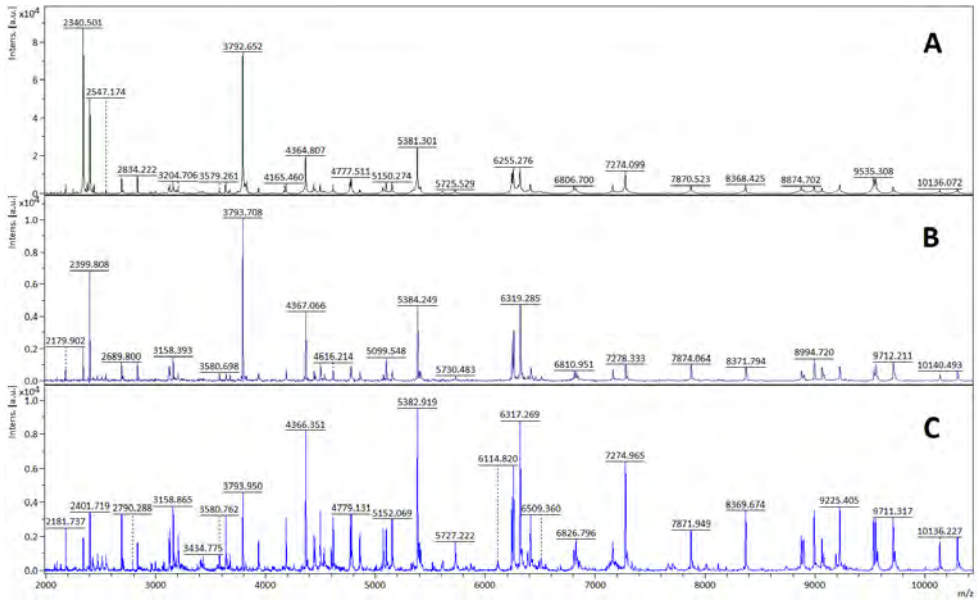

Fig. 3 Spectra obtained for *Escherichia coli* with usage of different matrices: (A) α-cyano-4-hydroxycinnamic acid, (B) 2,5-dihydroxybenzoic acid, (C) super DHB, i.e. mixture 9:1 of 2,5-dihydroxybenzoic acid and 2-hydroxy-5-methoxybenzoic acid.

from *Bacillus* family, which is considered to be environmental bacteria [4]. The commercial databases used for the MALDI approach contain less reference spectra for environmental microorganisms, in comparison with BLAST type repositories containing data about sequences of 16S rDNA [5].

The usage of different matrices has a big influence both on the view of obtained spectra and microorganisms identification rate (Fig. 3). The main differences that were observed with usage of 2,5-dihydroxybenzoic acid and sDHB as matrices compared to α-cyano-4-hydroxycinnamic acid were changes in intensity, signal/noise rate and appearance of different signals. In the identification process in MALDI approach the comparison of the most intense signals (peak list) of obtained spectra with that one from dataBase take place [7]. The highest peaks of each spectrum are compared taking into account the borders of the initial mass error, therefore the differences in intensity, peak appearance and peak shifts have a big influence on microorganisms identification rate. Generally the identification rate was higher with usage of 2,5-dihydroxybenzoic acid as a matrix, compared to other matrices.

4. Conclusions

The standard method for microorganisms identification supplied by Bruker Daltonik was optimized. The method allows obtaining high quality mass spectra and therefore to identify microorganisms isolated from urine with high efficiency. The usage of MALDI-TOF MS technique shows the efficiency of such approach for differentiation of uropathogens. Moreover, it was shown that usage of different matrices can improve identification rate.

Acknowledgments

This work was supported by Opus 11 No. 2016/21/B/ST4/02130 (2017-2020) from the National Science Centre, Poland.

References

[1] Michno M., Sydor A.: Zakażenia układu moczowego u osób dorosłych. *Przegląd Lekarski* **73** (2016), 504–508 (In Polish.)

[2] Buszewski B., Rogowska A., Pomastowski P., Złoch M., Rrailean-Plugaru V.: Identification of microorganisms by modern analytical techniques. *J. AOAC Int.* **100** (2017), 1607–1623

]3] Kandi V., Palange P., Vaish R., Bhatti A.B., Kale V., Kandi M.R., Bhoomagiri M.R.: Emerging bacterial infection: Identification and clinical significance of Kocuria species. *Cureus* **8** (2016), e731.

[4] Celandroni F.: Identification and pathogenic potential of clinical bacillus and paenibacillus isolates. *PLoSOne* **11** (2016), e0152831.

[5] Clark A.E., Kaleta E.J., Arora A., Wolk D.M.: Matrix-assisted laser desorption ionization-time of flight mass spectrometry: A fundamental shift in the routine practice of clinical microbiology. *Clin. Microbiol. Rev.* **26** (2013), 547–603

[6] Janda J.M., Abbott S.L.: 16S rRNA gene sequencing for bacterial identification in the diagnostic laboratory: Pluses, perils, and pitfalls. *J. Clin. Microbiol.* **45** (2007), 2761–2764.

[7] Zhang Y., Liu Y., Ma Q, Song Z., Zhang Q., Wang X., Chen F.: Identification of *Lactobacillus* from the saliva of adult patients with caries using matrix-assisted laser desorption/ionization time-of-flight mass spectrometry. *PLoS One* **9** (2014), e106185.

Zinc ions binding to β-lactoglobulin: proteomic study and physicochemical characteristic

Agnieszka Rodzik[a, b, *], Viorica Railean-Plugaru[a, b], Katarzyna Rafińska[a, b], Tomasz Kowalkowski[a, b], Paweł Pomastowski[b], Bogusław Buszewski[a, b]

[a] *Department of Environmental Chemistry and Bioanalysis, Faculty of Chemistry, Nicolaus Copernicus University, 7 Gagarin Street, 87-100 Toruń, Poland* ✉ *agnieszka.rodzik1@gmail.com*
[b] *Center for Education and Research in Separation Methods & Bioanalytics BioSep, Centre for Modern Interdisciplinary Technologies, Nicolaus Copernicus University, 4 Wileńska Street, 87-100 Toruń, Poland*

Keywords
β-lactoglobulin
interaction metal-protein
MALDI-TOF MS

Abstract
Metal ions are an extremely important element of many biological systems and play an essential role in the functioning of many proteins. Metal ions have an influence on the structure protein and provide overall structural stability. In the conducted studies to characterize β-lactoglobulin, MALDI-TOF MS analysis was performed and isoelectric point was determined. The kinetics of immobilization (sorption) of metal cations on the protein was investigated in order to determine the mechanism of binding Zn ions to β-lactoglobulin. Kinetic research allows us to understand the factors influence on binding process. Obtained metal complexes create a potential application in medicine: therapeutically to diagnose or treat various diseases or food industries.

1. Introduction

Proteins are the basic organic compounds present in living organisms [1]. They are the building material of cells, a biological active agents such representatives as enzymes, hormones, antibodies. Proteins determine the structure of the system, the proper functioning and development of organisms. They control every cellular process, including DNA/RNA replication, transcription, splicing and translation [2].

β-Lactoglobulin is the most abundant group of whey proteins in cow's milk, constituting more than 50% of all whey proteins. This protein is not present in human milk. β-Lactoglobulin is a source of essential and branched amino acids such as leucine, isoleucine and valine [3]. Based on the β-lactoglobulin structure, it is believed to bind ligands and transport small hydrophobic ligands. β-Lactoglobulin is capable of binding to vitamins A and D, palmitic acid and other

hydrophobic compounds. In addition, β-lactoglobulin has a strong affinity to fatty acids, phospholipids and aromatic compounds. The binding of these molecules to β-lactoglobulin may change their biological activity [4]. In addition, this protein has a high affinity for metal cations. The combination of proteins with metal cations creates new opportunities for their application in medicine or nutrition. Obtaining biologically active protein-metal complexes serves as a perfect tool to determine their influence on the metabolism of the examined organism [1]. Proteomic studies use highly specialized, multidimensional and electrophoretic analytical techniques coupled with mass spectrometry. This combination allows simultaneous, fast and precise identification of most proteins in the biological system. In addition, they create new possibilities of data interpretation. The essence of proteomics research is not only identification of specific proteins, but first of all methods searching for isolation of proteins from biological samples. It is important to study the expression of a given protein, analyze interactions and post-translational modifications and correlate the function of proteins with the activity of the test organism. Gel electrophoretic study hyphenated with spectrometric methods is a good combination for proteomic analysis [5].

This work focuses on the synthesis of complex β-lactoglobulin-zinc compounds. Characteristics of proteins by spectrometric, spectroscopic and microscopic methods and kinetics of zinc immobilization on β-lactoglobulin will allow formulating conclusions concerning the course and mechanisms of β-lactoglobulin-zinc complexes formation. Knowledge of processes and mechanisms of zinc binding to β-lactoglobulin creates potential applications.

2. Experimental

2.1 Reagents and chemicals

β-lactoglobulin purchased from Sigma Aldrich (Germany). All chemicals for the MALDI-MS analyses were supplied at the highest commercially available purity by Fluka Feinchemikalien (NeuUlm, Germany). Ultra-pure water was obtained from a Milli-Q RG system by Millipore (MilliporeIntertech, Bedford, MA, USA).

2.2 Characteristics of β-lactoglobulin

2.2.1 Electrophoresis in native conditions and SDS-PAGE

Electrophoresis was carried out in native and denaturing conditions. Initially, the concentration of protein was obtained equal to the concentration of 1 mg mL^{-1}. SDS-PAGE electrophoresis was carried out using Mini Gel Tank (ThermoFisher Scientific) according to procedure [6].

2.2.2 Matrix-Assisted Laser Desorption Ionization–Time of Flight Mass Spectrometry (MALDI-TOF/TOF-MS) Analysis

For MALDI-TOF MS analysis α-cyano-4-hydroxycinnammic acid was used as a matrix for intact proteins as well as proteins with tryptic digestion. Protein Calibration Standards II and Peptide Calibration Standard II for intact and trypsin digested proteins respectively (all from Bruker Daltonics, Bremen) were used as a matrix.

2.2.3 Isoelectric point determination

The isoelectric point of β-lactoglobulin was measured using the Zetasizer Nano Series (Malvern Instruments, Malvern, Great Britain). First, the protein was suspended in 0.09% NaCl (Sigma-Aldrich, Poland) at pH = 2, 3, 4, 5, 6, 7, 8, 9, 10 and 11 respectively at a final concentration of 0.4 mg/mL just before analysis. Next, the solution was sonicated for 10 sec.

2.3 Kinetic study of zinc binding to β-lactoglobulin

β-lactoglobulin (50 mg/10 mL) was suspended in 0.09% NaCl solution at pH = 4.6 (pI of β-lactoglobulin). The solution was sonicated for 5 min. 0.5 mL of β-lactoglobulin suspension was transferred to a 2 mL Eppendorf tube and mixed with 0.5 mL $Zn(NO_3)_2$ (Sigma-Aldrich, Poland) stock solution with zinc ions concentration of 60 mg L^{-1}. After incubation the solutions were certrifuged (4°C, 15,000 rpm, 5 min). 0.1 mL of supernatant was transferred to a 2 mL Eppendorf tube with 1.53 mL 65% HNO_3 and mineralization at the temperature 80°C for 2 h were carried out. Thereafter, the solution was transferred to a 100 ml volumetric flask to obtain a 1% HNO_3 solution. The concentration of zinc cations was determined using an Inductively Coupled Plasma-Mass Spectrometry ICP-MS.

3. Results and discussion

3.1 Characteristics of β-lactoglobulin

In order to precisely determine the mass of β-lactoglobulin, intact protein analysis using MALDI-TOF MS in linear ion positive mode was performed, as shown in Fig. 1. The mass of β-lactoglobulin was 18 301±0.132 Da, which is in accordance with the literature data [7]. More detailed structural identification was carried out after tryptic digestion and analysis of fingerprints and MS/MS spectra of selected peptides obtained in positive mode with reflector as shown in Fig. 2. In both cases, the mass spectra were collected and processed using the flexControl and flex-Analysis software. In case of tryptic digestion of β-lactoglobulin components, the highest MS and MS/MS peak values obtained were identified using BioTools software.

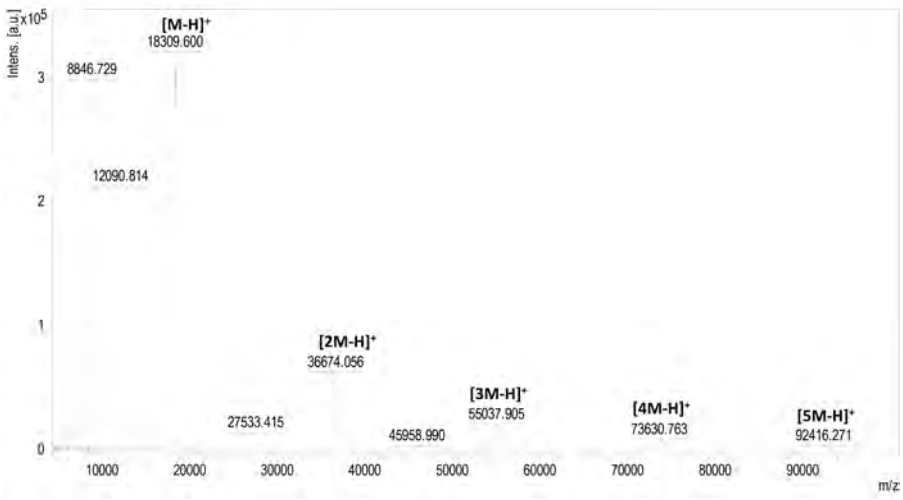

Fig. 1 Mass spectra of β-lactoglobulin components in the intact state.

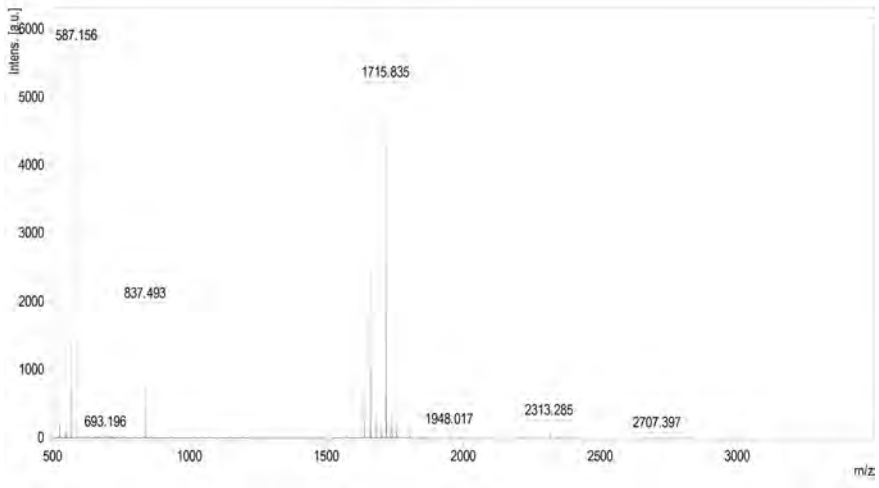

Fig. 2 The tryptic digestion spectrum recorded for β-lactoglobulin.

The determination of the isoelectric point of protein was performer by zeta potential measurements. Zeta potential values at pH values 2 and 3 ranged from 19 to 21mV. Then, at pH values 4 and 5 a decrease in potential values from +18.5 to –12.3 mV was observed. Zeta potential values above pH 5 are unstable and indicate protein degradation. The isoelectric point of β-lactoglobulin was 4.6, which is according to the literature [8, 9].

Table 1
Kinetic models parameters for the zinc ions sorption by β-lactoglobulin.

Kinetics model	Parameter
Zero order	
First step	k_0 = 4.233 mg L^{-1} min^{-1}
Second step	k_0 = 0.488 mg L^{-1} min^{-1}
Third step	k_0 = 1.535 mg L^{-1} min^{-1}
Pseudo first-order	q_e = 8.160 mg g^{-1}
	k_1 = 0.045 min^{-1}
	$A_{approx.}$ = 57.181 %
Intra-particle diffusion	A = 2.117 mg g^{-1}
	K_{ip} = −0.007 mg $g^{-1}min^{-0.5}$

3.2 Kinetic study of the zinc binding process

Kinetic research allows us to understand the factors influencing the speed of the binding process. Therefore, the experimental kinetic data obtained were subjected to zero order, pseudo-first order and Weber-Morris intra-particle diffusion kinetic model. The analysis of adsorption kinetics shows that it is not a homogeneous process but a differentiated one consisting of 3 steps and chemical equilibrium. In order to calculate the constant velocities of zinc ions for the 3 steps obtained, the zero-order kinetics model was applied, as it describes in a simple way the individual sorption steps. The unit of constant velocity obtained using this model is the real physical parameter characterizing the speed of the process. The rate constant values are summarized in Table 1. In order to more accurately present the received experimental data, the pseudo first-order kinetics model was used; Table 1 summarized the calculated kinetics constants. In order to determine the mechanism involved in adsorption process the obtained kinetic data was also tested against the Weber-Morris intra-particle diffusion model, as shown in Table 1.

4. Conclusion

Spectrometric studies of MALDI-TOF MS allowed obtaining information on precise determination of protein mass. Kinetics of binding zinc ions to protein is a heterogeneous process involving 3 steps process: first fast step, while steps 2 and 3 were steps in gradual sorption.

Acknowledgments

This work was financially supported by National Science Centre in frame of Opus 14 project No. 2017/27/B/ST4/02628 (2018-2021).

References

[1] Garcia J.S, Magalh C., Schmidt A.M., Arruda Z.: Trends in metal-binding and metalloprotein analysis. *Talanta* **69** (2006), 1–15.
[2] Berg J.M., Tymoczko J.L., Stryer L.: *Biochemia*. Warszawa, PWN 2007, s. 41–109. (In Polish.)
[3] Marshall K.: Therapeutic applications of whey protein. *Altern. Med. Rev.* **9** (2004), 136–156.
[4] Tai C.S., Chen Y.Y., Chen W. L.: β-Lactoglobulin influences human immunity and promotes cell proliferation. *Biomed. Res. Int.* 2016:7123587.
[5] Nebija D., Kopelent-Frank H., Urban E., Noe C.R, Lachmann B.: Comparison of two dimensional gel electrophoresis patterns and MALDI-TOF MS analysis of therapeutic recombinant monoclonal antibodies trastuzumab and rituximab. *J. Pharm. Biomed. Anal.* **56** (2002), 684–691.
[6] www.thermofisher.com/order/catalog/product/A25977 (accessed 11th June, 2019)
[7] Zhan L., Liu Y., Xie X., Xiong C., Nie Z.: Heat-induced rearrangement of the disulfide bond of lactoglobulin characterized by multiply charged MALDI-TOF/TOF Mass Spectrometry. *Anal. Chem.* **90** (2018),10670–10675.
[8] Gebhardt R., Toro-Sierraa J., Kulozik U.: Pressure dissociation of β-lactoglobulin oligomers near their isoelectric point. *Soft Matter*. **8** (2012), 11654–11660.
[9] Engelhardt K., Lexis M., Gochev G., Konnerth C., Miller R., Willenbacher N., Peukert W., Braunschweig B.: pH effects on the molecular structure of β-lactoglobulin modified air-water interfaces and its impact on foam rheology. *Langmuir* **29** (2013), 11646–11655.

Novel construction of renewable silver amalgam film electrode for voltammetric analysis

JÚLIUS GAJDÁR*, JIŘÍ BAREK, JAN FISCHER

UNESCO Laboratory of Environmental Electrochemistry, Department of Analytical Chemistry, Faculty of Science, Charles University, Hlavova 8, 128 43 Prague 2, Czech Republic
✉ *julius.gajdar@natur.cuni.cz*

Keywords
electrochemistry
renewable surface
silver amalgam film electrode
voltammetry

Abstract
This contribution outlines a development of a novel type of renewable silver amalgam film electrode. The electrode design is based on a previously published construction; however, it has been modified using a common retractable pen as a foundation of the electrode which also functions as a refreshing mechanism of amalgam film. We propose this electrode as a simple, inexpensive to construct and easily refreshable mercury-based electrochemical sensor for determination of organic pollutants.

1. Introduction

One of the best electrode materials for voltammetric analysis of metals and reducible organic compounds is mercury. However, some disadvantages like toxicity, liquid mercury handling, and complicated usage in online or field applications are propelling development of novel non-toxic mercury-based electrode materials [1]. One type of these electrodes is based on solid silver amalgam and they were developed by Yosypchuk and Novotny [2, 3]. In recent years, they were successfully used in a wide field of applications [4]. Around the same time Bas [5] proposed an easily renewable mercury film electrode using silver (silver amalgam) as a base substrate. These renewable silver amalgam film electrodes (Hg(Ag)FE) have been applied for voltammetric and potentiometric determinations of inorganic metallic cations and organic compounds. These works were summarized in a recent review [6]. Renewable silver amalgam film electrodes are based on a repeated renovation of the electrode surface by coating a silver wire with fresh liquid amalgam film (1% *w/w* Ag) before each experiment with satisfactory reproducibility between renovations of the amalgam film. These electrodes were reported to be stable in a timeframe of several months and used silver wire does not significantly degrade in a liquid amalgam. The amount of mercury used in this electrode is negligible; only approximately 10 μL of a liquid

amalgam are necessary. This electrode also offers very simple preparation and regeneration while it preserves the positive characteristics of mercury as an electrode material, e.g., a wide potential window and an excellent sensitivity [6].

The goal of this study is a development of a simple, inexpensive and easily refreshable electrochemical sensor based on Hg(Ag)FE for the determination of biologically active organic compounds in small volumes of samples. This work is a continuation of our previous publications [7–9] concerning the development of electrochemical microcells.

2. Experimental

All voltammetric measurements were carried out on Eco-Tribo Polarograph controlled by Polar Pro 5.1 software (both Polaro-Sensors, Czech Republic). Renewable silver amalgam film electrode Hg(Ag)FE was prepared using silver wire with 0.5 mm diameter. Voltammetric measurements were carried out in a three-electrode system with Ag|AgCl|3 mol L^{-1} KCl reference electrode (Elektrochemicke detektory, Turnov, Czech Republic) and a platinum wire auxiliary electrode (Eco-Trend Plus, Czech Republic). Working electrode had to be activated at the start of the day according to procedures usually carried out with solid silver amalgam electrodes [10] by applying potential −2.2 V for 10 mins in a solution of 0.2 mol L^{-1} KCl. Hg(Ag)FE was then cycled in the used supporting electrolyte (20 scans) [11]. Working electrode pre-treated by this procedure then can be used for multiple experiments with just refreshing of liquid amalgam film as a cleaning process. Britton-Robinson buffer with pH = 4 was used as a supporting electrolyte for preliminary experiments with 4-nitrophenol based on optimal conditions found in [12].

3. Results and discussion

A novel type of Hg(Ag)FE was constructed based on a common retractable plastic pen; more precisely its clicking retractable mechanism. An ink cartridge was replaced by an insulated copper wire with a smaller silver wire (d = 0.5 mm) soldered to its bottom end. This silver wire was used as a substrate for Hg(Ag)FE. Beforehand, the silver wire was pre-treated as described in [5, 13]. The wire was at first polished on alumina and then washed with water and acetone. The wire was then placed in a liquid amalgam (1% *w/w* Ag) for three days. During this time solid silver amalgam is formed in a thin layer of the silver wire and was reported to be stable for several months [5]. The pen's frame was modified by attaching a plastic vial to its end, which was capped with a septum. This septum was used as a seal that divided solution and liquid amalgam reservoir; and also provided a cleaning of a silver amalgam wire from excess liquid amalgam. Refreshing of the electrode surface was performed very simply just by "clicking" the pen two times, during which the silver wire is dipped in a liquid amalgam reservoir. This process provided a fresh amalgam film.

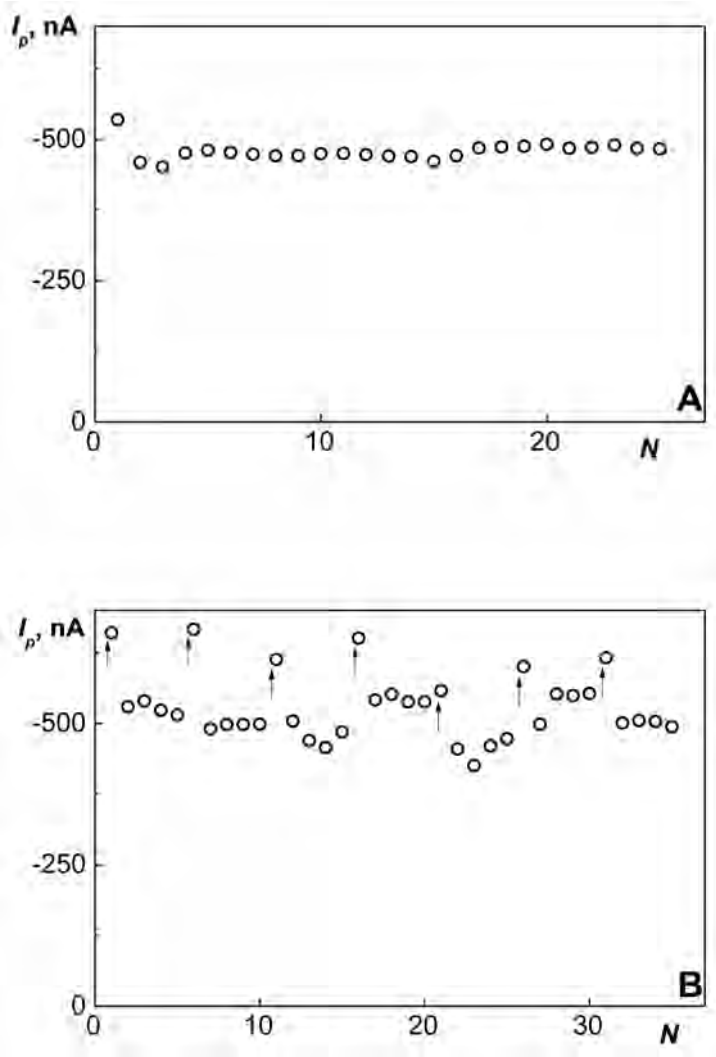

Fig. 1 Dependency of peak heights of 4-nitrophenol (0.1 mmol L^{-1}) on number of measurement in a series obtained at Hg(Ag)FE in Britton-Robinson buffer pH = 4 by DP voltammetry on (A) one refreshed amalgam film, and on (B) 7 refreshed amalgam films. Arrows denote a refresh of amalgam film.

Preliminary experiments were carried out with 4-nitrophenol as a model organic pollutant. Pre-treated electrode gave very good reproducibility (*RSD* = 2%, *c* = 0.1 mmol L^{-1}) after 25 scans by DP voltammetry without the refreshing of an amalgam film. Reproducibility between measurements during which amalgam film was refreshed gave worse results (*RSD* = 7%, 7 new amalgam films). In all experiments the very first scan had to be eliminated from the calculations as an outlier. The comparison of reproducibility of renewal of amalgam film is illustrated on Fig. 1. Additionally, a shift of reduction potential of 4-nitrophenol was observed in a range of approximately 50 mV (from −450 mV to

–500 mV) most probably caused by refreshing of amalgam film which is quite unfavorable for electrochemical studies. More complex pre-treatment [13] or regeneration [12] procedures might help to achieve better reproducibility in the following experiments.

4. Conclusions

Simple Hg(Ag)FE was successfully constructed and tested with 4-nitrophenol as a model substance. This electrode will be used as a base for an electrochemical sensor for analysis in small volumes.

Acknowledgments

This research was carried out within the framework of Specific University Research (SVV 260440) and it was supported by the Czech Science Foundation (project 17-03868S).

References

[1] Barek J., Fischer J., Navrátil T., Pecková K., Yosypchuk B., Zima J.: Nontraditional electrode materials in environmental analysis of biologically active organic compounds. *Electroanalysis* **19** (2007), 2003–2014.
[2] Novotny L., Yosypchuk B.: Solid silver amalgam electrodes. *Chem. Listy* **94** (2000), 1118–1120. (In Czech.)
[3] Yosypchuk B., Novotný L.: Electrodes of nontoxic solid amalgams for electrochemical measurements. *Electroanalysis* **14** (2002), 1733–1738.
[4] Danhel A., Josypcuk B., Barek J., Fojta M.: Possibilities and prospects of silver amalgam in electroanalytical chemistry. *Chem. Listy* **110** (2016), 215–221. (In Czech.)
[5] Baś B., Kowalski Z.: Preparation of silver surface for mercury film electrode of prolonged analytical application. *Electroanalysis* **14** (2002), 1067–1071.
[6] Bobrowski A., Królicka A., Bobrowski R.: Renewable silver amalgam film electrodes in electrochemical stripping analysis—a review. *J. Solid State Electr.* **20** (2016), 3217–3228.
[7] Gajdár J., Barek J., Fischer J.: Electrochemical microcell based on silver solid amalgam electrode for voltammetric determination of pesticide difenzoquat. *Sens. Actuator B-Chem.* submitted (2019).
[8] Gajdár J., Barek J., Fojta M., Fischer J.: Micro volume voltammetric determination of 4-nitrophenol in dimethyl sulfoxide at a glassy carbon electrode. *Monatsh. Chem.* **148** (2017), 1639–1644.
[9] Gajdár J., Goněc T., Jampílek J., Brázdová M., Bábková Z., Fojta M., Barek J., Fischer J.: Voltammetry of a novel antimycobacterial agent 1-hydroxy-*N*-(4-nitrophenyl)naphthalene-2-carboxamide in a single drop of a solution. *Electroanalysis* **30** (2018), 38–47.
[10] Yosypchuk B., Barek J.: Analytical applications of solid and paste amalgam electrodes. *Crit. Rev. Anal. Chem.* **39** (2009), 189–203.
[11] Vajdle O., Guzsvany V., Skoric D., Anojcic J., Jovanov P., Avramov-Ivic M., Csanadi J., Konya Z., Petrovic S., Bobrowski A.: Voltammetric behavior of erythromycin ethylsuccinate at a renewable silver-amalgam film electrode and its determination in urine and in a pharmaceutical preparation. *Electrochim. Acta* **191** (2016), 44–54.
[12] Fischer J., Vanourkova L., Danhel A., Vyskocil V., Cizek K., Barek J., Peckova K., Yosypchuk B., Navratil T.: Voltammetric determination of nitrophenols at a silver solid amalgam electrode. *Int. J. Electrochem. Sci.* **2** (2007), 226–234.
[13] Bas B.: Refreshable mercury film silver based electrode for determination of chromium(VI) using catalytic adsorptive stripping voltammetry. *Anal. Chim. Acta* **570** (2006), 195–201.

Flow amperometric biosensor based on two enzymatic reactors (acetylcholinesterase-choline oxidase) for the detection of neurotransmitter acetylcholine

Sofiia Tvorynska[a, b, *], Jiří Barek[a], Bohdan Josypčuk[b]

[a] *UNESCO Laboratory of Environmental Electrochemistry, Department of Analytical Chemistry, Hlavova 2030/8, Faculty of Science, Charles University, 128 43 Prague 2, Czech Republic,* ✉ *sofiia.tvorynska@jh-inst.cas.cz*

[b] *J. Heyrovský Institute of Physical Chemistry of the Czech Academy of Science, Dolejskova 3, 182 23 Prague 8, Czech Republic*

Keywords
acetylcholine
amperometric biosensor
acetylcholinesterase
choline oxidase
enzymatic reactor
flow injection analysis

Abstract
A stable amperometric biosensor with separated bienzymatic (acetylcholinesterase (AChE)–choline oxidase (ChOx)) part has been successfully developed for the determination of acetylcholine (ACh) in FIA for the first time. The bienzymatic part consists of two consecutively connected enzymatic reactors, which were independently prepared by covalent immobilization of AChE or ChOx on mesoporous silica powder (SBA-15). The amperometric measurements are based on the detection of consumed oxygen. The wall-jet cell with working silver solid amalgam electrode covered by mercury film to carry out four-electron oxygen reduction at the highly negative potential was used. The experimental parameters such as amounts of immobilized enzymes, pH of carrier solution, detection potential, flow rate, and injection volume of ACh were optimized. The detection limit was found to be 4.1 μmol L^{-1}. The developed amperometric ACh biosensor showed good repeatability and long-term stability. The same enzymatic reactors were successfully used for 500 measurements during 90 days.

1. Introduction

Acetylcholine (ACh) is one of the most important neurotransmitter, which plays a vital role in central and peripheral nervous system. It is implicated in many human behaviour, such as arousal and attention, and plays a key role in memory formation and learning [1]. The dysfunction in ACh regulation in the brain causes neuropsychiatric disorders such as Parkinson's disease, Alzheimer's disease [2] and schizophrenia. Therefore, the determination of ACh is important for the characterization of cholinergic transmission in normal and pathological

physiology. Moreover, the development of the fast, simple and sensitive methods of ACh determination could be useful in early diagnostic of above-mentioned neurological diseases.

Among the enzymatic biosensors, the amperometric enzyme-based biosensors are especially promising because of their potential high sensitivity, selectivity, simplicity, and good repeatability. The principle of ACh detection with the amperometric enzymatic biosensor is based on the two following sequential biochemical reaction:

$$\text{acetylcholine} + H_2O \xrightarrow{\text{AChE}} \text{choline} + \text{acetic acid} \quad (1)$$

$$\text{choline} + H_2O + 2\,O_2 \xrightarrow{\text{ChOx}} \text{betaine} + 2\,H_2O_2 \quad (2)$$

The enzyme acetylcholinesterase (AChE) catalyses the hydrolysis of ACh to form choline and acetic acid (1) and followed by the second reaction choline oxidase (ChOx) oxidizes choline generating betaine and hydrogen peroxide as the end products (2). The amperometric measurements can be based on the detection of produced hydrogen peroxide or consumed oxygen.

To our knowledge, most previously reported amperometric ACh biosensors are based on the immobilization of AChE and ChOx on working electrode surface through additional supports which are applied in the batch arrangement [3, 4]. Such type of enzymatic biosensor shows good sensitivity due to the immobilized enzymes on the electrode surface. However, it exhibits low stability. Also in this case the rule applies: one electrode – one biosensor. The flow amperometric biosensors based on the separated enzymatic (reactor) and detection (working electrode) part enable to overcome main limitations of the biosensors with the classic construction. First of all, the biosensors with the enzymatic reactor possess long-term stability because of the much larger amount of the immobilized enzyme. Moreover, there is a possibility to replace one bioreactor by another one in a few seconds and immediately start to work with other enzymatic system.

This work is focused on the development of a simple, rapid and long-time functional amperometric acetylcholine biosensor based on the separated bienzymatic (AChE–ChOx) and detection parts in FIA.

2. Experimental

2.1 Reagents and chemicals

All chemicals were of p. a. or better grade. Acetylcholinesterase from Electrophorus electricus (AChE, EC 3.1.1.7, 245 U mg^{-1}), choline oxidase from Alcaligenes sp. (ChOx, EC 1.1.3.17, 13.8 U mg^{-1}), acetylcholine chloride, choline chloride (≥ 98%), glutaraldehyde (GA), (3-aminopropyl)triethoxysilane, disodium ethylenediaminetetraacetate (Na_2EDTA), mesoporous silica powder SBA-15 (particle

size 2–6 μm, pore size ≈ 7 nm, surface area ≈ 600 m^2g^{-1}) were purchased from Sigma Aldrich.

2.2 Instrumentation

Amperometric measurements were carried out at room temperature using computer-controlled electrochemical stand (Polaro-Sensors, Czech Republic) with MultiElchem v. 3.1 software (J. Heyrovský Institute of Physical Chemistry of the CAS). FIA with the three-electrode laboratory-made wall-jet cell was used: working electrode – silver solid amalgam electrode covered by mercury film (MF-AgSAE, laboratory-made, amalgam disc diameter 0.50 mm), reference electrode – a miniaturized saturated calomel electrode based on silver paste amalgam (laboratory-made [5], it has the same potential as classical saturated calomel electrode, auxiliary electrode – platinum wire (diameter 0.25 mm, length 10 mm). The reproducible mercury film was formed at the beginning of each working day by dipping the end of AgSAE into a small glass tube with about 1 mL liquid mercury and intensively agitating for 15 s. An electrochemical activation of MF-AgSAE was carried out by imposition of −2200 mV for 300 s in 0.20 mol L^{-1} KCl.

3. Results and discussion

Two enzymatic reactors based on the mesoporous silica powder (SBA-15) as filling material covalently bounded with enzyme (AChE or ChOx) have been independently prepared. A detailed protocol of the preparation procedure of SiO2-powder covalently covered by enzyme is described in our previous paper [6]. Two enzymatic reactors (AChE–SBA15 and ChOx–SBA15) were consecutively connected in front of the detector in flow system (the analyte first passes through AChE–SBA15 reactor).

The principle of ACh detection is based on the amperometric measurements of oxygen consumed by two sequential enzymatic reactions (1)–(2). The decrease of dissolved oxygen concentration in the carrier solution (CS), shown on the amperometric curve as a downward peak, is directly proportional to ACh concentration. It is obvious that using four-electron oxygen reduction at the highly negative potentials results in a higher sensitivity. The wide range of working potentials and the high negative potential of hydrogen evolution on the different types of silver solid amalgam electrodes (AgSAEs) enable their application as the detectors to carry out four-electron oxygen reduction. It follows from our previous paper [7] based on the comparison of two flow cells with working two types of AgSAEs for the determination of Ch using amperometric biosensor with ChOx–SBA15 reactor that the wall-jet cell with working MF-AgSAE provides the better analytical characteristics.

The key parameters, which greatly influence on the response of the proposed amperometric biosensor based on the bienzymatic AChE–SBA5/ChOx–SBA15 reactors for ACh detection in FIA, were optimized.

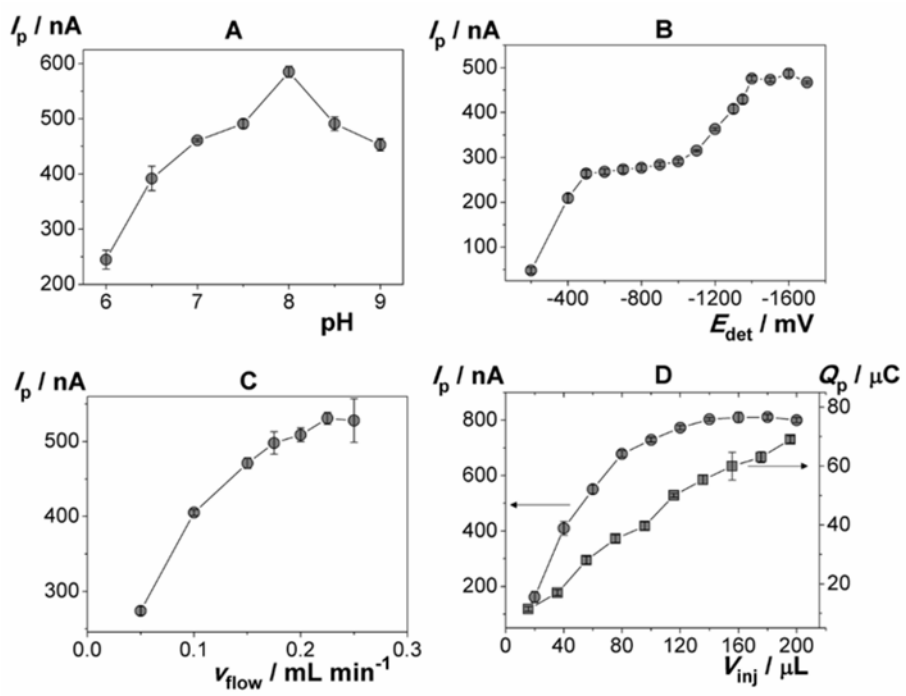

Fig. 1 Dependence of the peak current (circles) and peak area (squares) (only for D) on: (A) pH of the carrier solution; (B) the detection potential; (C) the flow rate of the carrier solution; (D) the injection volume of acetylcholine. Experimental conditions: *c*(acetylcholine) = 500 μmol L^{-1} , *v*(flow) = = 0.2 mL min^{-1} (A, B, D), E_{det} = −1400 mV (A, C, D), *CS*: [0.1 mol L^{-1} phosphate buffer; 0.001 mol L^{-1} Na_2EDTA, pH = 8.0] (B–D).

To investigate the effect of the immobilized amount of AChE, it was found that 1 mL of AChE solution with activity 274.4 U mL^{-1} (for 50 mg of the filling SBA-15) is sufficient to reach a complete enzyme coverage during the preparation of AChE-SBA15 powder. Regarding to the optimal immobilized amount of ChOx, it was found in our previous paper [7] that 1 mL of ChOx solution with activity ≥ 13.8 U mL^{-1} (for 50 mg of the filling powder SBA-15) should be used to achieve maximum enzymatic immobilized capacity.

The effect of pH of CS [0.1 mol L^{-1} phosphate buffer, 0.001 mol L^{-1} Na_2EDTA] on the peak response of the biosensor with AChE–SBA15/ChOx–SBA15 reactors to 500 μmol L^{-1} ACh was investigated in the range pH 6.0 – 9.0. As shown in Fig. 1A, amperometric response reached its maximum at pH = 8.0, which was selected as optimal. The solution of Na2EDTA was added into the CS to avoid possible inhibition of ChOx by the heavy metal cations (e.g., Co^{2+}, Cu^{2+}, Hg^{2+}, Ag^{+}).

The effect of the detection potential (E_{det}) on the amperometric signal to 500 μmol L^{-1} ACh was studied in the wide range (from −200 mV to −1700 mV). It can be seen in Fig. 1B that the dependence I_p–E_{det} consists of two waves, which well correspond to the two two-electron steps of oxygen reduction (similar as with liquid mercury electrode). As expected, the highest current response was

Table 1
Analytical characteristics for the determination of acetylcholine with the developed flow amperometric biosensor based on the bienzymatic AChE–SBA15/ChOx–SBA15 reactors; E_{det} = −1400 mV, v(flow) = 0.2 mL min^{-1}, *CS*: [0.1 mol L^{-1} phosphate buffer; 0.001 mol L^{-1} Na_2EDTA, pH = 8.0].

V_{inj}/μL	Linear range/μmol L^{-1}	*LOD*/μmol L^{-1}	*LOQ*/μmol L^{-1}	*RSD* (n = 11)/% (c(acetylcholine) = 200 μmol L^{-1})
60	50–600	18.4	61.2	2.9
120	10–200	4.1	13.5	2.8

obtained at the highly negative potentials to carry out four-electron oxygen reduction. A value of −1400 mV was chosen as the optimal for maximum sensitivity of ACh determination.

Investigation of the influence of the flow rate (v_{flow}) on the biosensor response revealed that with the increase of v_{flow} in the range of 0.05–0.225 mL min^{-1}, the peak height increased (Fig. 1C). To provide the best compromise among of the analysis time, sensitivity, and the consumption of CS, the optimal v_{flow} value 0.2 mL min^{-1} was chosen.

The construction of the apparatus and automatization program enable to change the injection volume of ACh (V_{inj}). As shown in Fig. 1D, the current response increased with the increasing of V_{inj} to 120 μL and then it kept constant until 200 μL. However, the peak area (Q_p) is linear function of V_{inj} in the whole investigated range. It is recommended to use higher value of V_{inj} if higher sensitivity is required. Under the optimized conditions, the linear range, limit of detection (*LOD*) and limit of quantification (*LOQ*) for ACh were found (Table 1).

No decrease of the current response during 90 days was observed, indicating high stability of the developed biosensor. The same enzymatic reactors were successfully used for 500 measurements during 90 days.

4. Conclusions

The novel stable amperometric biosensor based on the separated bienzymatic (AChE–SBA15/ChOx–SBA15) and detection (working MF-AgSAE) parts has been successfully developed and tested for the determination of ACh in FIA for the first time. The proposed biosensor showed acceptable sensitivity, good repeatability, long-term stability, and reusability.

Acknowledgments

This work was financially supported by Grant Agency of the Czech Republic (Project 17-05387S) and it was carried out within the framework of Specific Charles University Research (SVV 260440).

References

[1] Hasselmo M.E.: The role of acetylcholine in learning and memory. *Curr. Opin. Neurobiol.* **16** (2006), 710–715.

[2] Lombardo S., Maskos U.: Role of the nicotinic acetylcholine receptor in Alzheimer's disease pathology and treatment. *Neuropharmacology* **96B** (2015,), 255–262.
[3] Bolat E.O., Tig G.A., Pekyardimci S.: Fabrication of an amperometric acetylcholine esterase-choline oxidase biosensor based on MWCNTs-Fe3O4NPs-CS nanocomposite for determination of acetylcholine. *J. Electroanal. Chem.* **785** (2017), 241–248.
[4] Chauhan N., Pundir C.S.: Amperometric determination of acetylcholine – A neurotransmitter, by chitosan/gold-coated ferric oxide nanoparticles modified gold electrode. *Biosens. Bioelectron.* **61** (2014), 1–8.
[5] Josypčuk B., Barek J., Josypčuk O.: Preparation and properties of reference electrodes based on silver paste amalgam. *Electroanalysis* **23** (2011), 2226–2231.
[6] Josypčuk O., Barek J., Josypčuk B.: Electrochemical biosensors based on enzymatic reactors filled by various types of silica and amalgam powders for measurements in flow systems. *Electroanalysis* **28** (2016), 3028–3038.
[7] Tvorynska S., Barek J., Josypčuk B.: Amperometric biosensor based on enzymatic reactor for choline determination in flow systems. *Electroanalysis* **31** (2019), DOI:10.1002/-elan.201900237.

Effect of different types of divalent metal ions on *Lactobacillus paracasei* electrophoretic determination

Anna Król[a, b, *], Paweł Pomastowski[b], Viorica Railean-Plugaru[a, b], Bogusław Buszewski[a, b], Małgorzata Szultka-Młyńska[a]

[a] *Department of Environmental Chemistry and Bioanalytics, Faculty of Chemistry, Nicolaus Copernicus University, Gagarina 7, 87-100 Toruń, Poland* ✉ *annkrol18@gmail.com*
[b] *Interdisciplinary Centre of Modern Technology, Nicolaus Copernicus University, Wileńska 4, 87-100 Toruń, Poland*

Keywords
adhesion
aggregation
divalent ions
capillary electrophoresis
probiotic strains

Abstract
Nowadays, the use of capillary electrophoresis for the analysis, identification, and characterization of different types of microorganisms has received much attention. Adhesion to the capillary surface and uncontrolled aggregation of bacterial cells is a significant drawback of this approach. In our study, the influence of the probiotic strain (*Lactobacillus paracasei*) surface modification by different types of divalent metal ions (Cu^{2+}, Mg^{2+}, and Zn^{2+}) at 10 mM concentration was tested. Capillary electrophoresis analysis were performed in a pseudo-isotachophoretic mode using TBH (inlet) and TB (outlet) buffer at pH = 7.3 and 8.0, respectively. In addition, the fluorescence microscopy approach were chosen to point out if capillary electrophoresis cause any changes in the microbial cells (e.g., death or damage of bacteria). Therefore, this comprehensive study may be very helpful as a potential method for evaluating the aggregation activity of different types of metal ions against microbial cells.

1. Introduction

Nowadays, the use of capillary electrophoresis (CE) for the analysis, identification, and characterization of different types of microorganisms has received much attention. Capillary electrophoresis has been found to provide many advantages such as high separation efficiency and short analysis time [1]. There is a few examples of the CE use for the determination of bacterial pathogens, yeast cells or viruses. Unfortunately, this analytical method has limitations such as uncontrolled aggregation of bacterial cells and their adhesion to the capillary surface [2]. Microorganisms are often consider as a biocolloids, mainly due to the complex structure of their cell wall, and the understanding of the electrophoretic process is more complicated for such a particles. The cell wall composition is characteristic

for various types of bacterial species – they have different content of proteins, phospholipids, polysaccharides or another organic components [3]. All compounds present in the bacterial cell wall structure strongly affects the surface charge of microorganisms. It can be explained by the presence of many functional groups undergoing the protonation process [3, 4]. Therefore, understanding of the aggregation processes and the influence of different ions on microbial surfaces, as well as their potential use for further modifications, is pivotal for analytical chemistry. In the consequence, the main goal of this work was to determine the electrophoretic behaviour of *Lactobacillus paracasei* modified with different types of divalent metal ions at 10 mM concentration during CE analysis and to examine the possible mechanism of the bacterial cells aggregation. The electrophoretic determination of probiotic strain has been supplemented by application spectrometric in infrared range measurements (FT-IR) which will allow indicating that the main groups involved in the bacterial cells aggregation process. Additionally, the fluorescence microscopy approach was used to underlined the potential changes in microbial cells direct after CE. Then, such a comprehensive study may be a potential method for evaluating the aggregation activity of different types of bivalent metal ions against microbial cells.

2. Experimental

2.1 Reagents and chemicals

All solvents and materials were purchased from Avantor Gliwice (Poland). Ultrapure water was obtained from Milli-Q RG system by Millipore (Millipore Intertech, USA). Lactobacillus paracasei used in this study, was isolated from whey and cultured in M19 medium (Oxoid).

2.2 Instrumentation

2.2.1 Sample preparation for CE analysis

The required number of cells in 1 mL of the suspension was achieved by the serial dilution. The bacterial pellet were then suspended in the solution of cooper, magnesium, calcium or zinc nitrate at the 10 mM concentration and incubated for 1 hour at the room temperature. After the incubation, the suspension was centrifuged (20 °C, 9000 rpm, 15 min) and the obtained precipitate was washed twice with distilled water and transferred to the outlet TB buffer (Tris and boric acid; pH = 8.0). As a control, unmodified *Lactobacillus paracasei* cells were used.

2.2.2 Capillary electrophoresis analysis

Capillary electrophoresis analysis were performed using PA 800 plus (Beckman Coutner system, USA) equipped with a DAD with the use of fused silica capillary

(i.d. = 75 μm; L_{tot} = 33.5 cm; L_{eff} = 25 cm; Composite Metal Services, UK). The bacterial samples were injected into the capillary with a pressure mode (5 psi, 8 s) and the analysis were performed at a constant voltage (20 kV) and the temperature at 23 °C. As the inlet buffer, TBH (Tris, boric acid and hydrochloric acid; pH = 7.3) were choose.

2.2.3 Fluorescence microscopy

Determination of Lactobacillus paracasei cells viability after the CE analysis was performed by using fluorescence microscopy approach according to the [5]. During the CE analysis, fractions of bacterial cells not and modified with metal ions were collected. Obtained bacterial samples were then stained and analyzed using a Zeiss Axiocom D1 (Germany) fluorescence microscope with the set of filters (43 He and 38). Recorded images were analyzed with Axio Vision 4.8. software.

2.2.4 Fourier transform infrared spectroscopy analysis

The determination of active functional groups present on the *Lactobacillus paracasei* surface before and after Me^{2+} modification were performed using FT-IR method (Direct Detect spectrophotometer, Merck Millipore, Germany). All IR spectra were recorded at room temperature in the range of 1350–1850 cm^{-1}.

3. Results and discussion

In this study, Gram(+) *Lactobacillus paracasei* modified with the different types of metal divalent ions (Cu^{2+}, Mg^{2+}, and Zn^{2+}) were examined in an applied voltage of 20 kV. Bacterial strain without any surface modification was tested as a control sample (Fig. 1). Application of electrophoretic buffers with different ionic strength (TB and TBH) resulted in the formation of bacterial aggregates with different size and surface charge in unmodified *Lactobacillus paracasei* (Fig. 1). The use of $Cu(NO_3)_2$ at 10 mM concentration as a surface modification allowed focusing the zone of probiotic strain at the electromigration time of 2.6146 min (*RSD* = 4.67%) (Fig. 2A) . Similar results were obtained by using Mg^{2+} at the same concentration; the electromigration time of bacteria zone was determine as a 3.0275 min (*RSD* = 0.218 %) (Fig. 2B). Pomastowski et al. [6] have observed the peak of *Lactococcus lactis* ATCC 11454 at migration time of about 2 minutes. In case of zinc modification, the increasing number of signals in the electropherograms were observed (Fig. 2C). It is in a good correlation with the results presented in the work of Król et. al [7] which have shown that modification of another probiotic strain (*Lactococcus lactis*) by Zn^{2+} caused their agglomeration. All electrophoretic analysis were reproducible because of the similar migration times (Fig. 3).

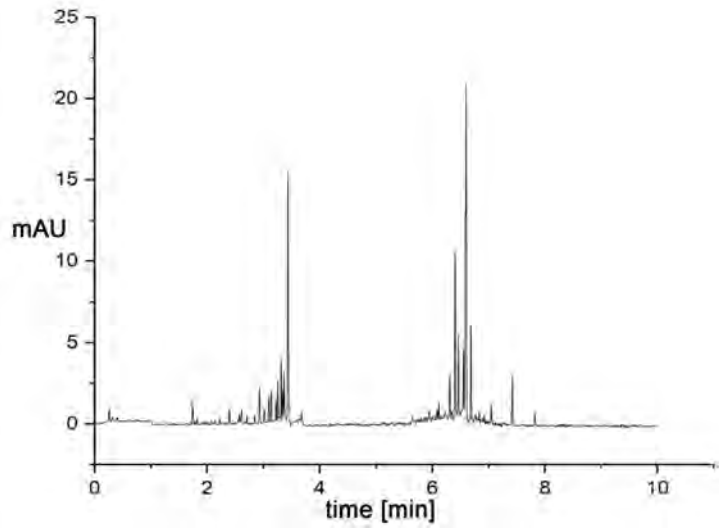

Fig. 1 Electropherogram of non-modified *Lactobacillus paracasei*. Conditions: inlet buffer: TBH (pH = 7.3), outlet buffer: TB (pH = 8.0), suspensive buffer: TB (pH = 8.0); I = 100 μA, U = 20 kV, t = 23 °C, λ = 214 nm, L = 33.5 cm, L_{eff} = 25 cm, φ = 100 μm, injection: 5 psi, t = 8 s.

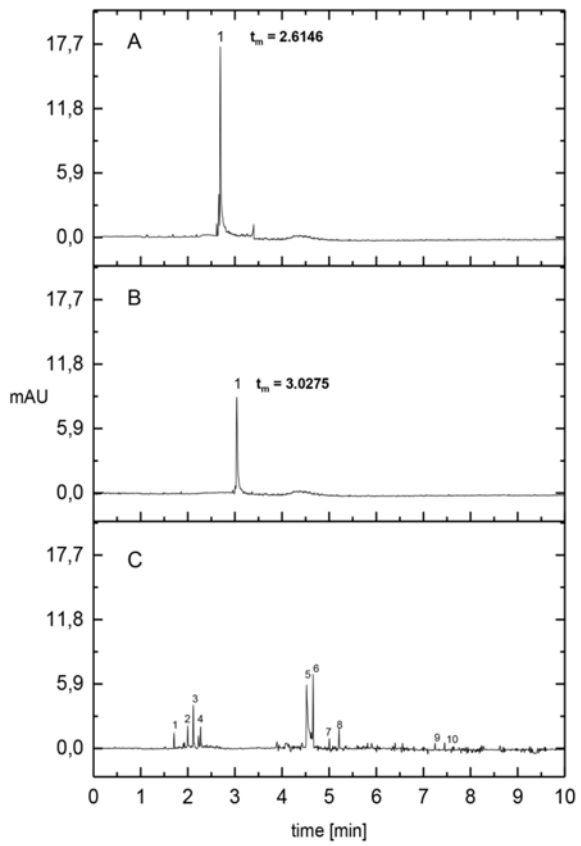

Fig. 2 Electropherogram modified *Lactobacillus paracasei* by (A) 10 mM $Cu(NO_3)_2$, (B) 10 mM $Mg(NO_3)_2$, and (C) 10 mM $Zn(NO_3)_2$. Conditions: inlet buffer: TBH (pH = 7.3), outlet buffer: TB (pH = 8.0), suspensive buffer: TB (pH = 8.0); I = 100 μA, U = 20 kV, t = 23 °C, λ = 214 nm, L = 33.5 cm, L_{eff} = 25 cm, φ = 100 μm, injection: 5 psi, t = 8 s.

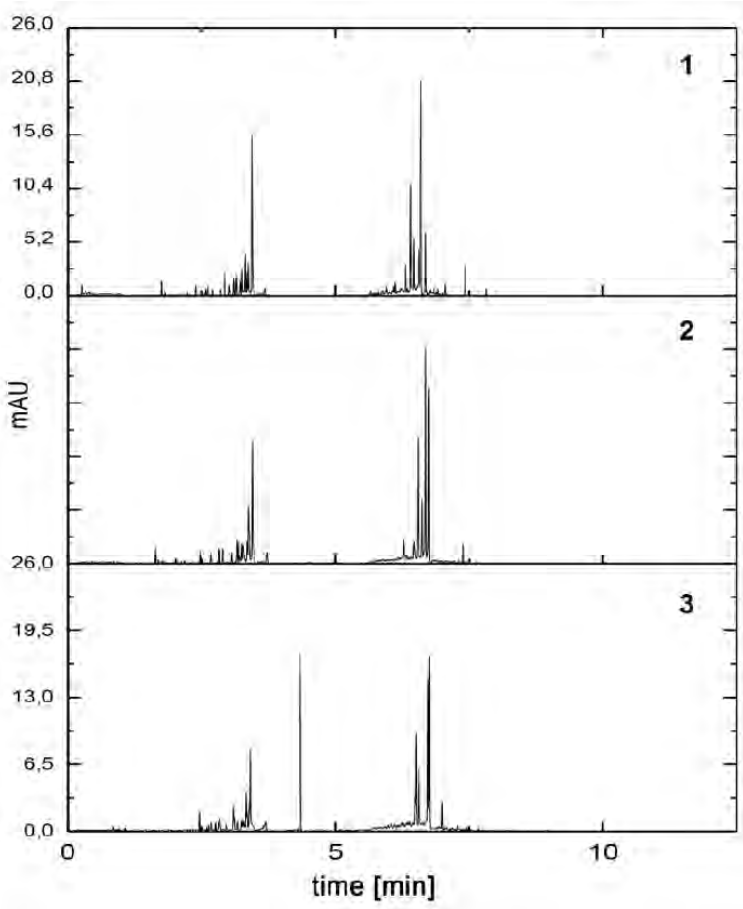

Fig. 3 The reproducibility of electroforetic determination of nonmodified *Lactobacillus paracasei*: (1)–(3) are number for subsequent measurements.

Figure 4 shows the FT-IR spectra of *Lactobacillus paracasei* unmodified and modified by Me^{2+} ions. The biggest changes are observed for the spectra of probiotic strain modified with Cu^{2+}. The main group involved in this process is characteristic band appears at 1440 cm^{-1} which may derives from the stretching vibration of C–N and N–H bond from surface microbial proteins [8]. Moreover, there is also band at 1650–1680 cm^{-1} corresponds with amide groups of bacterial proteins as well as the signal at 1720 cm^{-1} related with the stretching vibration of carbonyl groups (C=O) [8]. The intensity of this bands are lower in comparison with unmodified bacterial cells (Fig. 3). In the case of *Lactobacillus paracasei* surface modification by another divalent metals, practically no changes were observed for Mg^{2+}. Modification by zinc ions resulted in the appearing of spectral bands at 1530–1560 cm^{-1} which can derive from both aminoacids of bacterial proteins and peptidoglycan of their cell wall [8]. Among the common use of

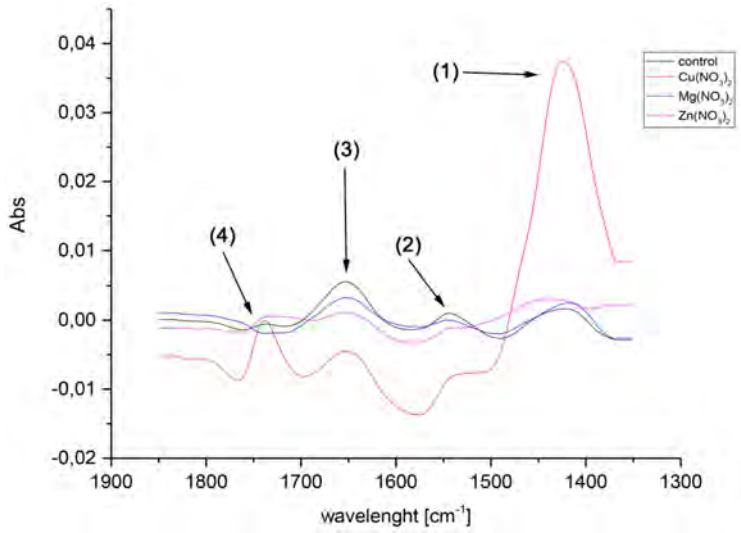

Fig. 4 FT-IR spectra for non-modified and modified *Lactobacillus paracasei*: (1) 1420–1480 cm^{-1}, (2) 1530–1560 cm^{-1}, (3) 1650–1680 cm^{-1}, (4) 1720–1750 cm^{-1}.

capillary electrophoresis in the identification of pathogens, yeast cells and various types of viruses [2], a CE approach has also been applied for the direct detect of the cell viability determination. As it is known from the work of Szumski et al. [9], the bigger peptidoglycan layer of Gram(+) (*Staphylococcus aureus*) cell wall make them more tough and resistant to capillary electrophoresis conditions. Data received Buszewski et al. [10] have shown that capillary electrophoresis do not cause the death of probiotic microbial cells but only their damage; in the fluorescence microscopy assay the amount of total cells before CE were compared to the control after the CE analysis. The results of their fluorescent microscopy analysis indicated that capillary electrophoresis do not cause the death of microbial cells but only their damage.

4. Conclusions

Capillary zone electrophoresis allows for the determination of a variety of biological systems such as bacteria, yeast and fungi. However, the complexity of the microorganism surface morphology forced us to carry out a series of research on the physicochemical properties in order to interpret the phenomena occurring at the interface of (bio)colloids. In this work, CE was used to evaluate the effect of different types of divalent metal ions at 10 mM concentration level on the *Lactobacillus paracasei* cells aggregation. This study confirms the occurrence the formation of bacterial cells agglomerates before the specific surface modification. The application of divalent ions such as cooper and magnesium allowed focusing the zone of probiotic strain. According to the FT-IR data, the main groups involved

in those process are carboxyl and amid groups which may derive from surface bacterial proteins. The described work might shed new light on several important issues, including an interpretation of probiotic bacteria aggregation process and understanding the influence of divalent metal ions on microorganisms surfaces and their potential use for further modifications, which seems to be crucial for separation science field.

Acknowledgments

This work was supported by the Opus 11 No. 2016/21/B/ST4/02130 (2017–2020) from the National Science Centre, Poland

References

[1] Desai M.J., Armstrong D.W.: Separation, identification, and characterization of microorganisms by capillary electrophoresis. *Microbiol. Mol. Biol. Rev.* **67** (2003), 38–51.
[2] Dziubakiewicz E., Buszewski B.: Capillary electrophoresis of microbial aggregates. *Electrophoresis* **35** (2014), 1160–1164.
[3] Salton M.R.J.: Studies of the bacterial cell wall: IV. The composition of the cell walls of some gram-positive and gram-negative bacteria. *Biochim. Biophys. Acta* **10** (1953), 512–523.
[4] Buszewski B., Szumski M., Kłodzińska E., Dahm H.: Separation of bacteria by capillary electrophoresis. *J. Sep. Sci.* **26** (2003), 1045–1049.
[5] Railean-Plugaru V., Pomastowski P., Rafinska K., Wypij M., Kupczyk W., Dahm H., Buszewski B.: Antimicrobial properties of biosynthesized silver nanoparticles studied by flow cytometry and related techniques. *Electrophoresis* **37** (2016), 752–761.
[6] Pomastowski P., Szultka-Młyńska M., Kupczyk W., Jackowski M., Buszewski B.: Evaluation of intact cell Matrix-Assisted Laser Desorption/Ionization Time of- Flight Mass Spectrometry for Capillary Electrophoresis detection of controlled bacterial clumping. *J. Anal. Bioanal. Tech.* **S13** (2015) 008. DOI: 10.4172/2155-9872.S13-008.
[7] Król A., Railean-Plugaru V., Pomastowski P., Złoch M., Buszewski B.: Mechanism study of intracellular zinc oxide nanocomposites formation. *Colloids Surf. A* **553** (2018) 349–358.
[8] Naumann D., Keller S., Helm D., Schultz C., Schrader B.: FT-IR spectroscopy and FT-Raman spectroscopy are powerful analytical tools for the non-invasive characterization of intact microbial cells. *J. Mol. Struct.* **347** (1995), 399–405.
[9] Szumski M., Kłodzińska E., Dziubakiewicz E., Hrynkiewicz K., Buszewski B.: Effect of applied voltage on viability of bacteria during separation under electrophoretic conditions. *J. Liq. Chromatogr. Relat. Technol.* **34** (2011), 2689–2698.
[10] Buszewski B., Król A., Pomastowski P., Railean-Plugaru V., Szultka-Młyńska M.: Electrophoretic fetermination of *Lactococcus lactis* modified by zinc ions. *Chromatographia* **82** (2019), 347–355.

Complementary approach on bacteria and antibiotics investigation

Katarzyna Pauter[a,*], Małgorzata Szultka-Młyńska[a], Paweł Pomastowski[b], Michał Złoch[b], Bogusław Buszewski[a, b]

[a] *Department of Environmental Chemistry and Bioanalytics, Faculty of Chemistry, Nicolaus Copernicus University, Gagarina 7, 87-100 Toruń, Poland* ✉ *kpauter@wp.pl*
[b] *Interdisciplinary Centre of Modern Technology, Nicolaus Copernicus University, Wileńska 4, 87-100 Toruń, Poland*

Keywords
antibiotics
biofilm
capillary electrophoresis
MALDI-TOF MS
saliva

Abstract
Intensive antibacterial treatment may lead to the development of antibiotic resistance. Therefore, it is necessary to develop new, more effective methods for the determination of both bacteria and drugs in biological materials. The aim of the study was to identify bacteria isolated from saliva by MALDI-TOF MS and optimize the electrophoretic separation of antibiotics. MALDI-TOF MS technology is a good tool for the identification of clinical bacteria strains, providing reliable results in a shorter time than other methods. Due to its low cost of use, small sample size and short analysis time, capillary electrophoresis can be an alternative to chromatographic techniques for antibiotic determination. The complexity of the structure of the biofilm and its high antibiotic resistance may cause difficulties in the treatment of biofilm-related infections. Saliva may be an alternative to biological matrices commonly used in diagnostic laboratories (urine, blood, faeces).

1. Introduction

The toothless oral cavity of infants is colonized by the so-called pioneering species, such as *Streptococcus salivarius*, *Streptococcus mitis*, *Streptococcus oralis*. Over the past years, the microflora of the oral cavity of the human body becomes more and more diverse; the new Gram-negative bacteria of the genus *Veillonella* or *Neisseria* have been appeared. Moreover, oral microflora is colonized by new species of bacteria such as *Streptococcus sanguinis*, *Streptococcus sorbinus*, *Streotococcus mutans* (caries), *Porphyromonas gingivalis* (paradontosis) and *Eneterococccus faecalis* (endodontic infections) [1]. The pathogenic bacteria present in saliva have the ability to adhere to hard dental tissues and to cause oral diseases as well. The use of saliva as a diagnostic material is not limited to recognize oral diseases. Saliva can also be used to diagnose infectious, endocrine and cardiac diseases, as well as to determine the presence and level of drugs [2].

A promising approach that can be widely used in clinical laboratories as a diagnostic potential is the identification of microorganisms using mass spectrometry. MALDI-TOF MS techniques allows for identification of pathogenic bacteria due to the significant automation and a very wide database that allows for a significant reduction in the time of microbiological diagnostics. This technique, based on the protein profile of the examined microorganisms, being a specific and unique for the species "molecular fingerprint" [3].

Modern medicine is associated with many therapeutic possibilities, but also with a great risk of developing infections. Unfortunately, intensive antibacterial treatment may result in bacterial resistance to antibiotics. Therefore, it is necessary to develop new, more effective and sensitive methods for the determination of drugs in biological materials. Apart from chromatographic techniques, the capillary electrophoresis (CE) is an increasingly popular method of choice among many methods used in the analysis of drugs. Optimization of electrophoretic mobility conditions allows determining a number of antibacterial drugs in biological fluids [4].

An important role in the emergence of bacterial infections is also played by the ability of bacteria to create a biofilm (a complex structure of microbial cells surrounded by a layer of metabolic products). The most common strains forming the biofilm include *Enterococcus faecalis*, *Staphylococcus aureus*, *Staphylococcus epidermidis*, *Escherichia coli* and *Pseudomonas aeruginosa*. Biofilm formation is a complex and multi-stage process. The initiation stage is the process of adhesion of single cells to the surface of biomaterials, foreign bodies and tissues. Microorganisms growing in the biofilm population are much less sensitive to antibiotics than their primary forms. The therapeutic problems resulting from the development of biofilm-related infections are the reason to the search and development of new methods for elimination and prevention of such infections [5].

The purpose of this research was to use the MALDI-TOF method to identify different strains of bacteria isolated from saliva of patients using antibiotic therapy. Moreover, the influence of antibiotics on molecular profile changes of selected bacterial strains was performed. Additionally, the optimization of electrophoretic mobility of selected antibiotics (selection of appropriate analysis parameters) has been investigated.

2. Experimental

2.1 Collection and isolation of pure bacterial colonies

The saliva was collected from patients group into sterilized falcon tubes. In the control group (14 patients), two people smoked cigarettes. Infected patients (9 patients) took antibiotics such as amoxicillin, clindamycin, ciprofloxacin and metronidazole.

All reagents to bacteria isolation and identification were delivered by the Sigma Aldrich (Germany).

The serial dilutions of the samples were prepared in peptone water solution. Bacteria were isolated by spreading the diluted samples (100 µl) in petri dishes containing three different culture media: Brain Heart Infusion Agar, Vancomycine Resistante Enterococci Agar Base and Azide Blood Agar. All plates were incubated at 37 °C for 24 hours. Then, the bacterial colonies were purified by reducing method.

2.2 Bacteria identification

Bacterial isolates obtained were identified by MALDI Ultraflextreme II technique (Bruker, Bremen, Germany). The identification process was performed according to Bruker sample preparation protocols. The procedure was preceded by the pre-extraction of proteins using ethanol and formic acid. After centrifugation, 1 µl of bacterial supernatant was transferred to the MALDI target, dried in air and a solution of the matrix (α-cyano-4-hydroxycinnamic acid) was applied. Mass spectra were analyzed using the MALDI BioTyper database (Bruker, Daltonik) in the molecular weight range. The following criteria for the identification of isolates were applied depending on the score value obtained: 2.300–3.000 for highly probable species identification: 2.000–2.299 for probable species identification; 1.700–1.999 for probable genus identification; 0.000–1.699 for unreliable identification.

2.3. Antibiotic determination

Antibiotics: amoxicillin, cefotaxime, clindamycin, ciprofloxacin, linezolid and metronidazole were provided from Sigma Aldrich (Schnelldorf, Germany). All solvents were obtained from Avantor Gliwice (Poland). The research was carried out on an HP3D CE system (Agilent Technologies, Waldbronn, Germany), equipped with a diode array detector (DAD) and an Agilent ChemStation software. A fused-silica capillary (L_{tot} = 64.5 cm, L_{eff} = 56 cm, i.d. = 50 µm) was used. The analytical wavelength of individual antibiotics was determined on the basis of their spectrophotometric spectra. Several factors (composition, concentration and pH of background electrolyte, injection time, voltage, temperature, electrophoretic migration and influence of organic modifier) were taken into account when working out the electrophoretic separation parameters.

3. Results and discussion

In the present study, 81 bacterial strains were isolated. 37 of them were identified as belonging to the species and 38 to the genus, while the remaining strains were unidentified. The obtained mass spectra (Fig. 1) reflect protein profiles are specific for the identified bacterial species in the control and studied groups, respectively. The predominant bacterial species included *Streptococcus salivarius*,

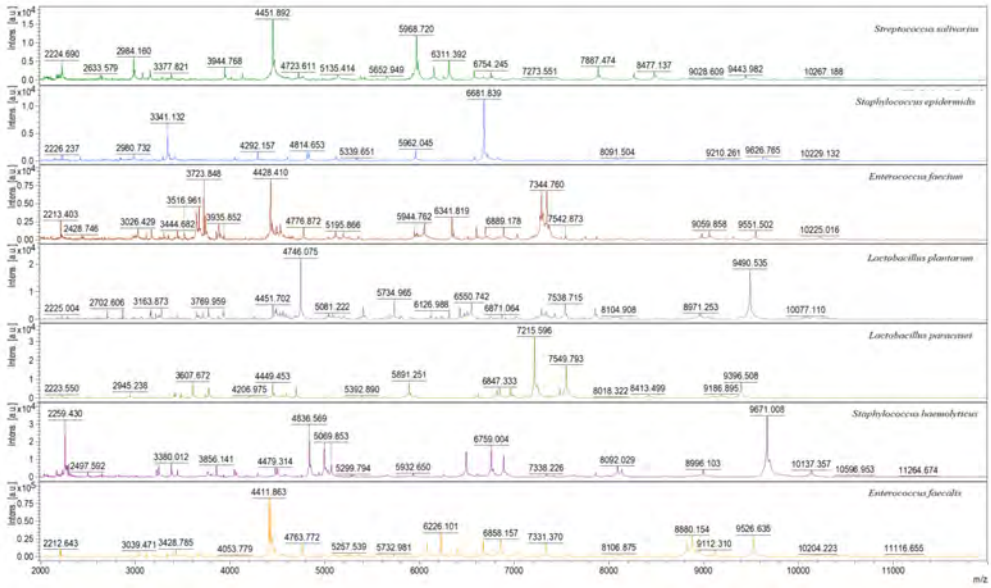

Fig. 1 MALDI-TOF MS profiles of studied bacteria isolates.

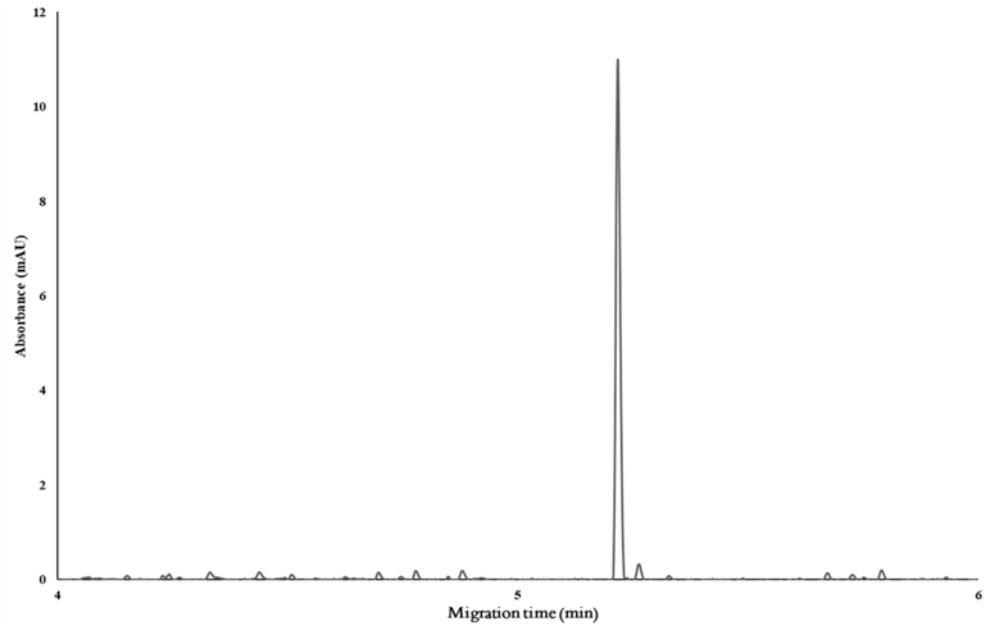

Fig. 2 Electropherogram obtained from the analysis of linezolid. Experimental conditions: fused silica capillary (L_{tot}= 64.5 cm, L_{eff} = 56 cm, i.d. = 50 μm,), running electrolyte 10 mM ammonium acetate (pH = 3.0), separation field 25 kV, t = 25 °C, λ = 254 nm.

Streptococcus mitis and *Streptococcus oralis*. Comparing with the control samples has been noticed that *Enterococcus genus* bacteria and *Candida glabrata* were found only in case of patients treated with antibiotics.

Moreover, using capillary electrophoresis have been investigated different parameters, that can influence the antibiotics mobility, such as: composition, concentration, pH of background electrolyte and injection time, voltage, temperature, influence of organic modifier. Furthermore, various properties of different antibiotic groups were accommodated. All analysed parameters affected the performance, repeatability, selectivity and precision of the determinations to varying degrees. The applied parameters of electrophoretic analysis made it possible to separate antibiotics from different chemical groups (Fig. 2).

4. Conclusions

Time to identify the causative factor plays a key role in the treatment process. In this context, new methods for rapid microbiological diagnosis are being sought. Such methods include, among others, MALDI-TOF MS, which may significantly reduce the time of identification of pathogens. MALDI-TOF MS technology is a good tool for the identification of clinically derived bacteria, ensuring reliable results in less time than molecular methods. Due to its low cost of use, small sample size and short analysis time, capillary electrophoresis may be an alternative method to chromatographic techniques for the determination of antibiotics. The complexity of the biofilm structure and its high resistance to antibiotics may cause difficulties in the treatment of biofilm-related infections. Saliva may be an interesting alternative to the biological matrices commonly used in diagnostic laboratories such as urine, blood or faeces.

Acknowledgments

This work was supported by research project Opus 11 No. 2016/21/B/ST4/02130 (2017-2020) from the National Science Centre, Kraków, Poland.

References

[1] Paster B.J., Stokes L.N., Olsen I., Dewhirst F.E., Aas J.A.: Defining the normal bacterial flora of the oral cavity. *J. Clin. Microbiol.* **43** (2005), 5721–5732.

[2] Pfaffe T., Cooper-White J., Beyerlein P., Kostner K.: Diagnostic potential of saliva: Current state and future applications. *Clin. Chem.* **57** (2011), 675–687.

[3] Buszewski B., Rogowska A., Pomastowski P., Złoch M., Railean-Plugaru V.: Identification of microorganisms by modern analytical techniques. *J. AOAC Int.* **100** (2017), 1607–1623.

[4] Greño M., Castro-Puyana M., García M.Á., Marina M.L.: Analysis of antibiotics by CE and CEC and their use as chiral selectors: An update. *Electrophoresis* **39** (2018) 235–259 .

[5] Caputo P., Di Martino M.C., Perfetto B., Iovino F., Donnarumma G.: Use of MALDI-TOF MS to discriminate between biofilm-producer and non producer strains of *Staphylococcus epidermidis*. *Int. J. Environ. Res. Public Health* **15** (2018), 1695.

Novel probe fabrication method for simultaneous scanning electrochemical microscopy and scanning ion conductance microscopy measurements

Stefan Wert*, Timo Raith, Frank-Michael Matysik

Institute of Analytical Chemistry, Faculty of Chemistry and Pharmacy, University of Regensburg, Universitätsstraße 31, 93053, Regensburg, Germany ✉ *stefan.wert@chemie.uni-regensburg.de*

Keywords
electroanalytical chemistry
probe fabrication
scanning electrochemical microscopy
scanning ion conductance microscopy

Abstract
Scanning electrochemical microscopy (SECM) has proven to be a powerful method for the investigation of electrochemical properties of surfaces, whereas scanning ion conductance microscopy (SICM) can be utilized for acquiring information about the sample topography. The hyphenation of these two techniques can be realized by using a micropipette with an integrated ring ultramicroelectrode (UME) as probe. Therefore, a novel and cost-efficient approach for the fabrication of a ring UME pipette probe is presented. The fabrication of probes was realized by isolating platinum-coated, pulled glass capillaries with a photoresist. Multiple layers had to be applied for obtaining functional UMEs. The coating process was investigated by optical microscopy imaging and cyclic voltammetry. To test the applicability of probes, the electrochemical behavior and the topography of the contact pads an electrochemical sensor, serving as a model substrate, was investigated by means of combined SECM and SICM. Electrochemical experiments were carried out with ferrocenemethanol (1.5 mM) as redox mediator and potassium nitrate (0.2 M) as supporting electrolyte.

1. Introduction

Scanning electrochemical microscopy (SECM) is a powerful technique for the investigation of electrochemical and topographical properties of surfaces. [1]. It belongs to the family of scanning probe techniques and features small electrodes as probes with diameters of 25 µm or less, which are termed ultramicroelectrodes (UMEs). Measurements are usually performed in a solution containing a reversible redox-active species, the so-called redox mediator. In the amperometric mode of SECM, a potential is applied at the UME, leading to the conversion of the mediator associated with a faradaic current that can be recorded. As the probe is

scanned over the surface of a substrate in close proximity, the current changes with respect to the surface properties. However, if the substrate of interest exhibits inhomogeneous topography and conductivity, distinguishing both kinds of information becomes challenging. In addition, maintaining a constant probe-to-substrate distance is difficult to achieve above surfaces with such properties. To overcome these issues, SECM can be coupled with other techniques such as atomic force microscopy [2, 3]. In this method, however, contact between the probe and the sample is established, which can damage fragile substrates and the probe itself. As a non-contact technique for acquiring topographical information and probe distance control, scanning ion conductance microscopy (SICM) [4] can be utilized. For this technique, a small micropipette is employed as probe. As it is filled with supporting electrolyte and has a Ag/AgCl electrode placed within the interior of the pipette, a potential can be applied between the inner electrode and another Ag/AgCl electrode located in the bulk solution. This results in an ionic current flowing between the pipette interior and the surrounding solution. Moving the pipette close to the surface leads to a hindered migration at the pipette orifice, increasing the resistance and yielding a lower current.

Performing SECM and SICM measurements simultaneously enables distinguishable acquisition of topographical and electrochemical information of surfaces. For the hyphenation of both techniques, probes with both an integrated UME for SECM and a micropipette for SICM are required. Established techniques [5, 6] for the preparation of such probes often require high-priced equipment such as pipette pullers, physical vapour deposition and focused ion beam systems. In this work, a novel and cost-efficient approach for the preparation of ring UME pipette probes is presented, using commercially available, pulled fused silica capillaries with platinum coating and isolating them with photoresist.

2. Experimental

2.1 Reagents and chemicals

All experiments were carried out with ferrocenemethanol (c = 1.5 mM, FcMeOH, 99%, ABCR, Germany) as redox mediator. To prepare aqueous solutions, Milli-Q water (Milli-Q Advantage A10 system, Merck Millipore, Germany) was used. Potassium nitrate (c = 0.2 M, analytical grade, Merck KGaA, Germany) and KCl (c = 0.2 M, analytical grade, Merck KGaA, Germany) served as supporting electrolytes. A 10:1 mixture of SU8.5 photoresist (MicroChem Corp., USA) and ethanol (Merck Millipore, USA) was utilized as isolating material.

2.2 Instrumentation

Probes were fabricated by modifying platinum-coated emitters for electrospray ionization (New Objective, USA). Initially, the capillaries were pushed through

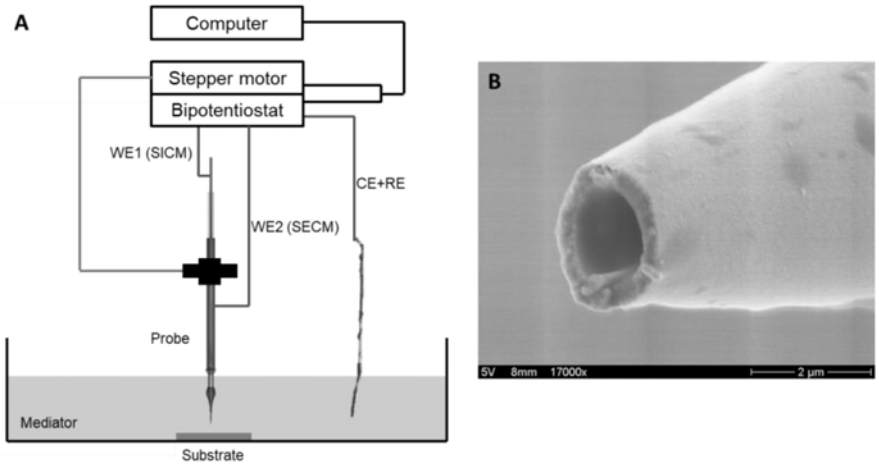

Fig. 1 (A) Schematic overview of the SECM/SICM experimental setup. Measurements were carried out in mediator solution containing FcMeOH. The position of the probe was controlled via a stepper motor and a piezoelectric element. The first working electrode channel (WE1) was connected to the Ag/AgCl wire placed inside the probe for SICM measurements and the second channel (WE2) was used for SECM by connecting it to the copper tubing. A Ag/AgCl wire placed in the bulk solution served both as counter and reference electrode (CE+RE). (B)SEM image of the probe tip.

copper tube (1.1 mm I.D., 2.0 mm OD, 3.0 cm length, Albion Alloys, UK) for establishing electrical contact to the platinum surface of the probes. Contact between copper and platinum was established using silver conductive paint (VS Electronic, Germany) and adhesive (UHU Max Repair Extreme, UHU GmbH & Co. KG, Germany). Afterwards, photoresist was applied under N_2 flow, cured by UV light (350 nm, 30 s) and heated in an oven at 95 °C for 5 min to evaporate the remaining solvent. The quality of the coating was investigated by CV and the coating process was repeated if the measured currents were too high. If larger probes are desired, an alternative way to expose a ring electrode surrounding the orifice was polishing the tips with diamond lapping sheets (0.1 micron, Precision Surfaces International, USA) while water was flushed through the pipette to prevent clogging. Eventually, probes were filled with supporting electrolyte and a Ag/AgCl wire was inserted. Figure 1B shows an image of a finished tip recorded with a scanning electron microscope (SEM).

Experiments with the fabricated probes were performed with a second Ag/AgCl wire placed in the bulk solution employed as both counter and reference electrode for SECM measurements (Fig. 1A). The mentioned potentials herein refer to this reference system.

Measurements were performed using a commercially available SECM 920C (CH Instruments, USA), with the first electrode channel being connected to the internal Ag/AgCl wire of the ring UME pipette for recording SICM current and the second channel connected to the copper tube for measuring SECM current.

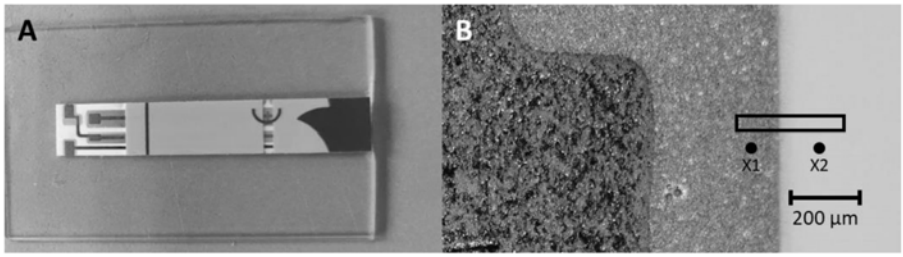

Fig. 2 (A) Image of the investigated screen-printed electrochemical sensor. (B) Micrograph of the electrode area. The black box indicates the area scanned by SECM/SICM. X1 and X2 indicate the spots where positive and negative feedback PACs were recorded, respectively.

The approach response of the fabricated probes was investigated by performing probe approach curves (PACs) over both gold and polymer of a screen-printed electrochemical sensor (Fig. 2, GlucoSmart® Swing, MSP bodmann GmbH, Germany) as conductive and non-conductive surfaces, respectively. A potential of 0.3 V (SECM) was applied and the probe was approached until the SECM current increased to 135% (conductor) or decreased to 85% (insulator) with respect to the current measured in bulk solution. In addition, a quiet time of 60 s was applied prior to approaching and the scan rate was set to 1.25 µm/s. For simultaneous SECM and SICM measurements, the contact pads of the same sensor served as a model substrate. Its roughness and the transition between conducting and isolating surface were investigated. Potentials of 0.3 (SECM) and 0.1 V (SICM) were applied, respectively. The scan rate of the probe was 40 µm/s.

3. Results and discussion

The coating of the fabricated ring UME pipette probes was investigated by means of CV. Figure 3 shows a CV recorded with a probe being coated six times according to the procedure described in the experimental section. The oxidation current measured corresponds well to ring UME theory [7] for a ring electrode with a diameter of 2 µm. This electrode size fits to the SEM image recorded of an insulated probe tip (Fig. 1B). The radius of the pipette aperture remains at 500 nm after the coating process.

Using polished probes, 4 successive PACs (Fig. 4) performed both above conducting and insulating area of the model substrate indicate good reproducibility of probe placement prior to the imaging process. Both positive and negative feedback responses are observable above conducting and insulating surfaces, respectively.

Images of the screen-printed model substrate were recorded to test the usability of the fabricated probes to perform simultaneous local topographical and conductivity studies. Figure 5 shows the SECM (A) and SICM (B) response at the edge of the conductive electrode area. The SECM image clearly shows a sharp

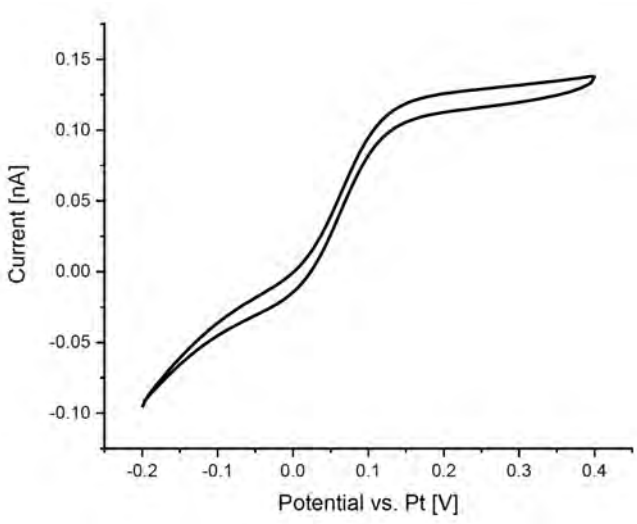

Fig. 3 Cyclic voltammogram of a probe coated 6 times with photoresist, recorded in 1.5 mM FcMeOH. Scan rate: 20 mV/s. Quiet time: 0 s. Sweep segments 5 and 6 are shown of 6 segments in total.

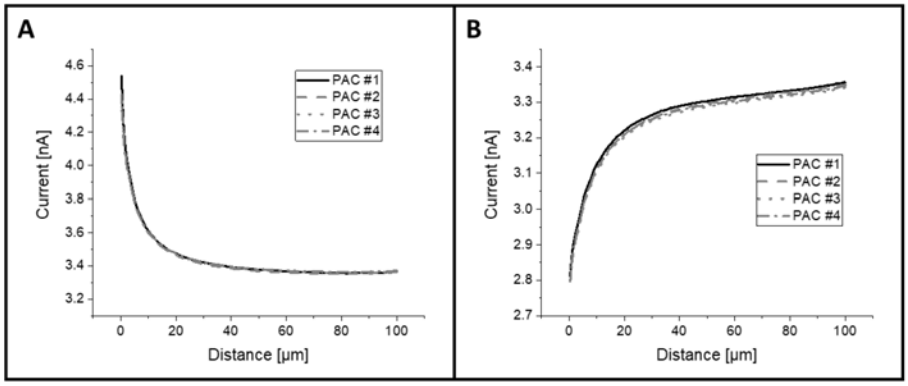

Fig. 4 Successive PACs in SECM mode above conducting (A) and insulating (B) surface. PACs were recorded using a probe with an OD of 25 µm. The probe approached until 135% (A) and 85% (B) of bulk current was reached. *E* (probe): 0.3 V. Scan rate: 1.25 µm/s. Quiet time: 20 s.

current transition from the conducting gold area in the left half of the image to the insulating polymer in the right half, as positive and negative feedback were measured on the left and right side, respectively. The SICM response indicates a significant roughness over the entire area of the sensor. In addition, an overall current increase from the conducting to the insulating area shows that the sensor is thicker at the electrode area, since the electrode material was printed onto the polymer carrier. Both observations could be confirmed by laser scanning micrographs.

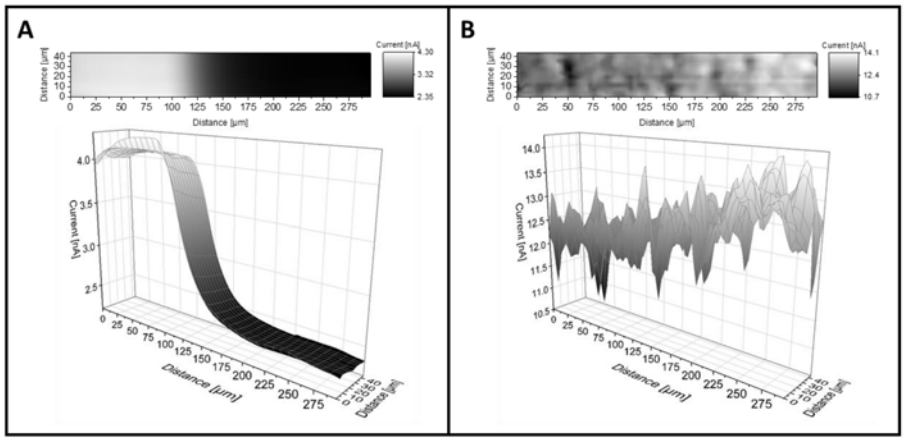

Fig. 5 Simultaneously recorded SECM (A) and SICM (B) images of the contact pads of the sensor shown in Fig. 3. At the top and the bottom, 2- and 3-dimensional plots of the measured currents are shown, respectively. *E*(SICM): 0.1 V. *E*(SECM): 0.3 V. Scan rate: 40 µm/s. *x* distance: 300 µm. *y* distance: 50 µm. Quiet time: 10 s.

4. Conclusions

A novel and cost-efficient probe fabrication method for simultaneous SECM and SICM imaging was developed and the functionality of the prepared ring UME pipettes was characterized by CV, PACs and simultaneous SECM-SICM imaging experiments. The ring UME pipette probes have proven to be suitable for obtaining topographical and conductivity information concurrently, making them suitable for the investigation of delicate substrates which require noncontact imaging.

References

[1] Bard A.J., Mirkin M.V.: *Scanning Electrochemical Microscopy.* 2nd ed. Boca Raton, CRC Press 2012.
[2] Macpherson J.V., Unwin P.R.: Combined scanning electrochemical-atomic force microscopy. *Anal. Chem.* **72** (2000), 276–285.
[3] Velmurugan J., Agrawal A., An S., Choudhary E., Szalai V.A.: Fabrication of scanning electrochemical microscopy-atomic force microscopy probes to image surface topography and reactivity at the nanoscale. *Anal. Chem.* **89** (2017), 2687– 2691.
[4] Hansma P.K., Drake B., Marti O., Gould S.A.C., Prater C.B.: The scanning ion-conductance microscope. *Science* **243** (1989), 641–643.
[5] Page A., Kang M., Armitstead A., Perry D., Unwin P.R.: Quantitative visualization of molecular delivery and uptake at living cells with self-referencing scanning ion conductance microscopy-scanning electrochemical microscopy. *Anal. Chem.* **89** (2017), 3021–3028.
[6] Takahashi Y., Shevchuk A.I., Novak P., Murakami Y., Shiku H., Korchev Y.E., Matsue T.: Simultaneous noncontact topography and electrochemical imaging by SECM/SICM featuring ion current feedback regulation. *J. Am. Chem. Soc.* **132** (2010), 10118–10126.
[7] Lee Y., Amemiya S., Bard A.J.: Scanning electrochemical microscopy. 41. Theory and characterization of ring electrodes. *Anal. Chem.* **73** (2001), 2261–2267.

Analysis of red lipstick traces: development of sampling procedure

Marta Gładysz*, Małgorzata Król, Adrianna Chudecka, Paweł Kościelniak

Department of Analytical Chemistry, Faculty of Chemistry, Jagiellonian University in Krakow, Gronostajowa St. 2, 30-387 Krakow, Poland ✉ *marta.gladysz@doctoral.uj.edu.pl*

Keywords
attenuated total reflectance spectroscopy (ATR)
GC-MS
lipsticks sampling
MEKC
red lipsticks traces

Abstract
The aim of this research was to develop the procedure of lipsticks sampling and to determine the area of lipstick trace, which is required to analysis. The results indicated that the 3 dots (i.d. 2 mm) cut out from paper (with smudged lipsticks) using a puncher were sufficient to achieve whole information about composition of investigated samples. Samples applied on shirt or glass were prepared using dry cotton swab and removing smudged lipstick from 0.5 cm^2 area. Moreover, the effect of the thickness of lipstick layer applied on surfaces was studied using three analytical techniques (ATR, GC-MS, MEKC) and three kinds of layer (thin, medium, thick). It was observed that the separation technique are less sensitive to changes in the thickness of the layer than the spectroscopic one.

1. Introduction

The number of objects than can be considered in the crime scene is large. In recent time, traces of cosmetics, especially traces of lipsticks, have been very popular. Despite such traces do not constitute unambiguous proof of crime, they can provide an investigative aid or corroborative evidence confirming the relationship of the suspect with the victim or crime scene. Hence, it is reasonable to develop new methods enabling comparative analysis of lipsticks located at a crime scene (as traces) with these found in the possession of a suspect.

The presented research is one of the stages aimed at developing a methodology for analyzing red lipsticks for forensic purpose. In the previous articles, authors developed three analytical methods: attenuated total reflectance spectroscopy (ATR) [1], gas chromatography coupled to mass spectrometry (GC-MS) [2] and micellar electrokientic capillary chromatography (MEKC) [3], allowing discrimination of red lipsticks. In most cases, lipsticks found at crime scene are applied on various surfaces, thus the main aim of this stage of research was to develop sampling procedure. Authors focused on: (i) determining the procedure and amount of sampling lipsticks found on different surfaces (absorbent, non-absorbent), (ii) examining the effect of the thickness of layer of lipstick (applied on the surfaces) on the information obtained about samples.

2. Experimental

2.1 Reagents and chemicals

The chemicals used throughout experiments: sodium tetraborate decahydrate, sodium dodecyl sulphate, acetonitrile, acetone, 2-propanol, methanol and sodium hydroxide were supplied by Sigma-Aldrich (Germany). Hydrochloric acid was purchased from POCH (Poland). Ultrapure water (18.2 MΩ cm, < 3ppb TOC) was produced in the laboratory with the Milli-Q system by Merck-Millipore (Germany).

Lipstick samples were purchased in local shops or donated by Inglot Sp. z o.o (Poland). Five red lipstick samples selected from all collection (43 items) were used in this research (L16 – Catrice 430, L28 – Inglot 176, L34 – Inglot 12, L36 – Manhattan 45N, L41 – Freedom 108).

2.2 Instrumentation

An ATR analyses were carried out using a Thermo Nicolet iS50 FTIR (Thermo Fisher Scientific, USA) with a Smart Orbit micro-ATR accessory. All spectra were collected from 650 to 4000 cm^{-1} with 4 cm^{-1} of resolution and using 20 number of scans. A GC-MS apparatus was constituted by a 6850 Series II gas chromatograph coupled to a 5975 MSD mass spectrometer (Agilent Technologies, USA). The detailed parameters of the GC-MS method can be found in [2]. A PA800 plus capillary electrophoresis system (Beckman-Coulter, USA) equipped with a diode array detector was also utilized. The detailed parameters of the MEKC method can be found in [3]. The UAE extraction was carried out using a Sonic 3 ultrasound bath (Polsonic, Poland) working at frequencies of 40 kHz.

2.3 Sample preparation

The sample was prepared prior to GC-MS and MEKC analysis in few steps. Firstly, the lipstick trace was taken from a surface. Depending on the type of surface on which the lipstick marks were applied, two kinds of sample preparation procedure were proposed. Samples smudged on the paper were cut out in the form of dots (i.d. 2 mm) using a Harris Micro Punch (Whatman, United Kingdom) whereas traces on the mirror or shirt were removed using a dry disposable cotton swab (Equimed, Poland). Then, the dots or swabs were transferred to a glass microtube and extraction process was performed. The optimal conditions of UAE extraction were different depending on the further analytical technique. In the case of GC-MS analysis, the extracts were obtained at 35 °C for 21 min., using 100 µL mixture of acetonitrile:methanol:acetone (50:30:20, *v/v/v*) as an extraction agent. In the next step, the obtained extracts were centrifuged (14 800 rpm, 5 min) by Microfuge 16 (Beckmann-Coulter, USA), the supernatants were

transferred to 1.5 mL vials and diluted 1:1 (*v/v*) with extracting agent prior to GC-MS analysis. The optimal extraction parameters for MEKC method were: 22 min – time, 45 °C – temperature of ultrasonic bath, 100 μL of extraction agent (background electrolyte: borate buffer at pH = 9.0 enriched with 80 mM sodium dodecyl sulphate(VI)). After the extraction, the extracts were centrifuged (14 800 rpm, 5 min), then the supernatants were transferred to a PCR tube and diluted with sample solution (100-fold water diluted optimal background electrolyte). Prior to MEKC analysis, the prepared samples were centrifuged again in order to remove air bubbles.

3. Results and discussion

3.1 Determination of the area of lipstick trace required to analysis

All measurements were performed using five lipsticks. They were chosen according to their various consistencies, which reflect in the traces left. Each lipstick was applied on surfaces (paper, shirt and glass) by gently spreading and then the appropriate areas of traces were used. In the case of paper: 1, 2, 3 and 5 dots (i.d. 2 mm) they were cut out using a puncher. Samples from shirt and glass were removed from approximately 0.5, 1.0, and 2.0 cm^2 area using a swab. Next, samples were prepared according to the description in Section 2.3 and analyzed using GC-MS and MEKC method. Due to the fact that ATR technique is non-destructive one, there was no need to determine the amount of lipsticks required to measurements. The required area of trace was limited by the diameter of crystal in ATR apparatus (i.d. 3.5 mm).

The obtained results, including comparison to pure lipsticks (prepared according to procedure described in [2] for GC-MS and in [3] for MEKC), are presented in Fig. 1 (GC-MS) and Fig. 2 (MEKC). As can be seen, the sample area required to analyses is the same for both methods. When the lipstick is applied on paper it is necessary to cut at least 3 dots to avoid losing any information about investigated samples. In the case of lipsticks smudged on shirt or glass, sample removed from 0.5 cm^2 area allows to achieve reliable results. The greater area of lipstick trace does not provide any additional information but only increases the consumption of sample – not recommended from the forensic point of view.

3.2 Examination of the effect of the thickness of lipstick layer applied on surfaces

It was also crucial to investigate how the thickness of the lipstick layer applied on the surface affects obtained information about samples and, in consequence, how it influences on the possibility of comparison of two lipsticks. Samples were prepared using three surfaces: paper, shirt, glass and five lipsticks. Each time three different layers were prepared: thin – transfer of the lipstick to the surface after earlier spreading on the glove; medium – gently spreading the lipstick on the

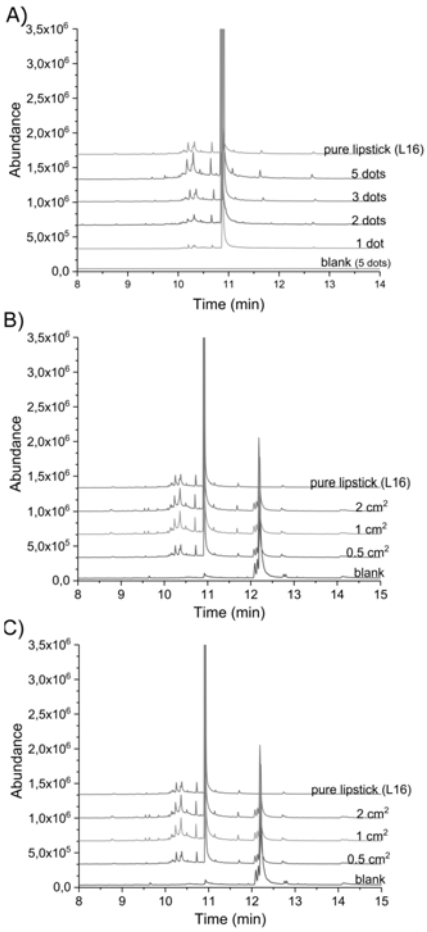

Fig. 1 Search for the trace area required to the GC-MS analysis of lipstick L41 applied on (A) paper: dots of i.d. 2 mm, (B) shirt :areas of lipstick removed from surface using swab, (C) glass: as in (B).

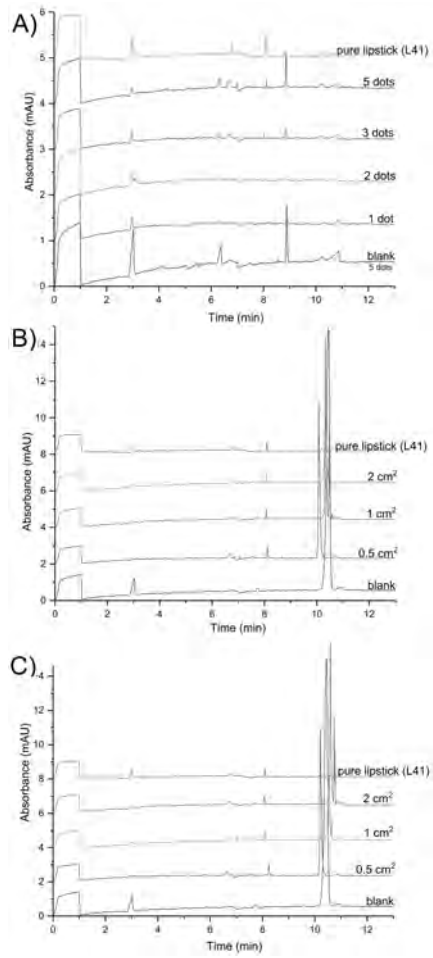

Fig. 2 Search for the trace area required to the MEKC analysis of lipstick L41 applied on (A) paper: dots of i.d. 2 mm, (B) shirt: areas of lipstick removed from surface using swab, (C) glass: as in (B).

surface; thick – spreading the lipstick on the surface twice in the same place. In the case of ATR analysis, five replicates were performed for each layer in order to minimize changes due to uneven spreading of the lipsticks. The relation (calculated as Person correlation coefficient, *CC*) between spectra registered for pure lipsticks and various layers of lipsticks applied on examined surfaces are presented in Fig. 3 (only three lipsticks). It was observed that the surface has a strong influence on registered spectrum. The thinner layer of lipstick, the smaller value of *CC* and thus the greater impact of the substrate. Hence, the comparison between two lipstick marks should be made with great caution. It was also noticed that non-absorbent surface (glass) causes the least interference.

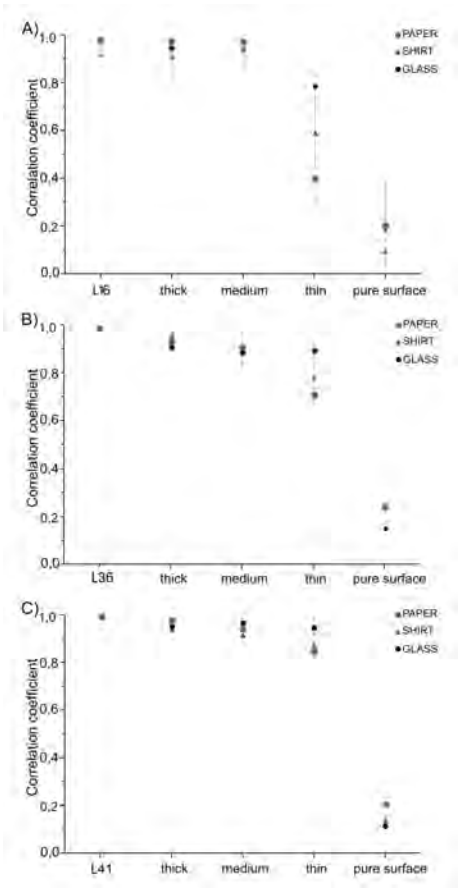

Fig. 3 The correlation coefficients between the ATR signals obtained for pure lipsticks (A) L16, (B) L36, and (C) L41) and of their layers of different thickness applied on the surfaces of paper, shirt, and glass.

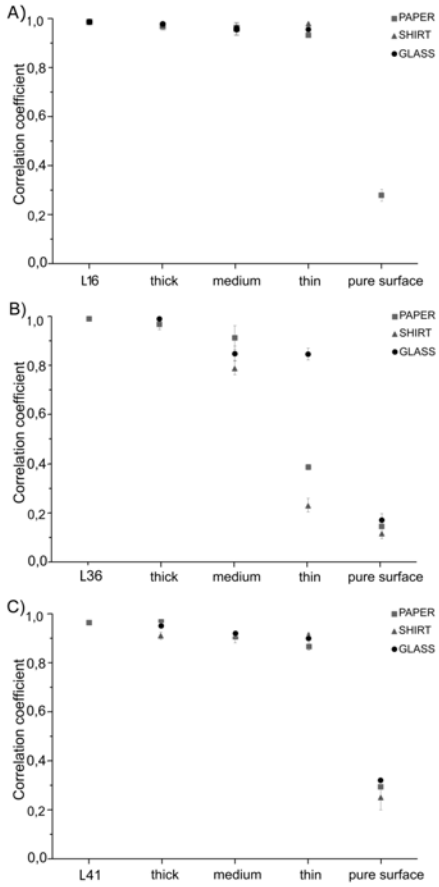

Fig. 4 The correlation coefficients between the GC-MS signals obtained for pure lipsticks (A) L16, (B) L36, and (C) L41 and of their layers of different thickness applied on the surfaces of paper, shirt, and glass.

Analogous experiments were carried out using separation techniques. This time, three samples were prepared from each layer and each sample was analyzed three times. The comparison of *CC* between pure lipsticks and various layers of lipsticks applied on investigated surfaces for GC-MS analysis are presented in Fig. 3 (only three lipsticks). The data analysis included the subtraction of peaks coming from compounds introduced to the samples (paper or swab) during their preparation. Also in this case, the decrease of *CC* value associated with a thinner lipsticks layer was observed. This changes, however, were much smaller than in

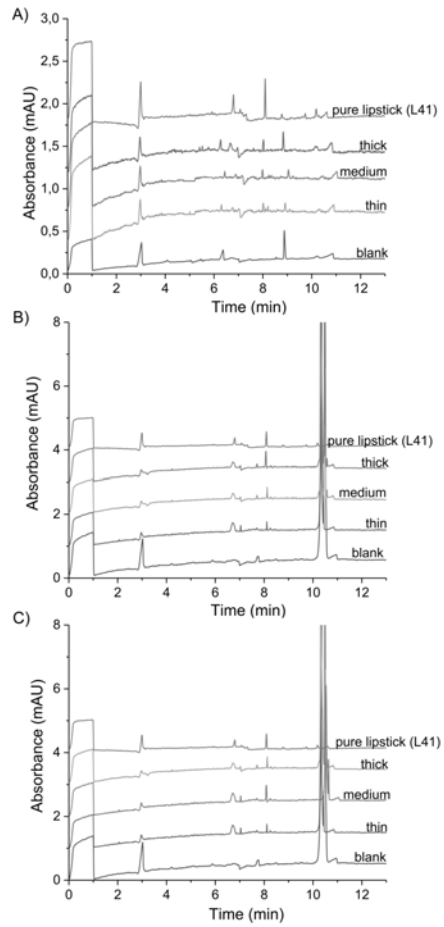

Fig. 5 The comparison between the MEKC signals obtained for pure lipstick L41 and for its layers of different thickness applied on the surfaces of (A) paper, (B) shirt, and (C) glass.

ATR analysis (with one exception: L36). Moreover, even though some low-intensity peaks disappeared, the whole chromatographic profile remains very similar to pure lipstick and it is possible to make correct comparative analysis.

Due to the nature of electrophoretic process (peaks shift, changes in baseline), it is not possible to calculate reasonable *CC* value for two electropherograms. For this reason, in the case of MEKC analysis, the effect of the thickness of lipstick layer applied on surfaces was examined by visual comparison of whole electropherogram profiles. As can be seen (Fig. 5), there are no changes in the obtained information about examined samples (the same number of peaks) dependent on the analyzed thickness of lipstick layer. Observations are the same for all investigated lipsticks (in Fig. 5 result for only one lipstick are presented) and for all studied surfaces.

4. Conclusions

In this research, the manner and the amount of lipsticks required to analysis (with the use of separation techniques) were defined. The optimal area of lipstick traces were found as follows: paper – 3 dots cut out by a puncher (i.d. 2 mm), shirt and glass – 0.5 cm^2 area removed by dry cotton swab.

The effect of the thickness of lipstick layer applied on surfaces was also examined. It was concluded that the separation technique are less sensitive to the changes associated with the thickness of the layer of lipstick smudged on the surface than the spectroscopic one.

Acknowledgments

The authors gratefully acknowledge the Inglot Company for donating lipsticks. The research was carried out with equipment purchased thanks to the financial support of the European Regional Development Fund (in Poland) within the framework of the Polish Innovation Economy Operational Program (contract no. POIG.02.01.00-12-023/08). The equipment has been used according to the contract policy.

References

[1] Gładysz M, Król, M, Kościelniak P.: Differentiation of red lipsticks using the attenuated total reflection technique supported by two chemometric methods. *Forensic Sci. Int.* **280** (2017), 130–138.

[2] Gładysz M, Król, M, Własiuk P., Piwowar M., Zadora G., Kościelniak P.: Development and evaluation of semi-destructive, ultrasound assisted extraction method followed by gas chromatography coupled to mass spectrometry enabling discrimination of red lipstick samples. *J. Chromatogr. A.* **1577** (2018), 92–100.

[3] Gładysz M, Król, M, Mystek K., Kościelniak P.: Application of micellar electrokinetic capillary chromatography to the discrimination of red lipstick samples. *Forensic Sci. Int.* **299** (2019), 49–58.

Development of extraction method for the isolation of antidepressants from human blood

Magdalena Świądro[a,*], Renata Wietecha-Posłuszny[a], Dominika DUDEK[b], Paweł Kościelniak[a]

[a] *Laboratory of Forensic Chemistry, Department of Analytical Chemistry, Faculty of Chemistry, Jagiellonian University in Krakow, Gronostajowa 2, 30-387, Krakow, Poland*
✉ *magda.swiadro@doctoral.uj.edu.pl*
[b] *Department of Affective Disorders, Jagiellonian University Medical College in Krakow, Kopernika 21A, 31-501 Krakow, Poland*

Keywords
antidepressants
extraction methods
human whole blood
UHPLC-MS

Abstract
The aim of this study was to develop a new, effective sample preparation method for isolation of psychotropic drugs, such as citalopram, fluoxetine, paroxetine, sertraline and venlafaxine. In this research six, various extraction agents were investigated in order to achieve the highest efficiency of the conducted process. Moreover, three different extraction techniques were investigated: liquid-liquid extraction, ultrasound-assisted extraction and microwave-assisted extraction. The obtained extracts were analysed using ultra-efficient liquid chromatography with mass spectrometry. The conducted research indicated that the most promising extraction agent was ethyl acetate. It is the first step to develop methods enabling the reliable determination of antidepressants in whole blood for the toxicological and clinical purposes.

1. Introduction

The most commonly used antidepressants are venlafaxine belonging to the serotonin-norepinephrine reuptake inhibitor and a number of medicines belonging to the selective serotonin reuptake inhibitors group. Citalopram, fluoxetine, paroxetine and sertraline are the first-line antidepressants. Selective serotonin reuptake inhibitors are a class especially used as antidepressants in the treatment of depression. The main mechanism of action of selective serotonin reuptake inhibitors is inhibition of reabsorbtion (reuptake) of serotonin. Moreover, selective serotonin reuptake inhibitors are called selective because they seem to primarily affect serotonin, not other neurotransmitters. All drugs of this group work in a similar way. They can cause similar side effects, despite better overall safety and tolerability than older antidepressants [1, 2]. There are the most

frequently prescribed medications due to their positive properties and high treatment effectiveness. There is a lack of methods for determining the level of medicines, which would facilitate the therapeutic drug monitoring of patient and better adjustment of doses to the treatment of an individual patient. Therefore, it is important to develop new analytical methods for the determination of selective serotonin reuptake inhibitors and the serotonin-norepinephrine reuptake inhibitor drugs in the human body. Extraction procedure is a very important step in the quantitative analysis of substances in biological fluids. If the extraction efficiency is high, it guarantees the good isolation of drugs. The effective procedure may be useful in clinical, toxicology and forensic analysis in dissecting the more matrix complex [3, 4]. Therefore, the purpose of this research was to choose the most promising extraction agent for isolation of antidepressant drugs from whole human blood using three different techniques: liquid-liquid extraction, ultrasonic-assisted extraction, and microwave-assisted extraction.

2. Experimental

2.1 Reagents and chemicals

Drug standards and their deuterated analogue were purchased from Lipomed AG (Switzerland): citalopram, fluoxetine, paroxetine, sertraline, venlafaxine, fluoxetine-D5, paroxetine-D5, and venlafaxine-D5. Drug stock solutions (1 mg/mL) and internal standards (1 mg/mL) were stored in methanol in freezer at –20 °C. The whole blood was provided by the local blood bank (Krakow, Poland). The other chemicals used throughout experiments: chloroform, form acid, *n*-hexane, acetic acid and sodium tetraborate decahydrate, were purchased from Sigma-Aldrich (USA). Acetonitrile, methyl alcohol and methanol were supplied by Fluka Analytical (Germany), whereas isoamyl alcohol was obtained from Chempur (Poland). Ultrapure water (18.2 MΩ cm, < 3 ppb TOC) used to prepare all aqueous solutions was generated with the Milli-Q system by Merck-Millipore (Germany).

2.2 Instrumentation

The measurements were carried out using UltiMate 3000 RS liquid chromatography system (Dionex, USA) coupled to a mass spectrometer MicrOTOF-Q II with a time of flight mass analyzer (Bruker, Germany). The mobile phase consisted of 0.1% formic acid in ultrapure water (A) and acetonitrile (B). The following gradient programme (B) at the flow rate of 0.4 mL/min was used: 0 min – 5%; 14 min – 70%; 16.5 min – 5%; 20 min – 5%. Separation was carried out in a Hypersil Gold Phenyl column (50×2.1 mm, 1.9 µm, injection: 5 µL, Dionex) at 20 °C. The ESI ion source conditions were as follows: nebulizer pressure: 2.5 bar, dry gas: 5.5 l/min heated to 200 °C. Data were recorded in the positive ion mode and

profile spectra were acquired in the mass range 100–1000 *m/z*. Cluster mass calibration was performed using a mixture of 10 mM sodium formate and isopropanol before each run.

Ultrasonic-assisted extraction experiments were performed using ultrasonic bath SONIC-3 (Polsonic, Poland), which works at frequensices of 40 kHz. For microwave-assisted extraction process, MARS 5 microwave-assisted sample preparation system (CEM Matthews NC, USA) equipped with 24 Xpress PHA vessels (75 mL) were used.

2.3 Sample preparation

The stock solutions of selective serotonin reuptake inhibitors and venlafaxine were prepared at a concentration of 100 ng/mL in methanol, next evaporated under nitrogen in the temperature of 40 °C. After that 300 μL of whole blood and 300 μL of borate buffer (pH = 9.5) were added to each probe and then vortexed (Vortex Heidolph, Germany) for 5 minutes. The samples prepared in such way were extracted using three techniques: liquid-liquid extraction, ultrasonic-assisted extraction and microwave-assisted extraction and testing six extraction solvents: chloroform, *n*-hexane, ethyl acetate, ethyl acetate:*n*-hexane (10:90, *v/v*), methanol:acetonitrile (1:1, *v/v*), and isoamyl alcohol:*n*-hexane (1:99, *v/v*). Each sample were dosed by 1 mL of an extraction solvent and gently agitated for 10 minutes using the platform shaker (liquid-liquid extraction) or sonicated by 10 minutes at 25 °C (ultrasonic-assisted extraction). Microwave-assisted extraction was performed for 10 min at 50 °C and 800 W using 3 ml of extraction solvent. After that, each sample was vortexed for 2 minutes and filtrated using PTFE filters (0.25 μm). Then, the supernatant was transferred to new probe and evaporated under nitrogen. Prior to UHPLC-MS analysis, 100 μL of mobile phase (acetonitrile 0.1% formic acid, 1:9, v/v) was added.

3. Results and discussion

In the beginning, six different solvents were selected as the extraction agents, but two of them (chloroform and methanol:acetonitrile) were rejected due to a problem with blood preparation (contamination). Each time, three samples were prepared and analysed three times using UHPLC-MS technique. The obtained results (Fig. 1) were compared by means of the extraction efficiency relating to an analyte. It was calculated according to SWGTOX [5] as the ratio of the analytical signal obtained for an analyte after extraction process to the signal measured for the appropriate standard drug solution.

As can be seen, the most promising extraction agents (i.e. suitable for all investigated compounds) are different for each examined techniques. In the case of liquid-liquid extraction and ultrasonic-assisted extraction, the best results were obtained using isoamyl alcohol:*n*-hexane. However, ethyl acetate was

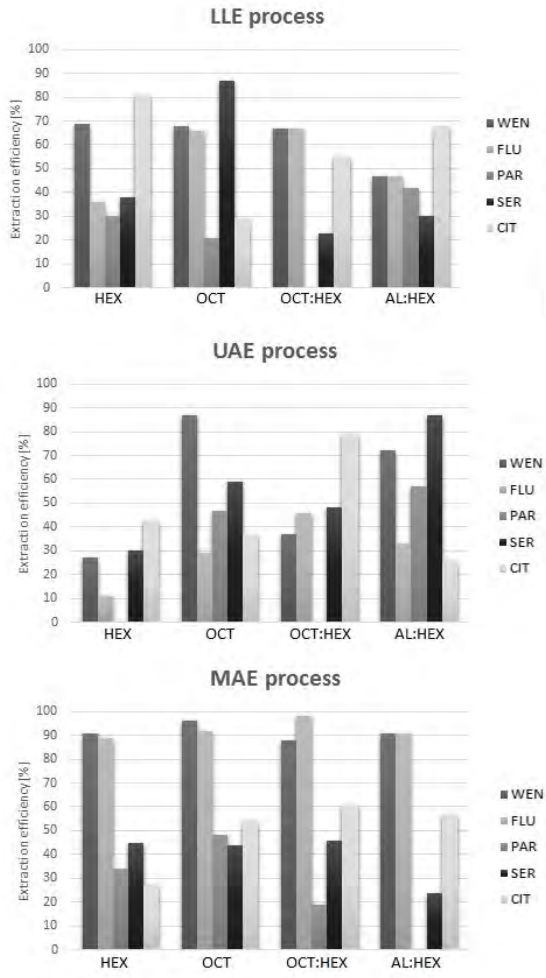

Fig. 1 Comparison of the extraction efficiency of venlafaxine (WEN), fluoxetine (FLU), paroxetine (PAR), sertraline (SER), citalopram (CIT) isolated from whole blood with the use of the liquid-liquid extraction (LLE), ultrasonic-assisted extraction (UAE), and microwave-assisted extraction (MAE), and various extraction solvents: *n*-hexane (HEX), ethyl acetate (OCT), ethyl acetate: hexane (10:90, *v/v*; OCT:HEX), and isoamyl alcohol:*n*-hexane (1:99, *v/v*; AL:HEX).

enabled to achieve high extraction efficiency for the same compounds and, in addition; it was the best in the case of microwave-assisted extraction.

The comparison of extraction efficiency between investigated techniques clearly indicated that the Microwave-assisted extraction allows achieving the best efficiency. Certainly, it is due of the character of the performed process, as the microwaves action prompt destruction of the blood cells (from the inside). The chromatogram obtained for the microwave-assisted extraction is presented in Fig. 2. It can be seen that all of the investigated compounds are separated from

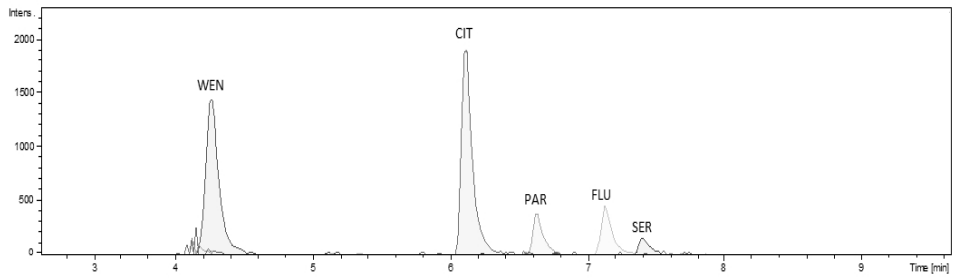

Fig. 2 UHPLC-MS chromatogram obtained for venlafaxine (WEN), citalopram (CIT), paroxetine (PAR), fluoxetine (FLU), sertraline (SER) after microwave-assisted extraction with the use ethyl acetate.

each other. They are also characterized by well shape and symmetry what is important from the point of view of quantitative analysis.

4. Conclusions

The extraction techniques play a crucial role in the analytical process, because it allows isolation of the analytes from their matrix. For this reason, different extraction techniques and extraction solvents for isolation drugs from human whole blood were tested. Ultimately, ethyl acetate conjunction with microwave-assisted extraction was excellent for isolation citalopram, fluoxetine, sertraline, paroxetine, and venlafaxine. These conclusions may facilitate the research of isolation antidepressants from blood. It may prove to be a useful contribution to therapeutic drug monitoring (i.e., patients with depression) or in forensic and toxicology analysis.

Acknowledgments

Magdalena Świądro acknowledges the support of InterDokMed project no. POWR.03.02.00-00-I013/16. The research was carried out with equipment purchased thanks to the financial support of the European Regional Development Fund within the framework of the Polish Innovation Economy Operational Program (contract no. POIG.02.01.00-12-023/08).

References

[1] Bingcong Z., Zhigang L., Yuanzheng W., Xuehong M., Xiangqun W., XueqinW., Jianping L., Yong H., Jianbin Z., Liqin L., Xiaoyang H., Jinfeng J., Shanshan Q., Qianyun C., Meng S., Xinjing Y., Tuya B., Yutong F.: Manual or electroacupuncture as an add-on therapy to SSRIs for depression: A randomized controlled trial. *J. Psychiatr. Res.* **114** (2019), 24–33.

[2] Jarema M.: *Depresja w praktyce lekarza*. Warsar, POZ Wydawnictwo Lekarskie PZWL 2017. (In Polish.)

[3] Fernadez P., Taboada V., Regenjo M., Morales L., Alvarez I., Carro A.M.: Optimalization of ultrasound assisted dispersive liquiud-liquid microextraction of six antidepressants in human plasma using experimental design. *J.Pharm. Biomed. Anal.* **124** (2016), 189–197.

[4] Snamina M., Wietecha-Posłuszny R., Zawadzki M.: Postmortem analysis of human bone marrow aspirate: Quantitative determination of SSRI and SNRI drugs. *Talanta* **204** (2019), 607–612.
[5] Scientific Working Group for Forensic Toxicology, Scientific Working Group for Forensic Toxicology (SWGTOX): Standard practices for method validation in forensic toxicology. *J. Anal. Toxicol.* **37** (2013) 452–474.

Application of double disc glassy carbon electrode for voltammetric determination of viloxazine

Maria Madej[a,*], Jolanta Kochana[a], Bogusław Baś[b]

[a] *Department of Analytical Chemistry, Faculty of Chemistry, Jagiellonian University, Gronostajowa 2, 30-387, Kraków, Poland* ✉ *marysia.madej@doctoral.uj.edu.pl*
[b] *Department of Analytical Chemistry, Faculty of Materials and Ceramics, AGH University of Science and Technology, Adama Mickiewicza 30, 30-059, Kraków, Poland*

Keywords
differential pulse voltammetry
electrochemistry
glassy carbon electrode
viloxazine

Abstract
This work deals with the verification of potential applicability of double disc glassy carbon electrode (DDGCE; d = 1.0 mm) for pharmaceuticals quantitative analysis, on the example of an antidepressant drug, viloxazine, determination using differential pulse voltammetry. For that purpose, the viloxazine oxidation peak current density, the sensitivity, linearity and limit of detection values obtained using DDCGE were compared to the results received at the conventional glassy carbon electrode (GCE; d = 3.0 mm). The research has shown that employing DDGCE allowed to obtain higher current density in comparison to GCE, and consequently better sensitivity and lower detection limit. The DDGCE was successfully employed for viloxazine determination in spiked Vistula water and waste water certified reference standard samples with good recovery (96.0–99.2%).

1. Introduction

The continuous increase in the consumption of drugs and the use of inappropriate drug disposal procedures are only two of many factors that have an impact on the growing environmental pollution of medicinal substances and their metabolites, including antidepressants [1]. Commonly used wastewater treatment procedures do not allow for effective removal of drug residues present in the environment, and thus the concentration of pharmaceuticals in environmental waters is constantly growing [2]. Viloxazine, the antidepressant drug from the group of selective norepinephrine reuptake inhibitors, exhibit one of the lowest degree of drug metabolism from all antidepressants, therefore it can occur in the environment in unchanged form even at a micromole level and thus pose a risk to aquatic organisms [3]. These observations prove that it is essential to develop new analytical methods that will allow for monitoring the concentration of antidepressants, like viloxazine, not only in biological, but especially in environmental

samples. Particular attention should be paid to the use of electrochemical methods, which give the possibility of performing cheap, fast, and accurate analyses, without any sample preparation.

Voltammetry is one of the most commonly used electrochemical techniques, wherein the analytical signal is recorded as a dependence of a current in a function of a potential applied to the working electrode. In constant measurement conditions, the registered current is directly proportional to the analyte concentration. In the case of differential pulse voltammetry (DPV) this dependence can be described by following equations

$$I_{\mathrm{p}} = \frac{n\boldsymbol{F}AD^{1/2}c}{\pi^{1/2}t^{1/2}}\left(\frac{1-\sigma}{1+\sigma}\right) \tag{1}$$

$$\sigma = \exp\left(\frac{n\boldsymbol{F}\Delta E}{2\boldsymbol{R}T}\right) \tag{2}$$

where I_{p} is peak current, n is number of electrons involved in the redox process, $\boldsymbol{F}$ is Faraday constant (96485 C mol^{-1}), A is electrode surface, D is diffusion coefficient, c is electroactive compound concentration, t is pulse width, ΔE is potential step , $\boldsymbol{R}$ is gas constant (8.314 J K^{-1}mol^{-1}), and T is thermodynamic temperature [4].

The aim of this work was to verify the usefulness of double disc glassy carbon electrode in voltammetric measurements, on the example of viloxazine determination. For this purpose, the DPV measurements using conventional glassy carbon electrode (d = 3.0 mm) and double disc glassy carbon electrode (d = 1.0 mm) were carried out. The influence of electrode surface area on recorded signals was compared, particularly in terms of analytical method sensitivity.

2. Experimental

2.1 Reagents and chemicals

The following reagents were used: MicroPolish Alumina suspension with grain size 0.5 µm (Buechler, USA); potassium chloride (Poch, Poland); viloxazine hydrochloride (LGC, Great Britain); acetic acid (Poch, Poland); sodium acetate (Merck, Germany); Vistula water collected in Krakow; certified reference standard EnviroMAT Waste Water, High EU-H-3 (SCP Science, Canada); distilled water derived from a HLP 5 system (Hydrolab, Poland).

2.2 Instrumentation

The voltammetric measurements were conducted with the M161 electrochemical analyzer (Mtm-Anko, Poland). The EALab 2.1 software was used for data

acquisition. The measurements were carried in three-electrode system in quartz vessel of 10 mL volume covered with a plastic cover with four holes that matched the size of each electrode and an additional hole for adding standard solution. The double disc glassy carbon electrode (DDGCE) consisting of two, separate glassy carbon layers (d = 1.0 mm) placed on the long side of steel wire covered with glass coating (surface area: 0.0157 cm^2) and conventional glassy carbon electrode (d = 3.0 mm) placed in teflon holder (MTM Anko M10X1) (surface area: 0.0707 cm^2) were used as a working electrodes. Silver chloride electrode (Ag/AgCl, 3M KCl; MTM Anko M6) was used as a reference electrode and platinum wire placed in teflon holder was used as an auxiliary electrode. Also magnetic stirrer MS 11 (Wigo, Poland) were used.

3. Results and discussion

According to equation (1) peak current recorded in differential pulse voltammetric measurements is directly proportional to the working electrode surface, therefore the application of the same type of working electrodes but with different surface area with maintaining the constant measurement conditions should result in registration of different peak current values. However, this results could be comparable only when analytical signal is presented in a form of current density, so the current value per electrode surface unit (expressed as A cm^{-2}). To verify the impact of electrode surface area on recorded current, the differential pulse voltammograms for antidepressant drug viloxazine were recorded using two glassy carbon electrodes, with different surface areas: the conventional glassy carbon electrode (d = 3.0 mm) and double disc glassy carbon electrode (d = 1.0 mm). According to previously optimized analytical procedure for viloxazine determination [5] the measurements were carried in 0.1 mol L^{-1} acetate buffer solution pH = 5.0 containing viloxazine at concentration of 10 μmol L^{-1} in potential range from 0.50 to 1.55 V. The example of recorded DP voltammograms are presented in Fig. 1. As can be seen, the current recorded using conventional GCE is almost three times higher than using DDGCE, however when the signal is converted into current density the viloxazine oxidation peak current density obtained at GCE and DDGCE are equal 52.0 and 64.0 μA cm^{-2}, respectively. This results clearly shows that despite application of the same type of working electrode, but with different surface areas, the obtained current density values differs significantly. The higher current density received at DDGCE results mainly from the enhanced mass-transport and faster electron exchange process observed in measurement conducted in electrodes with small surface area [4].

Consequently, the DP voltammograms for viloxazine in concentration range from 0.5 to 40.0 μmol L^{-1} using both tested working electrodes were recorded. On the calibration graphs obtained using DDGCE (Fig. 2) and GCE (Fig. 3) two linear relationships, 0.5–15.0 and 15.0–40.0 μmol L^{-1}, could be distinguished. The limit of detection was calculated as 3.3 times standard error of intercept obtained from

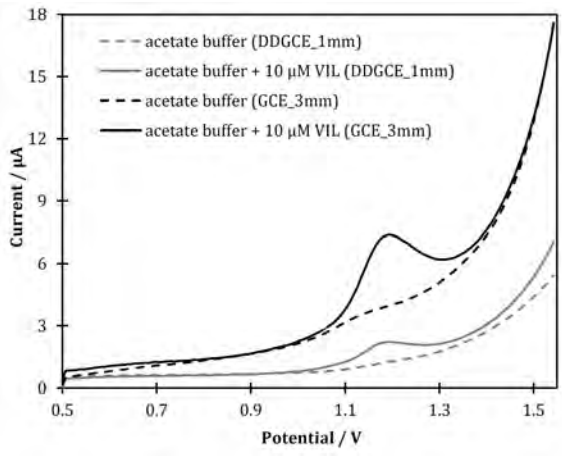

Fig. 1 Voltammograms recorded for 10 µmol L^{-1} viloxazine (solid lines) in 0.1 mol L^{-1} acetate buffer solution pH = 5.0 (dotted line) using glassy carbon electrode *d* = 3.0 mm (black lines) and double disc glassy carbon electrode *d* = 1.0 mm (grey lines) using differential pulse voltammetry. Conditions: (potential step 7 mV; pulse width 10 ms; pulse amplitude 50 mV; accumulation potential 500 mV; accumulation time 10 s.

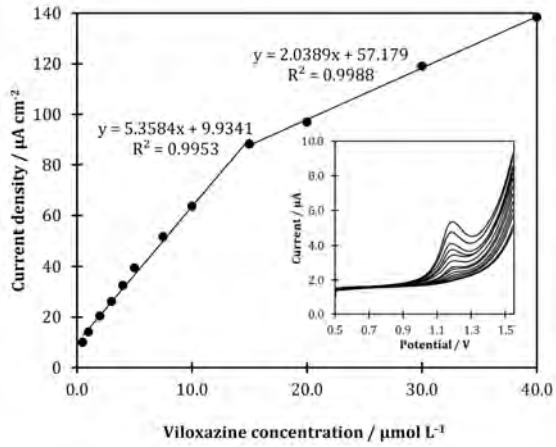

Fig. 2 Calibration dependence obtained using double disc glassy carbon electrode *d* = 1.0 mm in differential pulse voltammetric measurements conducted in 0.1 mol L^{-1} acetate buffer solution pH = 5.0 containing viloxazine with corresponding DP voltammograms (insert). Conditions: potential step 7 mV; pulse width 10 ms; pulse amplitude 50 mV; accumulation potential 500 mV; accumulation time 10 s.

linear estimation of calibration graphs over the calibration slope [6]. The obtained analytical parameters were summarized in Table 1. The received analytical data indicates that both considered electrodes present a good linear response in the same concentration ranges, however the measurements conducted using DDGCE results in higher sensitivity and lower limit of detection value in comparison to conventional GCE.

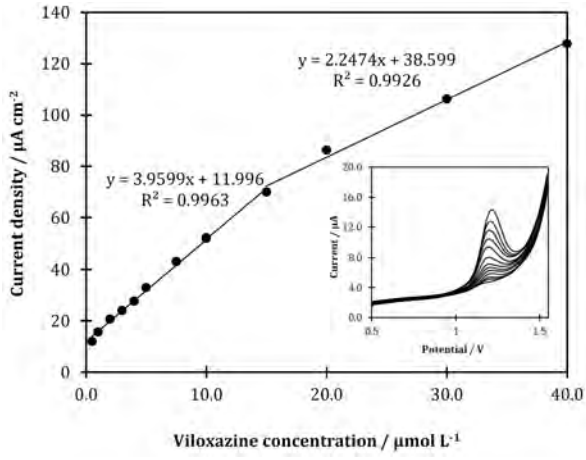

Fig. 3 Calibration dependence obtained using conventional glassy carbon electrode d = 3.0 mm in differential pulse voltammetric measurements conducted in 0.1 mol L^{-1} acetate buffer solution pH = 5.0 containing viloxazine with corresponding DP voltammograms (insert). Conditions: potential step 7 mV; pulse width 10 ms; pulse amplitude 50 mV; accumulation potential 500 mV; accumulation time 10 s.

Table 1
The comparison of analytical parameters of viloxazine determination obtained for glassy carbon electrode and double disc glassy carbon electrode.

Electrode type	Linear range / µmol L^{-1}	Sensitivity / µA L µmol^{-1}cm^{-2}	*LOD*/µmol L^{-1}
GCE, d = 3.0 mm	0.5–15.0	3.96	0.31
	15.0–40.0	2.25	
DDGCE, d = 1.0 mm	0.5 – 15.0	5.36	0.22
	15.0 – 40.0	2.04	

The usefulness of DDGCE in real sample analysis was verified by viloxazine determination in Vistula water and waste water certified reference standard samples spiked with the analyte to obtain concentration of 1.0 and 5.0 µmol L^{-1}. For each spiked water the 5.0 mL of sample was added to the 5.0 mL of supporting electrolyte and then measurements were conducted according to standard addition calibration method. The quantification procedure was repeated three times for each sample and then the recovery with confidence intervals (significance level 0.05) and relative standard deviation (*RSD*) were calculated (Table 2). The received recovery values for both samples at two concentration levels ranged between 96.0 and 99.2% with confidence intervals less than 1.2% and RSD lower than 0.5%. The obtained results indicate that employing DDGCE allows for accurate and precise determination of viloxazine with good repeatability even in samples with complex matrix.

Table 2
Results of viloxazine determination in spiked water samples using double disc glassy carbon electrode.

Matrix	Amount/μmol L^{-1}		Recovery/%	*RSD*/%
	Added	Received		
Vistula water	1.0	0.976	97.8 ± 0.3	0.2
		0.980		
		0.978		
	5.0	4.954	99.2 ± 0.6	0.1
		4.958		
		4.961		
Waste Water CRS	1.0	0.955	96.0 ± 0.8	0.5
		0.960		
		0.950		
	5.0	4.916	98.2 ± 1.2	0.1
		4.908		
		4.902		

4. Conclusions

The conducted study proved that application of double disc glassy carbon electrode (d = 1.0 mm) instead of conventional glassy carbon electrode (d = 3.0 mm) results in significant sensitivity increase (ca. 35%) and limit of detection reduction (ca. 305%), thus allowed for accurate and precise determination of viloxazine in tested water samples. Additionally, good recovery suggests that analytical method based on DDGCE can be successfully used for water sample analysis without any special sample pretreatement. The obtained results indicate that application of DDGCE in voltammetric measurements represents a good alternative for commercially available glassy carbon electrodes.

Acknowledgments

This research has been partly supported by the EU Project POWR.03.02.00-00-I004/16.

References

[1] Weber F., Beek T., Bargman A.: *Pharmaceuticals in the Environment: The Global Perspective.* Dessau-Roßlau, German Environmental Agency 2014.
[2] Langford K.H., Thomas K.V.: Determination of pharmaceutical compounds in hospital effluents and their contribution to wastewater treatment works. *Environ. Int.* **35** (2009), 766–770.
[3] Finder M., Brogden R.N., Speight T.M., Avery G.S.: Viloxazine: A review of its pharmacological properties and therapeutic efficacy in depressive illness. *Drugs* **13** (1977), 401–420.
[4] Bard A., Faulkner L.R.: *Electrochemical Methods: Fundamentals and Applications.* New York, Wiley 2001.
[5] Madej M., Kochana J., Baś B.: Determination of viloxazine by differential pulse voltammetry with boron-doped diamond electrode. *Monatsh. Chem.* (2019), in press. DOI: 10.1007/s00706-019-2380-6
[6] Shrivastava A., Gupta V.B.: Methods for determination of limit of detection and limit of quantitation analytical methods. *Chron. Young. Sci.* **2** (2011), 21–25.

Application of stripping voltammetry for monitoring of vitamin B_2 *in vitro* synthesis by *Bacillus subtillis*

Radosław Porada*, Katarzyna Jedlińska, Justyna Lipińska, Bogusław Baś

Department of Analytical Chemistry, Faculty of Materials Science and Ceramics, AGH University of Science and Technology, Mickiewicza 30, 30-059 Kraków, Poland ✉ *rporada@agh.edu.pl*

Keywords
bacteria
supernatant
vitamin B_2
voltammetry

Abstract
This work presents the electrochemical procedure for vitamin B_2 determination by means of differential pulse voltammetry with adsorptive preconcentration step. The experimental conditions were investigated and optimised, leading to methods validation. The method was then applied to characterize and monitor the process of vitamin B_2 production by *Bacillus subtillis* bacteria in *in vitro* conditions. The research has shown that protein-based cultivation medium strongly handicapped the analysis by blocking the working electrode surface, therefore, decreasing the method sensitivity. The amount of produced vitamin has changed with the breeding time, displaying an abrupt increase after 72 h of bacteria growth.

1. Introduction

Vitamin B_2 is an important micronutrient, essential for proper function of human body and retention of its health. It is commonly known as riboflavin, which resembles the fact, that vitamin B_2 molecule is composed of ribitol side-chain and flavin ring-moiety, responsible for its yellow colour. Common sources of vitamin B_2 involve eggs, meat, cheese and yeast. In solid state its solubility in water is mediocre (10–13 mg L^{-1}), but it can be greatly increased by alkali addition [1, 2]. In human body vitamin B_2 not only plays an important role in glucose and amino acids biotransformation, but also factors in immunity. At the very early stage of its deficiency mucosa fragmentation and photophobia may be observed. In more advanced stage it can lead to skin inflammation or anaemia [2, 3]. Vitamin B_2 deficiency is mostly caused by inappropriate supplementation, various diseases and excessive alcohol consumption [1, 3]. Owing to the great importance of vitamin B_2, as well as the negative consequences of its deficiency or excess, novel and non-hazardous vitamins sources with extended assimilability are in demand.

Bacteria are commonly used in biotechnology for manufacturing most of dairy products and in meat fermentation. Recently it has been discovered that bacteria

possess the ability to synthesize some vitamins by means of fermentation or genetic engineering. There is also a possibility to use bacteria as a bioreactor, in which the outcome of distinct metabolic processes is the essential vitamins. This methodology has many advantages, including the reduction of production costs or elimination of toxic chemicals. Moreover, the assimilability of vitamins of natural origin is higher than those from artificial sources, like pharmaceuticals [4]. Burgess [5] described the synthesis of some B-group vitamin, mainly B_2, B_9, and B_{12}, by *Escherichia coli* and *Bacillus subtillis* as a result of guanosine triphosphate fermentation. This feature offers the possibility to manufacture food products designed for a particular social group, containing the proper composition of dietary ingredients. The amount of these components in wheat decreases during various processing stages. Addition of the human-safe lactic acid bacteria, as a fermentations starter can countervail this effect [6]. Current research in the field of biotechnological vitamins synthesis focus on selection of proper bacteria strain [4], elucidating the enzymatic reactions mechanism [5] and possible application of that methodology in the industry [4, 6]. A little attention is devoted to development of analytical procedures, which allows to quantify the amount of produced vitamins. An example of successful attempt hitherwards utilized differential pulse voltammetry with Refreshable Silver Liquid Amalgam Film multi-Electrode [7].

This paper aims at characteristic of vitamin B_2 production in *in vitro* conditions, which includes the study of vitamin dispersion among three fraction and variation in the produced amount with the breeding time. The influence of the cultivation medium, as an example of complex biological matrix, on the recorded voltammograms was investigated. Prior to that, the applied analytical procedure by means of differential pulse voltammetry with adsorptive preconcentration (DP AdSV) step was optimised and validated.

2. Experimental

2.1 Reagents and chemicals

All applied reagents were of analytical grade. 0.04 mol L^{-1} solution of boric, phosphate and acetic acid was titrated with 0.2 mol L^{-1} sodium hydroxide till required pH of prepared Britton-Robinson buffer was obtained. Standard solution of vitamin B_2 was made by dissolving an appropriate amount of riboflavin secondary standard (Sigma Aldrich) in 0.1 mol L^{-1} NaOH. 3 mol L^{-1} potassium chloride and 2.5 mol L^{-1} potassium nitrate aqueous solution were prepared using corresponding weighted portion of KCl and KNO_3 respectively (Merck, Suprapur, ≥ 99%) and fourfold distilled water. During bacteria breeding standard cultivation Tryptic Soy Broth medium, which is an aqueous solution of tryptone, soytone, dextrose, NaCl and K_2HPO_4 [8], was used.

2.2 Instrumentation

Growth of bacteria required the use of: Petri dishes, sterile test tubes with plastic cork, 1 μL plastic inoculation loop, vortex mixer Bio Vortex V1 (BIOSAN), incubator, laboratory centrifuge LMC-4200R (BIOSAN) and filters with submicrometric pore size. All voltammetric measurements were conducted in 10 mL quartz cell with Controlled Growth Mercury Drop Electrode (μCGMDE) acting as the working electrode, self-made double junction Ag|AgCl|3 mol L^{-1} KCl|2.5 mol L^{-1} KNO_3 reference electrode and Pt wire as the auxiliary electrode. Their work was controlled by M164 electrode stand associated with M161 electrochemical analyzer (mtm-anko, Kraków). For measurement of Britton-Robinson buffer pH value, the CPI-505 laboratory pH/ion meter (ELMETRON) was utilized.

2.3 Bacteria cultivation

In this study *Bacillus subtilis* 1, *Bacillus subtilis* 2 and their mixture of ratio 1:1, isolated from naturally fermented soy, were used. At the beginning, 8 loops of 1 μL of the seeded bacteria *Bacillus subtilis* 1 were transferred from the Petri dishes to the test tube containing 50 mL of cultivation medium. Next, it was shaken out to increase the contact area between bacteria cells and nutrient ingredients in the medium and later placed in the incubator in 37 °C. The period, when the test tubes are in the incubator, is called the breeding time. Afterwards, the content of the test tube was centrifugated to separate the liquid fraction, called supernatant and containing vitamin B_2 expelled from bacteria cells, from bacteria precipitate–pellet. The latter was rinsed with distilled water, infiltrated and subsequently frozen at –80 °C for 4 h and defrosted. The water fraction contains the vitamin B_2 adsorbed at the bacteria surface, whereas the refrigeration step allowed to extract the vitamin placed inside the bacteria cell. The same procedure was applied for *Bacillus subtilis* 2 and the mixture of both strains.

2.4 Voltammetric measurements

Voltammetric measurements were always conducted in deaerated solution of supporting electrolyte. No less than three consecutive potential scans were recorded per each measurement and averaged. In case of analysis of biological samples, the influence of the cultivation medium on the recorded voltammograms was first investigated. Based on [9, 10] an attempt toward its elimination with trichloroacetic acid was made. According to Sivaraman, for protein precipitation the trichloroacetic acid concentration must be properly selected to avoid protein solubility. The changes in vitamin B_2 in vitro production with breeding time were finally studied.

Table 1
Optimal parameters for differential pulse voltammetry with adsorptive preconcentration determination of riboflavin.

Parameter	Value
Supporting electrolyte	0.1 mol L^{-1} Britton-Robinson buffer, pH = 3.0
Start potential, E_0	–1.3 V
End potential, E_k	+0.1 V
Accumulation potential, E_{acc}	–1.3 V
Accumulation time, t_{acc}	15 s
Step potential, E_s	4 mV
Pulse amplitude, dE	40 mV
Pulse width, t_{imp}	20 ms

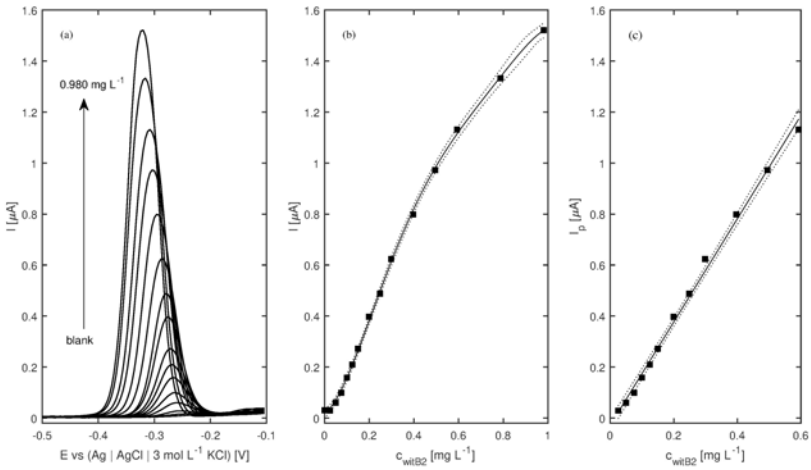

Fig. 1 (a) DP AdSV voltammograms of vitamin B_2 reduction recorded in the supporting electrolyte for increasing concentration of vitamin B_2. Concentration from bottom to top: 0, 0.010, 0.025, 0.050, 0.075, 0.100, 0.125, 0.150, 0.199, 0.249, 0.298, 0.397, 0.495, 0.593, 0.787, 0.980 mg L^{-1}. (b) Relationship between peak current and vitamin B_2 concentration. (c) Concentration range of linear response. Experimental conditions as in Table 1.

3. Results and discussion

3.1 Determination procedure

To find the measurement conditions, which will assure the high sensitivity and reliability of the proposed analytical method, an univariate optimisation was conducted. Concentration and pH-value of supporting electrolyte as well as parameters for differential pulse voltammetry with adsorptive pre-concentration step were systematically changed and based on the peak shape, height, and repeatability the optimal value were chosen and summarized in Table 1. The peak

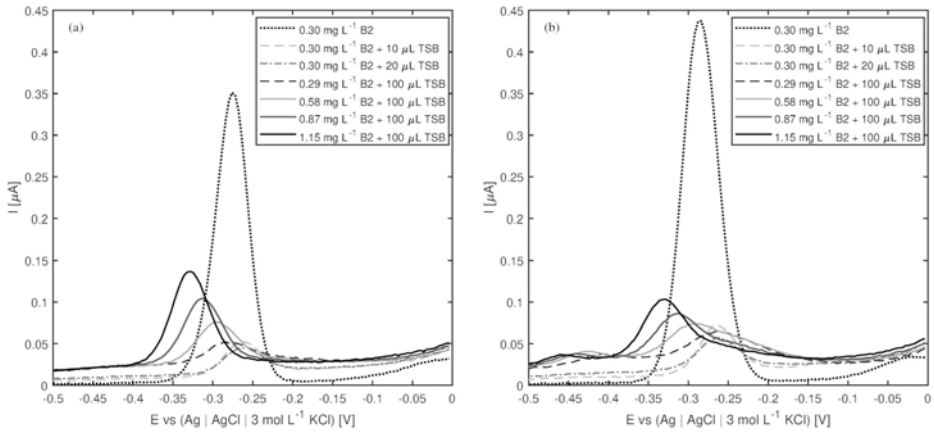

Fig. 2 Influence of the bacteria culture medium on the (a) oxidation and (b) reduction signal of vitamin B_2. Breeding time: 72 h, other conditions as in Table 1.

current for both oxidation and reduction of vitamin B_2 increased with analyte concentration, but the relationship was not linear in the whole range of tested concentrations, therefore the narrower scope was selected for further analysis (Fig. 1). Using the cross-validation approach the parameters of calibration curves (separately for anodic and cathodic voltammograms) were obtained. The linear range, detection limit and sensitivity for cathodic curves were 0.011 to 0.60 mg L^{-1}, 0.003 mg L^{-1} and 1.869 ± 0.062 μA L mg^{-1} respectively.

3.2 Influence of the cultivation medium

The presence of cultivation medium in the analysed solution decreased the signal of vitamin, for which the non-specific adsorption of medium protein on the working electrode is responsible (Fig. 2). With each addition of the medium the background signal grew, significantly hindering the interpretation of the obtained curves. After the addition of vitamin B_2 standard solution the peak current increased, meaning that despite the reduced sensitivity the quantitative analysis is still possible. For oxidation process the signal maintained the shape of singular peak, whereas for reduction overlapped peaks were observed.

Trichloroacetic acid addition in concentration range between from 0 to 0.15 % (*m:v*) did not cause the protein to be extracted from the studied sample, but it increased the background signal in the whole studied potential range by one order of magnitude. Also, a new, broad peak between –1.2 and –0.8 V appeared (Fig. 3), whose height was proportional to the amount of added trichloroacetic acid. It indicates, that trichloroacetic acid should be extracted from the studied sample prior to carrying out the measurement. Owing to the presented drawbacks, the further measurement were conducted without trichloroacetic acid addition.

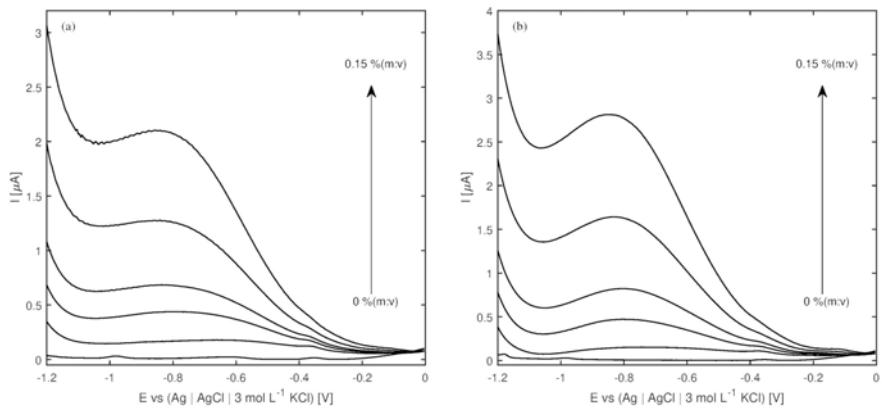

Fig. 3 Influence of the trichloroacetic acid addition on (a) oxidation and (b) reduction signal of vitamin B_2 in Tryptic Soy Broth medium. Trichloroacetic acid concentration from bottom to top: 0, 0.02, 0.04, 0.06, 0.10, 0.15% (*m:v*), concentration of vitamin B_2: 30 mg L^{-1}, other conditions as in Table 1.

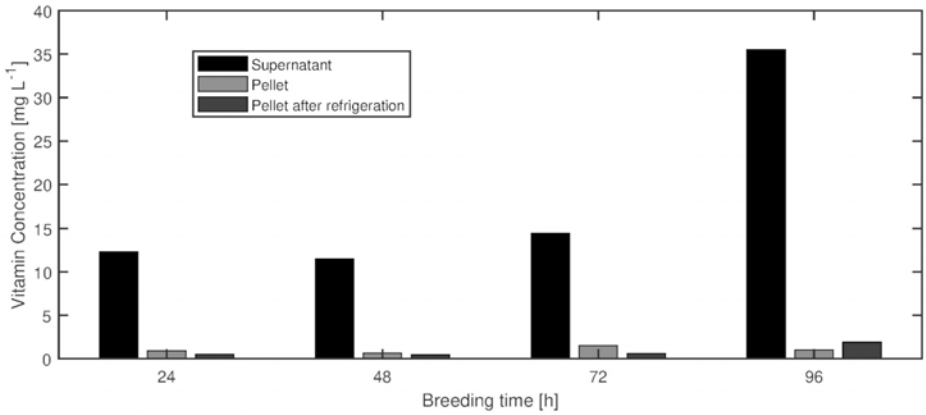

Fig. 4 Changes in the vitamin B_2 amount with the breeding time for three fractions: supernatant, pellet and pellet after refrigeration.

3.3 Effect of the breeding time

After 18 h of breeding cell division ends and the cells start to devour one another. Voltammetric analysis for 24, 48, 72 and 96 h breeding time indicated, that the amount of produced vitamin B_2 changes for supernatant, whereas for pellet and pellet after refrigeration remains almost constant (Fig. 4). This phenomenon can be attributed to the solubility of vitamin B_2 in water, which was the main constituent of the cultivation medium. The observed increase in vitamin B_2 production after 72 h may provide a possibility for gradual and relatively prolonged release.

4. Conclusions

Differential pulse adsorptive stripping voltammetry allows for fast and reliable determination of vitamin B_2 in range from 0.011 to 0.60 mg L^{-1}. The developed procedure was successfully applied to characterize the vitamin B_2 *in vitro* synthesis by *Bacillus subtillis* bacteria. The recorded voltammograms were distorted by the presence of protein components in the cultivation media, which blocked the surface of the working electrode. Vitamin B_2 shows strong affinity to aquatic supernatant and its amount it this phase changes strongly with time. On the other hand, the amount of vitamin B_2 adsorbed on the cell surface and accumulated inside bacteria does not depend on breeding time and in comparison to the amount in supernatant is negligible.

Acknowledgments

RP and JL have been partly supported by the EU Project POWR.03.02-00-00-I004/16.

References

[1] Combs G.F.: *The Vitamins: Fundamental Aspects in Nutrition and Health.* 3rd ed. Ithaca, Elsevier Academic Press 2008.
[2] Mindell E.: *Biblia witamin.* Warszawa, Wiedza i życie 1996. (In Polish.)
[3] Petteys B.J., Frank E.L.: Rapid determination of vitamin B_2 (riboflavin) in plasma by HPLC. *Clin. Chim. Acta* **412** (2011), 38–43.
[4] Duliński R.: Biotechnologiczne metody produkcji witamin z wykorzystaniem mikroorganizmów. *Żywn. Nauk. Technol. Ja.* **68** (2010), 5–19.
[5] Burgess C.M., Smid E.J., van Sinderen D.: Bacterical vitamin B_2, B_{11} and B_{12} overproduction: An overview. *Int. J. Food Microbiol.* **133** (2009), 1–7.
[6] Capozzi V., Russo P., Duenas M.T., López P., Spano G.: Lactic acid bacteria producing B-group vitamins: A great potential for functional cereal products. *Appl. Microbiol. Biotechnol.* **96** (2012), 1383–1394.
[7] Jedlińska K., Strus M., Baś B.: A new electrochemical sensor with the Refreshable Silver Liquid Amalgam Film multi-Electrode for sensitive voltammetric determination of vitamin K2 (menaquinone). *Electrochim. Acta* **265** (2018), 355–363.
[8] https://www.atcc.org/~/media/F11236DC0E36489ABFA10BF4A411C525.ashx (accesed 11th May 2018).
[9] Sivaraman T.: The mechanism of 2,2,2-trichloroacetic acid-induced protein precipitation. *J. Protein Chem.* **16** (1997), 291–297.
[10] Rajalingam D., Loftis C., Xu J.J., Kumar T.K.: Trichloroacetic acid-induced protein precipitation involves the reversible association of a stable partially structured intermediate. *Protein Sci.* **18** (2009), 980–993.

Aldrithiol-2 as a new derivatization agent for double bond localization in unsaturated compounds by mass spectrometry

TIMOTEJ STRMEŇ[a, b, *], JOSEF CVAČKA[a, b]

[a] *Institute of Organic Chemistry and Biochemistry of the Czech Academy of Sciences, Flemingovo náměstí 2, 166 10 Prague 6, Czech Republic* ✉ *timotej.strmen@uochb.cas.cz*
[b] *Department of Analytical Chemistry, Faculty of Science, Charles University, Hlavova 8, 128 43 Prague 2, Czech Republic*

Keywords
aldrithiol-2
double bond
electrospray
lipids
mass spectrometry

Abstract
A new method for localizing double bonds in lipids using derivatization with 2,2′-dipyridyl disulfide (Aldrithiol-2) and electrospray ionization mass spectrometry (ESI-MS) is presented. The derivatization introduces a permanent charge to the molecules. When collisionally activated, the derivatives provide diagnostic peaks useful for establishing the position of the original double bond. Since the permanent charge of the derivative significantly increases the detectability of analytes, the method works well also for lipids of very low polarity like hydrocarbons.

1. Introduction

The positions of double bonds in lipids have significant implications for their chemical, biochemical and biophysical roles [1]. For example, the double bond position in phosphatidylcholines influences the physical properties of lipid bilayer [2]. Another example is the effect of the position of the double bond on the pheromonal activity of hydrocarbons. While (*Z*)-tricos-7-ene is a male sex hormone of *Drosophila melanogaster* [3], (*Z*)-tricos-9-ene is a female sex pheromone of *Musca domestica* [4].

Double bond positions in lipids cannot be determined by mass spectrometry directly in most cases. Therefore, chemical derivatization of the analytes is required. In GC-EIMS, double bonds are often modified with small functional groups like an oxirane ring [5], methylthio groups [6] or hydroxy groups [7]. The original double bond position is established from characteristic peaks corresponding to cleavages near the newly introduced functional groups [8]. GC-EIMS is not appropriate for compounds with high molecular weight or high polarity, for which electrospray ionization suits the best. Derivatization of double bonds with 5-nitro-2-pyridine sulphenyl chloride was suggested for the enhancement of detection but the possibility of double bond localization was not discussed [9].

In this study, we present Aldrithiol-2 derivatization for ESI-MS as an efficient method for double bond localization in unsaturated lipids.

2. Experimental

2.1 Chemicals

Aldrithiol-2, (*E*)-tetradec-7-ene, and (*Z*)-tricos-9-ene were purchased from Sigma-Aldrich (USA). Vaccenyl alcohol, oleyl alcohol, oleic acid, methyl linoleate and triolein were purchased from Nu-Chek Prep (USA). Methanol and toluene were obtained from Merck (Germany). Chloroform (stabilized with 1% of ethanol) from Penta (Czech Republic) was distilled before use. Iodine and sodium thiosulfate were obtained from Lachema (Czech Republic). Water was prepared using a Milli-Q integral system (Merck Millipore, USA). Heptacosa-6,9-diene was isolated from *Periplaneta americana* and kindly provided to us by Vladimír Vrkoslav.

2.2 Derivatization procedure

The derivatization procedure was analogous to protocols used for the reaction with dimethyl disulfide [6, 10]. The unsaturated compound (1.0 to 1.5 mg) and Aldrithiol-2 (2.5–3.5 mg) were dissolved in 200 µl of chloroform. Then, 30 µl of iodine solution in toluene (60 mg/ml) was added. The reaction mixture was heated at 45 °C for 24 hours and shaken at the speed of 600 rpm using an Eppendorf ThermoMixer comfort (Germany). After 24 hours, an aqueous solution of sodium thiosulfate was added to eliminate the unreacted iodine. The organic phase was then transferred to a new vial, evaporated to dryness and the product was re-dissolved in methanol. The solution was further diluted in methanol prior to the mass spectrometry analysis.

2.3 Mass spectrometry detection

Low- and high-resolution data were recorded with LTQ Orbitrap XL (Thermo Fisher Scientific). The basic source parameters were set as follows: Spray voltage 4.86 kV; sheath gas flow rate 35.0 a.u.; auxiliary gas flow rate 5.0 a.u.; capillary voltage 9.0 V, capillary temperature 275 °C; tube lens voltage 150 V.

3. Results and discussion

3. 1 Structure of the derivatives

The scheme of the reaction of Aldrithiol-2 with unsaturated compounds is depicted in Fig. 1. Similar compounds were recently synthesized using an

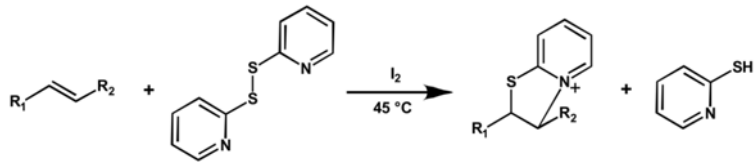

Fig. 1 Scheme of Aldrithiol-2 reaction with monounsaturated lipids.

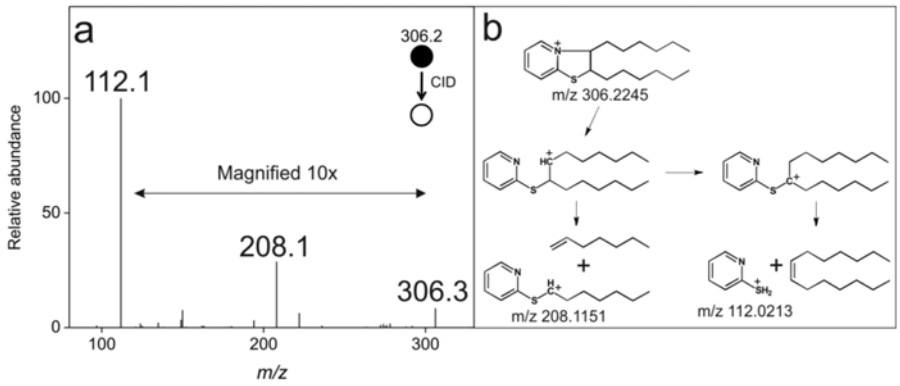

Fig. 2 CID MS^2 spectrum of (a) (*E*)-tetradec-7-ene derivative, and (b) proposed mechanism of fragmentation with exact ion masses obtained by high-resolution MS.

analogous procedure [11]. The reaction products were soluble in water. In our case, more hydrophobic compounds were derivatized, which resulted in products with limited solubility in water.

3.2 Fragmentation of the derivatives

3.2.1 Derivatives of symmetric monounsaturated compound

(*E*)-Tetradec-7-ene was chosen as a symmetrical compound. The fragmentation mass spectrum of its derivative successfully revealed double bond position. The precursor at *m/z* 306 provided two fragments, *m/z* 208 and *m/z* 112 (Fig. 2a). Both fragments were most likely formed by charge site-initiated fragmentation and subsequent loss of olefin. While the ion at *m/z* 112 does not say anything about the derivative structure, less abundant fragment ion at *m/z* 208 clearly indicates the fragmentation of the hydrocarbon chain at the position of the former double bond. Thus, the ion *m/z* 208 shows the position of the double bond and can serve as a diagnostic ion.

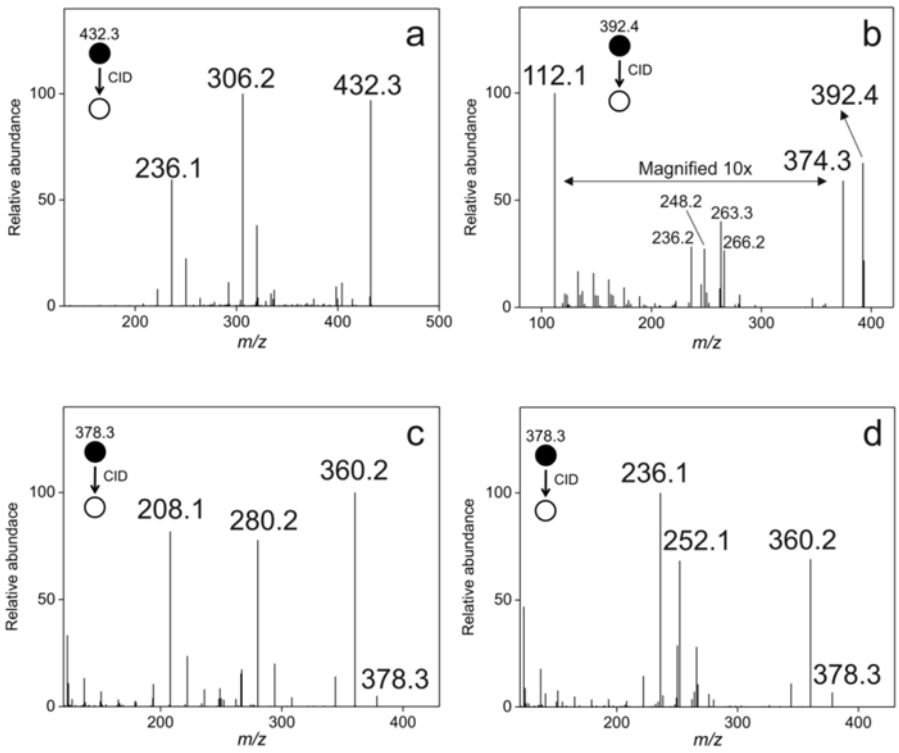

Fig. 3 Fragmentation mass spectra of (a) (*Z*)-tricos-9-ene derivative, (b) oleic acid derivative, (c) vaccenyl alcohol derivative, and (d) oleyl alcohol derivative.

3.2.2 Derivatives of asymmetric monounsaturated compounds

(*Z*)-Tricos-9-ene and oleic acid were successfully derivatized and the former double bond positions were easily identified from the corresponding fragmentation mass spectra. Since the unsaturated compounds were asymmetric, two major diagnostic peaks were formed. Fragmentation mass spectrum of (*Z*)-tricos-9-ene derivative contained main diagnostic peaks *m/z* 236 and *m/z* 306 (Fig. 3a). Fragmentation mass spectrum of oleic acid derivative was more complicated because of the carboxylic group. In addition to diagnostic peaks *m/z* 236 and *m/z* 266, signals at *m/z* 374 (loss of water from the parent molecule) and *m/z* 248 (loss of water from *m/z* 266) were present. The major fragment at *m/z* 112 was mercaptopyridinium cation (Fig. 3b).

To compare compounds that differ only by the position of double bond, two isomeric fatty alcohols, (*Z*)-octadec-9-en-1-ol (oleyl alcohol) and (*Z*)-octadec-11-en-1-ol (vaccenyl alcohol) were derivatized with Aldrithiol-2. Fragmentation mass spectrum of oleyl alcohol derivative contained expected diagnostic peaks (*m/z* 236 and *m/z* 252), which differed from fragments of vaccenyl alcohol derivative (*m/z* 208 and *m/z* 280); Fig. 3c–d. Both alcohol derivatives eliminated water (*m/z* 360), similarly to the oleic acid derivative.

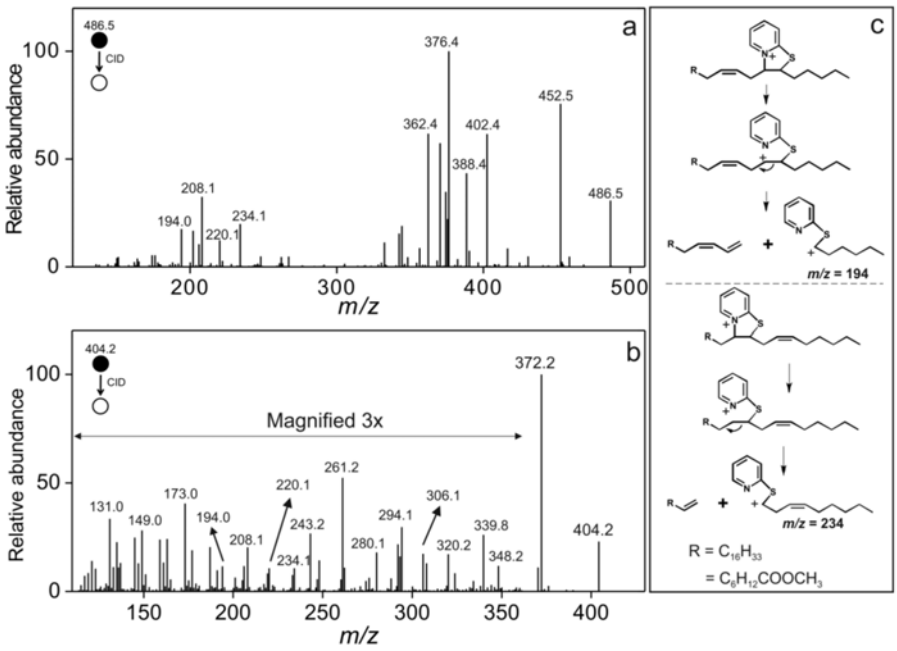

Fig. 4 Fragmentation mass spectra of (a) monosubstituted heptacosa-6,9-diene and (b) monosubstituted methyl linoleate, (c) formation of diagnostic peaks 194 and 234 with a proposed fragmentation mechanism.

3.2.3 Diunsaturated compounds

Two diunsaturated compounds (heptacosa-6,9-diene and methyl linoleate) with methylene-interrupted double bond arrangement were successfully derivatized with Aldrithiol-2. In mass spectra of heptacosa-6,9-diene and methyl linoleate, the monosubstituted derivative was observed almost exclusively. Disubstituted derivatives were formed only negligibly most likely because of the electrostatic repulsion between the two charged sites, which would be formed.

Fragmentation mass spectra of monosubstituted heptacosa-6,9-diene and monosubstituted methyl linoleate contained the same peak pattern composed of *m/z* 194, *m/z* 208, *m/z* 220, and *m/z* 234 (Fig. 4a and 4b) because both molecules share the same structural motif (see proposed fragmentation scheme in Fig. 4c). This peak pattern pointed out the position of the original double bonds. The fragments generated from the other side of the molecules differed because of their different structures. The monosubstituted heptacosa-6,9-diene provided *m/z* 362, *m/z* 376, *m/z* 388, and *m/z* 402 (Fig. 4a), while the monosubstituted methyl linoleate gave *m/z* 280, *m/z* 294, *m/z* 306, and *m/z* 320, together with additional peaks like neutral loss of methanol (*m/z* 372); Fig. 4b.

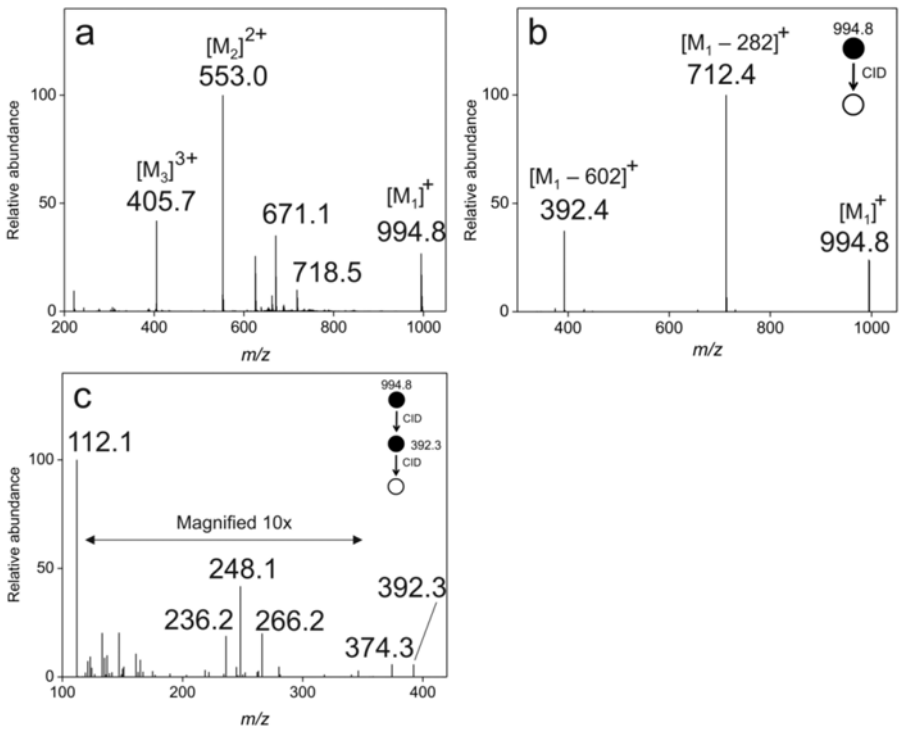

Fig. 5 Full-MS mass spectrum of (a) triolein derivatives, (b) fragmentation mass spectrum of monosubstituted triolein, and fragmentation mass spectrum (MS^3) of *m/z* 394.2 from Fig. 4b.

3.2.4 Triunsaturated compound

Trielaidin formed mono- di- and trisubstituted derivatives and the charge state of derivatized molecules was equal to the degree of substitution. Full-MS mass spectrum of trielaidin showed three major products; *m/z* 994.7 (monosubstituted derivative, M_1); *m/z* 553.0 (disubstituted derivative, M_2), and *m/z* 405.6 (trisubstituted derivative, M_3); Fig. 5a. Monosubstituted derivative was fragmented to two main ions, $[M_1–282]^+$ (*m/z* 712) that corresponds to the neutral loss of elaidic acid and $[M–602]^+$ (*m/z* 392) that is structurally an elaidic acid/aldrithiol-2 derivative (Fig. 5b). Fragmentation of *m/z* 392 provided mass spectrum (Fig. 5c) similar oleic acid derivative (Fig. 3b). Fragmentation mass spectra of multiply substituted derivatives were not suitable for double bond localization because they were mostly fragmented to less substituted derivatives and therefore additional fragmentation steps in the elucidation process would be required.

4. Conclusions

We have developed a method for localization of double bond in unsaturated compounds using derivatization with Aldrithiol-2. The reaction introduced permanent charge into the molecules, which resulted in enhanced detectability of rather hydrophobic analytes in ESI-MS. The reaction was successfully applied to various lipids. In the case of di- and polyunsaturated compounds, the structure of the reaction products depends on the arrangement of double bonds. For methylene-interrupted double bonds, only monosubstituted product was formed under the reaction conditions. Double bonds far away from each other (in the case of trielaidin) were derivatized all and mono-, di-, and trisubstituted derivatives were observed in MS. The charge was raised by 1 with each substituted double bond.

References

[1] Ma X., Xia Y.: Pinpointing double bonds in lipids by Paternò-Büchi reactions and mass spectrometry. *Angew. Chem. Int. Ed.* **53** (2014), 2592–2596.

[2] Martinez- Seara H., Róg T., Pasenkiewicz-Gierula M., Vattulainen I., Karttunen M., Reigada R.: Effect of double bond position on lipid bilayer properties: Insight through atomistic simulations. *J. Phys. Chem. B* **111** (2007), 11162–11168.

[3] Grillet M., Dartevelle L., Ferveur J.-F.: A *Drosophila* male pheromone affects female sexual receptivity. *Proc. Biol. Sci.* **273** (2006), 315–323.

[4] Sundar B., Ravi Latha B., Vijayashanthi R., Pandian S.S.: (*Z*)-9-Tricosene based *Musca domestica* lure study on a garbage dump yard using plywood sticky trap baited with fish meal. *J. Parasit. Dis.* **40** (2016), 32–35.

[5] Bierl-Leonhardt B.A., DeVilbiss E.D., Plimmer J.R.: Location of double-bond position in long-chain aldehydes and acetates, by mass spectral analysis of epoxide derivatives. *J. Chromatogr. Sci.* **18** (1980), 364–367.

[6] Nichols P.D., Guckert J.B., White D.C.: Determination of monounsaturated fatty acid double-bond position and geometry for microbial monocultures and complex consortia by capillary GC-MS of their dimethyl disulphide adducts. *J. Microbiol. Meth.* **5** (1986), 49–55.

[7] Niehaus W.G., Ryhage R.: Determination of double bond positions in polyunsaturated fatty acids by combination gas chromatography-mass spectrometry. *Anal. Chem.* **40** (1968), 1840–1847 .

[8] Zaikin V., Halket J.: *A Handbook of Derivatives for Mass Spectrometry*. Chichester, IM Publications LLP 2009.

[9] Van Berkel G.J., Quirke J. Martin E., Adams C.L.: Derivatization for electrospray ionization-mass spectrometry. 4. Alkenes and alkynes. *Rapid Commun. Mass Spectrom.* **14** (2000), 849–858.

[10] Yuan G., Yan J.: A method for the identification of the double-bond position of isomeric linear tetradecenols and related compounds based on mass spectra of dimethyl disulfide derivatives. *Rapid Commun. Mass Spectrom.* **16** (2002), 11–14.

[11] Potapov V.A., Ishigeev R.S., Amosova S.V., Borodina T.M.: Synthesis of a novel family of water-soluble 2*H*,3*H*-[1,3]thia- and -selenazolo[3,2-a]pyridin-4-ium heterocycles by annulation reactions. *Tetrahedron Lett.* **60** (2019), 475–479.

Electrochemical quantification of arrow poison, tubocurarine: application on biological fluids

Sladjana Djurdjic[a,*], Vesna Stankovic[b], Ľubomir Švorc[c], Jelena Mutic[a], Dalibor Stankovic[d]

[a] *Faculty of Chemistry, University of Belgrade, Studentski trg 12-16, 11000 Belgrade, Serbia* ✉ *sladjanadj@chem.bg.ac.rs*
[b] *Institute of Chemistry, Technology and Metallurgy, University of Belgrade, Njegoseva 12, 11000 Belgrade, Serbia*
[c] *Faculty of Chemical and Food Technology, Slovak University of Technology in Bratislava Radlinského 9, Bratislava, Slovak Republic*
[d] *The Vinca Institute of Nuclear Sciences, University of Belgrade, 11001 Belgrade, Serbia*

Keywords
arrow poison
electrochemistry
tubocurarine

Abstract
The electrochemical behavior and quantitative analysis of the natural alkaloid, tubocurarine (arrow poison), were studied. Electrochemical behavior was investigated using several organic solvents and aqueous buffers, at different pH, as supporting electrolytes. After selection of the most appropriate supporting electrolyte and investigation of its electrochemical behavior, analytical procedures for quantitative analysis of tubocurarine were developed in acetonitrile:methanol (80:20, *v/v*) mixture and in 1 mol L^{-1} nitric acid. Remarkable selectivity and good sensitivity were obtained after the tubocurarine quantification method was optimized, allowing application of the developed method for tubocurarine quantification in biological fluids.

1. Introduction

Tubocurarine, also well known as d-tubocurarine, is a natural plant alkaloid isolated from the plant *Chondrodendron tomentosum*, which is a species of the *Menispermaceae* family [1, 2]. *Chondrodendron tomentosum* is a tropical liana widely found in Central and South American regions. Tubocurarine was initially used as arrow poison, while later, this compound was used during surgeries as a muscle relaxant. This alkaloid competes with acetylcholine for the nicotinic receptors at the neuromuscular junction of skeletal muscles, thereby inhibiting the action of acetylcholine and blocking the neural transmission without depolarizing the postsynaptic membrane [3, 4]. This can lead to skeletal muscle relaxation and paralysis. Tubocurarine is known also as the chief alkaloid in

tobacco products and can have several influences on the central nervous system, including stereo-selectively binding to nicotinic-cholinergic receptors at the autonomic ganglia in the adrenal medulla, at neuromuscular junctions, and in the brain. Due to this knowledge of the electrochemical behavior and quantitative analysis of tubocurarine should be beneficial for further research dealing with this compound [5, 6].

Therefore, the aims of this work were to investigate the electrochemical behavior of tubocurarine, to propose an analytical procedure for tubocurarine quantification. This study was conducted using an unmodified and green electrochemical sensor – a boron doped diamond electrode (BDDE) in both organic and aqueous supporting electrolytes. The effects of possible interfering compounds were examined, and the developed method was successfully applied to quantify tubocurarine in biological fluids.

2. Experimental

2.1 Reagents and chemicals

All reagents used were analytical grade and supplied by Merck, Germany. A standard solution of tubocurarine (1×10^{-3} mol L^{-1}) was prepared by dissolving the powder with the minimum amount of methanol and diluting in appropriate solvent (organic or aqueous).

2.2 Instrumentation

All measurements were obtained using a potentiostat/galvanostat CHI 760b (USA). Three electrode cells with total volume of 10 mL were used for electrochemical experiments. A boron doped diamond electrode (3 mm diameter, 1000 mg L^{-1} of boron doping level, Windsor Scientific, UK) was used as the working electrode, while a 3 mol L^{-1} KCl Ag/AgCl electrode and a large surface platinum wire were used as reference and counter electrodes, respectively.

2.3 Supporting electrolytes

The electrochemical behavior of tubocurarine was examined in organic and aqueous supporting electrolytes. Dimethylsulfoxide, *N,N*-dimethylformamide, and a mixture acetonitrile:methanol (80:20, *v/v*) were used as organic supporting electrolytes. All organic supporting electrolytes contained 0.1 mol L^{-1} tetrabutylammonium hexa-fluorophosphate. Nitric acid and Britton-Robinson buffer solution were used as aqueous supporting electrolytes.

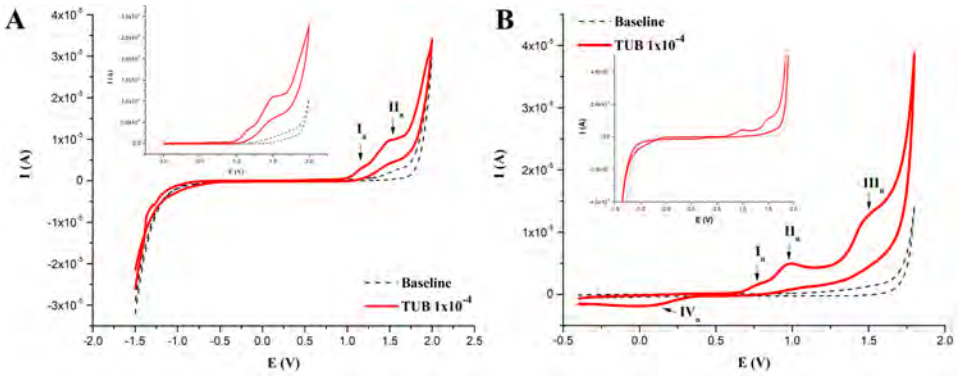

Fig. 1 Cyclic voltammogram of 1×10^{-4} mol L^{-1} tubocurarine in (A) acetonitrile:methanol mixture (80:20, *v/v*), and (B) in 0.1 mol L^{-1} nitric acid (pH = 1.0) at the BDDE. Scan rate 100 mV s^{-1}.

2.4 Biological sample preparation

Fresh urine samples (0.5 mL) were diluted to 5 mL with supporting electrolyte (1 mol L^{-1} nitric acid, pH = 0.0). Blood samples were prepared according this reference [7]. Samples were spiked with different aliquots of tubocurarine stock solution. Concentrations of tubocurarine in urine and blood serum samples were calculated from a calibration curve. Recovery tests were conducted by adding known amounts of tubocurarine into urine and sera.

3. Results and discussion

3.1 Electrochemical behavior of tubocurarine

Cyclic voltammetry was used to study the electrochemical behavior of tubocurarine (1×10^{-4} mol L^{-1}) in the potential range of –1.5 to +2.0 V, with scan rate 100 mV s^{-1}. In the supporting electrolytes *N,N*-dimethylformamide and Britton-Robinson buffer solution, no oxidation or reduction peaks were noticed and no electrochemical activity of tubocurarine at the BDDE was observed. Oxidation of tubocurarine at the BDDE occurred in the supporting electrolytes dimethylsulfoxide, the acetonitrile:methanol (80:20, *v/v*) mixture (Fig. 1A), and in 0.1 mol L^{-1} nitric acid (pH = 1.0) (Fig. 1B). Also, reductions in corresponding peaks currents were noticed in the solution of nitric acid as supporting electrolyte. Taking into account peak currents and shapes, the acetonitrile:methanol (80:20, *v/v*) mixture was selected as the organic supporting electrolyte, and for 0.1 mol L^{-1} nitric acid was selected as the aqueous supporting electrolyte for further investigating the electrochemical behavior of tubocurarine.

In the acetonitrile:methanol (80:20, *v/v*) mixture, two well-defined and sharp oxidation peaks of tubocurarine at potentials 1.15 V (I_a) and 1.45 V (II_a) were observed (Fig. 1A). Also, neither of the corresponding peaks were reduced, which

indicates irreversible oxidation of tubocurarine occurred in the acetonitrile:methanol supporting electrolyte at the BDDE. The inset in Fig. 1A shows the electrochemical behavior of tubocurarine in the positive potential region of the acetonitrile:methanol (80:20, *v/v*) mixture at the BDDE.

In 0.1 mol L^{-1} nitric acid (pH = 1.0), in the anodic potential range, three well separated oxidation peaks of tubocurarine were observed. At a potential of around 0.75 V, oxidation of tubocurarine occurred with low current intensity (I_n), but at potentials of around 1.0 V (II_n) and 1.5 V (III_n), two well-defined and sharp oxidation peaks of tubocurarine were measured (Fig. 1B). Also, cathodic electroactivity of tubocurarine at potential of around 0.0 V (IV_n) was recorded, from which it can be concluded that the redox behavior of tubocurarine occurs as a quasi-reversible process. The influence of different pH of nitric acid were then examined. The best electrochemical response of tubocurarine was noted at pH = 0.0. Therefore, for further analysis, 1 mol L^{-1} nitric acid (pH = 0.0) was used as the aqueous supporting electrolyte.

3.2 Development of the selected electroanalytical method

Electrochemical responses of 1×10^{-4} mol L^{-1} tubocurarine in organic (acetonitrile:methanol mixture) and aqueous (1 mol L^{-1} nitric acid) supporting electrolytes were initially measured using two voltammetric methods, square wave voltammetry (SWV) and differential pulse voltammetry (DPV). For both types of supporting electrolyte, the SWV technique provided well defined peak shape and higher peak current, so for this reason, this method was used for all further studies. In order to increase SWV performance, the important parameters of amplitude and frequency were optimized. Also, oxidation peaks of tubocurarine in both supporting electrolytes were monitored during optimization and quantification of the parameters (amplitude 80 mV and frequency 50 Hz for acetonitrile:methanol mixture; amplitude 50 mV and frequency 40 Hz for 1 mol L^{-1} nitric acid, pH = 0.0).

3.3 Analytical performance of the proposed method

Working linear ranges for tubocurarine quantification at the BDD electrode in both supporting electrolytes were measured under optimized SWV parameters. In the acetonitrile.methanol mixture, tubocurarine was studied in the concentration range of 4×10^{-6} to 1×10^{-4} mol L^{-1}. In this concentration range, the oxidation peak of tubocurarine at potential of 1.15 V (I_a) was not well defined. Linear dependence of concentrations and corresponding currents was monitored using the oxidation peak of tubocurarine at potential of 1.45 V (II_a); Fig. 2. The inset of Fig. 2 shows the calibration curve for these measurements. The limit of detection of tubocurarine in the acetonitrile:methanol mixture at the BDDE was calculated from the calibration curve and it was 3.07×10^{-6} mol L^{-1}.

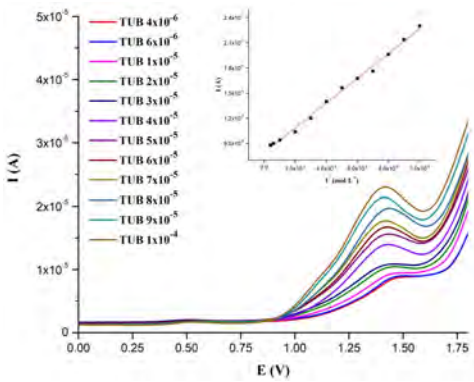

Fig. 2 SW voltammogram obtained for different concentrations of tubocurarine in acetonitrile:methanol (80:20, *v/v*) mixture. Insert figure shows the corresponding calibration curve.

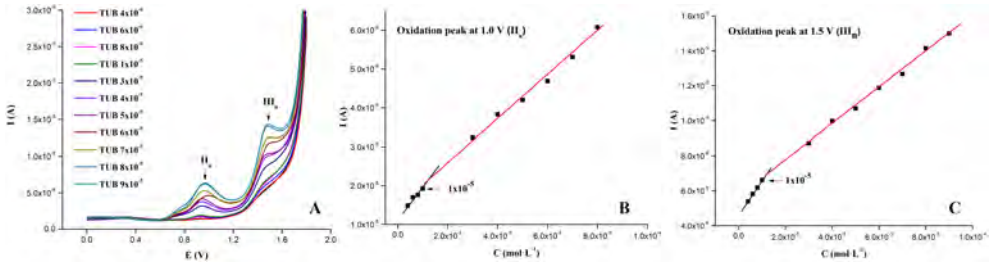

Fig. 3 SW voltammogram of 4×10^{-6} to 9×10^{-5} mol L^{-1} tubocurarine in (a) 1 mol L^{-1} nitric acid (pH = 0.0). Calibration curve for (B) II_n oxidation peak, and (C) III_n oxidation peak.

A similar concentration range of tubocurarine was studied in 1 mol L^{-1} nitric acid, pH = 0.0 (4×10^{-6} to 9×10^{-5} mol L^{-1}). In this case, the oxidation peaks of tubocurarine were measured at 1.0 V (II_n) and 1.5 V (III_n), while for first oxidation peak and reduction peak, this dependence was not linear; Fig. 3A. Tubocurarine shows one type of linearity in concentration range from 4×10^{-6} to $1x10^{-5}$ mol L^{-1} for both oxidation peaks. Another type of linear dependence tubocurarine also shows in the concentration range from 2×10^{-6} mol L^{-1} to 9×10^{-5} mol L^{-1} ; Fig. 3B, 3C. Limits of detection for tubocurarine in 1 mol L^{-1} nitric acid (pH = 0.0) were calculated for oxidation peaks II_n and III_n in the same way as for the organic supporting electrolyte mixture, and were 2.45×10^{-6} mol L^{-1} and 5.28×10^{-7} mol L^{-1}, respectively.

When we compared the electrochemical behavior of tubocurarine in organic and aqueous supporting electrolytes, it was clear that tubocurarine oxidation produced more desirable characteristics in 1 mol L^{-1} nitric acid at the BDDE .

3.5 Application in real biological samples

The accuracy and precision of the proposed electroanalytical method for quantifying tubocurarine were measured in urine and blood samples. Urine and blood serum samples were prepared as described in section 2. Diluted urine and blood

Table 1
Comparison of theoretical tubocurarine contents from artificially spiked biological samples with the results obtained using the new method.

Matrix	c(tubocurarine)/mol L^{-1}			Recovery/%	
	Spiked	Found		II_n peak	III_n peak
		II_n peak	III_n peak		
Blood	8×10^{-6}	7.63×10^{-6}	7.85×10^{-6}	95	98
	$5x10^{-5}$	4.96×10^{-5}	4.57×10^{-5}	99	91
Urine	$3x10^{-5}$	2.79×10^{-5}	2.83×10^{-5}	93	94
	$4x10^{-5}$	3.97×10^{-5}	3.87×10^{-5}	99	97

serum samples were spiked with different volumes of tubocurarine stock solution. Using the optimized method to quantify tubocurarine in these artificially spiked biological samples resulted in good agreement of the results obtained with the calculated tubocurarine concentrations (Table 1). Recovery values indicated good selectivity, excellent accuracy and precision of the optimized method. We also found minimal impact of the biological matrix during tubocurarine quantification in these biological samples.

4. Conclusions

In summary, the electrochemical behavior and quantification of tubocurarine was investigated in various electrolytes. Tubocurarine behaves differently in organic solvent than in water. The combination of pulse method with the advantages of using an unmodified BDDE resulted in the development of a selective, sensitive, accurate, and precise method for tubocurarine quantification, which should be suitable for application in various biological fluid matrices.

Acknowledgments

This work was supported by the Ministry of Education, Science and Technology, the Republic of Serbia, Project No. OI 172030.

References

[1] Aronson J.K.: *Meyler's Side Effects of Drugs.* 16th ed. Oxford, Elsevier 2016.
[2] *Encyclopedia of Toxicology.* 3th ed. P. Wexler (ed.). Oxford, Academic Press 2014.
[3] Goličnik M., Fournier D., Stojan J.: Acceleration of *Drosophila melanogaster* acetylcholinesterase methanesulfonylation: Peripheral ligand d-tubocurarine enhances the affinity for small methanesulfonylfluoride. *Chem. Biol. Interact.* **139** (2002), 145–157.
[4] Stojan J., Pavlic M.: On the inhibition of cholinesterase by d-tubocurarine. *Biochim. Biophys. Acta* **1079** (1991), 96–102.
[5] Burr S.A., Leung Y.L.: Curare (d-Tubocurarine). In: *Encyclopedia of Toxicology.* 3th ed. P. Wexler (ed.). Oxford, Academic Press 2014.

[6] Atallah M.M., Daif A.A., Saied M.M.A., Sonbul Z.M.: Neuromuscular blocking activity of tubocurarine in patients with diabetes mellitus. *Br. J. Anaesth.* **68** (1992), 567–569.
[7] Stankovic D., Svorc L., Mariano J.F.M. L., Ortner A., Kalcher K.: Electrochemical determination of natural drug colchicine in pharmaceuticals and human serum sample and its interaction with DNA. *Electroanalysis* **29** (2017), 2276–2281.

Determination of food additives quinine and indigo carmine in pharmaceutical drugs by the fluorimetry

Alena Nikolaeva*, Elena Korotkova

Department of Chemical Engineering, Engineering School of Natural Resources , National Research Tomsk Polytechnic University, Lenin avenue 30, 634 050 Tomsk, Russia ✉ *ivanovaaa@tpu.ru*

Keywords
drugs
fluorimetry
indigo carmine
quinine

Abstract
Fluorimetric approaches for determining of food additives quinine and indigo carmine in pharmaceutical preparations have been developed. These approaches are distinguished by high sensitivity compared with the known methods. For the quinine: the excitation wavelength is 353 nm, the luminescence wavelength is 452 nm and the sulfuric acid concentration is 0.01 M. For the indigo carmine: the excitation wavelength is 270 nm, the luminescence wavelength is 410 nm and the sodium hydroxide concentration is 1.00 M. Indigo carmine dye was determined by the luminescence signal of a leuco compound formed during the reduction of indigo carmine in alkali. The results of the determination of quinine and indigo carmine in pharmaceutical preparations have a good agreement with the results obtained by known methods – spectrophotometric and chromatographic. The detection limit of the developed fluorimetric method is: for quinine 0.0012 mg l^{-1}, for indigo carmine 0.0033 mg l^{-1}. The obtained detection limit is lower than the known methods for analyzing drugs.

1. Introduction

Food additives are substances that are added to food in the process of their production, packaging, transporting, and storage to give them certain expected properties [1]. For example, to the necessary flavor (flavors), a certain color (dyes), a long shelf life (preservatives), taste, the desired consistency, and so on. Currently, food additives are used not only in the food industry, but also in the pharmaceutical industry. Dyes are the most popular additives in the pharmaceutical industry, which are used for coloration of capsules and tablets.

The most widespread and numerous classes of food additives are dyes and flavors. Therefore, two food additives from these classes were selected for research; this is the flavoring additive quinine and the synthetic food dye indigo carmine.

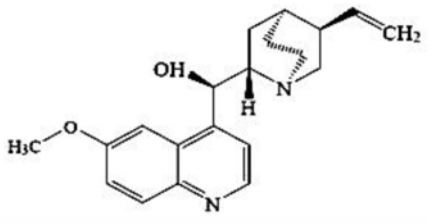

Fig. 1 Structural formula of quinine.

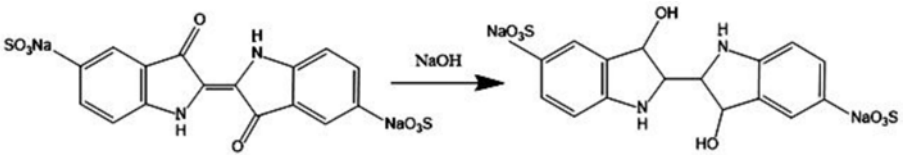

Fig. 2 The reaction of the formation of leuco compound of indigo carmine in alkaline medium.

Quinine (6'-methoxycinchonan-9-ol) is the main alkaloid of the cinchona bark, which is known as the most effective anti-malarial drug. The structural formula of quinine is shown in Fig. 1. Quinine has antipyretic and analgesic properties [2]. Quinine is also used in obstetric practice [3] to enhance labor activity, but an abortion may occur during an overdose [4]. Recent exploring in rats has shown that quinine completely blocks ovulation and causes oxidative stress in the ovary of rats [5]. In combination with analginum, quinine is used against headaches.

Indigo carmine (E132, Indigotine, Food Blue 1, Acid Blue 74, Indigo Blue, Pigment Blue 66, Vat Blue 1) belongs to the class of indigoid dyes, the main feature of which is the ability to restore to a water-soluble colorless leuco compound (Fig. 2) in alkaline medium [6].

Advantageous for industry food additives are often toxic to people's health, especially for children. For this reason, control over the use of food additives in the food and pharmaceutical industries has been increasing in recent years. The use of known methods of analysis of food additives is often difficult due to the high cost of equipment and the need to use hazardous chemicals.

Analysis of the literature data showed that to date for the determination of food additives the most popular methods are chromatographic, spectrophotometric, electrochemical and capillary electrophoresis. All of the above methods for determining food additives in medicines have their advantages and disadvantages, so research in the field of qualitative and quantitative analysis of food additives is still relevant.

In addition to the above methods for the determination of food additives, there are references in the literature about fluorimetric methods for the determination of food additives. The method of fluorimetry has a number of advantages compared with the known methods: high sensitivity, a wide range of detectable concentrations, ability to analyze complex mixtures, expressivity, simplicity and low cost of equipment. All these advantages allow the use of the fluorimetric

method for the determination of the dietary additives of quinine and indigo carmine, not only in food products, but also in medicinal preparations.

The aim of the work is to develop fluorimetric methods for the determination of food additives quinine (flavoring additive) and indigo carmine (synthetic food dye) in pharmaceutical preparations.

2. Experimental

2.1 Reagents and chemicals

Work solutions were prepared with a basic substance content of at least 95%. Quinine powder was dissolved in 0.01 M sulfuric acid; indigo carmine powder was dissolved in 1.00 M sodium hydroxide.

The following pharmaceutical drugs were selected for analysis:

- tablets *Analgin-quinine,* manufacturer Sopharma, Bulgaria;
- tablets *Levomitsetin Aktivit*, Russia (antibacterial agent: chloramphenicol);
- vitamins for children *Pikovit*, manufacturer of JSC KRKA, Slovenia.

2.2 Instrumentation

The investigations were performed on the instrument Fluoforat-02-Panorama spectrofluorometer. The device is designed to record the transmission spectrum of solutions in the UV and visible regions, as well as to record the luminescence spectrum.

2.3 Sample preparation

Sample preparation of the investigated objects consisted in the preliminary dissolution of the drug in 20 ml of 0.01 M sulfuric acid for the determination of quinine and in 20 ml of 1.00 M sodium hydroxide for the determination of indigo carmine. The resulting solution was centrifuged and diluted 100 times. The intensity of the diluted solution was measured and the concentrations of quinine and indigo carmine were calculated and recalculated into 20 ml of the initial solution.

3. Results and discussion

3.1. Quinine

For the quantitative determination of quinine in pharmaceutical drugs, a calibration dependence of the intensity of the luminescent signal on the concentration of

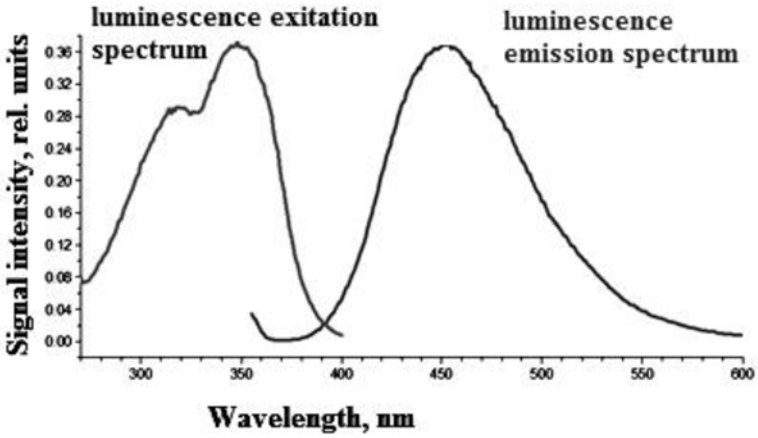

Fig. 3 The excitation spectrum and the emission spectrum of quinine in 0.01 M sulfuric acid.

Table 1
Results of the determination of the quinine and the indigo carmine in drugs by fluorimetric, spectrophotometric and chromatographic methods; $n = 3$, $p = 0.95$, $t_{table} = 2.78$.

Sample	Food additive	Fluorimetry		Spectrophotometry		Chromatography		$t_{calc.}$
		c/mg L^{-1}	s_r	c/mg L^{-1}	s_r	c/mg L^{-1}	s_r	
Analgin-quinine	quinine	51.41±0.43	0.0033	52.3±2.7	0.021	–[a]	–[a]	0.017
Levomitsetin	indigo carmine	0.01307±0.09	0.027	–[a]	–[a]	0.01642±0.00049	0.012	2.7
Pikovit	indigo carmine	0.0047±0.0011	0.098	–[a]	–[a]	0.00415±0.00102	0.099	0.63

[a] Not determined.

quinine in 0.01 M sulfuric acid (Fig. 3) was built in the concentration range from 0.10 to 1.00 mg l^{-1} with the regression equation

$$y = 0.3533\,C + 0.0022 \quad (1)$$

To assess the correctness of the results of the developed fluorimetric method, a spectrophotometric analysis method was used at an absorption wavelength of 331 nm. For the comparison method, the calibration dependence of the optical density of the solution on the concentration of quinine in sulfuric acid was constructed in the concentration range from 1.00 to 10.00 mg l^{-1} with the regression equation

$$y = 0.0152\,C + 0.1125 \quad (2)$$

The results are presented in Table 1.

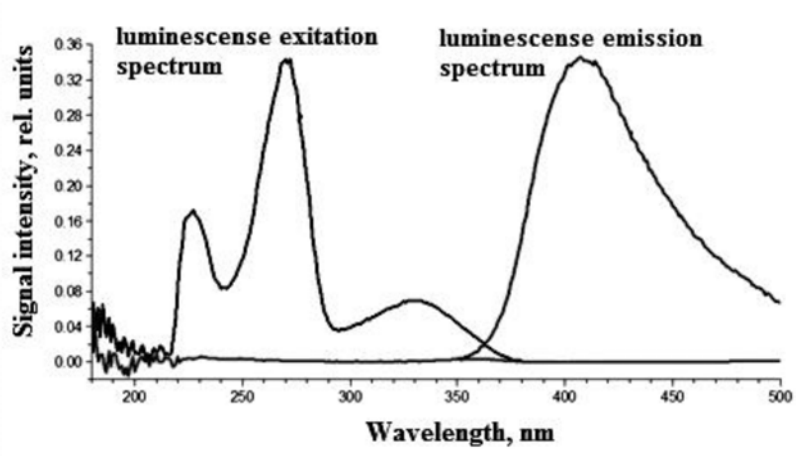

Fig. 4 Spectrum of excitation and emission of leuco compound of synthetic food dye indigo carmine.

3.2. Indigo carmine

From the synchronous scanning mode an optimal excitation wavelength of 270 nm was established, at which the most intense luminescence of indigo carmine leuco compound at a wavelength of 410 nm was observed (Fig. 4).

For the quantitative determination of the indigo carmine, a calibration graph of the intensity of the luminescent signal versus the concentration of indigo carmine leuco compound in 1.00 M sodium hydroxide was constructed in the concentration range from 0.10 to 1.00 mg l^{-1} with the regression equation

$$y = 0.1287\,C + 0.0041 \tag{3}$$

To assess the correctness of the results of the fluorimetric method being developed, high-performance liquid chromatography was used with UV detection at 610 nm. The average retention time was 5.10 minutes. For the comparison method, the calibration dependence of the peak area on the retention time of an aqueous solution of indigo carmine dye was constructed in the concentration range from 0.10 to 100.00 mg l^{-1} with the regression equation

$$y = 37.133\,C - 3.5983 \tag{4}$$

The results are presented in Table 1. As can be seen, there is a good convergence of the results of quinine and indigo carmine determination by fluorimetric, spectrophotometric and chromatographic methods of analysis.

4. Conclusions

For the first time, a method for determining quinine in pharmaceutical drugs using fluorimetry was developed. A new approach has been developed for the fluorimetric determination of indigo carmine synthetic food dye in medicinal preparations based on the luminescence signal of its leuco compound in alkali. Under the found conditions for the determination of quinine in drugs, the detection limit was 0.0012 mg l.$^{-1}$ The detection limit of indigo carmine by the fluorimetric method was 0.0033 mg l^{-1}. A high detection limit for quinine and indigo carmine was obtained in comparison with the majority of well-known works [7–11].

Acknowledgments

This investigation was supported by State Program RF "Science". Project N 4.5752.2017.

References

[1] Martins F.C.O., Sentanin M. A., De Souza D.: Analytical methods in food additives determination: compounds with functional applications. *J. Food Chem.* **272** (2019), 732–750.
[2] Samanidou V. F., Evaggelopoulou E. N., Papadoyannis I. N.: Simple and rapid HPLC method for the determination of quinine in soft drinks using fluorescence detection. *J. Liq. Chromatogr. Relat. Technol.* **27** (2004), 2397–2406.
[3] Gopi P., Sarveswari S.: Effective water mediated green synthesis of polysubstituted quinolines without energy expenditure. *Monatsh. Chem.* **148** (2016), 1043–1049.
[4] www. pubchem.ncbi.nlm.nih.gov/compound/Quinine#section=Top (accessed 10th May, 2019).
[5] Gbotolorun S.C., Inikori O., Bamisi O.D., Osinubi A.A.A., Okanlawon A.O.: Quinine inhibits ovulation and produces oxidative stress in the ovary of cyclic Sprague-Dawley rats. *Afr. Health Sci.* **18** (2018), 253–259.
[6] http://www.xumuk.ru/encyklopedia/1679.html (accessed 3th June, 2019).
[7] https://www.perkinelmer.com/lab-solutions/resources/docs/APP_Quinine_in_Tonic_Water_014133_01.pdf (accessed 25th July, 2019).
[8] Kluska M., Marciniuk-Kluska A., Prukała D., Prukała W.: Analytics of quinine and its derivatives. *Crit. Rev. Anal. Chem.* **46** (2015), 139–145.
[9] Reijenga J.C., Aben G.V.A., Lemmens A.A.G., Verheggen T.P.E.M., De Bruijn C.H.M.M., Everaerts F.M.: Determination of quinine in beverages, pharmaceutical preparations and urine by isotachophoresis. *J. Chromatogr. A* **320** (1985), 245–252.
[10] Altınöz S., Toptan S.: Simultaneous determination of Indigotin and Ponceau-4R in food samples by using Vierordt's method, ratio spectra first order derivative and derivative UV spectrophoto-metry. *J. Food Comp. Anal.* **16** (2003), 517–530.
[11] Boley N. P., Crosby N. T., Roper P., Somers L. Determination of Indigo Carmine in boiled sweets and similar confectionery products. *Analyst* **106** (1981), 710–713.

Application of GC-MS/MS technique for the determination of benzodiazepines in blood samples

Laura Banaszkiewicz*, Mateusz Kacper Woźniak, Agata Kot-Wasik

Department of Analytical Chemistry, Faculty of Chemistry, Gdańsk University of Technology, 11/12 Narutowicza Street, 80-233 Gdańsk, Poland ✉ *laura.banaszkiewicz@pg.edu.pl*

Keywords
benzodiazepines
GC-MS/MS
new psychoactive substances
blood samples

Abstract
Benzodiazepines are widely used as pharmaceuticals in medicine. However, due to psychostimulatory effect of benzodiazepines, in the last decade, they are more and more often used as drugs of abuse. These compounds produce similar effects to classical illicit drugs and are sold as "legal" alternatives to them as new psychoactive substances. Currently new benzodiazepines, named designer benzodiazepines, are synthesized each year by a simple modification of registered drug structure or their metabolites. The misuse and abuse of benzodiazepines has become an increasing problem in many countries. Due to this phenomenon there is a strong need to develop new analytical methods for the determination of a whole range of substances in biological specimens for forensic toxicology. A rapid, sensitive and robust GC-MS/MS-based method with a simple liquid-liquid extraction for the determination of 10 benzodiazepines in whole blood samples was developed. The assay achieved satisfactory validation parameters, such as: inter-day accuracy (91.8–118.6%), and precision (2.8–14.9%). The limit of detection and limit of quantification were in the range of 0.02–0.53 ng mL^{-1} and 1–2 ng mL^{-1}, respectively. The developed procedure can be widely applicable for rapid screening of new drugs of abuse in forensic or clinical cases.

1. Introduction

Benzodiazepines, due to their anxiolytic, hypnotic, anticonvulsive, and muscle-relaxant properties, are widely used in medicine for treatment of various mental illnesses. These compounds are typically prescribed by medical professionals for insomnia, anxiety, agitation, muscle spasms, seizures, alcohol withdrawal or as a premedication for medical procedure because of a wide spectrum of therapeutic result [1, 2]. However, due to psychostimulatory effect of benzodiazepines, a phenomenon involving misuse or abuse these types of compounds (as drugs of abuse) is observed. Moreover, in recent years, many new compounds belonging to

benzodiazepines group were synthesized as modification of existing substances and were introduced into illicit trade. New benzodiazepines are typically sold as "designer benzodiazepines" giving recreation feeling similar to the other new psychoactive substances [3, 4]. The easy availability both classical and designer benzodiazepines consists a serious societal problem and leads to health risks.

Chemically benzodiazepines are the fusion of benzene and diazepine ring with various substituents of side chains, what gives these compounds unique physico-chemical properties. The extensive research associated with these structures resulted in an introduction a variety of psychoactive substances that never got a marketing authorization which leads to illegal distribution these substances in drug market and appearance of more new derivatives.

Problems associated with the detection of benzodiazepines in complex matrices, such as blood and urine, consist an interesting area in various scopes to develop rapid and sensitive analytical procedures. Currently, many methods for benzodiazepines determination have been used. They mainly utilizing immuno-assays techniques and hyphenated techniques (LC-MS/MS and GC-MS), allowing to obtain a valuable source data set useful in clinical research, quality control and legal studies [5]. However, in toxicology analysis, new analytical procedures are still strongly required in order to simplify sample preparation step and to reduce volume of sample required for the extraction. The determination of benzodiazepines in biological specimen is still challenging owing mainly due to a large number of these compounds available. Such results can be useful for toxicological analysis in order to establish magnitude of the abuse problem of these compounds or in the cause of death [6].

Despite the large number of published data associated with the determination of benzodiazepines, to the best of our knowledge, there is a lack of information concerning the application of GC–MS/MS for the analysis of these compounds in human biological fluids. Therefore, the aim of this study was to verify potentiality of application of a GC-MS/MS technique for the detection and quantification of benzodiazepines in whole blood samples for occupational and forensic purposes.

2. Experimental

2.1 Standards, reagents and chemicals

The certified standards of benzodiazepines used in this study were purchased from LGC Standards (UK), Cayman Chemical Company (USA), and Cerilliant (USA) as separate solutions in methanol at a concentration of 1 mg mL^{-1}. The standards have a minimum purity of 98%. Diazepam-D_5 was used as the internal standard. Diisopropyl ether, ethyl acetate, and methanol were supplied by Sigma-Aldrich (USA). All solvents used were of HPLC grade. Analytical-grade sodium carbonate and sodium bicarbonate powder were obtained from POCH S.A. (Poland). Both salts were used for the preparation of carbonate buffer solution at pH = 9.2 by

dissolving appropriate mass of powder in ultrapure water. Water was purified by a Millipore Milli-Q Gradient A10 water system(Merck, Warszawa, Poland). Stock solutions of analytes (as a mixture) and the internal standard stock solution were prepared by dilution of the certified standards with methanol and were stored at –20 °C until use.

2.2 Biological specimens

Blank (drug-free) blood samples were collected from volunteers non-consumers of any drugs and were obtained from a regional blood donation bank (Gdańsk, Poland). Blank blood samples were used for the development and validation of the method and were also stored in –20 °C prior to analysis.

2.2 Instrumentation

The analysis were performed using GC-2010 PLUS system with TQ8050 triple quadrupole mass spectrometer (Shimadzu, Japan). Chromatographic separation of the analytes was achieved on Zebron ZB-5MSi capillary column (30 m × 0.25 mm i.d., 0.25 µm; Torrance, USA). Hellium (grade 5.0) was used as carrier gas with an initial flow rate of 1 mL min^{-1}. Then, a constant gas linear velocity was maintained at 38 cm s^{-1}. The splitless injection mode for 1 min under High Pressure Injection mode (300 kPa; 0.5 min) was used followed by split mode (20:1). The oven temperature gradient program was as follows: from 150 °C (held 1 min) to 200 °C at 20 °C min^{-1} (held 1 min), then ramp to 285 °C at 10 °C min^{-1} (held 5 min) and finally ramp to 310 °C at 10 °C min^{-1} (held 4 min). The temperature of the injection port, MS transfer line and ion source were set at 260, 285 and 250 °C, respectively. MS was operated in positive electronic ionization mode. The ion source temperature was set at 250°C. Argon (grade 5.0) was used as the collision-induced dissociation gas. Quantification was performed using multiple reaction monitoring transitions. The specific transitions with optimum collision energies for all compounds are shown in Fig. 1. Data acquisition and processing were performed using the GCMS Solution and Insight GCMS software (version 4.45, Shimadzu Corporation). Injection volume was 2 µL.

2.3 Extraction, calibration and method validation

The analytes were extracted from 0.5 mL of blood sample using diisopropyl ether after addition of the internal standard stock solution and carbonate buffer to obtain alkaline condition (pH = 9.2). After evaporation of solvent, dry residue was dissolved in 100 µl of ethyl acetate. The calibration solutions were prepared in triplicate (n = 3) in the range of 1–200 ng mL^{-1} by spiking blank blood samples with the appropriate volume of the stock solution of the analytes and the internal standard stock solution. Then, extraction procedure was performed. Quality

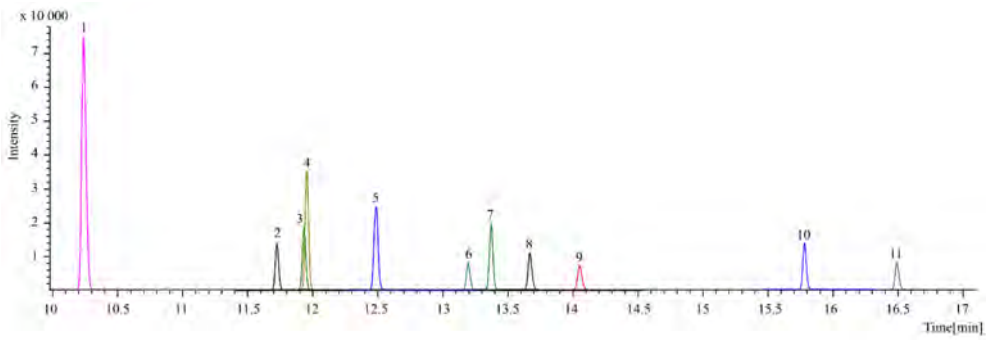

Fig. 1 GC-MS/MS chromatogram (in MRM mode) of standard benzodiazepine mixture in blood in blood samples (t_r – retention time, *CE* – collision energy, *RA* – relative abundance of quantifier/qualifier transitions.

Peak	Compound	t_r/min	Quantifier		Qualifier		*RA*
			Transition	*CE*/V	Transition	*CE*/V	
1	Medazepam	10.24	242.1 → 207.2	15	207.1→ 165.1	24	100/38
2	Lorazepam	11.72	274.0 → 239.1	15	239.0 → 177.1	24	100/79
3	Diazepam-D_5	11.93	261.0 → 226.2	12	261.0 → 170.2	30	100/31
4	Diazepam	11.95	256.1 → 221.1	12	256.1 → 165.1	36	100/50
5	Nordiazepam	12.48	242.0 → 207.1	12	242.0 → 152.1	33	100/47
6	Midazolam	13.19	310.1 → 95.1	9	310.1 → 75.1	42	100/38
7	Flunitrazepam	13.37	312.1 → 266.1	36	286.1 → 240.1	42	100/59
8	Prazepam	13.67	269.1 → 240.1	15	269.1 → 116.1	33	100/86
9	Lormetazepam	14.05	305.0 → 111.1	15	305.0 → 193.0	15	100/59
10	Clonazepam	15.78	280.1 → 234.1	15	314.0 → 268.0	15	100/76
11	Estazolam	16.49	259.1 → 205.1	12	205.1 → 151.1	15	100/47

control samples were prepared similar to the calibration solutions at three concentration levels (at various steps depending on calibration range) listed in Table 2. Quality control samples were used for the evaluation of precision and accuracy.

The developed GC-MS/MS-based method for the quantification of benzodiazepines in blood samples was validated according to the international guidelines [7, 8]. Several parameters relevant to a quantitative method such as: linearity, precision, accuracy, matrix effect, limit of detection, and limit of quantification were evaluated.

3. Results and discussion

A liquid–liquid extraction based method utilizing GC-MS/MS technique for the determination of 10 benzodiazepines in whole blood samples was developed. Specific multiple reaction monitoring transitions and collision energies were optimized using Shimadzu MRM Optimization Tool and Shimadzu Smart Database

Table 1
Quantification and calibration data (*LOD* – limit of detection, *LOQ* – limit of quantification, *r* – correlation coefficient).

Compound	Calibration curverange /ng ml^{-1}	Weighting factor	Calibration equation	*r*	*LOD* /ng ml^{-1}	*LOQ* /ng ml^{-1}
Medazepam	1–100	$1/x$	$y = 0.07220\,x + 0.0137$	0.9994	0.21	1
Lorazepam	2–100	–	$y = 0.00701\,x - 0.0040$	0.9992	0.30	2
Diazepam	1–100	$1/x$	$y = 0.03164\,x + 0.0020$	0.9994	0.09	1
Nordiazepam	1–100	$1/x$	$y = 0.02498\,x - 0.0024$	0.9995	0.09	1
Midazolam	1–200	$1/x$	$y = 0.00691\,x - 0.0006$	0.9998	0.08	1
Flunitrazepam	2–200	$1/x^2$	$y = 0.01329\,x - 0.0006$	0.9953	0.11	2
Prazepam	1–100	$1/x$	$y = 0.01005\,x - 0.0003$	0.9996	0.12	1
Lormetazepam	2–100	$1/x^2$	$y = 0.00137\,x - 0.0010$	0.9951	0.44	2
Clonazepam	2–100	$1/x$	$y = 0.09301\,x - 0.0080$	0.9966	0.02	2
Estazolam	2–200	–	$y = 0.01179\,x - 0.0111$	0.9998	0.53	2

software. Chromatography separation time was short and peaks for the analytes were totally resolved, excepting peaks for Diazepam and Diazepam-d_5 (Fig. 1). However, due to use of specific multiple reaction monitoring transitions, chromatographic separation is not required in such cases. Up to now, in most GC-based procedures published in the literature [9], derivatization has been performed to obtain low limit of detection and limit of quantification. In our developed method, due to the use of MS/MS detection, the derivatization step could be omitted and low limit of detection and limit of quantification were obtained at similar levels as for LC-MS/MS-based methods [10].

The validation data are shown in Fig. 1 and Table 1. Calibration curves were linear in various ranges depending on MS responses with correlation coefficient above 0.99. Weighted least squares regression was applied to the calibration curves to improve the accuracy, especially at in low concentration level range. The limit of detection, based on a signal-noise ratio (*S/N*) equal to 3, was between 0.02–0.53 ng mL^{-1} and the limit of quantification was assumed to be the lowest point of the calibration curve (1 or 2 ng mL^{-1}) due to the linearity.

GC-MS/MS matrix effect was calculated by comparing the MS response for extract of blank blood spiked with analytes at known amounts with MS response recorded for sample prepared in methanol at the same concentration level. The negative and positive values for matrix effect were obtained what indicates signal enhancement and suppression. Therefore, matrix-match internal standard calibration, instead of external calibration, was used in this study. The intra-day accuracy varied from 83.7 to 117.6%, while the inter-day accuracy was 91.8 to 118.6%, respectively. Precision (as coefficient of variation) varied from 0.1 to 12.7% for intra-day and from 1.9 to 14.9% for inter-day assay.

Table 2
Summary of the validation test performed in this study: accuracy, precision (*CV*), and matrix effect.

Compound	C/ng ml^{-1}	Intra-day assay		Inter-day assay		Matrix effect/%
		Accuracy/%	*CV*/%	Accuracy/%	*CV*/%	
Medazepam	5	101.1	4.6	91.9	10.4	–6
	20	98.8	7.0	97.6	9.7	11
	80	104.5	4.5	118.6	14.9	0
Lorazepam	5	105.6	0.8	106.4	10.8	36
	20	111.8	2.7	113.3	9.9	2
	80	117.6	12.7	117.9	9.8	37
Diazepam	5	96.0	1.3	93.5	9.8	–10
	20	103.7	0.5	95.4	9.0	7
	80	103.8	1.9	113.0	13.8	18
Nordiazepam	5	97.1	1.8	96.8	9.3	0
	20	103.6	0.9	96.8	7.1	12
	80	107.6	0.4	115.2	10.6	37
Midazolam	5	98.4	1.0	95.1	6.9	1
	50	101.9	3.8	109.5	9.8	2
	150	107.9	0.5	114.2	7.7	12
Flunitrazepam	10	95.7	1.3	91.8	3.8	5
	50	104.6	4.6	112.1	3.7	1
	150	104.7	1.3	112.9	7.5	10
Prazepam	5	99.3	0.1	97.1	9.0	–10
	20	103.2	1.0	95.9	8.6	8
	80	103.6	1.7	112.1	1.9	22
Lormetazepam	5	102.5	0.2	104.4	4.6	–[a]
	20	106.5	3.1	102.4	6.7	–2
	80	110.1	3.5	105.8	3.5	52
Clonazepam	5	109.1	4.8	109.9	2.8	49
	20	115.4	1.4	106.9	7.6	4
	80	94.6	2.2	111.5	8.6	44
Estazolam	10	83.7	0.9	99.2	6.4	3
	50	99.5	3.5	118.4	5.7	–3
	150	112.2	5.1	115.1	9.5	6

[a] Due to high signal enhancement in matrix, intensity of peak (*S/N*) in the solvent was below 3.

4. Conclusions

A liquid–liquid extraction procedure followed by GC–MS/MS analysis was developed for the quantification of 10 benzodiazepines in whole blood samples using only 500 µL of sample. The whole procedure was rapid and simple. Blood is one of the most commonly used matrix in forensic toxicology analysis for drug or other toxic substances screening. Importantly, the developed procedure can be easily expanded for more substances. Based on the obtained validation parameters, our procedure can be used as an alternative tool to LC-MS/MS-based

methods for the determination of benzodiazepines for clinical laboratories and forensic toxicology.

Acknowledgments

Special thanks to the employees of the Department of Forensic Medicine of Medical University of Gdańsk for their great support and providing standards. We would like to honor the memory of Prof. Jacek Namieśnik, Head of the Department of Analytical Chemistry of Gdańsk University of Technology, who has sadly passed away. His words were always supporting and encouraged us. He will remain in our memory for ever.

References

[1] Samadi F., Sarafraz-Yazdi A., Es'haghi Z.: An insight into the determination of trace levels of benzodiazepines in biometric systems: Use of crab shell powder as an environmentally friendly biosorbent. *J. Chromatogr. B* **1092** (2018), 58–64.
[2] Zawilska J.B., Wojcieszak J.: An expanding world of new psychoactive substances: Designer benzodiazepines. *Neurotoxicol.* **73** (2019), 8–16.
[3] Nozawa H., Minakata K., Yamagishi I., Hasegawa K., Wurita A., Gonmori K.: MALDI-TOF mass spectrometric determination of eight benzodiazepines with two of their metabolites in blood. *Leg. Med.* **17** (2014), 150–156.
[4] Høiseth G., Tuv S.S., Karinen R.: Blood concentrations of new designer benzodiazepines in forensic cases. *Forensic Sci. Int.* **268** (2016), 35–38.
[5] Ashrafi H., Mobed A., Hasanzadeh M., Babaie P., Ansarin K., Jouyban A.: Monitoring of five benzodiazepines using a novel polymeric interface prepared by layer by layer strategy. *Microchem. J.* **146** (2019), 121–125.
[6] Álvarez-Freire I., Brunetti P., Cabarcos-Fernández P., Fernández-Liste A., Tabernero-Duque M.J., Bermejo-Barrera A.M.: Determination of benzodiazepines in pericardial fluid by gas chromatography–mass spectrometry. *J. Pharm. Biomed. Anal.* **159** (2018), 45–52.
[7] Scientific Working Group for Forensic Toxicology (SWGTOX): Standard practices for method validation in forensic toxicology. *J. Anal. Toxicol.* **37** (2013) 452–474.
[8] US Food and Drug Administration: *Guidance for Industry: Q2B Validation of Analytical Procedures: Methodology*. Rockville 1996; https://www.fda.gov/media/71725/download.
[9] Gunnar T., Ariniemi K., Lillsunde P.: Determination of 14 benzodiazepines and hydroxy metabolites , zaleplon and zolpidem as tert -butyldimethylsilyl derivatives compared with other common silylating reagents in whole blood by gas chromatography – mass spectrometry. *J. Chromatogr. B.* **818** (2005), 175–189.
[10] Øiestad E.L., Johansen U., Marit Å., Øiestad L., Christophersen A.S.: Drug screening of whole blood by ultra-performance liquid chromatography – tandem mass spectrometry. *J. Anal. Toxicol.* **35** (2011), 280–293.

Determination of L-arginine in dietary supplement by voltammetry on glassy carbon electrode

MARIA PONOMAREVA, VALENTINA POPOVA*, ELENA KOROTKOVA

Chemical Engineering Department, National Research Tomsk Polytechnic University, 30 Lenin Avenue, 634050 Tomsk, Russia ✉ *vap25@tpu.ru*

Keywords
L-arginine
dietary supplements
glassy carbon electrode
voltammetry

Abstract
A simple and sensitive voltammetric method was developed to determine of L-arginine in a dietary supplement at glassy carbon electrode in 0.1 M sodium hydroxide with pH = 13.0. The L-arginine was preaccumulated on the electrode surface at +0.3 V for 30 s. A well-defined oxidation peak was obtained at 0.9 V. Differential pulse voltammetry was applied for the calibration plot and detection limit (1.34×10^{-6} mol L^{-1}).

1. Introduction

L-Arginine is a molecule of tremendous clinical importance [1]. The conversion of arginine to nitric oxide by nitric oxide synthase can be used for the treatment of various diseases such as cardiovascular, atherosclerosis, vascular headaches and chest pain [2]. L-arginine is often taken as a dietary supplement, especially by athletes to increase muscle mass. The use of dietary supplements has always been associated with risk [3], mainly due to the fact that during the production process, additives can be contaminated and not satisfies to the stated quality. Despite the fact that all substances of a biologically active additive should be displayed on the label, there is no guarantee that the product does not contain any prohibited substances.

A large number of registered positive results of doping control among the athletes was due to contamination and incorrect labeling of additives. Therefore, it is necessary to develop fast, sensitive and cheap methods for the determination of L-arginine in dietary supplements.

2. Experimental

2.1 Reagents and chemicals

All solutions were prepared with pure water. Britton-Robinson buffer solution was prepared by mixing of 0.2 mol L^{-1} sodium hydroxide with the mixture of

0.04 mol L^{-1} of boric, acetic and phosphoric acid. The object of research was the dietary supplement "L-arginine 500 mg" produced by Solgar (USA). As a standard substance was L-arginine powder produced by Alfa Aesar (Germany). In the regard that the amount of L-arginine in the dietary supplement was 99.9%, sample preparation of the dietary supplement was not carried out.

2.2 Instrumentation

All voltammetric measurements were conducted with the PalmSens 4 (Netherlands) instrument equipped with PSTrace 5 software. The three-electrode electrochemical cell was equipped with the working electrode (glassy carbon electrode), the auxiliary electrode (platinum wire) and the reference electrode (Ag/AgCl/1 M KCl), The working electrode was polished by Al_2O_3 before each experiment. The pH was measured with a pH-meter/ionomer ITAN, Tomanalyt, Russia. Cyclic voltammetry (CV) was used at first for the examination of L-arginine voltammetric behavior on glassy carbon electrode. Differential pulse voltammetry (DPV) with following parameters was applied for the determination of L-arginine in dietary supplements: scan rate 60 mV s^{-1}, pulse height 0.2 V, pulse width 0.02 s, step potential 0.01 V, potential range from 0.3 V to 1.3 V.

3. Results and discussion

Firstly, the electrochemical behavior of 1 mmol L^{-1} L-arginine in 0.1 mol L–$^{-1}$ sodium hydroxide (pH = 13.0) was investigated by cyclic voltammetry. L-Arginine oxidation on glassy carbon electrode occurred at +0.7 V (Fig. 1). Further, DPV was

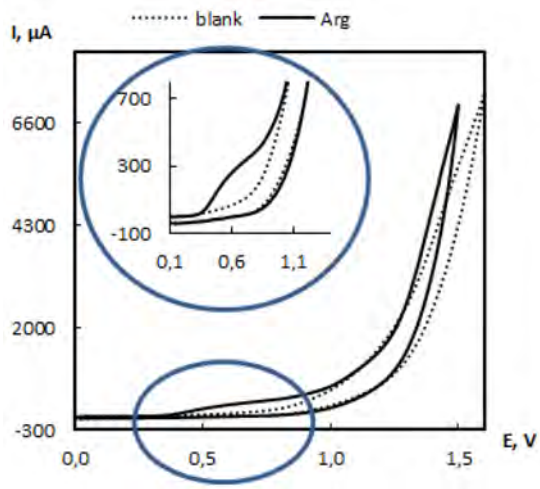

Fig. 1 Cyclic voltammograms of 10^{-3} mol L^{-1} L-arginine in 0.1 M sodium hydroxide at glassy carbon electrode. Scan rate 60 mV s^{-1}.

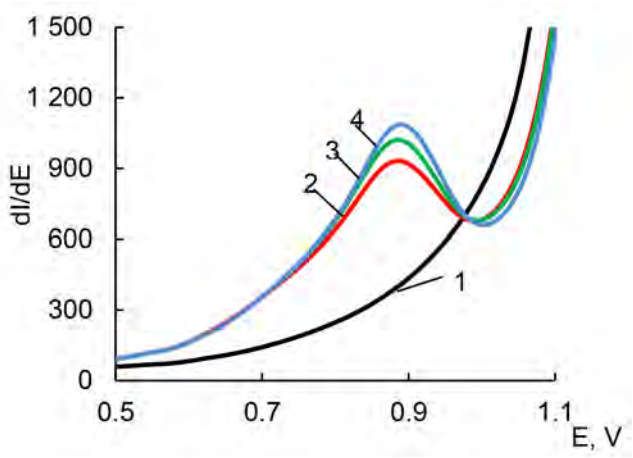

Fig. 2 DP voltammograms of L-aginine obtained on glassy carbon electrode: (1) blank, (2) sample, c_x, (3) c(L-arginine) = 2.5×10^{-4} mol L^{-1}, (4)c(L-arginine) = 3.0×10^{-4} mol L^{-1}. Parameters: 0.1 mol L^{-1} NaOH (pH = 13.0), E_{in} = 0.3 V, E_{fin} = 1.3 V, scan rate 60 mV s^{-1}, pulse height 0.2 V, pulse width 0.02 s, step potential 0.01 V.

used to select the optimal conditions for the determination of L-arginine in dietary supplements. Secondly, the optimal pH for L-arginine determination was found. The Britton-Robinson buffer solution in the pH range from 2.4 to 12 and 0.1 mol L^{-1} sodium hydroxide were controlled. The highest and the best-developed peak was obtained in the 0.1 mol L^{-1} NaOH with the pH = 13.0. Sodium hydroxide with the pH = 13.0 was chosen as the optimal medium.

The influence of potential and time pre-accumulation has been tested. Optimal working conditions are potential pre-accumulation +0.3 V; time pre-accumulation 30 s. The dependence of the peak current on the concentration of L-arginine was linear in the range from 2.0×10^{-4} to 4.5×10^{-4} mol L^{-1} with the regression equation of

$$I[\mu A] = 3.0522\, c[\text{mg L}^{-1}] - 0.2853 \quad (1)$$
$$R^2 = 0.9952$$

The detection limit calculated by equation

$$c_{min} = 3s/b \quad (2)$$

where s is the standard deviation in the measurement of the signal of a blank sample, and b is the instrumental sensitivity factor of the slope of the straight section of the calibration curve. The calculated detection limit was 1.34×10^{-6} mol L^{-1}.

To quantify L-arginine in the dietary supplement, the background was tested. After that, a standard substance was added (Fig. 2). The content of L-arginine in

the dietary supplement was calculated by the additive method. The amount of arginine in the dietary supplement corresponded to the stated.

4. Conclusions

In this research, the electrochemical behavior of L-arginine on glassy carbon electrode was studied and its amount in the dietary supplement was controlled.

Acknowledgments

The authors thank Tomsk Polytechnic University for financial support of this work (Russian Fund for Basic Research, research project No. 4.5752.2017/BP, Russian State assignment "Science").

References

[1] Fuhrmann J., Schmidt A., Spiess S., Lehner A., Turgay K., Mechtler K., Charpentier E., Clausen T.: McsB is a protein arginine kinase that phosphorylates and inhibits the heat-shock regulator CtsR. *Science* **324** (2009), 1323–1327.
[2] Boger R.H.: The pharmacodynamics of L-Arginine. *J. Nutri.* **137** (2007), 1650–1655.
[3] Fürst P., Stehle P.: What are the essential elements needed for the determination of amino acid requirements in humans. *J. Nutr.* **134** (2004), 1558–1565.

Application of analytical methods for determining properties of selenium nanoparticles

MAGDALENA BOROWSKA*, KRZYSZTOF JANKOWSKI

Department of Analytical Chemistry, Faculty of Chemistry, Warsaw University of Technology, Noakowskiego 3 Street, 00-664 Warsaw, Poland ✉ *mbartosiak@ch.pw.edu.pl*

Keywords
green chemistry
photochemical vapor generation
selenium nanoparticles
single particle mode spectrometry

Abstract
Selenium plays an important role in effective binding of mercury compounds. Selenium nanoparticles due to their lower toxicity and higher bioavailability compared to other selenium species, have a high bioapplicability potential as a new source of selenium. The properties of selenium nanoparticles depend on the choice of synthesis route. Analytical methods based on microwave assisted headspace solid phase microextraction (MA-HS-SPME) and microwave-induced plasma optical emission spectrometry (MIP-OES), single particle microwave plasma optical emission spectrometry (MWP-OES), and photochemical vapor generation (PCVG) coupled with SPME-MIP-OES were used for determination of synthesis efficiency, identification of selenium in single yeast cell and investigation of selenium-mercury interactions, respectively. These methods allows us to confirm the presence of the selenium nanoparticles inside yeast cells as observed by scanning electron microscopy (SEM).

1. Introduction

Selenium is an essential element for life. Its excess or deficiency causes pathological states of the body. It becomes toxic when the concentration exceeds the safe limit. The selenium concentration required by the human body is in the range 0.10–0.30 μg kg^{-1}. Selenium shows antagonistic properties against mercury. Inorganic sodium selenite, selenomethionine, or selenium yeasts rich in selenomethionine are the most frequently used selenium supplement forms [1]. Nowadays, selenium nanoparticles are more and more being listed as a potential source of selenium being alternative to common forms of the element. It is noteworthy, that the toxicity of inorganic selenium is definitely higher than the toxicity for elemental selenium at nano size. Moreover, selenium nanoparticles exhibit higher bioavailability than that of both inorganic selenium species and organic selenium-containing amino acids [2]. The properties of selenium

nanoparticles depend on the choice of synthesis route and the appropriate control of nanoparticle parameters such as shape, size, surface functionalization and particle composition. Among methods of synthesizing nanoparticles, chemical, physical and biological methods can be distinguished [1]. In recent years, the biological synthesis of selenium nanoparticles has gained enormous popularity due to the low cost and the availability of raw materials as well as the low toxicity and the high pharmacological potential of selenium nanoparticles [3].

Various analytical techniques have been used for monitoring nanoparticles synthesis efficiency and selenium nanoparticles characterization. Vogel et al. [4] determined unreacted selenite in supernatant after separation of selenium-based nanoparticles using hydride generation atomic absorption spectrometry. Alternatively, they determined total selenium concentration by ICP-MS after acid digestion of the nanoparticles sample. Also, Nie et al. [5] applied acid digestion followed by ICP-OES for determining total selenium content in selenium nanoparticles dispersion. Moreno et al. [6] used flow field-flow fractionation coupled with dynamic light scattering for sizing selenium nanoparticles, and Jiménez et al. [7] used single particle ICP-MS for detection and characterization of biogenic selenium nanoparticles in selenium-rich yeast, as alternative to transmission electron microscopy measurements. While the single characterization methods of selenium nanoparticles have been long reported, little has been published about using the wide spectrum of combined techniques in analytical protocols for characterization of selenium nanoparticles. The goal of this study was the determination of the yield of synthesis, characterization of selenium nanoparticles produced by yeast and investigation of their interactions with inorganic mercury using MA-HS-SPME-TD-MIP-OES, SP-MWP-OES and PCVG-SMPE-MIP-OES, respectively.

2. Experimental

2.1 Reagents and chemicals

For selenium nanoparticles synthesis, analytical grade reagents were used (Sigma Aldrich). For optimization and calibration of MA-HS-SPME-TD-MIP-OES methods, Se(IV) stock solution was prepared by dissolving selenium dioxide (Sigma Aldrich) in 2% (*v/v*) nitric acid. Working solutions were freshly prepared daily by serial dilution of the stock solutions with distilled water, and subsequent addition of appropriate volume of 1% ethanolic solution of 4,5-dichloro-*o*-phenylenediamine (Sigma Aldrich). For optimization and calibration PCVG-SPME-MIP-OES, mercury stock solution was prepared by dissolving mercury chloride (Sigma Aldrich) in 3% (*v/v*) nitric acid. Working solutions were freshly prepared daily by serial dilution of the stock solutions with distilled water, and subsequent addition of appropriate volume of 99.5% (*v/v*) formic acid (POCh, Poland). For optimization of SP-MWP-OES lyophilized samples of synthesized selenium nanoparticles were used.

2.2 Instrumentation

2.2.1 Microwave assisted MA-HS-SPME-TD-MIP-OES

A TD-MIP-OES apparatus consisted of a modified Beenakker-type cavity with a microwave power generator (Ertec, Poland) and miniature optical spectrometer AvaSpec-3648 (Avantes, The Netherlands). Pure (99.998%) helium (Multax, Poland) was used as plasma and carrier gas. SPME was supported by microwave radiation (TEM-type cavity with microwave power generator; Ertec, Poland).

2.2.2 PCVG-SPME-MIP-OES

An experimental set-up was described above. Pure (99.998%) argon (Multax, Poland) was used as plasma and carrier gas. Both PCVG of Hg species and thermal desorption of Hg vapor sorbed on fiber (DVB/CAR/PDMS) were accomplished in a continuous stop-flow mode using modified liquid-gas sample introduction system. The 3 mm i.d. and 68 cm-long quartz reactor was layered along a low pressure 11 W UV-C lamp (Osram).

2.2.3 SP-MWP-OES

An experimental set-up consisted of six-phase rotating field MWP source (Ertec, Poland) and AvaSpec-3648-UE (Avantes, Netherland) operated in time resolved analysis (TRA) mode to output signal of cps versus time providing simultaneous detection. Pure (99.998%) helium (Multax, Poland) was used as plasma and carrier gas.

2.3 Procedures

2.3.1 Selenium nanoparticles synthesis using yeast *Saccharomyces cerevisiae boulardii*

Selenium nanoparticles were synthesized using a biological approach described in [8] based on intracellular formation of selenium nanoparticles in yeast cells. The color of the culture changed from colorless to orange-red. Yeast cells were then harvested by centrifugation at 10000×g for 10 min. Supernatant was collected for further analysis. A portion of the obtained pellets was washed three times with distilled water and lyophilized for analysis using SP-MWP-OES. Second portion was collected for further analysis using MA-HS-SPME-TD-MIP-OES. The third portion was used for mercury sorption experiments. The second and third portion of pellets were purified using a protocol described in [8].

2.3.2 Selenium nanoparticles analysis using MA-HS-SPME-TD-MIP-OES

The suspension of selenium nanoparticles with yeast cell as well as the pellet and the supernatant obtained after centrifugation were digested with nitric acid on the hot block. Once excess nitric acid was evaporated, the residues were dissolved in 4 mL of hydrochloric acid. Next, 0.2 mL of 4,5-dichloro-*o*-phenylenediamine was added and the SPME fiber was exposed. Both derivatization and sorption stage last 20 min each.

2.3.3 Selenium nanoparticles analysis in yeast cell using SP-MWP-OES

A few milligrams of lyophilized sample nanoparticles was placed in the sample chamber maintaining MWP-OES system the sample was transferred particle by particle to helium plasma with carrier gas and emission spectra were registered in the TRA mode.

2.3.4 Selenium nanoparticles and mercury investigation using PCVG-SPME-MIP-OES

10 mL of selenium nanoparticles suspension was incubated with Hg^{2+} for 24 hours (37 °C, pH = 7.4). Samples (1mL) of reaction medium were collected periodically. Each sample was centrifugated, next the supernatant was sampled and diluted 1:10, and formic acid was added to obtain 2% (*v/v*) in analyzed sample. The solution was pumped through the quartz reactor where UV radiation exposure time of about 85 s. Then, the resulting vapors were collected in glass vessel and the SPME fiber was exposed within 2 min. Liquid sample was removed from glass vessel.

3. Results and discussion

3.1 Biosynthesis of selenium nanoparticles using yeast Saccharomyces cerevisiae boulardii

Selenium nanoparticles were produced in green synthesis using cells of yeast *Saccharomyces cerevisiae boulardii*. Biogenic selenium nanoparticles do not require any addition of stabilizing agents because they are stabilized by natural organic molecules present in the yeast culture. The color of the culture changed from colorless to orange-red as the incubation proceeded. The selenium nanoparticles production was confirmed using scanning electron microscopy (SEM). In the first step of synthesis, intracellular formation was observed [9]. After that selenium nanoparticles were excreted extracellular. The mean particle diameter was about 250 nm (Fig. 1).

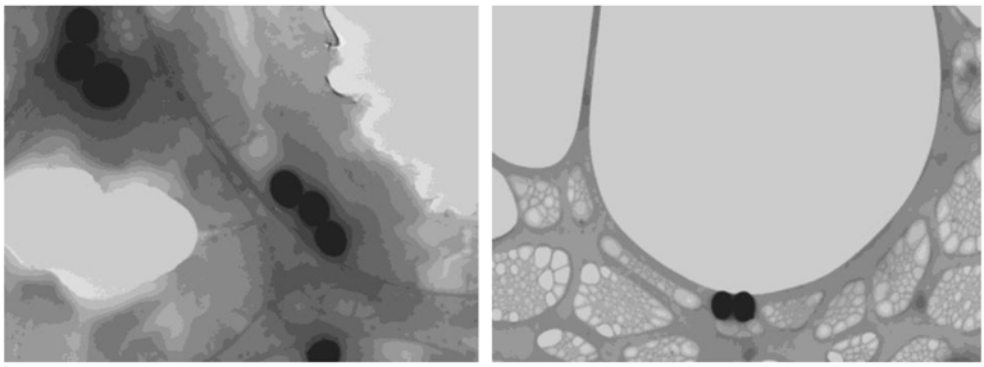

Fig. 1 Scanning electron microscopy images of selenium nanoparticles inside living yeast cells.

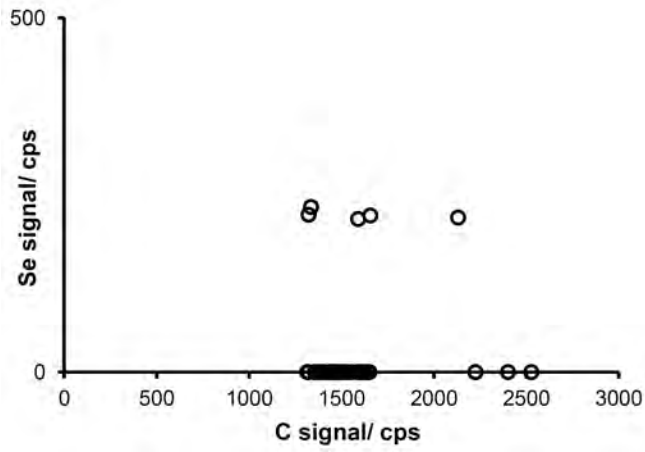

Fig. 2 Correlation between selenium and carbon for yeast culture sample .

3.2 Single-cell analysis using SP-MWP-OES

SP-MWP-OES technique can evaluate the macroscopic properties of the single powdered nanomaterial including agglomeration or aggregation of particles because it employs a statistical analyzing process. Both adequate time resolution and low particle number flow rate are required to ensure that each pulse signal corresponds to one particle only. Time scans of sample at an integration time 50 ms were recorded and regular pulse distribution was observed. SP-MWP-OES provided information about elemental composition of yeast culture after selenium nanoparticles. Correlation between selenium and carbon events for selenium nanoparticles sample was evaluated by the observation of synchronized pulses distribution. As shown in Fig. 2, correlation between selenium and carbon was not observed for all recorded events. This observation confirmed selenium nanoparticles synthesis in selected yeast cells and is in a good agreement with SEM scans.

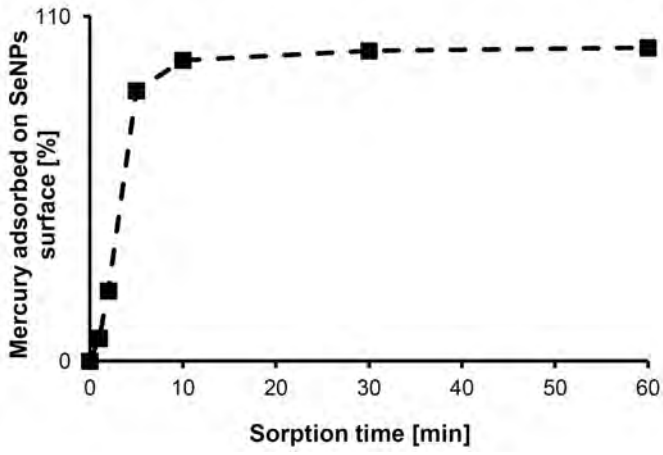

Fig. 3 Percentage of mercury adsorbed on selenium nanoparticles surface during reaction time.

3.3 Selenium nanoparticles synthesis yield determination using MA-HS-SPME-TD-MIP-OES

For determining the selenium nanoparticles synthesis yield, the selenium content was measured both in the supernatant and in the pellet and the yield of synthesis was calculated. 4,5-dichloro-*o*-phenylenediamine was used as a derivatizating agent because it is resistant to microwave field. The selenium nanoparticles synthesis yield was found to be about 100%.

3.4 Selenium nanoparticles and mercury investigation using PCVG-SPME-MIP-OES

Mercury concentration was monitored before and after sorption experiments using selenium nanoparticles as an adsorbent under conditions simulating human body fluids (pH ~ 7.3, 37 °C). For the analysis, mercury ions present in the sample solution were converted into volatile species by UV irradiation in the presence of 2% (*v/v*) formic acid. For analytical monitoring of selenium nanoparticles mercury-antagonistic properties PCVG-SPME-MIP-OES was successfully applied and it was stated that after 10 minutes almost 100% of mercury present in solution was adsorbed (Fig. 3).

4. Conclusions

Three analytical methods based on MIP-OES were successfully used for both determining the yield of selenium nanoparticles biological synthesis and characterizing selenium nanoparticles. The presence of selenium nanoparticles in yeast cell and in extracellular space is demonstrated and the selenium concentration in different phases of selenium nanoparticles suspension can be determined. The

yield of selenium nanoparticles synthesis was 100%. Furthermore, selenium nanoparticles were successfully applied for detoxification of inorganic mercury.

Acknowledgments

This work was supported by the National Science Centre, Poland (2017/27/N/ST4/00338).

References

[1] Skalickova S., Milosavljevic V., Cihalova K., Horky P., Richtera L., Adam V.: Selenium nanoparticles as a nutritional supplement. *Nutrition* **33** (2017), 83–90.
[2] Zhang J.S., Gao X.Y., Zhang L.D., Bao Y.P.: Biological effects of a nano red elemental selenium. *Biofactors* **15** (2001), 27–38.
[3] Husen A., Siddiqi K.S.: Plants and microbes assisted selenium nanoparticles: Characterizaton and application. *J. Nanobiotech.* **12** (2014), 1–10.
[4] Vogel M. Fischer S., Maffert A., Hübner R., Scheinost A.C., Franzen C., Steudtner R.: Biotransformation and detoxification of selenite by microbial biogenesis of selenium-sulfur nanoparticles. *J. Hazard. Mater.* **344** (2018), 749–757.
[5] Nie T., Wu H., Wong K.H., Chen T.: Facile synthesis of highly uniform selenium nanoparticles using glucose as the reductant and surface decorator to induce cancer cell apoptosis. *J. Mater. Chem. B* **4** (2016), 2351– 2358.
[6] Moreno-Martin G., Pescuma M., Pérez-Corona T., Mozzi F., Madrid Y.: Determination of size and mass-and number-based concentration of biogenic Selenium nanoparticles synthesized by lactic acid bacteria by using a multimethod approach. *Anal. Chim. Acta.* **992** (2017), 34–41.
[7] Jimenez J., Abad-Álvaro I., Bierla K., Laborda F., Szpunar J., Lobinski R: Detection and characterization of biogenic selenium nanoparticles in selenium-rich yeast by single particle ICPMS. *J. Anal. At. Spectrom.* **33** (2018), 452–460.
[8] Bartosiak M., Giersz J., Jankowski K.: Analytical monitoring of selenium nanoparticles green synthesis using photochemical vapor generation coupled with MIP-OES and UV-Vis spectrophotometry. *Microchem. J.* **145** (2019), 1169–1175.
[9] Wadhwani S., Shedbalkar U.U., Singh R., Chopade B.A.: Biogenic selenium nanoparticles: current status and future prospects. *Appl. Microbiol. Biotechnol.* **100** (2016), 2555–2566.

Signal increment standard addition method: new calibration approach in potentiometric measurements

Marek Dębosz[a,*], Marcin Wieczorek[a], Paweł Kościelniak[b], Jan Migdalski[b]

[a] *Department of Analytical Chemistry, Faculty of Chemistry, Jagiellonian University in Krakow, Gronostajowa 2, 30-387, Krakow, Poland* ✉ *marek.debosz@doctoral.uj.edu.pl*
[b] *Department of Analytical Chemistry, Faculty of Materials Science and Ceramics, AGH-University of Science and Technology in Cracow, al. Mickiewicza 30, Kraków, Poland*

Keywords
analytical calibration
ion selective electrodes
potassium and chloride determination

Abstract
The present work is focused on the implementation of a new calibration approach, termed the Signal Increment Standard Addition Method (SI-SAM), to the potentiometric determination of potassium and chloride ions in the synthetic samples. Potentiometry is the method of choice due to its simplicity, rapid measurements, wide linear range and fulfilment of green analytical principles. However, the week point is the calibration as various versions of the standard addition method, which are commonly used in potentiometry, may create some problems leading to serious systematic analytical errors. It has been proved here that SI-SAM allows for elimination of this drawback and, consequently, for determination of the considered analytes with improved results, especially in terms of accuracy.

1. Introduction

Among a variety of analytical methods electrochemical ones play an important role. One of them, potentiometry, can be particularly recommended as being simple, fast, low-cost and sensitive. Ion selective electrodes, a group of selective potentiometric devices, have been widely employed for environmental analysis. However, the use of ion selective electrodes is limited due to interferences, which are caused by e.g. different levels of complexing equilibria or poisoning effects of colloidal electrolytes in the matrix of analysed samples. Such issues can be overcome through addition of an ionic strength adjuster to both the sample and the standard solutions. In conditions of equal ionic strength it is possible to release an analyte from complexes and to buffer the samples contributing to the elimination of pH interference.

Similarly to most of analytical methods, the potentiometric determinations need to be calibrated using standard solutions. For this purpose different calibration approaches are exploited, including calibration curve method (direct

potentiometry), single standard addition method (SA-SAM), Gran's method (multiple standard addition method), or methods based on mathematical models [1, 2]. When the interference effects are expected, SA-SAM and Gran's method are usually applied. Both of them require to know the exact value of the empirical sensitivity of the electrode in order to make the dependence of the signal on the logarithm of the analyte concentration linear [2]. Moreover, SA-SAM leads to results with high uncertainty. Classical standard addition method (SAM) cannot be performed in potentiometry since the extrapolation of the calibration curve to the signal measured for the blank solution (without the analyte) may lead to the erroneous analytical results.

The calibration method allowing the extrapolation-related problem to be overcome is the Signal Increment Standard Addition Method (SI-SAM). This method was already applied to the determination of Cr(VI) using electroanalytical method based on the electrostriction phenomenon [3, 4]. This method enables minimizing the systematic error committed in such cases, when the course of the calibration graph in the extrapolation are is unknown or uncertain. As the SAM's version, it is also able to compensate a systematic error caused by multiplicative interferent effect.

In this paper, the suitability of this calibration method in potentiometric measurements was verified on the example of determination of potassium and chloride in synthetic samples.

2. Experimental

2.1 Reagents and samples

All chemicals were of analytical grade. The following chemicals purchased from Sigma Aldrich (Germany) were used for membrane preparation: high molecular weight polyvinyl chloride, bis(2-ethylhexyl)sebacate, tetrahydrofuran, potassium tetrakis(*p*-chlorophenyl)borate, valinomycin (potassium ionophore I). Other chemicals, such as inorganic salts: potassium chloride (Chempur, Poland), calcium chloride (POCH, Poland), were also utilized. Ultrapure water (18.2 MΩ cm) from an HLP 5 system (Hydrolab, Poland) was used throughout the work.

Stock standard solutions of potassium chloride (0.2 mol L^{-1}), calcium chloride and sodium nitrate were prepared by dissolving adequate amount of chloride salts.

2.2 Instrumentation

Potentiometric measurements were performed using 16-channel LawsonLab (USA) potentiometer with EMF Suite version 2.0 data logging program. Potentials were measured against Ag/AgCl/(3 mol L^{-1}) KCl reference electrodes obtained from Mineral, Warsaw. All measurements were performed at 20±2 °C. The potentiostatic electrodeposition was performed with the M161 electrochemical

analyzer (Mtm-Anko, Poland). The EALab 2.1 software was used for the data acquisition. The measurements were carried out in the three-electrode system in quartz vessel of 25 cm^3 volume covered with a PMMA cover with five holes matched the size of each electrode and an additional hole for adding standard solution. Magnetic stirrer (Wigo, Poland) was also used.

2.3 Preparation of working electrodes

Prior to preparation of each electrode, the silver electrodes were polished with 0.3 μm alumina, rinsed thoroughly with deionized water and ultrasonicated for at least 4 minutes. Solid contact potassium ion selective electrodes were prepared on silver electrode (diameter 2 mm) by drop casting method. The solution used for casting the ion selective membranes was 15% dry fraction solution in tetrahydrofuran. The dry fraction was consisted of 65.8% plasticizer (bis(2-ethylhexyl)-sebacate), 1% ionophore (Valinomycin), 33% polymer (polyvinyl chloride) and 0.2% ion exchanger (potassium tetrakis(*p*-chlorophenyl)borate). 15 μL of the membrane cocktail was deposited by drop casting on the ion-selective electrode surface. Then, the electrodes were left overnight to ensure evaporation of tetrahydrofuran from the membranes. Subsequently, the electrodes were conditioned in 0.1 mol L^{-1} potassium chloride (pH = 7.0) for at least 24 hours. The chloride selective electrode was prepared by potentiostatic electrodeposition of the silver chloride on the surface of silver (wire) electrode. The silver electrode was inserted into 0.1 mol L^{-1} potassium chloride solution and 125 mV was applied against the Ag/AgCl/(3 mol L^{-1}) KCl reference electrode for 10 minutes. A platinum wire was used as the auxiliary electrode. After that, the electrode were left to dry. In this case, the conditioning was not necessary. The value of the applied potential was chosen to enable the process of solid silver oxidation and, as a result, to start the reaction between chloride and silver ions.

2.4 Calibration procedure

The presented calibration method is a modification of the standard addition method. In the first step of the calibration procedure the signal R_0 is measured for the first standard solution (so-called "blank test solution") with optimised concentration of the analyte. In the next step, the volume ΔV_s of a sample (with unknown analyte concentration) is added to the blank solution and signal R_1 is measured. Then, the appropriately increased volumes of the standard are added to the mixture of sample and standard solution and signals R_2, …, R_n are measured one after the other. On the basis of received data, the calibration graph is constructed as the relationship between signal R and cumulative concentration ΔC of added standard (Fig. 1). Finally, the calibration graph is extrapolated to the intersection with the signal of the blank test solution (first standard solution) and after projecting this point onto abscissa axis, the analytical result is obtained.

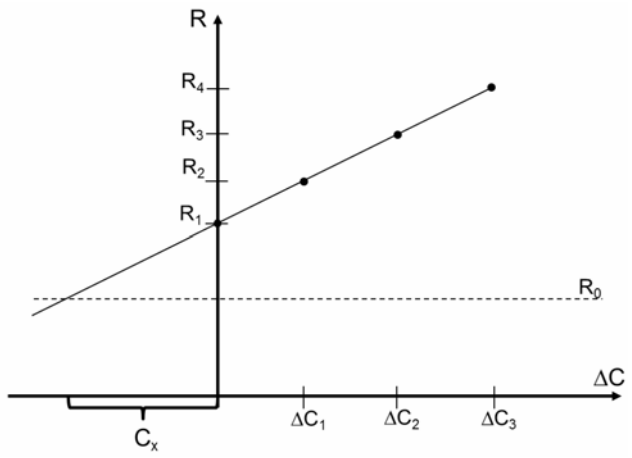

Fig. 1 The principle of signal increment standard addition method.

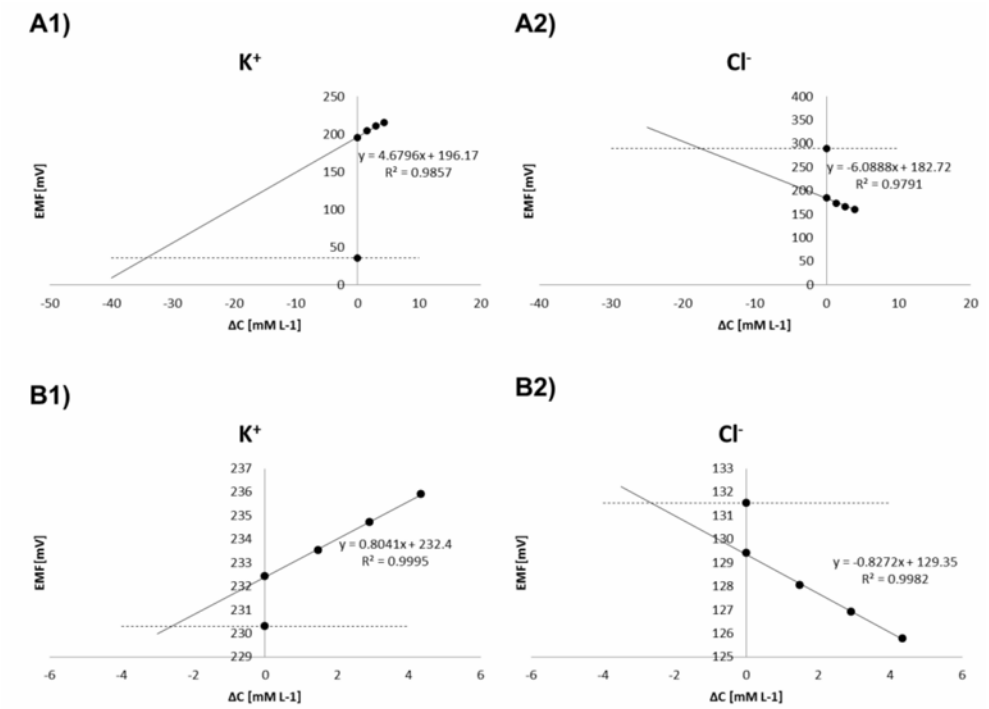

Fig. 2 The Signal Increment Standard Addition Method calibration plots for the potassium and chloride determination when water (A1, A2) and the standard solution (B1, B2) played a role of the blank test solution.

Table 1
Results of potassium ion determination in synthetic samples, expected concentration 2.57 mmol L^{-1}.

Composition of synthetic sample	Blank test solution	Found concentration/mmol L^{-1}	*RE*/%	*RSD*/%
KCl	Water	34.4	1240.30	2.11
	23 mmol L^{-1} KCl	2.53	–1.56	3.56
KCl + NaCl	23 mmol L^{-1} KCl	2.37	–7.88	0.16
KCl + $Ca(NO_3)_3$	23 mmol L^{-1} KCl	2.54	–1.17	1.72
KCl + $Ca(NO_3)_3$ + NaCl	23 mmol L^{-1} KCl	2.30	–10.64	1.38

Table 2
Results of chloride ion determination in synthetic samples, expected concentration 2.57 mmol L^{-1}.

Composition of synthetic sample	Blank test solution	Expected concentration/mmol L^{-1}	Found concentration/mmol L^{-1}	*RE*/%	*RSD*/%
KCl	Water	2.57	19.82	671.4	2.21
	23 mmol L^{-1} KCl	2.57	2.57	0.00	1.92
KCl + NaCl	23 mmol L^{-1} KCl	5.14	4.85	–5.58	2.57
KCl + $Ca(NO_3)_3$	23 mmol L^{-1} KCl	2.57	2.59	0.72	2.23
KCl + $Ca(NO_3)_3$ + NaCl	23 mmol L^{-1} KCl	5.14	4.34	–15.56	1.48

3. Results and discussion

In the present work potassium and chloride ions were determined. Figure 2 presents the results obtained by SI-SAM when extrapolation is carried out to the signal measured for the blank solution (water). It is seen that the calibration curves have to be extrapolated in definitely too large area in comparison with the experimental one (i.e., covered by the measurement points) to have a chance for obtaining reliable results of the determination of both analytes. One may expect that the sample dilution could be an appropriate solution of this problem, but taking the nature of electrodes into account the obtained results would be biased due to the ion flux membrane effect.

To overcome this problem SI-SAM was applied. This method modifies this classical SAM procedure by using the standard solution as a blank solution. By doing so the difference between extrapolation and experimental areas became acceptable as shown in Fig. 2B. The analyte concentration in the standard playing the role of blank solution was chosen to meaured the signals for all calibration solutions in the range of circa 5 mV.

In terms of analytical parameters, the SI-SAM method delivered much better results in terms of accuracy than the SAM method. Both potassium and chloride ions were determined with accuracy of up to 2% (see Table 1 and 2 for potassium and chloride ions determination, respectively). The precision of the analytical results was also acceptable in all considered cases (up to 3.56 %).

The contribution of other ions on the results was also examined keeping the rule that the ratio of the concentration of determined ion to the interfering one is 1:1. In case of potassium ions the sodium chloride and calcium nitrate were added separately and together. The accuracy was worsened when sodium was present in the sample matrix (Table 1). The addition of sodium chloride also influenced the determination of chloride ions in the samples (Table 2). Thus, the interference displayed by sodium and chloride ions was more evident in comparison to the interference caused by nitrate or calcium ions. This influence might be a result of the difference between the ionic strengths of standard solutions and synthetic samples [5].

4. Conclusions

The presented approach to calibration by SI-SAM is not only simple and fast but, what is much more important, delivers more accurate results in comparison with SAM and does not require to know what is the empirical sensitivity of the electrode. Moreover, as a version of SAM, it offers the possibility of reducing the systematic error caused by the multiplicative interference effect.

This preliminary study ought to be followed by the inspection of the applicability to the real samples. In this case, the ionic strength adjuster should be considered, since the difference between the ionic strength of pure standard solutions and of real sample will surely influence the analytical parameters.

Acknowledgments

M.D. has been partly supported by the EU Project POWR.03.02.00-00-I004/16.

References

[1] Thomas J.D.R.: Ion-selective electrodes in environmental and toxicological analysis. In: *Analytical Techniques in Environmental Chemistry.* J. Albaiges J. (ed.). Elsiever 2013, p. 543–562.
[2] Banica F.G.: *Chemical Sensors and Biosensors – Fundamentals and Applications.* Wiley 2012.
[3] Wieczorek M., Kochana J., Knihnicki P., Wapiennik K., Kościelniak P.: Novel electroanalytical method based on the electrostriction phenomenon and its application to determination of Cr(VI) by the flow injection technique. *Talanta* **166** (2017), 383–390.
[4] Kościelniak P., Wieczorek M.: Univariate analytical calibration methods and procedures. A review. *Anal. Chim. Acta* **944** (2016), 14–28.
[5] Mohan M.S., Bates R.G.: Calibration of ion-selective electrodes for use in biological fluids. *Clin. Chem.* **21** (1975), 864–872.

Stabilized lactate biosensors based on composite alkoxysilane-Nafion membranes

Ksenia Andreeva*, Daria Vokhmyanina, Arkady Karyakin

Chemistry Department, Moscow State University,
1–3 Leninskiye Gory, 119991, Moscow, Russia ✉ *tabulette@gmail.com*

Keywords
biosensors
immobilization
lactate oxidase
operational stability
Prussian Blue

Abstract
Operational stability of lactate biosensors is limited by leaching and inactivation of the enzyme and by instability of transducer, therefore it is insufficient for their use in clinical diagnostics. To increase the stability of lactate biosensors we immobilize lactate oxidase into γ-aminopropyltriethoxysilan-Nafion membranes by suspending the enzyme in a water-isopropanol mixture with a high (>90%) isopropanol content, mixed with the dissolved γ-aminopropyltriethoxysilan and Nafion, and then allowing the enzyme-polyelectrolytes solution to dry at the electrode surface. We report on improvement of operational stability by almost three times, proposing lactate biosensors based on composite alkoxysilane-Nafion membranes, while maintaining the range of the determined contents and high sensitivity coefficients.

1. Introduction

Lactate is considered as one of the most important metabolites in clinical analysis. It can be used as a marker for glycolysis, which might cause death of tissues, and is controlled in blood for patients with lactic acidosis [1]. Moreover, in sports medicine it is crucial to control the concentration of lactate in blood at a certain level for the training to be the most effective as intensive physical activity can cause an increase in blood lactate concentrations up to 10–15 times [2].

Biosensors are convenient analytical tools, which have immense applications in clinical diagnostics, environmental monitoring, food industry, and other areas where precise and reliable analysis is required [3]. Biosensors consist of two main parts: biological recognition element, generally called bioreceptor, and physicochemical transducer. As bioreceptor we use enzymes (lactate oxidase in particular). For coupling oxidase-catalysed and electrochemical reactions the most progressive way is the detection of hydrogen peroxide. The most advantageous transducer for hydrogen peroxide is Prussian Blue [4], which electroactivity is known to be pH independent.

When preparing a biosensor, the immobilization of the enzyme plays crucial role. By proposing successful immobilization technique advanced membranes, which show high enzyme activity and stability, can be obtained. Previously, in the laboratory of electrochemical methods we proposed immobilization protocol, involving exposing of proteins to water-organic mixtures with the high content of organic solvent [5]. We used diluted solvents of Nafion for immobilization of lactate oxidase. Such biosensors were stable in flow injection analysis (FIA), however their sensitivity was rather low for the practical use. Instead of Nafion we tried using γ-aminopropyltriethoxysilan as the main component for membranes. Although these lactate biosensors showed high sensitivity, stability in FIA was not enough for them to be used in clinical diagnosis. Hence, developing both stable and sensitive lactate biosensors is essential for their efficient use.

2. Experimental

2.1 Reagents and chemicals

All used materials (inorganic salts, γ-aminopropyltriethoxysilane, Nafion, organic solvents, hydrogen peroxide) were obtained at the highest purity from Sigma-Aldrich (USA) and used as received. Sodium lactate (40% solution) was purchased from ICN. Lactate oxidase (EC 1.1.3.2) from Pediococcus sp. (lyophilized powder, activity 72 IU) was purchased from Sorachim, Switzerland.

2.2 Instrumentation

Screen printed electrodes were purchased from Rusens LTD (Moscow, Russia) and modified with Prussian Blue. The flow injection system consisted of a Cole Parmer (Vernon Hills, IL) peristaltic pump (7519-10), homemade flow-through wall-jet cell with a 0.5 mm nozzle positioned at 1–2 mm distance from the surface of the planner electrode, homemade injector, and PalmSens electrochemical interface connected to an IBM PC.

3. Results and discussion

3.1 The causes of the low stability of lactate biosensors

In this work, the main causes of the low stability of lactate biosensors based on polyalkoxysilane membranes were studied. The loss of stability was investigated in the flow of lactate (0.2 mM), in the flow of phosphate buffer (pH = 6.0) and in the stationary buffer solution. Also, the behaviour of lactate biosensors was studied in the open air to evaluate the stability of the biosensors in such conditions. The results are presented in Fig. 1. The greatest loss of sensitivity is observed for biosensors placed in the flow of lactate, mainly because the membrane gets

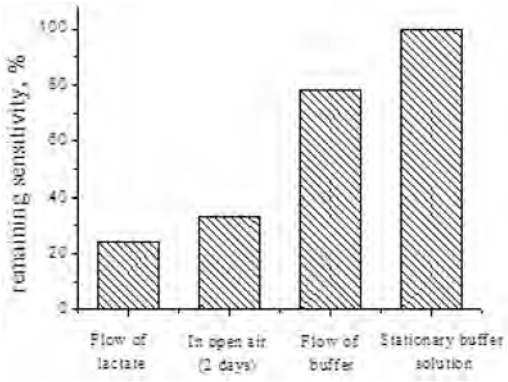

Fig. 1 The causes of the low stability of lactate biosensors.

destroyed by the interaction with the flow. Moreover, constant presence of hydrogen peroxide on the electrode surface leads to the instability of the transducer [6]. The flow of buffer causes the loss of sensitivity for biosensors as well, which is however less significant (approximately 20%) than in the first case. The main reason for that might be the mechanical effect of the flow. The experiment in the stationary buffer solution did not show any considerable loss of the sensitivity. Biosensors in the open air also showed a great loss in sensitivity due to the inactivation of the enzyme.

In the result, we suppose that the main causes of the low stability of lactate biosensors are the leaching of the enzyme, the inactivation of the enzyme, and the instability of the transducer.

3.2 Composite lactate biosensors based on the polyalkoxysilan-Nafion membranes

Improving the stability of lactate biosensors while maintaining the range of detectable contents is a necessary condition for their use in clinical medicine. To increase the stability of enzyme-containing membranes, it was proposed to add small (0.1–0.5%) concentrations of Nafion to the membrane-forming mixture (based on γ-aminopropyltriethoxysilan) before applying it to the electrode surface.

The sensitivity of biosensors based on the polyalkoxysilan-Nafion membranes was determined in FIA and Batch modes. According to the results of the experiment (Fig. 2), the addition of Nafion to the membrane leads to a decrease in the sensitivity of the biosensors in both modes of analysis. Nafion contains negatively charged groups that shield the positively charged enzyme, which affects the sensitivity coefficient. However, when adding 0.2% Nafion to the membrane, an optimum is observed - biosensors with a membrane composition of 1.5% siloxane + 0.2% Nafion have the best sensitivity compared to other biosensors based on mixed membranes.

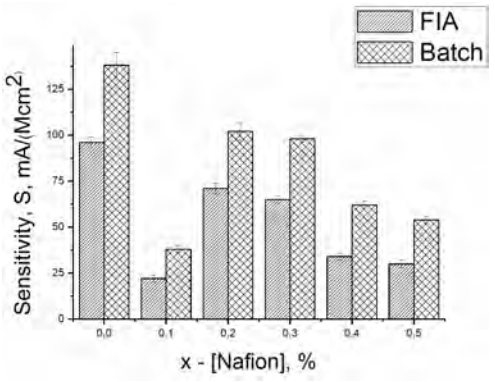

Fig. 2 The sensitivity for lactate biosensors based on composite membranes in FIA and batch mode.

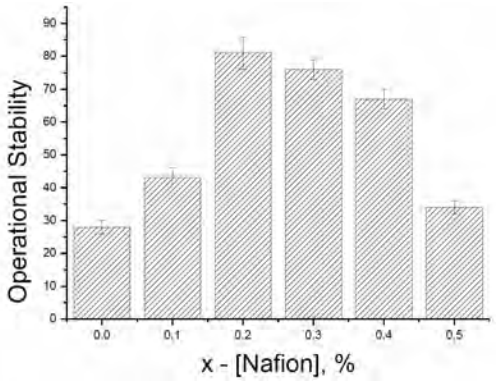

Fig. 3 Operational stability for lactate biosensors based on composite membranes in FIA mode.

Operational stability is the number of injections that can be measured to a loss of 5% of the value of the initial response. The study the operational stability we performed the experiment in the FIA mode, which meets the needs of clinical diagnostics. Adding Nafion to the membrane improves stability for all biosensors (Fig. 3) based on mixed membranes, reaching a maximum for biosensors with a membrane composition of 1.5% siloxane + 0.2% Nafion, which corresponds to the optimum sensitivity for biosensors with the same membrane composition. Thus, it was possible to increase the stability of lactate biosensors by almost 3 times compared with previously used lactate biosensors based on polyalkoxysilan membranes only.

Therefore, we assume that the membrane composition (1.5% siloxane + 0.2% Nafion) creates the most favourable environment for lactate oxidase.

4. Conclusions

The optimal membrane composition (1.5% siloxane + 0.2% Nafion) was determined for lactate biosensors based on the polyalkoxysilan-Nafion membranes. Therefore, operational stability for these composite lactate biosensors was increased by almost 3 times, while maintaining the range of the determined contents (1×10^{-6}– 5×10^{-4} M in the FIA mode) and sensitivity coefficients (71 ± 3 mA $M^{-1}cm^{-2}$). Although, Nafion shields the positively charged enzyme, the optimum 1.5% siloxane + 0.2% Nafion indicates the creation of the most favourable environment for the enzyme.

Acknowledgments

Financial support through Russian Science Foundation grant number 19-13-00131 is greatly acknowledged.

References

[1] Yashina E.I., Borisova A.V., Karyakina E.E., Shchegolikhina O.I., Vagin M.Yu., Sakharov D.A., Tonevitsky A.G., Karyakin A.A.: Sol-Gel immobilization of lactate oxidase from organic solvent: Toward the advanced lactate biosensor. *J. Anal. Chem.* **82** (2010), 1601–1604.

[2] Goodwin M.L., Harris J.E., Hernández A., Gladden L.B.: Blood lactate measurements and analysis during exercise: A guide for clinicians. *J. Diab. Sci. Technol.* **4** (2007), 558–569.

[3] Karyakin A.A.: Prussian Blue and its analogues: Electrochemistry and analytical applications. *J. Electroanal.* **13** (2001), 813–819.

[4] Karyakin A.A., Karaykina E.E.: Prussian blue based artificial peroxidase as a transducer for hydrogen peroxide detection. Application to biosensors. *J. Sens. Actuators.* **57** (1999), 268–273.

[5] Pribil M.M., Karyakina E.E., Karyakin A.A.: Rapid optimization of a lactate biosensor design using soft probes. *J. Electroanal. Chem.* **731** (2014), 112–118.

[6] Karpova E.V., Karyakina E.E., Karyakin A.A.: Communication-accessing stability of oxidase-based biosensors via stabilizing the advanced H_2O_2 transducer. *J. Electrochem. Soc.* **164** (2017), B3056–B3058.

Investigation of Ru, Rh, Pd, Os, Ir, Pt, Au chlorocomplexes sorption preconcentration in static and dynamic mode on the new polyvinylpyridine sorbents

Yulia A. Krasilnikova[a, *], Alexander S. Dubenskiy[a, b], Irina F. Seregina[a], Mikhail A. Bolshov[a], Lyudmila A. Pavlova[c], Vladimir A. Davankov[c]

[a] *Analytical Chemistry Division, Chemistry Department, Lomonosov Moscow State University, 1–3 Leninskie Gory, 119991 Moscow, Russian Federation* ✉ *yu.a.krasilnikova@mail.ru*
[b] *Geological Institute of Russian Academy of Sciences, Pyzhevsky lane 7, 119017 Moscow, Russian Federation*
[c] *A. N. Nesmeyanov Institute of Organoelement Compounds of Russian Academy of Sciences, Vavilova St. 28, 119991, Moscow, Russian Federation*

Keywords
dynamic sorption
noble metals
polyvinylpyridine sorbents
preconcentration
static sorption

Abstract
Sorption preconcentration of noble metals chlorocomplexes on new polyvinylpyridine sorbents was investigated. The new pyridinium-containing sorbents occur high sorption capacity in dynamic and static mode of preconcentration. It was established sorption degree of Ru, Rh, and Ir largely depends on form of these ones in solution. It is supposed that pyridinium-containing sorbents function as a complexing ion exchanger.

1. Introduction

The noble metals (Ru, Rh, Pd, Os, Ir, Pt, Au) are called "Vitamin of Modern Industry" by a reason of ones well thermal and electrical stability, catalytic activity, resistance toward corrosion. Natural sources of noble metals are exhaustible. Therefore, there is a growing interest in low-grade deposits with concentration 10^{-5}–10^{-3} wt. % of noble metals, which may be economically advantageous for the separation of valuable components if it will be possible to estimate the degree of noble metals extraction. The determination of noble metals within the concentration range of 10^{-8}–10^{-6} wt.% requires preconcentration and separation analytes from the matrix components even for very sensitive ICP-MS method. Sorption preconcentration is ecologically friendly, highly efficient and easy to use. Quantitative extraction of noble metals chlorocomplexes can be carried out on nitrogen atom(s) containing sorbents with heterocyclic functional groups. However, there are some problems with desorption of analytes by reason of

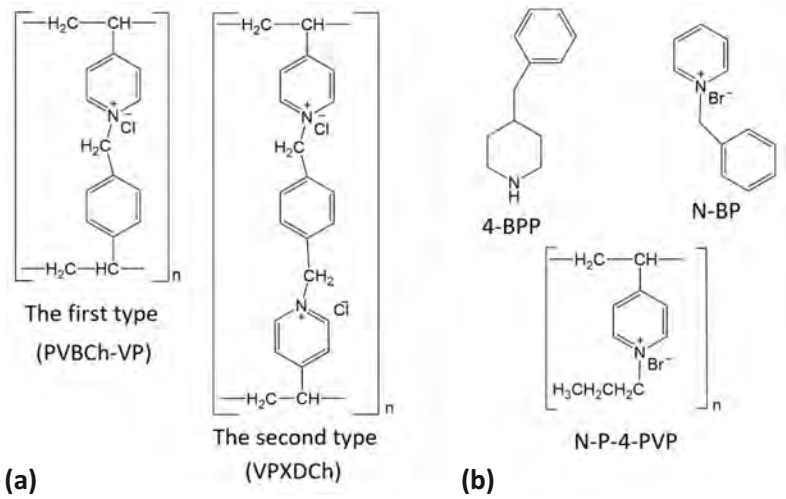

Fig. 1 The structures of used (a) sorbents: copolymer of 4-vinylpyridine and vinylbenzyl chloride (PVBCh-VP), and copolymer of *p*-xylylene dichloride and 4-vinylpyridine (VPXDCh); and (b) model monomer units: 4-benzylpiperidine (4-BPP), *N*-benzylpyridine bromide (N-BP), and *N*-propyl-4-polyvinilpyridine bromide (N-P-4-PVP).

a strong bond between nitrogen from sorbent and central atom of complexes. It requires a more detailed study for a selection of fitting desorption agent.

In this research, sorption of noble metals using new polyvinylpyridine sorbents was investigated.

2. Experimental

2.1 Reagents and chemicals

The following heterocyclic amines were used as model monomer units of using sorbents: 4-benzylpiperidine (≥ 99.0% for synthesis, Sigma-Aldrich, USA), *N*-benzylpyridine bromide and *N*-propyl-4-polyvinilpyridine bromide (synthesised by Davankov's group from A.N. Nesmeyanov Institute of Organoelement Compounds of Russian Academy of Sciences). Two types of hyper-crosslinked sorbents (synthesised by Davankov's group from A.N. Nesmeyanov Institute of Organoelement Compounds of Russian Academy of Sciences) were used for the preconcentration of noble metals chlorocomplexes. The first type containing one pyridinium group in a monomer unit is copolymer of 4-vinylpyridine and vinylbenzyl chloride (PVBCh-VP). The second type containing two pyridinium groups in monomer unit is copolymers of *p*-xylylene dichloride and 4-vinylpyridine (VPXDCh). The main characteristics of both sorbents types was: particle size 315 μm, surface area 40 m^2 g^{-1}. The structures of the model monomer units and sorbents are presented on Fig. 1.

The copper alloy SOMB-6 (SRM 7202-95, EZOCM JSC, Russian Federation) and the ICP-MS-68A-C multi-element standard solution, containing 10 mg L^{-1} Ru, Rh, Pd, Os, Ir, Pt, and Au, and single-element solutions (High-Purity Standards, USA) were used as sources of noble metals for different stock and model solutions. Concentrations of noble metals in the stock solution from SOMB-6 were 500 μg L^{-1} for Ru and 1250 μg L^{-1} for all other noble metals except Os. Single-element 1000 mg L^{-1} indium standard solution (High-Purity Standards, USA) was used for preparation of the internal standard solutions. All solutions were prepared using deionized water (18.2 MΩ cm, Millipore, France).

The following acids were used: concentrated nitric acid (65%, p. a. grade, Merck, Germany) and concentrated hydrochloric acid (37%, puriss. spec. grade, Sigma Tek, Russian Federation).

Carbonyl nickel powder (Ni content not less than 99.7%, Normetimpeks, Russian Federation), sulphur (puriss. spec. grade, LabTeh, Russian Federation), sodium carbonate (p. a. grade, MZHR, Russian Federation), sodium tetraborate decahydrate (borax) and silicon dioxide (silica) (all p. a. grade, ReaHim, Russian Federation) were used for NiS fire-assay of the copper alloy SOMB-6.

2.2 Instrumentation

All of the measurements were carried out with a quadrupole ICP-MS spectrometer, Agilent 7500c (Agilent Technologies, Japan). The data were acquired and processed with the ICP-MS ChemStation software package (version G1834B, Agilent Technologies). The following isotopes of noble metals were used: ^{99}Ru, ^{101}Ru, ^{102}Ru, ^{103}Rh, ^{108}Pd, ^{188}Os, ^{189}Os, ^{190}Os, ^{193}Ir, ^{195}Pt, ^{197}Au. Indium was used as internal standard to account for the matrix effect and temporal changes of the mass-spectrometer sensitivity curve. The concentration of indium in the analysed solutions was 5 μg L^{-1}. The detailed operating conditions of the mass-spectrometer and a list of auxiliary equipment are presented in our previous work [1].

Preconcentration experiments were carried out in dynamic and static mode. The scheme of dynamic preconcentration system is presented on Fig. 2. Sorption columns with sorbent bed depth from 4 mm to 39 mm were used.

Dynamic sorption preconcentration of noble metals was carried out after conditioning the column with the sorbent by pumping 5 mL of 0.7 M HCl solution. At the dynamic sorption preconcentration stage the model solution was pumped through the column at the rate of 1.3–2.3 mL min^{-1}. The solution passed through the column (waste solution) was collected in glass test-tubes for subsequent analysis. The whole system was then cleaned with 5–7 mL of 0.7 M HCl solution.

Portions of sorbent for static mode experiments were picked out by sorption column because these sorbents may become unserviceable after drying. At the static sorption preconcentration stage, portions of sorbent were collected in test-tubes, followed by addition of noble metals chlorocomplex solutions and shaking for a fixed time.

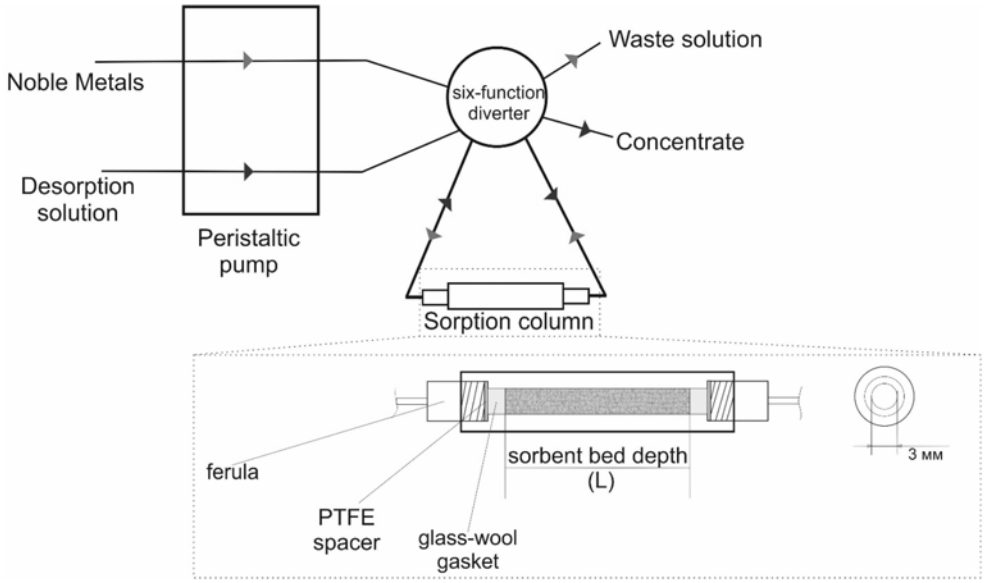

Fig. 2 The scheme of dynamic preconcentration system.

The efficiency of noble metals sorption on hyper-crosslinked polyvinylpyridine sorbents was estimated with the degree of sorption (S/%) as calculated using the following formula

$$S = 100\% - \frac{m_w}{m_0} \cdot 100\% \quad (1)$$

where m_0 is the initial content of noble metals in a model solution (μg); m_w is the content of noble metals in a waste solution (μg). The initial content of noble metals in freshly prepared model solutions used for sorption preconcentration was controlled by ICP-MS analysis each experimental day.

Spectrums of acid solutions of model monomeric units with noble metals were obtained by UV-Vis scanning spectrophotometer T-70 (PG Instruments Limited, UK). Wavelength range was 190–1000 nm. Unit increment was 1 nm.

3. Results and discussion

Primarily, sorption degree of noble metals in dynamic mode on two types of pyridinium-containig sorbents was estimated and there is presented in Table 1. Based on the data of Table 1, it was decided to carry out a subsequent preconcentration in dynamic mode on the sorbent of first type. The differences between the degrees of sorption for the first and second types of sorbents can be associated with larger pores of the first type of sorbent due to its less rigid structure.

Table 1
Comparison of noble metals sorption degree on two types of hyper-crosslinked sorbents containing pyridinium groups (n = 3, P = 0.95). Sorption preconcentration was carried out from solutions of noble metals-containing (except Os) copper alloy dissolved in aqua regia.

Noble metal	Degree of sorption S/%	
	VPXDCh[a]	PVBCh-VP[b]
Ru	72 ± 2	75 ± 3
Rh	66 ± 3	75 ± 5
Pd	100 ± 5	100 ± 2
Ir	98 ± 1	100 ± 5
Pt	97 ± 2	98 ± 2
Au	98 ± 5	100 ± 3

[a] Copolymer of *p*-xylylene dichloride and 4-vinylpyridine.
[b] Copolymer of 4-vinylpyridine and vinylbenzyl chloride.

Table 2
Forms of noble metals in different hydrochoric acid solutions.

Noble metal	c(HCl)/mol dm^{-3}	
	0.1–3.0	12
Ru	Predominantly $[Ru_2O_2(H_2O)_2Cl_6]^{2-}$ and $[Ru_2O(H_2O)_2Cl_8]^{2-}$	$[RuCl_6]^{2-}$
Rh	Predominantly $[Rh(H_2O)Cl_5]^{2-}$ and $[Rh(H_2O)_2Cl_4]^-$	$[RhCl_6]^{3-}$
Pd	$[PdCl_4]^{2-}$ and $[Pd(H_2O)Cl_5]^-$	$[PdCl_4]^{2-}$
Os	Predominantly $[Os(H_2O)Cl_5]^-$	$[OsCl_6]^{2-}$
Ir	*cis*– and *trans*– configurations of $[Ir(H_2O)_2Cl_4]^-$	$[IrCl_6]^{2-}$
Pt	$[PtCl_4]^{2-}$	$[PtCl_4]^{2-}$
Au	$[AuCl_4]^-$	$[AuCl_4]^-$

Second, influence of dissolution way of copper allow was investigated. It was determined, sorption preconcentration of all noble metals group occur quantitatively after the NiS fire-assay of the copper alloy in comparison to ordinary aqua regia dissolution. Example Ru and Rh sorption degrees increase from 75% to 97%. Sorption degrees of Ru, Rh and Ir largely depend on form of these ones in solution. Noble metals forms in solutions with different HCl concentrations are presented in Table 2 [2]. Chlorocomplexes of Ru, Rh, Ir turns to aquachloromplexes very quickly after dilution.

The dependence of the sorption degrees on the sorbent bed depth is presented in Table 3. Based on data of Table 3 it is quite within reason to suggest this type of sorbents occur high sorption capacity. It supposition was confirmed in static sorption mode too. Sorption degrees of all noble metals from 2500 ppb solution in static mode were more than 85%.

Table 3
The dependence of the sorption degrees (S/%) of all noble metals (n =3, P = 0.95) on the sorbent bed depth. Sorption preconcentration was carried out from solutions of noble metals-containing (except Os) copper alloy dissolved after the NiS fire-assay. Osmium was added to solution from single-element standard solution. Concentration of Ru was 12 ppb, concentrations of other noble metals were 25 ppb in solution for preconcentration.

Noble metal	Sorbent bed depth/mm	
	4	21
Ru	95 ± 1	95 ± 1
Rh	92 ± 4	95 ± 2
Pd	89 ± 1	95 ± 2
Os	97 ± 3	99 ± 1
Ir	98 ± 2	100 ± 1
Pt	99 ± 1	100 ± 2
Au	100 ± 1	100 ± 1

We suppose that pyridinium-containing sorbents function not only as ion exchanger but as a complexing ion exchanger. This supposition is confirmed, firstly, nonquantitative sorption of Ru, Ir, Rh aquachlorocomplexes from dilute acid solution, and secondly data obtained from spectrums of acid solutions of model monomeric units with noble metals.

According to the literature, pyridine has an absorption maximum at 250 nm and a molar absorption coefficient ε_{250} = 2000 $cm^{-1}mol^{-1}dm^3$ (ref. [3]). Model monomeric units such as *N*-benzylpyridine bromide and *N*-propyl-4-polyvinil-pyridine bromide have has absorption maximums at 259 nm (ε_{259} = = 4020 $cm^{-1}mol^{-1}dm^3$) and 258 nm (ε_{258} = 3292 $cm^{-1}mol^{-1}dm^3$) respectively, what probably correspond to the pyridinium ring with substituents introduced into it.

For ratio monomer:Me (in the case of *N*-propyl-4-polyvinilpyridine bromide is ratio N:Me) 2.5:1.0 for all noble metals significant increase of a molar absorption coefficient at 258–259 nm 3–7 times was observed. A similar effect with 4-benzyl-piperidine:Me at 260 nm was observed. In the interaction of the water-soluble model polymer *N*-propyl-4-polyvinilpyridine bromide with noble metals batho-chromic shift of the own absorption maximum of the chlorocomplexes of Os (from 344 to 351 nm), Pt (from 262 to 268 nm), and Au (from 313 to 330) was also observed, what was also accompanied by a hyperchromic shift. All this facts argue in favor of complexes or ionic associations' formation between model pyridinium-containing compounds and noble metals. It requires a more detailed study of the mechanisms of interaction between pyridinium-containing sorbents and noble metals chlorocomplexes.

4. Conclusions

The new pyridinium-containing sorbents occur high sorption capacity in dynamic and static mode of preconcentration. But sorption degree of Ru, Rh, and Ir largely depends on form of these ones in solution. Perhaps a nonquantitative sorption of Ru, Rh, and Ir aqua chlorocomplexes is associated with a large aqua coat or with steric difficulty. It is supposed that pyridinium-containing sorbents function as a complexing ion exchanger. This supposition is indirectly confirmed by the spectral behavior of model compounds with noble metals. In addition, it can be suggested that the quantitative sorption of metals is due to the formation of more durable complexes. It requires a more detailed study of the mechanisms of interaction between pyridinium-containing sorbents and noble metals chlorocomplexes.

Acknowledgments

The partial financial support from Russian Foundation for Fundamental Research (RFFR), Grant 17-03-01014 is acknowledged.

References

[1] Dubenskiy A.S., Yakurnova E.D., Seregina I.F., Pavlova L.A., Tsyurupa M.P., Davankov V.A., Bol'shov M.A.: On the features of sorption concentration of Ru on super-crosslinked polystyrenes during the analysis of rocks by the method of inductively coupled plasma mass spectrometry. *Inorg. Mater* **54** (2018), 1379–1386.

[2] *Аналитическая химия металлов платиновой группы.* Ю.А. Золотов, Г.М. Варшал, В.М.Иванов. (ред.). Москва, Едиториал УРСС 2003.

[3] Грандберг И.И.: *Практические работы и семинарские занятия по органической химии.* Москва, Высшая школа 1973.

DC amperometric flow-injection analysis of ions and neutral molecules transduced by electroactive polymers

Marina Zavolskova*, Vita Nikitina, Arkady Karyakin

Chemistry Department, Moscow State University,
1–3 Leninskiye Gory, 119991 Moscow, Russia ✉ *marina-zav@bk.ru*

Keywords
electroactive polymer
flow-injection analysis
lactate

Abstract
We first report on constant potential (dc) amperometric flow-injection analysis (FIA) transduced by electroactive (conductive) polymers. Amperometric response is caused by the polymer recharging in order to maintain the electrode potential at a constant level when (i) ions are crossing the film|solution interface and polarizing electrode| film interface, or (ii) ions or neutral molecules are specifically interacting with the polymer recharging it. In both constant flow and flow-injection regimes, the peak current is dependent on analyte concentrations. Obviously, the FIA mode provides more advantageous analytical characteristics. Constant potential amperometric flow-injection analysis is shown for boronate-functionalized polyaniline. As a proof of concept, the successful dc amperometric detection of lactate in human sweat with boronate-functionalized polyaniline has been shown. The proposed approach would revolutionize the field of conductive/electroactive polymer-supported ion sensing with the introduction of reliable and robust amperometry as a valuable alternative to existing potentiometry.

1. Introduction

It is known that conductive polymers have attracted a great interest of scientists in different fields including analytical chemistry. Of particular importance is the so-called "solid contact" for ion-selective electrodes [1], also referred to as "ion-to-electron interface" [2].

In addition to ion-selective electrodes, conductive polymers can also serve as transducers for neutral molecules. Among synthetic receptors, phenylboronic acid is particularly attractive due to binding selectivity to compounds possessing 1,2- or 1,3-diol functionalities, common structural elements of saccharides and hydroxy acids [3]. Involving phenylboronic acid in conductive polyaniline, the reagentless sensor which is able to generate an increase in its conductivity as a result of binding with polyols, has been elaborated [4].

Flow-injection analysis (FIA) [5] is of particular importance providing simple, cost-effective, and express analysis of multiple samples. In addition, FIA protocol involves a transducer washing step after each injection, which is important for its regeneration if it is inhibited by the analyte or the product of its transformation.

The most reliable detection principle for FIA is constant potential (dc) amperometry. However, for conducting polymer-based transducers, this detection principle has not been reported yet. The attractive performance characteristics of the proposed constant potential (dc) amperometric FIA transduced by electroactive polymers are the improved precision and signal-to-noise ratio, resulting in a wider calibration range, better reproducibility and short response time. As a proof of principle, the analysis of real objects has been demonstrated through successful amperometric lactate detection in human sweat.

2. Experimental

2.1 Reagents and chemicals

Potassium L-lactate, and D-fructose, 3-amino-phenylboronic acid hydrochloride were purchased from Sigma-Aldrich (Germany). Inorganic salts and acids were obtained of the highest purity from Reachim (Russia). Pilocarpine chloride (1%) was purchased from Ferein (Russia). Planar screen-printed three-electrode sensor structures (Rusens Ltd., Russia) had a carbon working electrode (diameter 1.8 mm) encircled with a carbon auxiliary electrode.

2.2 Instrumentation

Cyclic voltammetry was carried out using a μAUTOLAB III (Metrohm, The Netherlands), and constant potential amperometry was carried out using a PalmSens 3 (PalmSens, The Netherlands). Skin electro-phoresis was made using Potok-1 (Russia). The flow-injection setup consisted of a Perfusor Compact syringe pump (Braun, Germany), homemade flow-through wall-jet cell with a 0.5 mm nozzle, and injector (IDEX Health & Science LLC). The flow rate used was of 0.67 mL min^{-1}.

2.3 Methods

Cyclic voltammetry was carried out in a three-compartment electrochemical cell (with separated compart-ments of all electrodes) containing a glassy carbon auxiliary and Ag|AgCl in 1 M KCl reference. Boronate functionalized polyaniline was synthesized by electropolymerization of 3-aminophenylboronic acid from its 0.04–0.15 M solution in 0.1–0.3 M sulfuric acid containing potassium L-lactate (0.9 M) or sodium fluoride (0.2 M). The electropolymerization was carried out by cycling the applied potential at a sweep rate of 40 mV s^{-1}, and the anodic switching potential was in the range 0.85–0.90 V.

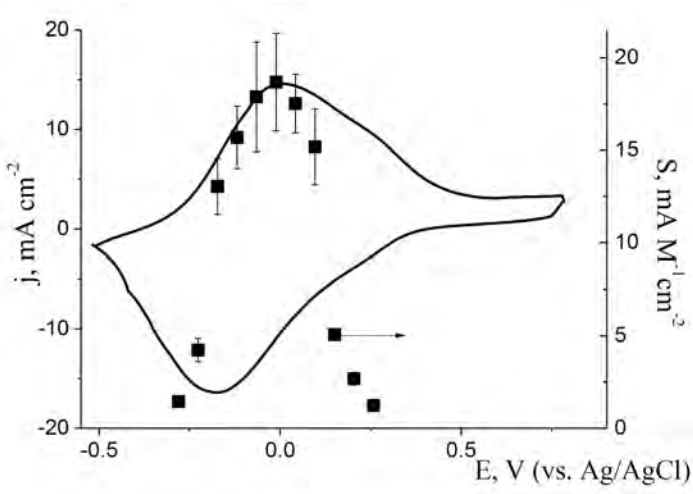

Fig. 1 Sensitivity of amperometric flow-injection lactate detection as a function of the applied (dc) potential (■) in comparison with cyclic voltammogram (sweep rate 40 mV s^{-1}) of boronate functionalized polyaniline; 0.1M phosphate buffer, pH = 6.0.

Sweat samples were collected from healthy human volunteers using a Macroduct Sweat Collector for 30 min after activation of the skin spot with 1% pilocarpine solution by means of electrophoresis. Informed content was obtained from all subjects. Samples were stored frozen at −18 °C. For standardization of the analytical procedure, sweat samples were 50 times diluted with buffer to a final phosphate concentration of 100 mM (pH = 6.0) and 0.7 M NaCl.

3. Results and discussion

An initial aim of this study was to improve nonenzymatic lactate detection in human sweat. Accordingly, lactate imprinted boronate-functionalized polyaniline [6] was deposited onto the screen-printed electrode surface. Cyclic voltammograms of the polymer growth in the potential range from 0.00 to 0.85 V, Ag|AgCl, display an increase in current at the anodic switching potential indicating the deposition of the conductive polymer. Cyclic voltammograms of the resulting modified electrode in monomer-free solutions indicate that electroactivity of the resulting polymer is similar to that of conventional conducting polyaniline (Fig.1).

3.1 dc Amperometric flow-injection analysis of saccharides and hydroxy acids

After injection of lactate, the FIA system with the integrated boronate-functionalized polyaniline (BFPAn)-modified electrode in constant potential mode generates a couple of current peaks: the anodic sharp peak followed with the cathodic peak. Injection of fructose results in a similar couple of peaks, but directed opposite (Fig. 2).

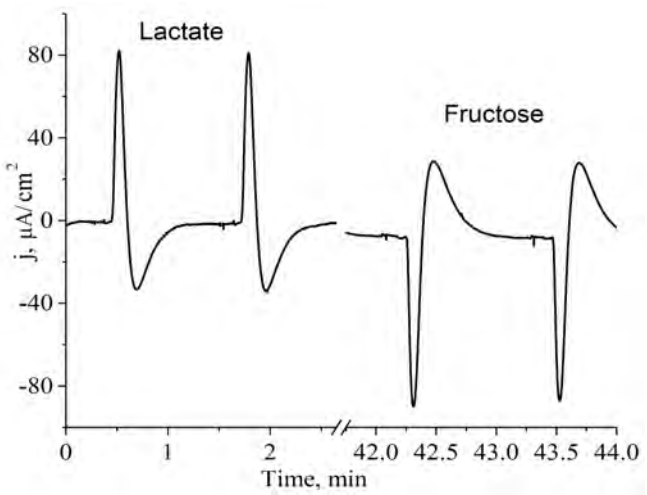

Fig. 2 Flow-injection current responses towards 5 mM L-lactate and 20 mM D-fructose; 0.1 M phosphate buffer, pH = 6.0; E_{dc} = 0.00 V.

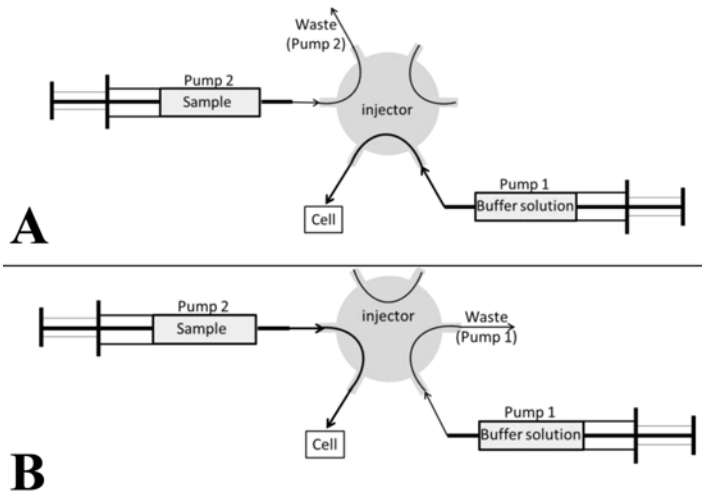

Fig. 3 Scheme of the two-pumps setup as a version of the flow-injection setup.

To understand the nature of the observed FIA responses, the system has been also studied in continuous flow mode. To minimize the hydrodynamic disturbance when one solution is changed to another, the injection loop has been disconnected from the injector and the latter inlet has been connected to the second pump (Fig 3). Accordingly, switching injector positions in the "two-pumps" setup results in changing of the solution flows between the continuously working pumps. Figure 4 displays that changing the carrier solution to the lactate-containing one results in a reproducible anodic peak, after which the current falls to the background. Changing the lactate-containing solution back to the carrier solution

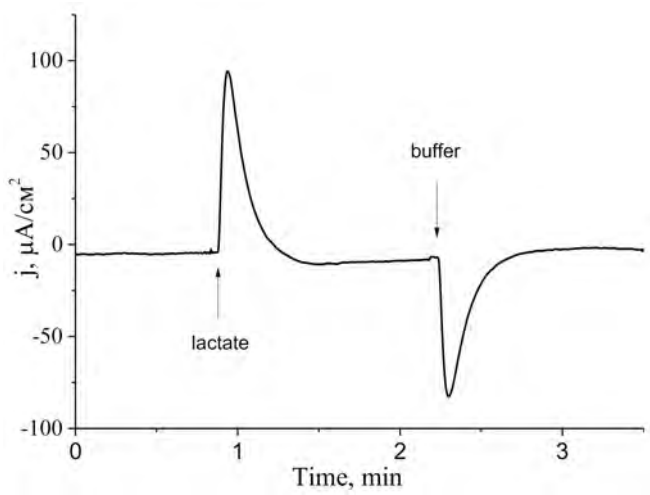

Fig. 4 Constant flow current responses towards 5 mM L-lactate; 0.1M phosphate buffer, pH = 6.0; E_{dc} = 0.00 V.

results in a cathodic peak. The peak height in continuous flow mode is concentration dependent for both lactate and fructose.

Accordingly, the couple of peaks in the flow-injection response can be explained as follows. An appearance of analyte in solution flow causes the current to increase in the corresponding direction. After emptying the injection loop, the carrier solution is changed back to the analyte-free buffer and the polymer has to be recharged causing a current response in the opposite direction. Hence, the first peak of the FIA response has to be considered for analysis. Intuitively, the dc potential for amperometric flow-injection analysis has been chosen close to the polymer redox potential. Indeed, the conductivity window of polyaniline with the rise of solution pH is narrowed and in neutral solutions polyaniline behaves as an electroactive material. As seen, the highest sensitivity of the dc amperometric FIA response coincides with the peak of the cyclic voltammogram.

3.2 Mechanism of dc amperometric response

Let us consider the one-dimensional model for the conductive polymer modified electrode. Obviously, in case of negligible current, the electrode potential is determined by the sum of the electrode|polymer ($E_{e/p}$) and polymer|solution ($E_{p/s}$) potentials.

When anions that are able to interact specifically with the polymer (for example lactate) charge the polymer chain and polarize the electrode|polymer interface. Hence, for maintaining the electrode potential, it is enough to depolarize the latter interface by removing electrons from the polymer film. Accordingly, the increase in lactate ion concentrations results in an anodic current response.

The case of neutral molecules specifically binding boronate-functionalized polyaniline (saccharides) is more complicated. Despite negative charges appearing in the polymer chain, this interaction is coupled with the consumption of hydroxyl, thus, decreasing local pH in the polymer film. Such a pH shift increases the redox potential of the polymer; hence, maintaining the electrode potential at a constant level requires cathodic current. The evidence of the local pH shift in the presence of saccharide has been obtained from square wave voltammograms of boronate functionalized polyaniline recorded at different solution pH values and in the presence of fructose.

3.3. dc Amperometric detection of lactate in human sweat

In order to validate the concept of dc amperometric FIA with electroactive polymer, the detection of lactate in human sweat has been demonstrated. This analytical tool is particularly useful as a noninvasive approach for assessing the training level of sportsmen. In contrast to the previously reported impedimetric lactate sensor based on the same transducer, the reported approach provides complete transducer regeneration. Validation of the proposed dc amperometric nonenzymatic FIA of sweat has been carried out using the previously reported highly specific biosensor based on Prussian Blue and the enzyme lactate oxidase as a reference method The measurements using both approaches are in a good agreement, with the Pearson correlation coefficient exceeding 0.9. Hence, the proposed dc amperometric FIA with electroactive polymers is suitable for analysis of real samples.

4. Conclusions

Constant potential (dc) amperometry is apparently the most universal electro-analytical tool because of its simplicity, robustness, and advantageous analytical performance characteristics. With the use of electroactive polymer as a transducer, the dc amperometric flow-injection analysis of ions and neutral molecules is possible. The proposed dc amperometric FIA is expected to improve the ion sensing by introducing more robust and reliable amperometry as a valuable alternative to existing potentiometry. The desired selectivity can be achieved by specific analyte interaction with the electroactive polymer, as shown here.

Acknowledgments

Financial support through the Russian Science Foundation Grant number 19-13-00131 is greatly acknowledged. We thank Mr. Nikolay Z. And Mrs. Elena V. Karpova for her help.

References

[1] Cadogan A., Gao Z.Q., Lewenstam A., Ivaska A., Diamondet D.: All-solid-state sodium-selective electrode based on a calixarene ionophore in a poly(vinyl chloride) membrane with a polypyrrole solid contact. *Anal. Chem.* **64** (1992), 2496–2501.

[2] Bobacka J.: Potential stability of all-solid-state ion-selective electrodes using conducting polymers as ion-to-electron transducers. *Anal. Chem.* **71** (1999), 4932–4937.

[3] Bosch L.I., Fyles T.M., James T.D.: Binary and ternary phenylboronic acid complexes with saccharides and Lewis bases. *Tetrahedron* **60** (2004), 11175–11190.

[4] Andreyev E.A., Komkova M.A., Nikitina V.N., Zaryanov N.V., Voronin O.G., Karyakina E.E., Yatsimirsky A.K., Karyakin A.A.: Reagentless polyol detection by conductivity increase in the course of self-doping of boronate-substituted polyaniline. *Anal. Chem.* **86** (2014), 11690–11695.

[5] Ruzicka J., Hansen E.H.: *Flow Injection Analysis*. 2nd ed. New York, Wiley 1988.

[6] Nikitina V.N., Zaryanov N.V., Kochetkov I.R., Karyakina E.E, Yatsimirsky A.K., Karyakin A.K.: Molecular imprinting of boronate functionalized polyaniline for enzyme-free selective detection of saccharides and hydroxy acids. *Sens. Actuators B* **246** (2017), 428–433.

Biopsy needles coated with the antimicrobial coatings

Małgorzata Borowska[a,*], Agata Kot-Wasik[a], Justyna Kucińska-Lipka[b]

[a] *Department of Analytical Chemistry, Faculty of Chemistry, Gdańsk University of Technology, 11/12 Gabriela Narutowicza Street, 80-233 Gdańsk, Poland* ✉ *malborow@student.pg.edu.pl*
[b] *Department of Polymer Technology, Faculty of Chemistry, Gdańsk University of Technology, 11/12 Gabriela Narutowicza Street, 80-233 Gdańsk, Poland*

Keywords
antimicrobial coatings
biopsy needles
drug delivery systems
polymer coatings

Abstract
Drug delivery systems are used to achieve higher therapeutic effects of medicaments in a specific diseased site with minimal toxicological effect. The used of biopolymers in drug delivery systems ensure the biocompatibility, biodegradability and low immunogenicity. Drug delivery systems enhance the drug delivery actively and can be used in different diseases. In this study, two types of polymer coatings were prepared and were applied on biopsy needles surface. High performance liquid chromatography is a very good solution to analysis of release the drug from antimicrobial coatings and it was used in this studies.

1. Introduction

Conventional methods of administering a drug substance do not fully use the therapeutic effect of medicaments. This is due to the distribution of the drug in the body, which begins when the drug is administered by the oral route. This reduces the chance of reaching a large amount of the dose to the destination, which forces it to increase in the applied preparation. Controlling the kinetics of drug release brings many health benefits to patients. It provides an improvement in the effectiveness of the therapeutic substance and reduces the severity of side effects. In addition, controlled drug release systems often also allow the active substance to be delivered accurately to the affected site. The conventional approach is the most often based on the oral intake of the right dose, in order to achieve the desired effect in a changed or painful place. Unfortunately, as it is difficult to control the distribution of the drug in the body, the medicinal substance "by the way" also reaches other places. The effect of this phenomenon is the occurrence of side effects and the need to increase the concentration of the drug substance, so as to be sure that it will produce the desired effect [1].

The use of drug delivery systems can to improve the pharmacological properties of conventional drugs drug delivery systems include particulate

carriers, composed primarily of lipids and/or polymers, and their associated therapeutics. Drug delivery systems are designed to alter the pharmacokinetics and biodistribution of their associated drugs, or to function as drug reservoirs (for example as sustained release systems) [2].

Biofilm-based infections can be as cause of percutaneous implant loss after medical device implantation. Microorganisms in the biofilm form are responsible for a substantial portion of healthcare-related infections. Over 65% of all human infections have been estimated to be biofilm-related. Bacteria's biofilm is an organized biological structure developed by microorganisms growing on a surface and enclosed in an exopolysaccharide matrix. Effective protection against antimicrobial substances provided by this matrix hinders the elimination of microorganisms and allows the infectious disease to diffuse further into tissue [3, 4].

The aim of this study was to prepare two type of coatings which were applied on biopsy needles. One of the coatings were consisted of polyurethane dissolved in dimethyl sulfoxide. The second type of coatings containing an antimicrobial agent like ciprofloxacin were prepared with two biodegradable polymers: polyvinylpyrrolidone and carboxymethyl cellulose. In this study, coatings that differed in the content of ciprofloxacin were prepared.

2. Experimental

2.1 Chemicals and reagents

Polyvinylpyrrolidone and standard ciprofloxacin powder were purchased from Sigma-Aldrich (USA). Carboxymethyl cellulose was purchased from Bresciani (Italy). Dimethyl sulfoxide (>99%) was purchased from TechlandLab (Poland). Polyurethane was purchased from Epaflex (Italy). Epaline 380A10 25 based on thermoplastic polyurethane was used. Analytical-grade ethyl acetate, ethyl alcohol (96%) and potassium phosphate monobasic dihydrate were purchased from POCh (Poland). Ortophosphoric acid solution 85% (analytical grade) was purchased from Chempur (Poland). Acetonitrile (HPLC grade) was purchased from Merck (Germany). Ultrapure water was prepared using HPL5 system from Hydrolab (Poland).

2.2 Sample preparation

Preparation of coatings on biopsy needles surface was proceeded in two stages. Firstly, coatings based on polyurethane were prepared. During first stage polymer coatings based on polyurethane were prepared through an appropriate amount of polyurethane in dimethyl sulfoxide was dissolved. Flasks with a mixture of polyurethane and dimethyl sulfoxide were heated to 80 °C and stirred using a magnetic stirrer until the polymer was completely dissolved. These solutions consisted 5 and 10% of polyurethane. After the polyurethane had dissolved, the

Table 1
Content of ingredients in the second polymer coating.

Ingredient	Content of ingredient			
	Variant 1	Variant 2	Variant 3	Variant 4
Ciprofloxacin[a]	0.05 g (0.10%)	0.10 g (0.20%)	0.15 g (0.30%)	0.20g (0.40%)
Deionized water	2.5 ml			
Ethyl alcohol (40 or 96%)	30 ml			
Ethyl acetate	20 ml			
Polyvinylpyrrolidone	0.40 g			
Carboxymethyl cellulose	0.04 g			

[a] The % content of ciprofloxacin in the coating is given in brackets.

biopsy needles were immersed in the polymer solution for about 30 seconds. For each polymer content (5 and 10% polyurethane) in the coating, biopsy needles with single and double polymeric layers were prepared. For needles with two coatings on the surface, the second layer was applied after the first was dried.

In the next step, second coating, coating including ciprofloxacin was prepared. In this stage, four variants of coatings were prepared that were differed in the content of ciprofloxacin. The composition of the second coating in all variants is presented in Table 1.

The second coatings were prepared by mixing two solutions. One of the solutions were consisted of ciprofloxacin dissolved in deionized water. In the second solution, the appropriate amounts of polyvinylpyrrolidone and carboxymethyl cellulose were dissolved in a mixture of ethyl acetate and ethyl alcohol. Needles that were prepared in the first stage (containing a polyurethane-based coating on the surface) were immersed in a solutions containing ciprofloxacin (second coatings) for 30 seconds. During the preparation of the second coatings two different ethyl alcohol were used. In the one case, 96% ethyl alcohol was used. In the second case dilute ethyl alcohols (40%) was used.

2.3 HPLC-UV

An Agilent 1100 series LC system consisted with binary pump, an on-line degasser, an autosampler and a thermostatted column compartment coupled with spectrophotometric detector type UV. ZORBAX Eclipse XDB-C8 (150×4.6 mm, 5µm; Agilent, USA) column was used during analysis. The system was operated isocratically at a flow rate of 0.8 ml/min. The injection volume was 50µL. The column was worked at 40°C. The UV detector was set at 277 nm. Analysis of one sample takes 5 minutes.

2.4 Preparation of the mobile phase

A 0.02 M phosphate buffer at pH = 2.7 was prepared using potassium dihydrogen phosphate and orthophosphoric acid. This was then eluted together with acetonitrile to make up a mobile phase of buffer and acetonitrile 80:20 (*v/v*).

2.5 Ciprofloxacin release studies

The coated biopsy needles (with a known coating weight on needle) were placed in 10 ml deionized water for 15, 30 and 60 minutes, respectively. After a predetermined time, a sample solution was taken and tested by HPLC-UV (procedure 2.3).

3. Results and discussion

3.1 Sample preparation

Firstly, coatings based on polyurethane were prepared. Solutions containing polyurethane in dimethyl sulfoxide were prepared in two different variants (5 and 10%). Biopsy needles with single and double polyurethane–based coatings were prepared. Preparation of polyurethane-based coatings is very long-term process. The dissolution of polyurethane in dimethyl sulfoxide proceeds gradually and slowly and requires the use of an elevated temperature (80 °C). During the preparation of a 10% polyurethane solution in dimethyl sulfoxide, approximately 6 hours were used to completely dissolve the polymer.

Secondary, coatings containing ciprofloxacin were prepared. In this step, two different ethyl alcohols were used. When we used 96% ethyl alcohol, it turned out that polymers used in this studies (polyvinylpyrrolidone and carboxymethyl cellulose) do not dissolve. The complete dissolution of polyvinylpyrrolidone and carboxymethyl cellulose was obtained only after dilute ethyl alcohol was used. The ethyl alcohol was diluted with deionized water. In addition, in this step, four different variants coatings containing ciprofloxacin were prepared. It turned out that for variant 4 with the highest content of ciprofloxacin, this drug is not dissolved in the solvents that make up the coating. A solution with this ciprofloxacin content was not applied to the needles.

3.2 Ciprofloxacin release from antimicrobial coatings

The analysis of the ciprofloxacin release rate from biopsy needle coatings was carried out at various time intervals (15, 30, 60 min). This is the time from placing the coated needle in deionized water to take a sample of the solution for analysis by HPLC-UV. At this stage of the research, the profile of release of the drug from coated needles cannot be determined yet. It is necessary to perform a more of

experiments. HPLC-UV analysis showed that ciprofloxacin is released from coatings on biopsy needles.

4. Conclusion

The conducted research proved that there is a possibility of effective coating of the surface of biopsy needles with an antimicrobial agent in the form of ciprofloxacin. It turned out that it is possible to prepare coatings containing a maximum of 0.3% ciprofloxacin. Higher content of ciprofloxacin in the coating is impossible due to incomplete dissolution of the drug. In addition, it turned out that increasing the amount of water during the preparation of the second coating allows the dissolution of all ingredients.

References

[1] Barbaresso R.C., Rău I., Zgârian R.G., Meghea A., Ghica M.V.: Niflumic acid-collagen delivery systems used as anti-inflammatory drugs and analgesics in dentistry. *Comptes Rendus Chim.* **17** (2014), 12–17.

[2] Allen T.M, Cullis P.R: Drug delivery systems: Entering the mainstream. *Science* **303** (2004), 1818–1822.

[3] Nguyen S., Hiorth M., Rykke M., Smistad G.: The potential of liposomes as dental drug delivery systems. *Eur. J. Pharm. Biopharm.* **70** (2011), 75–83.

[4] de Avila E.D., Castro A.G.B., Tagit O., Krom B.P., Löwik D., van Well A.A., Bannenberg L.J., Vergani C.E., van den Beucken J.J.J.P.: Anti-bacterial efficacy via drug-delivery system from layer-by-layer coating for percutaneous dental implant components. *Appl. Surf. Sci*. **488** (2019), 194–204.

Optimization of photochemical vapor generation of nickel with ICP-MS detection

Jakub Šoukal[a, b, *], Stanislav Musil[a]

[a] *Department of Trace Element Analysis, Institute of Analytical Chemistry of the Czech Academy of Sciences, Veveří 97, 602 00 Brno, Czech Republic* ✉ *soukalkuba@gmail.com*
[b] *Department of Analytical Chemistry, Faculty of Science, Charles University, Hlavova 8, 128 43 Prague, Czech Republic*

Keywords
inductively coupled plasma mass spectrometry
nickel
photochemical vapor generation

Abstract
This article deals with optimization of conditions of photochemical vapor generation of nickel for inductively coupled plasma mass spectrometry. The volatile species of nickel was generated in the flow arrangement, when sample was injected to a stream of a reaction medium using either formic acid or formic acid with the addition of formate anions. Efficient generation was accomplished using a 19W high-efficiency flow-through photoreactor and the generated volatile nickel tetracarbonyl was introduced to an inductively coupled plasma mass spectrometer for ultrasensitive detection. Formic acid concentration and the effect of additives were carefully studied with the aim to reach the highest generation efficiency. The limit of detection achieved at chosen optimal conditions was 1.6 pg mL^{-1}. The accuracy and feasibility of this sensitive methodology were successfully verified by analysis of river water certified reference material (SLRS-6) using a standard addition technique.

1. Introduction

Photochemical vapor generation (photochemical vapor generation) is an expanding and promising alternative sample introduction technique for analytical atomic spectrometry. With photochemical vapor generation, an analyte is converted to the volatile species through the action of UV-radiation. The presence of a photochemical agent in the liquid phase is required (typically formic acid or acetic acid). The photochemical generator usually consists of a source of UV radiation, most often a mercury UV tube lamp (emitting mainly at 254 nm), and a reaction coil that is tightly wrapped around and where the analyte in the photochemical agent is irradiated and converted to the volatile species. The material of the reaction coil must be made of a material transparent for UV radiation (quartz or teflon). The advanced photoreactors (high-efficiency flow-through photoreactors) utilize a modified mercury UV lamp where the sample is irradiated in the inner channel (quartz tube) that passes through the discharge of

the UV lamp. Since UV radiation has to transmit only the quartz wall of the inner channel, these photoreactors were shown to irradiate the sample with the photochemical agent more efficiently [1, 2].

The advantage of photochemical vapor generation over more established hydride generation lies in that it can be accomplished using only organic acids which can be obtained in high purity or can be purified in a laboratory. Photochemical vapor generation is more user friendly technique and is considered to be "greener" for the environment [3, 4]. Photochemical vapor generation is also applicable to a broader range of elements, not only to mercury and typical hydride forming elements (Se, As, Sb, Te, Pb, Bi) but also to nonmetals (I, Br, Cl, S) and many transition metals (Ni, Fe, Co, Cu, Cd, Os and very recently also Rh, Pt, Pd, Ag, Au, Ir and Mo) [5, 6].

2. Experimental

2.1 Reagents and chemicals

Deionized water (< 0.2 μS cm^{-1}, Ultrapur, Watrex, USA) was used for the preparation of all solutions. Formic acid (98%, p.a., Lach-Ner, Czech Republic) was purified in-house in a Teflon BSB-939-IR subboiling distillation apparatus (Berghof) and used for preparation of the reaction medium. Ammonium hydroxide (25%, p.a.) was obtained from Sigma-Aldrich (USA). A stock solution of 1000 μg mL^{-1} Ni was purchased from Analytika (Czech Republic) as well as stock solutions of 1000 μg mL^{-1} Cd, Co, Cu and Fe. The certified reference material of river water (SLRS-6) produced by National Research Council (Canada) was employed for method validation.

2.2 Instrumentation

A schematic diagram of the UV-photochemical vapor generation system in a flow-injection mode hyphenated to ICP-MS is depicted in Fig.1. Photochemical vapor generation was carried out using a 19W high-efficiency flow-through photoreactor (Beijing Titan Instruments, China). The generated volatile product was directed by an argon carrier gas to a plastic gas-liquid separator (50 mL) and introduced into a spray chamber of an Agilent 7700x inductively coupled plasma mass spectrometer (ICP-MS). A solution of 1% nitric acid mixed with a solution of 10 ng mL^{-1} rhodium internal standard (IS) was nebulized into the spray chamber creating more robust wet plasma conditions [7]. The typical conditions of ICP-MS used for detection are summarized in Table 1.

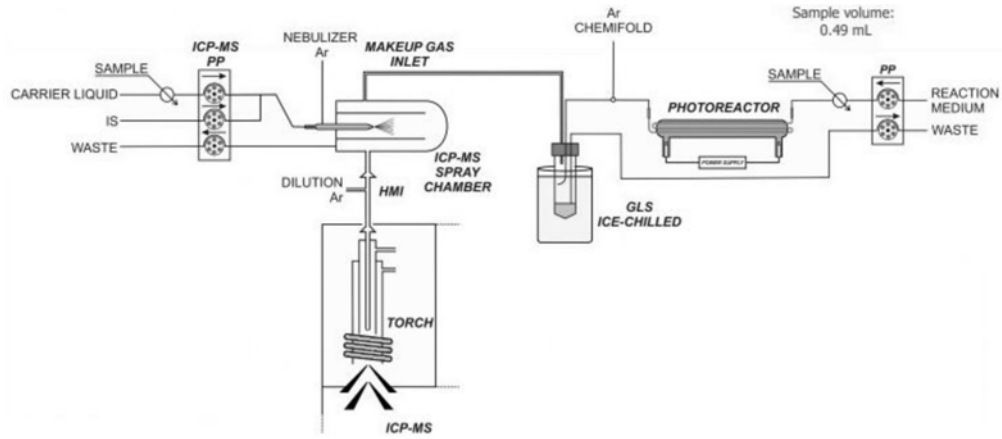

Fig. 1 Schematic diagram of the flow-injection photochemical vapor generation system hyphenated to ICP-MS for vapor introduction of volatile nickel species.

Table 1
Typical ICP-MS parameters for coupling with photochemical vapor generation.

RF power	1600 W
Nebulizer Ar	1.05 L min^{-1}
Dilution Ar (via HMI)	0 L min^{-1}
Ar (chemifold) for photochemical vapor generation	100 mL min^{-1}
ICP-MS pump	0.35 mL min^{-1} carrier liquid, 0.06 mL min^{-1} IS
Spray chamber temperature	2 °C
He collision cell gas	4.1 mL min^{-1}
Measurement mode	Time resolved analysis
Measured isotopes (dwell time)	^{58}Ni (0.1 s), ^{60}Ni (0.1 s), ^{103}Rh (IS, 0.05 s)

3. Results and discussion

Preliminary experiments, such as optimization of a flow rate of Ar (chemifold) and irradiation time, were carried out using atomic absorption spectrometry for detection with a miniature diffusion flame as an atomizer. The optimum flow rate of Ar (chemifold) was at 100 mL min^{-1}. The highest sensitivity was found at 1.5 mL min^{-1} of the reaction medium. This flow rate corresponds to irradiation time of 29 s in the photoreactor which is reflected on a total time of the measurement of 350 s per one sample injection.

Afterwards, a composition of the reaction medium was investigated which meant in particular: the concentration of formic acid, the influence of pH and the effect of metal additives. First of all, only formic acid was used as the reaction medium. The maximum sensitivity was found at 50% (*w/v*). Since the difference in the sensitivity measured with 30% and 50% formic acid was not so significant, 30% formic acid was chosen for all the other experiments from the economical

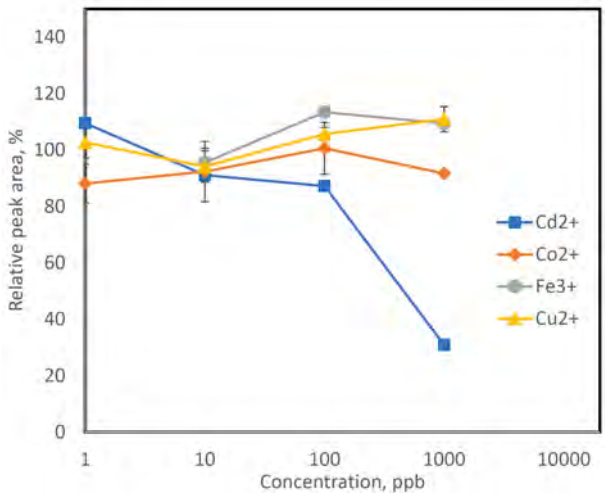

Fig. 2 Relative effects of added transition metals on photochemical vapor generation of 1 ng mL^{-1} Ni in 30% formic acid.

reason. Subsequently, various volumes of liquid ammonium were added, forming ammonium formate while keeping the concentration of formic acid constant at 30% in the final solution. The maximum response was achieved with formate concentration of 1.25 mol L^{-1} (pH ≈ 2.40) and the sensitivity was increased by seventy percent in comparison to the situation when no formate was added (pH ≈1.40).

An influence of various metal additives (Fe^{3+}, Cd^{2+}, Cu^{2+}, and Co^{2+} ions) with respect to potential enhancement in generation efficiency was also investigated. There was not any serious positive effect (Fig. 2). Cadmium ions caused even serious interference at 1000 ng mL^{-1}.

A special attention was paid to reduce the Ni contamination in the reaction medium and to decrease the measured baseline level of the signal intensity and thus limits of detection. The experiments showed that trace-cleaned glassware (by vapors of nitric acid) is required as well as using ultrapure water. It was also extremely important to use deionized water for preparation of all solutions directly from the ion exchanger. The achieved limit of detection at chosen optimal conditions (formic acid with formate) was 1.6 pg mL^{-1}. Limit of detection for 30% formic acid without addition of formate was 2.8 pg mL^{-1}. Repeatability of the measurement (RSD) at 1 ng mL^{-1} of Ni was excellent, better than 2% for both the reaction media.

The accuracy and feasibility of this sensitive methodology was successfully verified by analysis of the certified reference material river water (SLRS-6) with certified nickel content of 616±2.2 ng mL^{-1} . Due to HNO_3 presence used for stabilization of the certified reference material that interfered seriously, starting even at the concentration of 5 mmol L^{-1}, the material had to be diluted and

measured using a standard addition technique. The found concentration of nickel in the certified reference material SLRS-6 was 610±15.5 ng mL^{-1}

4. Conclusion

Photochemical vapor generation of Ni has been investigated in detail using ICP-MS as the detector. The method is extremely sensitive with a very good repeatability. $Ni(CO)_4$ is supposed to be the generated volatile product but this has to been confirmed. Very high efficiency of photochemical vapor generation has been reached using 30% formic acid which can be substantially improved by addition of ammonium formate. Accuracy of the developed method has been verified using river water certified reference material. Photochemical vapor generation is prone to serious interferences from nitrates which have to be taken into account with respect to real sample preparation.

Acknowledgments

The support of the Grant Agency of the Czech Republic (19-17604Y), Czech Academy of Sciences (Institutional support RVO: 68081715) and Charles University (project SVV260440) is gratefully acknowledged.

References

[1] Rybínová M., Červený V., Hraníček J., Rychlovský P.: UV-fotochemické generování těkavých sloučenin pro potřeby atomových spektrometrických metod. *Chem. Listy* **109** (2015), 930–937. (In Czech.)
[2] Sturgeon R.E.: Photochemical vapor generation: a radical approach to analyte introduction for atomic spectrometry. *J. Anal. At. Spectrom.* **32** (2017), 2319–2340.
[3] Yin Y.G., Liu J.F., Jiang G.B.: Photo-induced chemical-vapor generation for sample introduction in atomic spectrometry. *TrAC, Trends Anal. Chem.* **30** (2011), 1672–1684.
[4] He Y.H., Hou X.D., Zheng R.E., Sturgeon R.E.: Critical evaluation of the application of photochemical vapor generation in analytical atomic spectrometry. *Anal. Bioanal. Chem.* **30** (2007), 769–774.
[5] de Oliveira R.M.; Borges D.L.G.: UV photochemical vapor generation of noble metals (Au, Ir, Pd, Pt and Rh): A feasibility study using inductively coupled plasma mass spectrometry and seawater as a test matrix. *J. Anal. At. Spectrom.* **33** (2018), 1700–1706.
[6] Šoukal J., Sturgeon R.E., Musil S.: Efficient photochemical vapor generation of molybdenum for ICP-MS Detection. *Anal. Chem.* **90** (2018), 11688–11695.
[7] Musil S., Pétursdóttir Á.H., Raab A., Gunnlaugsdóttir H., Krupp, E., Feldmann, J.: Speciation without chromatography using selective hydride generation: Inorganic arsenic in rice and samples of marine origin. *Anal. Chem.* **86** (2014), 993–999.

Chemometric estimation of spectral profile of internal standard

IVAN KRYLOV

Department of Chemistry, Lomonosov Moscow State University,
1–3 Leninskiye Gory, 119991 Moscow, Russia ✉ *ikrylov@laser.chem.msu.ru*

Keywords
chemometrics
internal standard
optimization
simulated data

Abstract
The work is concerned with a multivariate internal standard method. A dataset of spectra containing multiple independent peaks is simulated, then each spectrum is multiplied by a random factor. Classical approach of dividing by the intensity of the internal standard peak is compared with the multivariate approach of evolving the internal standard profile to compute scalar products with each spectrum. Approaches are evaluated by root-mean-square error on leave-one-out cross-validation of a PLS model. A minor improvement is demonstrated using the multivariate technique.

1. Introduction

Internal standard is an important pre-treatment technique in cases where the scale of the analytical response may vary from experiment to experiment due to circumstances outside the experimenter's control. Ideally, the internal standard is chosen to prevent all interference from varying components of the samples, so that there is no overlap between predictor values affected by the internal standard and other sources of variance.

Chemometrics makes it possible to resolve overlapping spectral signals into individual components. What if the experiment conditions are so constrained that it is impossible to fully avoid interference? This work attempts to use chemometric techniques to obtain a multivariate internal standard profile from a set of simulated samples with known individual component concentrations by means of partial least squares (PLS) regression.

2. Experimental

The simulated dataset consists of 200 samples containing 6 independently distributed components, each having its own peak in the spectrum. Cachy-Lorentz function with center at x_0, half width at half maximum of w and total area of A was used as model peak profile:

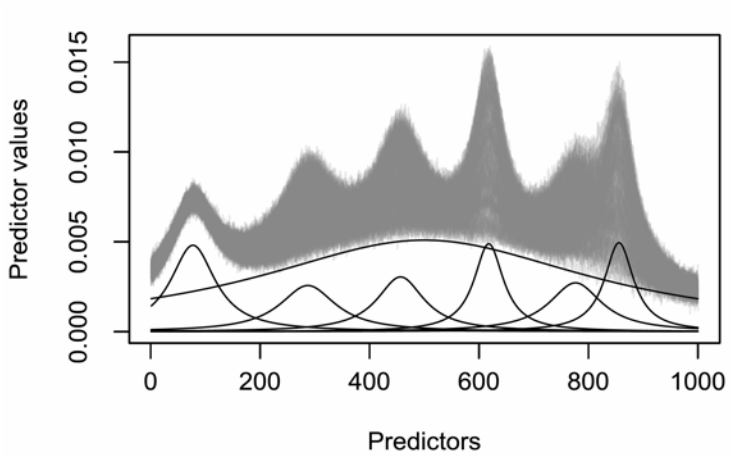

Fig. 1 The whole dataset of simulated spectra used in this work. Grey lines: predictor values, per sample. Black lines: true profiles of pure simulated components.

$$L(x) = \frac{2A}{\pi} \frac{w}{4(x - x_0)^2 + w^2} \tag{1}$$

Each simulated spectrum consisted of 1000 points, spanning x values from 1 to 1000.

The 6 model positions were uniformly scattered across the x value range; the peak widths were chosen to be 7±2% of the x range. In addition, a very wide peak (center at 50%, width of 75% of the spectrum) was added to model data to simulate background.

The peak #1 ($x_0 = 77.21$, $w = 99.29$) has been chosen to be the internal standard and had a fixed area of 0.75 in all samples. In addition, the background had the same area of 6 in all samples. For the rest of the peaks, an experimental design was generated using latin hypercube sampling [1] to get an orthogonal, uniformly-distributed (in [0,1]) design matrix, optimal with respect to the S optimality criterion, to supply the peak area values.

Given the design matrix **A**, with $a_{i,j}$ giving the area of peak number j in the modelled spectrum of the i-th sample, the predictor matrix **S** (with $s_{i,k}$ being the predictor number k in the i-th sample) was simulated using the following formula:

$$s_{i,k} = \sum_j L\left(x_k, x_{0,j}, w_j, A_{i,j}\right) + n_{i,k},\ x_k = 1 \ldots 1000,\ n_{i,k} \sim \mathcal{N}(0, \sigma) \tag{2}$$

The $n_{i,k}$ component amounts to independent and identically distributed random noise with $\sigma = 3 \times 10^{-4}$. See Fig. 1 for the overview of the simulated predictor values along with the "pure component" profiles.

Having calculated the model spectra, each one was multiplied by a normally distributed value to simulate a situation requiring the use of internal standard method:

$$x_{s,ij} = x_{ij} s_i;\ s_i \sim \mathcal{N}(1,0.2) \tag{3}$$

To evaluate the results of different internal standard correction methods, PLS [2] regression models were built to predict the profile area matrix **A** from the scaled predictor matrix $\mathbf{X}_S$. The number of components yielding the least root-mean-square error (RMSE) on leave-one-out (LOO) cross-validation (CV) was chosen as the model score on given dataset:

$$\mathrm{RMSE} = \sqrt{\frac{\sum_{i=1}^{n} (y_i - \hat{y}(x_i))^2}{n}} \tag{4}$$

The simplest form of the classical internal standard method is where predictors of a given sample are normalised by the value of a particular predictor (i.e., the peak of the internal standard):

$$\hat{x}_{ij} = x_{s,ij} / x_{s,ij_0} \tag{5}$$

In this work, it is suggested to normalise every predictor vector by its scalar product with the internal standard profile p

$$\hat{x}_{ij} = x_{s,ij} / (x_{s,ij} \cdot p) \tag{6}$$

which is obtained by minimizing the RMSECV of the PLS model resulting from a given dataset:

$$p = \operatorname{argmin} \mathrm{RMSECV}(\mathrm{PLS}(\hat{\mathbf{X}}(p), \mathbf{A})) \tag{7}$$

Despite the elements of p are constrained to the range of [0;1], the problem as stated is ill-posed (does not have a unique solution), since (subject to machine accuracy) a PLS model would predict the same results for a predictor matrix $\hat{\mathbf{X}}$ and for the same matrix multiplied by a constant, $c\hat{\mathbf{X}}$. Hence, the actual objective function being minimized contains a regularisation component, causing the optimization algorithm to look for the unique solution having the smallest norm:

$$\mathrm{Loss}(p) = \mathrm{RMSECV}(\mathrm{PLS}(\hat{\mathbf{X}}(p), \mathbf{A})) + ||p||^2 \tag{8}$$

The optimization algorithm used was an implementation of Subplex [3], which is an improved version of Nelder-Mead simplex algorithm [4] suitable for higher-

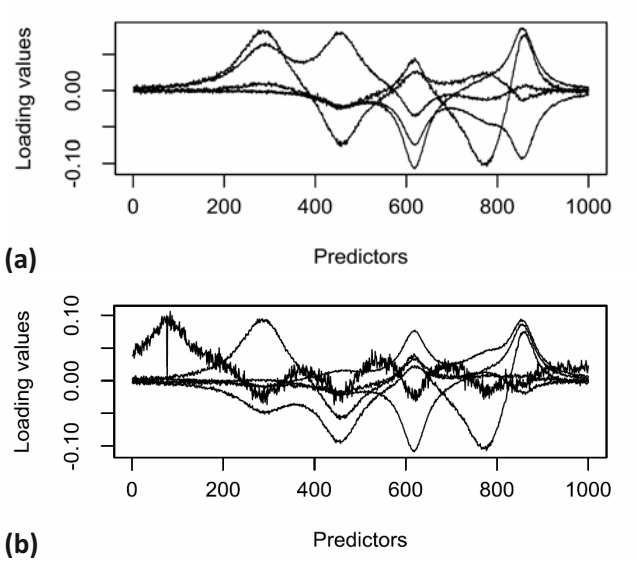

Fig. 2 Partial least squares loadings of (a) the source dataset, (b) the dataset after scrambling it by multiplying by a random variable, then correcting by the value of the internal standard peak.

dimensional problems. The author used a ready implementation of the algorithm available as a part of NLopt package [5].

3. Results and discussion

The "ground truth", i.e., the most optimal RMSECV value possible to obtain using PLS on raw predictor values before scrambling them by multiplying by random factor, has been determined to be 0.0284 (5 components). On the other hand, the RMSECV of the PLS model incorrectly built without any internal standard correction is 0.287 (5 components). The rest of RMSECV values fall between these edge cases.

Classic internal standard correction results in PLS RMSECV of 0.0853 (6 components). See Fig. 2 for the comparison of the loading values between the two models. The extra component appearing after the classic internal standard correction is slightly noisy, but is contains the systematic information about extra difference between each spectrum and the mean spectrum caused by imperfect reconstruction of the unscrambled signal.

Dividing each spectrum by its scalar product with the evolved internal standard profile (Fig. 3) makes it possible to lower the RMSECV further to 0.0496 (5 components).

Figure 4 displays the relationship between the true scale factors that were used to scramble the simulated spectra and their estimations obtained by the two methods discussed in this work. The multivariate approach yields values better

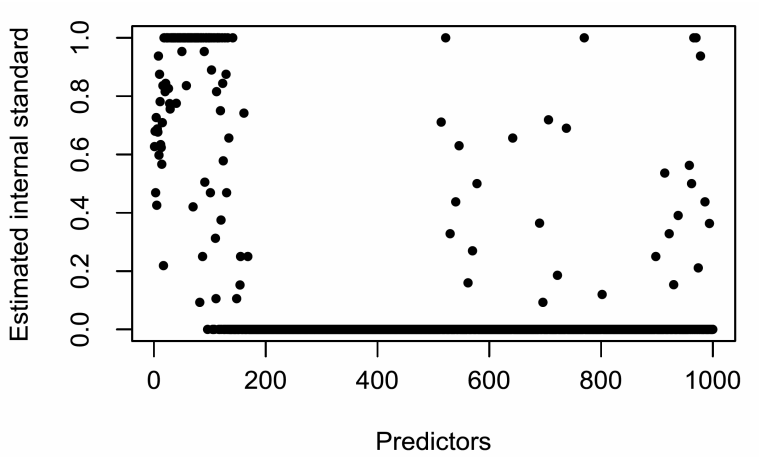

Fig. 3 Internal standard profile evolved by the optimization algorithm.

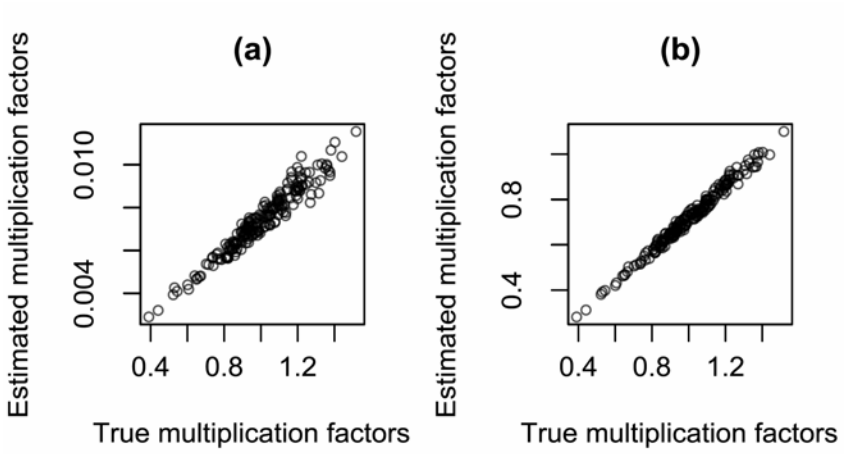

Fig. 4 Comparison of true scale factors used to scramble the simulated spectra and their estimations by means of (a) classic internal standard and (b) optimisation-based algorithm. Estimated scale factors are uncertain up to a constant multiplier but show correlation to the true scale factor.

correlating to the original multiplication factors ($\rho = 0.9928387$) than classical internal standard method ($\rho = 0.9691366$).

4. Conclusions

The use of optimization methods made it possible to obtain a multivariate internal standard profile that does not overlap with outher sources of variance in the predictor vectors, improving the regression model score; see Fig. 5 for the plot of RMSECV scores of all regression models obtained in this work.

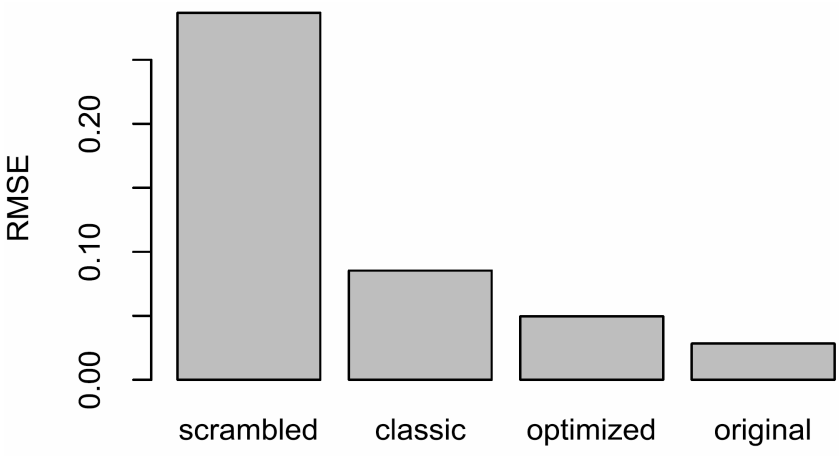

Fig. 5 Comparison of PLS RMSECV values obtained from different datasets in this work: "scrambled", each simulated spectrum multiplied by random factor; "classic", each scrambled spectrum divided by internal standard peak value; "optimized", each scrambled spectrum divided by scalar product with internal standard profile; "original", each simulated spectrum unmodified.

Although the technique shows good results, it is several magnitudes more computatinally expensive than classic internal standard methods. Additionally, the cost function suggested in this work is hard to optimize well and there may be stability and/or overfitting problems that should be addressed in the future work.

Acknowledgments

The author thanks Konstantin Melnikov from Unidragmet BSU, Minsk, Republic of Belarus for the fruitful discussion and some implementation ideas.

References

[1] Carnell R.: *lhs: Latin Hypercube Samples*. https://CRAN.R-project.org/package=lhs
[2] Mevik B.H., Wehrens R., Liland K.H.: *Pls: Partial Least Squares and Principal Component Regression*. https://CRAN.R-project.org/package=pls
[3] Rowan T.H.: *Functional Stability Analysis of Numerical Algorithms: PhD Thesis.* University of Texas at Austin, 1990.
[4] Nelder J.A., Mead R.: A simplex method for function minimization. *Comput. J.* **7** (1965), 308–313.
[5] Johnson S.G.: *The Nlopt Nonlinear-Optimization Package.* http://github.com/stevengj/nlopt

Non-invasive monitoring of diabetes and hypoxia based on continuous sweat analysis by flow-through biosensors

Elena V. Karpova*, Elizaveta V. Shcherbacheva, Elena E. Karyakina, Arkady A. Karyakin

Analytical Chemistry Department, Chemistry Faculty, M. V. Lomonosov Moscow State University, Lenin's Hills, 119991 Moscow, Russia ✉ *karpowa.ew@gmail.com*

Keywords
glucose
lactate
non-invasive diagnostics
oxidase-based biosensors
Prussian Blue

Abstract
Non-invasive diagnostics seems to be the best way for continuous monitoring of metabolites. We proposed operated in power generation mode biosensors based on Prussian Blue, stabilized by nickel hexacyanoferrate, for long-term monitoring of glucose and lactate in human sweat. Moreover, the universal design of non-invasive diabetes or hypoxia monitor based on glucose or lactate biosensor has been developed.

1. Introduction

Non-invasive methods, which exclude injury to blood vessels and damage to the skin surface, are preferred for diagnostics. These methods are painless and avoid potential infection and trauma to patients. Thus, non-invasive diagnostic methods are promising, and their development could help to improve the quality of millions of people life. However, despite continuing efforts, the problem of non-invasive evaluation of blood glucose or lactate concentration has not been solved yet.

Currently there are some devices on the market, called low-invasive devices. For example, devices for glucose detection are applied to 5 mm depth under the skin surface. Obviously, they are thus applied in the bulk of fat tissue. The latter is pierced by the network of blood capillaries, which cannot remain unbroken. Hence, obtained glucose levels are still blood levels, and the approach is still invasive even referred to as "low-invasive". Such devices can monitor for 10–14 days, however, they require blood calibration. Thus, a sufficient requirement for creating a non-invasive monitor would be a correlation between variation rates metabolite concentration in the blood and excretory liquid.

Saliva, urine, tears, exhaled breath condensate and sweat can be considered as excretory liquids suitable for analysis. In current research, we focused on the analysis of sweat, known to be one of the most promising liquids for non-invasive monitoring. Chemical analysis of sweat is very attractive. However, conventional

electrochemical clinical analyzers are not applicable for this purpose, since the sweat components inactivate platinum used as a transducer in the respective biosensors.

Oxidases serve as terminal ones for more than 90% of enzyme based biosensors. The most progressive way to couple the oxidase-catalyzed and the electrochemical reactions allowing to achieve the lowest detection limit is to detect H_2O_2, their side product [1]. At present, Prussian Blue (ferric hexacyanoferrate) is the most advantageous low-potential hydrogen peroxide transducer [2]. The only disadvantage of Prussian Blue is its inherent instability. Among a number of approaches used for stabilization of Prussian Blue, the building of multilayers with non-iron hexacyanoferrates isostructural to Prussian Blue seems to be the most progressive [3].

Here we report on the flow-through glucose and lactate biosensors with improved stability for continuous analysis of undiluted sweat. The proposed biosensors offer a prospect for real-time monitoring of blood glucose and lactate concentration thus representing a prototype of a non-invasive diabetes and hypoxia monitor.

2. Experimental

2.1 Reagents and chemicals

Experiments were carried out with Millipore Milli-Q water. All inorganic salts, perfluorosulfonated ionomerMF4 SK (Nafion analogue), organic solvents, and hydrogen peroxide (30% solution) were obtained at the highest purity from Reachim (Russia) and used as received. Pilocarpine (1% solution) was purchased from Ferein (Russia). D-Glucose and sodium lactate (40% solution) were purchased from Sigma (Germany). Glucose oxidase (EC 1.1.3.4) from *Aspergillus niger* (lyophilized powder, activity 270 IU) was purchased from Sigma (Germany). Lactate oxidase (EC 1.1.3.2) from *Pediococcus sp.* (lyophilized powder, activity 72 IU) was from Sorachim (Switzerland).

2.2 Instrumentation

Planar 3-electrode structures were made by screen-printing (Rusens, Russia) contained carbon working electrode (d = 1.8 mm). PalmSens potentiostat (Netherlands) and Digital multimeter Tektronix DMM4020 (USA) interfaced to PC were used. The flow-injection setup consisted of a syringe pump Perfusor Compact S (Braun, Germany), homemade flow-through wall-jet cell with 0.5 mm nozzle, and a homemade injector. For electrophoresis, we used Potok-1 (Russia). Sweat sampling was made with a sweat collector Macroduct (USA).

2.3 Methods

Interfacial synthesis of Prussian Blue was made by dipping a droplet of 2–4 mM $K_3[Fe(CN)_6]$ and 2–4 mM $FeCl_3$ in 0.1 M HCl and 0.1 M KCl and initiating by addition of H_2O_2 to a final concentration of 50–200 mM. Deposition of nickel hexacyanoferrate was made using 0.5 M KCl and 0.1 M HCl as a background electrolyte. Concentration of precursors ($NiCl_3 \cdot 6H_2O$, $K_3[Fe(CN)_6]$) was varied in the range 0.5–2.0 mM. After deposition modified electrodes were annealed at 100 °C for 1 h.

Biosensors were made by casting an enzyme containing drop (2 μL) onto the transducer surface with subsequent drying at a room temperature for one hour. Glucose oxidase casting mixture was prepared by suspending aqueous enzyme (10 mg/mL) by 0.3% Nafion analogue in 85% isopropanol. Lactate oxidase was suspended by 2% γ-aminopropyltriethoxysilane in 90% isopropanol or by 2.5% γ-aminopropyltriethoxysilane and 5% Nafion analogue in 90% isopropanol.

The flow-through biosensor was made by modifying the outer flat surface of a Macroduct-type collector with double side adhesive forming a channel of 1.5 mm width. Another side of the adhesive was linked to the power generating Prussian Blue based glucose/lactate biosensor [4].

3. Results and discussion

We already reported on the open circuit interfacial deposition of Prussian Blue-nickel hexacyanoferrate bilayer allowing to avoid electrochemical techniques, highly required for cost-effective mass production. In hard conditions under 1 mM hydrogen peroxide Prussian Blue-nickel hexacyanoferrate sensors do not display any decay in current response during more than one hour.

Operational stability of glucose and lactate biosensors has been investigated. Response of the biosensors made on the basis of Prussian Blue-nickel hexacyanoferrate is approximately 1.5 times less compared to the glucose/lactate-sensitive electrode using common Prussian Blue as a transducer (Table 1). However, the response current of the bilayer based biosensor is much more stable: the time of half inactivation ($t_{50\%}$) is almost twice of it for conventional Prussian Blue based biosensor. Analytical performance of corresponding biosensors were investigated in batch mode as well as flow-injection analyses (FIA) mode. Obtained data are presented in Table 1. Despite glucose/lactate biosensor made on the basis of Prussian Blue-nickel hexacyanoferrate bilayer displays lower response, for both biosensors the dynamic range is similar. Hence, a slightly lower sensitivity of the biosensor based on Prussian Blue-nickel hexacyanoferrate bilayer does not affect the dynamic range, and the biosensor is suitable for similar tasks as the biosensor based on conventional Prussian Blue.

It is known that there are positive correlations in the rates of glucose/lactate concentration increase for sweat and for blood [5, 6]. Obviously, it is not possible

Table 1
Comparison of analytical performance of glucose and lactate biosensors based on Prussian Blue and Prussian Blue-nickel hexacyanoferrate bilayer.

Analyte	Analytical performance	Transducer	
		Prussian Blue	Prussian Blue-nickel hexacyanoferrate
Glucose	Sensitivity/A $M^{-1}cm^{-2}$	0.042±0.003	0.023±0.002
	$t_{50\%}$/h (5 mM glucose)	14.0±0.5	27.5±1.2
	c_{min}/μM	4.1±0.2	4.5±0.3
	Operational stability in FIA-mode, injection number (5 mM glucose)	≈ 60	≈ 120
	Number of injections per 1 hour	> 100	> 100
Lactate	Sensitivity/A $M^{-1}cm^{-2}$	0.23±0.03	0.11±0.01
	$t_{50\%}$/h (0.25 mM lactate)	4.0±0.2	7.5±0.6
	c_{min}/μM	0.5±0.1	0.8±0.1
	Operational stability in FIA-mode, injection number (0.25 mM lactate)	≈ 30	≈ 60
	Number of injections per 1 hour	> 100	> 100

Fig. 1 The flow-through glucose or lactate biosensor.

to completely exclude the collection and analysis of blood samples, however, the development of a device for glucose/lactate monitoring in the sweat is very promising. To create such a device, it was necessary to combine a flow analysis system with an integrated biosensor and a sweat collector (Fig. 1).

Glucose biosensor integrated into the monitor was preliminarily calibrated. Glucose solutions were injected at a low speed and the current responses were observed. Based on the obtained data, a calibration graph was plotted (Fig. 2). The linear range of concentrations for biosensor operated in the non-invasive monitor system prolongs from 5 μM to 1 mM glucose, which covers the physiological range of glucose in sweat. The sensitivity is 24±2 mA $M^{-1}cm^{-2}$ ($n = 3$, $P = 0.95$).

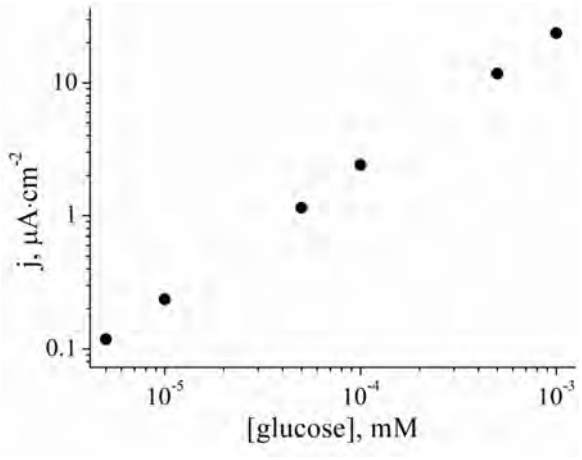

Fig. 2 Calibration graph for non-invasive glucose monitor (0.05 M KH_2PO_4/-K_2HPO_4, 0.1 M KCl, pH = 6.0).

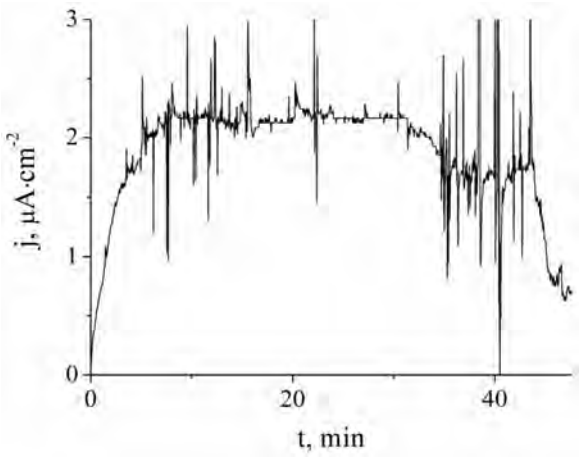

Fig. 3 Online readings of the non-invasive diabetes monitor representing sweat glucose level.

After 15 minutes of sweat gland stimulation, the monitor is applied to the same skin spot, and within the first one – two minutes the biosensor displays a response. Constant sweat flow after pilocarpine activation is observed during 20–30 minutes (Fig. 3). Afterwards the same skin spot should be reactivated.

The main problem with lactate analysis in undiluted sweat is the high lactate concentration, which is on average 10 times higher compared to blood. Lactate content in sweat of a healthy human is in the range from 4 to 25 mM, whereas after loading test it is increasing up to 50–80 mM. Hence, the upper detection limit of lactate biosensors has to be at least 80 mM. To increase the upper detection limit required for analysis of undiluted sweat, it is necessary to increase an apparent Michaelis constant of lactate oxidase. It was shown that lactate oxidase affinity to its substrate could be significantly decreased by addition of negatively charged polyelectrolyte (Nafion analogue) in siloxane gel [7].

The corresponding biosensor was integrated into proposed monitor (prototype of a wearable device) and tested in power generation mode. The current response after adding of the analyte immediately decreased and could be increase to the

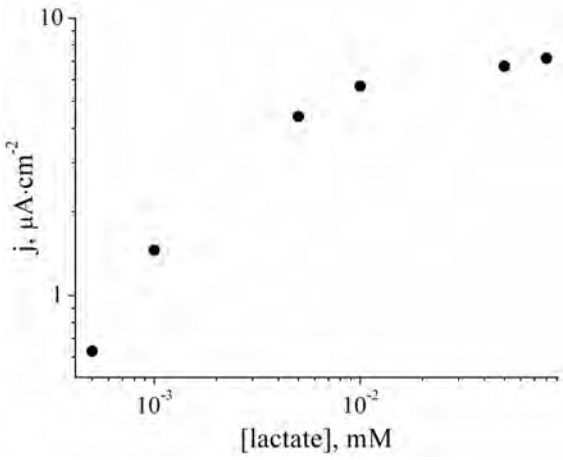

Fig. 4 Calibration graph for non-invasive lactate monitor (0.05 M KH_2PO_4/-K_2HPO_4, 0.1 M KCl, pH = 6.0).

initial value only with a continuous lactate flow. The response decreased so fast that it was impossible to record it. Thereby, this sensor is not suitable for continuous sweat analysis.

We achieved stable current responses to the lactate addition by reducing the concentration of the enzyme (0.1 mg ml^{-1} instead of 1 mg ml^{-1}) in the membrane (Fig. 5). The resulting Prussian Blue based biosensor allows continuous lactate detection up to 80 mM was integrated in a flow-through sweat collector for successful monitoring of lactate content in whole sweat.

4. Conclusions

Continuous monitoring of blood glucose concentration opens a possibility to cure diabetes or at least to decrease the insulin dependence of the patients. There are also severe cases of diabetes, among which there is a possibility of death of the patient in their sleep caused by hypoglycemia, and the best solution for them is non-invasive diabetes monitoring. We also proposed lactate biosensor for continuous sweat monitoring, which provides a possibility for non-invasive personification of sport training, as well as of hypoxia.

Acknowledgments

Financial support of the Russian Science Foundation through Grant No. 19-13-00131 is greatly acknowledged.

References

[1] Guilbault G.G., Lubrano G.J.: An enzyme electrode for the amperometric determination of glucose. *Anal. Chim. Acta* **64** (1973), 439–455.

[2] Karyakin A.A.: Prussian blue and its analogues: electrochemistry and analytical applications. *Electroanalysis* **13** (2001), 813– 819.

[3] Karpova E.V., Karyakina E.E., Karyakin A.A.: Iron–nickel hexacyanoferrate bilayer as an advanced electrocatalyst for H_2O_2 reduction. *RSC Adv.* **6** (2016), 103328–103331.

[4] Komkova M.A., Karyakina E.E., Karyakin A.A.: Noiseless performance of Prussian Blue based (Bio) sensors through power generation. *Anal. Chem.* **89** (2017), 6290–6294.
[5] Karpova E.V., Shcherbacheva E.V., Galushin A.A., Vokhmyanina D.V., Karyakina E.E., Karyakin A.A.: Noninvasive diabetes monitoring through continuous analysis of sweat using flow-through glucose biosensor. *Anal. Chem.* **91** (2019), 3778–3783.
[6] Karpova E.V, Laptev A.I., Andreev E.A., Karyakina E.E., Karyakin A.A.: Sweat vs blood lactate: Comment on "a soft, wearable microfluidic device for the capture, storage, and colorimetric sensing of sweat". *Science Translational Medicine* (2019), https://stm.sciencemag.org/content/8/366/366ra165/tab-e-letters
[7] Pribil M.M., Laptev G.U., Karyakina E.E., Karyakin A. A.: Noninvasive hypoxia monitor based on gene-free engineering of lactate oxidase for analysis of undiluted sweat. *Anal. Chem.* **86** (2014), 5215–5219.

Electroanalysis of cholesterol and its precursor 7-dehydrocholesterol on carbon-based electrodes

Lenka Benešová*, Eva Bláhová, Polina Yershova, Jan Klouda, Karolina Schwarzová

UNESCO Laboratory of Environmental Electrochemistry, Department of Analytical Chemistry, Faculty of Science, Charles University, Hlavova 8, 128 43 Prague 2, Czech Republic
✉ *benesole@natur.cuni.cz*

Keywords
boron-doped diamond electrode
cholesterol
7-dehydrocholesterol
glassy carbon electrode
voltammetry

Abstract
Electrochemical behaviour of cholesterol and its precursor 7-dehydrocholesterol was studied using cyclic voltammetry on boron-doped diamond and glassy carbon electrode. Inorganic acids (i.e., $HClO_4$, H_2SO_4, HNO_3, and H_3PO_4) were used for activation of sterol structure by dehydration reaction, similarly to Liebermann-Burchard reaction of cholesterol. Oxidation potentials of cholesterol and 7-dehydrocholesterol are circa +1.5 V and circa +0.8 V (vs. $Ag/AgNO_3$ in acetonitrile) in optimized supporting electrolyte containing 0.1 mol L^{-1} perchloric acid in acetonitrile. The approach is promising for simultaneous detection of both sterols using voltammetry in various physiological (serum) and food matrices.

1. Introduction

Cholesterol is an unsaturated sterol essential for the normal function of all animal cells as fundamental element of their membranes. It is also a precursor of various critical substances such as bile acids and adrenal and gonadal steroid hormones. Increase of its concentration level in plasma lead to genesis of various diseases as atherosclerosis, or cardiovascular diseases. Smith-Lemli-Opitz syndrome is characterized by decreased concentration levels of cholesterol and high concentration of its precursor 7-dehydrocholestrol in plasma due to inborn deficiency in biosynthesis of 7-dehydrocholesterol reductase. Smith-Lemli-Opitz syndrome is an autosomal recessive genetic disease leading to various degree of mental and physical retardation [1].

The most common method employed for determination of cholesterol is GC with mass spectrometric or flame ionization detection or HPLC with tandem MS [2] or UV detection. Electrochemically methods are mostly limited to detection using enzyme-based sensor [3], although non-enzymatic sensors were also

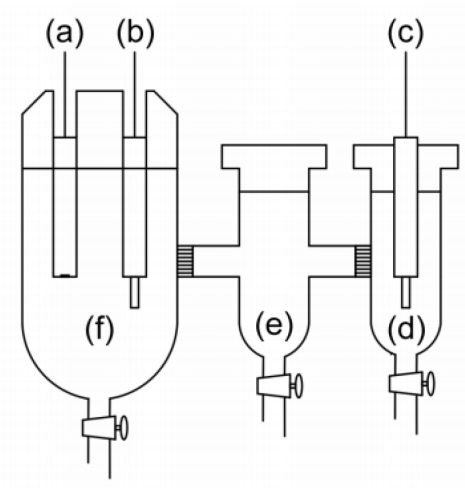

Fig. 1 Electrochemical detection cell for voltammetry in non-aqueous medium: (A) working electrode, (B) platinum auxiliary electrode, (C) non-aqueous $Ag/AgNO_3$ reference electrode, (D) solution of 0.01 mol L^{-1} $AgNO_3$ and 1 mol L^{-1} $NaClO_4$ both in acetonitrile, (E) salt-bridge 0.5 mol L^{-1} $NaClO_4$ in acetonitrile, and (F) working space.

described [4]. Methods based on direct transfer of electrons are applied peripherally due to limited redox activity of steroid core (review [5]). Modified electrodes were used to detect cholesterol within potential window of carbon-based electrodes in aqueous-organic media [6, 7].

Recently, an approach based on chemical activation of steroid core of bile acids using their dehydration succeeded as they could be consequently oxidized on boron doped diamond (BDD), platinum and glassy carbon (GC) electrode [8]. This reaction is analogous to Liebermann-Burchard reaction for colorimetric assay of cholesterol [9]. In this contribution, applicability of this approach consisting of chemical activation of cholesterol and its precursor 7-dehydrocholestrol and followed by electrooxidation on carbon-based electrode was tested.

2. Experimental

2.1 Reagents and chemicals

Solutions of supporting electrolytes containing inorganic acids, i.e. perchloric acid (70 %, Penta, Czech Republic), sulfuric acid (96 %, Lach:Ner, Czech Republic), nitric acid (65 %, Lach:Ner, Czech Republic), and phosphoric acid (85 %, Lach:Ner, Czech Republic), cholesterol and 7-dehydrocholesterol (both 99 %, Sigma-Aldrich) were prepared in acetonitrile (>99.9 %, Honeywell). Solution used for reference space and salt-bridge of voltammetric cell (Fig. 1) were prepared dissolving $AgNO_3$ (Ph. Eur. 3, Fluka) and $NaClO_4$ (Fluka) in acetonitrile.

2.2 Instrumentation

Voltammetric measurements were performed using Eco-Tribo Polarograph with PolarPro5.1 software (both Eco-Trend Plus, Czech Republic). Three-chamber detection cell (Fig. 1) was used for measurement with BDD electrode (d = 3 mm,

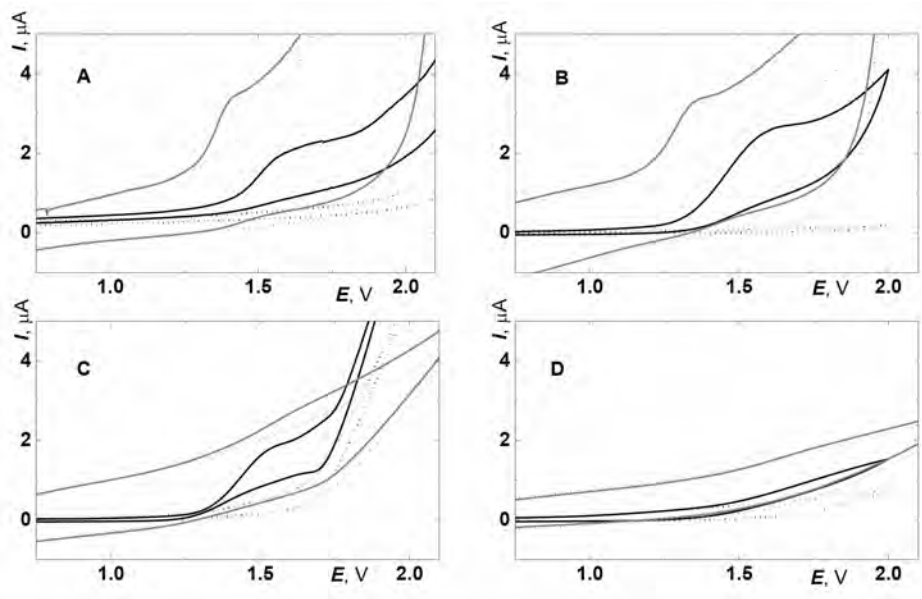

Fig. 2 Cyclic voltammograms of cholesterol on BDD electrode (black) and GC electrode (grey) in 0.1 mol L^{-1} inorganic acids in acetonitrile (dashed lines): (A) perchloric acid (0.43 % water content), (B) sulfuric acid (0.04 % water content), (C) nitric acid (0.34 % water content), and (D) phosphoric acid (0.17 % water content). Polarization rate 100 mV s^{-1}.

Windsor Scientific, UK) and GC electrode (d = 3mm, Metrohm, Switzerland) as working electrodes, platinum wire as auxiliary electrode (Electrochemické detektory, Turnov) and non-aqueous reference electrode ($Ag/AgNO_3$ in 0.01 mol L^{-1} $AgNO_3$ and 1 mol L^{-1} $NaClO_4$ in acetonitrile). Polishing of surface of working electrodes before each scan using Al_2O_3 was performed.

3. Results and discussion

In this study comparison of performance of BDD and GC electrode for voltammetric detection of cholesterol and 7-dehydrocholesterol using the same conditions was performed. Firstly, influence of four inorganic acids used simultaneously as dehydrating agent and supporting electrolyte on voltammetric response of cholesterol was investigated. 1 mol L^{-1} perchloric acid, sulfuric acid, nitric acid and phosphoric acid in acetonitrile were used for that purpose. In Fig. 2 illustrative comparison of cyclic voltammograms of cholesterol in these media with minimal water content on both electrodes is depicted. Signal of cholesterol is observable in medium containing perchloric (Fig. 2A) and sulfuric acid (Fig. 2B) on both working electrodes. Glassy carbon electrode exhibits higher background current than BBD electrode and detection potential of cholesterol +1.4 V, circa 0.1–0.2 V, more negative than BDD electrode. In solution containing nitric acid (Fig. 2C) the signal is observable only on BDD electrode. Phosphoric acid (Fig. 2D)

is inappropriate as no signal of cholesterol is developed on both working electrodes.

Further, influence of water content in solution containing 1 mol L^{-1} perchloric acid in acetonitrile was investigated. Downshift of potential from +1.5 V to +1.2 V and decrease of peaks heights was observed on BDD electrode, while on GC electrode increase of peak height was observed. The highest water content investigated was 40%.

Concentration dependences were measured using differential pulse voltammetry in 0.1 mol L^{-1} HClO4 in acetonitrile (0.43% water content) on both electrodes and micromolar detection limits were achieved.

The precursor of cholesterol, 7-dehydrocholesterol was studied in solution containing 0.1 moL^{-1} HClO4 in acetonitrile on BDD electrode. Two oxidation peaks at detection potentials of +0.8 V and +1.1 V are observable in medium with 0.43% content of water. While the first peak arises immediately, the second peak is probably due to genesis of another product of dehydration reaction in the media containing dehydrating acid. Further experiments leading to explanation of this feature and investigation of electrochemical behaviour of 7-dehydrocholesterol on glassy carbon electrode are in progress.

4. Conclusions

The voltammetric signal of cholesterol is observable on BDD and glassy carbon electrode at potential of circa +1.4 V to +1.5 V in media containing a dehydrating acid in acetonitrile. Simultaneous detection of cholesterol and its precursor 7-dehydrocholesterol on BDD electrode is possible due to difference in oxidation potentials. Development of voltammetric methods as well as FIA with multiple pulse amperometric detection aiming at simultaneous determination of these analytes in serum and food products are in progress.

Acknowledgments

The research was supported by the Czech Science Foundation (project 18-01710S) and the Specific University Research (SVV 260440) and the Grant Agency of Charles University (GAUK 1440217).

References

[1] Rizzo C., Dionisi–Vici C., D'Ippoliti M., Fina F., Sabetta G.: Federici G.: A simple and rapid HPLC method for simultaneous determination of plasma 7–dehydrocholesterol and vitamin E: Its application in Smith–Lemli–Opitz patients. *Clin. Chim. Acta* **291** (2000), 97–102.

[2] Raith K., Brenner C., Farwahan H., Muller G., Eder K, Neubert R.H.H.: A new LC/APCI–MS method for the determination of cholesterol oxidation products in food. *J. Chromatog. A* **1067** (2005), 207–211.

[3] Nantaphol S., Chailapakul O., Siangproh W.: Sensitive and selective electrochemical sensor using silver nanoparticles modified glassy carbon electrode for determination of cholesterol in bovine serum. *Sens. Actuators B* **207** (2015), 193–198.

[4] Anh T.T.N., Lan H., Tam L.T., Pham V.H., Tam P.D.: Highly sensitive nonenzymatic cholesterol sensor based on zinc oxide nanorods. *J. Electron. Mater.* **47** (2018), 6701–6708.

[5] Klouda J., Barek J., Nesmerak K., Schwarzova-Peckova K.: Non-enzymatic electrochemistry in characterization and analysis of steroid compounds. *Crit. Rev. Anal. Chem.* **47** (2017), 384–404.
[6] Derina K.V., Korotkova E.I., Taishibekova Y., Salkeeva L., Kratochvil B., Barek J.: Electrochemical non–enzymatic sensor for cholesterol determination in food. *Anal. Bioanal. Chem.* **410** (2018), 5085–5092.
[7] Derina K.V., Korotkova E.I., Dorozhko E.V., Voronova O.A.: Voltammetric determination of cholesterol in human blood serum. *J. Anal. Chem.* **72** (2017), 904–910.
[8] Klouda J., Barek J., Kocovsky P., Herl T., Matysik F.M., Nesmerak K., Schwarzova-Peckova K.: Bile acids: Electrochemical oxidation on bare electrodes after acid–induced dehydration. *Electrochem. Commun.* **86** (2018), 99–103.
[9] Xiong Q.B., Wilson W.K., Pang J.H.: The Liebermann-Burchard reaction: Sulfonation, desaturation, and rearrangment of cholesterol in acid. *Lipids* **42** (2007), 87–96.

The possibility to employ ethanol as an internal standard in quantification of volatile compounds in alcoholic products with GC-MS

Anton Korban[a, b, *], Lidia Sobolenko[a, b]

[a] *Department of Analytical Chemistry, Chemistry Faculty, Belarusian State University, Leningradskaya Str. 14, 220050 Minsk, Belarus* ✉ *karbonat7@gmail.com*
[b] *Institute for Nuclear Problems of Belarusian State University, Bobruyskaya Str. 11, 220006 Minsk, Belarus*

Keywords
alcoholic products
ethanol
GC-MS
quantification
volatile compounds

Abstract
In the current study ethanol was employed as an internal standard for the common procedure of volatile compounds quantification in alcoholic products. A number of standard solutions was prepared in a water-ethanol matrix and measured with GC-MS in the SIM mode. In order to avoid detector saturation during ethanol detection it was suggested to use less abundant *m/z* 47 as quantifiers. These ions mainly correspond to unfragmented heavy ethanol molecules containing one ^{13}C isotope. The experiment also included the determination of the linearity of the modified MS detector response relative to the ethanol content. Analysis of the obtained results revealed that volatile compounds can be successfully accurately determined with GC-MS by employing ethanol as an internal standard. Application of the suggested method is not limited to the reported volatile compounds and alcoholic products.

1. Introduction

According to the international legislative documents, volatile compounds are determined in alcoholic beverages using GC coupled to FID [1–3], although GC-MS methods are quite wide-spread among researchers. Internal standard methods are prescribed in the above-mentioned legislation and are mainly employed in scientific papers. Chemical compounds such as 1-pentanol or 3-pentanol, originally absent in the analysed sample, are usually employed as internal standard.

This paper is a further development of our previously published method, which employs ethanol as an internal standard during direct determination of volatile compounds in ethanol-containing products with GC-FID [4–5]. It was

Table 1
Description of the created SIM mode.

Compound	Window	Time/min	*m/z*
acetaldehyde methyl acetate ethyl acetate	1	0.00–8.85	29, 43
methanol	2	8.85–9.50	29, 31, 32
2-propanol	3	9.50–10.14	27, 43, 45
ethanol	4	10.14–12.00	47
1-propanol	5	12.00–13.70	31, 41–43
water	6	13.70–14.80	19
isobutanol 1-butanol isoamylol	7	14.80–20.00	31, 41–43, 55, 56

shown that employing ethanol as an internal standard creates great perspectives for this method in analysis of alcoholic beverages and products of their origin.

The main idea of the "Ethanol as internal standard" method is that ethanol concentration expressed in mg/L AA (absolute alcohol) units is constant and equal to its density. Any attempt to establish ethanol concentration in mg/L AA units by transfer from mg/kg or mg/L units will always lead to the same value. This method is beneficial because of the fact that according to the regulatory documents [1–3] volatile compounds concentrations must be finally expressed in mass per litre of absolute alcohol units (mg/L AA, g/L AA, etc.). The suggested method allows establishing volatile compounds concentrations in mg/L AA units directly without internal standard compound addition into test sample and its density or strength (alcohol by volume, ABV) establishment. Eventually, the usage of ethanol as an internal standard greatly simplifies the whole analysis and improves the reliability and accuracy of the obtained data.

Due to the high popularity of modern GC-MS instruments, we decided to discover whether this approach is also valid for GC-MS. To our knowledge, no study of the use of ethanol or another major component for quantification during GC-MS analysis has been carried out.

The main difficulty we encountered was control of the ethanol signal with respect to the MS detector response saturation. For overcoming this problem we have suggested to select a less abundant quantifier ethanol ion, e.g., *m/z* 47, which corresponds to the unfragmented ethanol molecule containing one of the heavy isotopes of carbon, oxygen or hydrogen. Thus, as the natural ^{13}C isotope content is 1.07 % compared to 0.04 % and 0.01 % of the ^{17}O and ^{2}H isotopes, respectively, the *m/z* 47 ion corresponds almost solely to $^{13}C^{12}CH_6O$.

A SIM method for the determination of 9 volatile compounds and ethanol containing 7 time windows with correspondingly selected quantifier ions was created (Table 1). By analogy with ethanol, water could be monitored at *m/z* 19, although it was not used in any calculations. It's also necessary to note that use of

Table 2
Volatile compounds concentrations and their uncertainties in gravimetrically prepared standard solutions.

Compound	Concentration/mg L^{-1}						
	SS-3	SS-2	SS-1	SS-D	SS-C	SS-B	SS-A
acetaldehyde	3.5±0.2	10.9±0.3	48.3±1.4	183±5	227±7	407±12	4828±49
methyl acetate	1.8±0.1	9.3±0.3	47.4±1.4	185±6	230±7	413±12	4918±49
ethyl acetate	1.8±0.1	9.4±0.3	47.8±1.4	186±6	232±7	417±13	4962±49
methanol	15.1±0.7	22.6±0.7	60.4±1.8	197±6	241±7	424±13	4899±49
2-propanol	3.1±0.1	10.4±0.3	47.4±1.4	181±5	225±7	403±12	4783±48
ethanol	789300						
1-propanol	2.8±0.1	10.4±0.3	48.5±1.5	186±6	231±7	415±12	4929±49
isobutanol	1.9±0.1	9.7±0.3	49.0±1.5	191±6	238±7	427±13	5088±49
1-butanol	1.8±0.1	9.4±0.3	47.6±1.4	185±6	231±7	415±12	4943±49
isoamylol	1.8±0.1	9.3±0.3	47.1±1.4	183±5	228±7	411±12	4888±49

the suggested method is not limited to the described compounds and can be used for any volatile substances that can be separated and detected with a standard GC-MS system.

2. Experimental

2.1 Reagents and chemicals

The following volatile compounds were analysed: acetaldehyde, methyl acetate, ethyl acetate, methanol, 2-propanol, 1-propanol, 2-methyl-1-propanol (isobutanol), 1-butanol, and 3-methyl-1-butanol (isoamylol). All the volatile organic compounds mentioned above, including ethanol, were of more than 99.9% purity (Sigma-Aldrich or Merck). Deionised water was used for the preparation. Table 2 contains the concentrations of volatile compounds in gravimetrically prepared standard solutions.

2.2 Instrumentation

A GCMS-QP2010 Shimadzu chromatograph was used for the measurements. A ZB-WAX plus capillary column, 60 m long with internal diameter of 0.25 mm and phase thickness of 0.5 μm was employed. The MS was operated in the electron impact ion source mode at 70 eV.

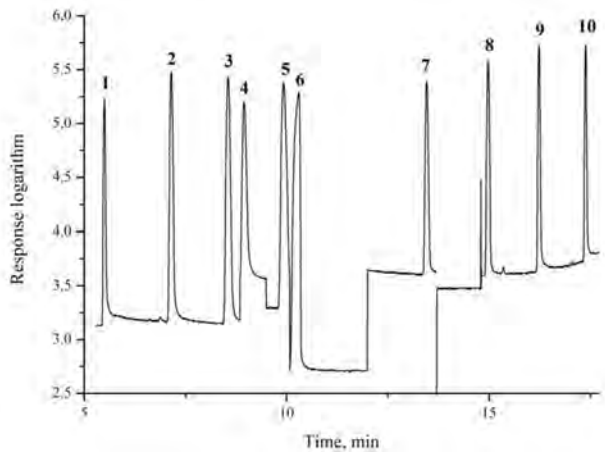

Fig. 1 The GC-MS chromatogram of the most saturated prepared standard solution SS-A: (1) acetaldehyde, (2) methyl acetate, (3) ethyl acetate, (4) methanol, (5) 2-propanol, (6) ethanol, (7) 1-propanol, (8) isobutyl alcohol, (9) 1-butanol, (10) isoamyl alcohol.

3. Results and discussion

Figure 1 depicts the GC-MS chromatogram of the most saturated standard solution SS-A (Table 2) and it can be seen that, for high concentrations of volatiles, their peak areas can be comparable or even larger than that of ethanol.

The standard solution SS-3 containing the lowest volatile amounts was used to determine the limits of quantification. Ten consecutive measurements of standard solution SS-3 were made and the limit of quantification was expressed as 10× the standard deviation of the concentration for both FID and MS. According to the obtained results, limit of quantification values for FID were in the range of 0.71–2.04 mg/L AA while for MS detector in the range of 0.31–0.84 mg/L AA.

Absolute biases were calculated for the trueness performance. The majority of the obtained values were below 3%. The standard solutions SS-2 and SS-3 as the most diluted samples exhibited slightly worse results. We already observed this phenomenon during our previous works with FID [4–5]. The reason for the worse biases could consist in chemical transformations of reactive acetaldehyde and esters or in the evaporation. Nevertheless, the results are still acceptable and the described method can be undoubtedly regarded as true.

The repeatability of the proposed method was investigated by calculation of the relative standard deviation of the volatile compound concentrations; the obtained values were lower than 5%. No any crucial dependence of the relative standard deviation values on the concentration was observed.

In order to establish the potential range of alcoholic substrates available for measurement via the proposed method, we checked the linear dependence of volatile compounds and ethanol MS detector response on their concentrations. For this purpose samples obtained by dilution of standard solution SS-A with water were measured. The coefficients of determination, R^2, obtained for all

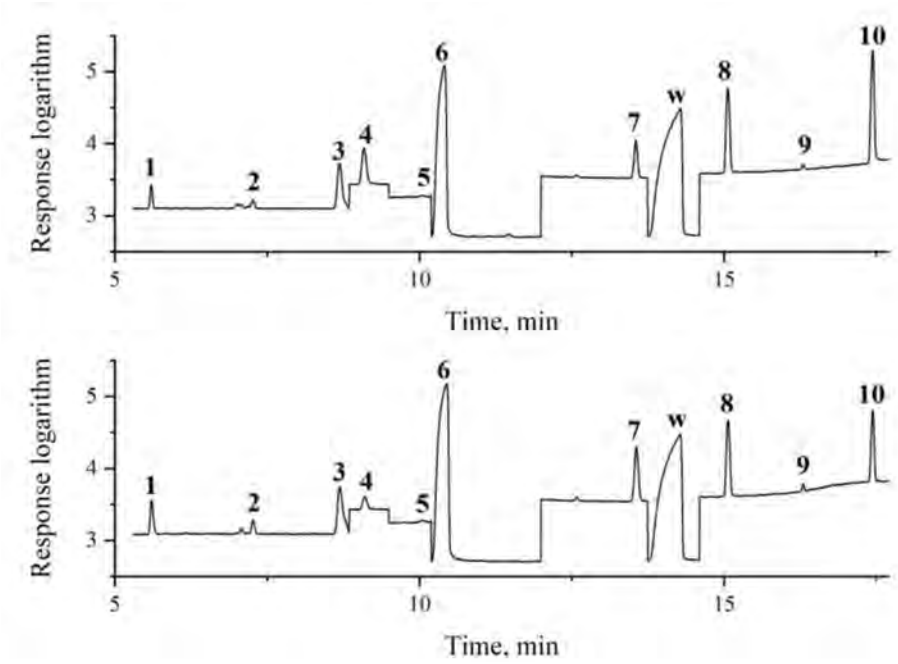

Fig. 2 The GC-MS chromatograms of the commercially purchased spirit samples 1 and 2 (from up to down): (1) acetaldehyde, (2) methyl acetate, (3) ethyl acetate, (4) methanol, (5) 2-propanol, (6) ethanol, (7) 1-propanol, (8) isobutyl alcohol, (9) 1-butanol, (10) isoamyl alcohol, (W) water.

Table 3
Volatile compounds concentrations obtained for two purchased spirits by both detectors.

Component	Concentration/mg L^{-1}			
	Sample 1		Sample 2	
	FID	MS	FID	MS
acetaldehyde	130.8	133.9	98.7	103.0
methyl acetate	9.4	10.3	8.4	8.5
ethyl acetate	151.1	140.3	219.5	211.8
methanol	51.0	53.9	316.3	322.4
2-propanol	0.0	1.6	0.0	1.7
1-propanol	403.1	407.6	267.3	280.3
isobutanol	601.4	606.7	1259	1287
1-butanol	10.0	9.2	7.4	7.5
isoamylol	642.9	628.0	3368	3266

analysed volatile compounds exceeded value of 0.9986. In addition, pure ethanol was diluted with water to obtain 12 samples with ABV levels from 100% to 1% (*v/v*). Analysis of the obtained graphs demonstrates the good linearity ($R^2 = 0.9959$) of the suggested method.

To demonstrate the applicability of the proposed method on real samples, two commercial spirits were purchased and analysed simultaneously by MS and FID (Fig. 2). As expected, the obtained results were very similar (Table 3). To evaluate if the difference between the results is significant Student's *t*-test of independent samples was used. It was found, that there was no statistical evidence that associated populations means differ significantly for all compounds ($p = 0.05$).

4. Conclusions

In this work, the procedure of employing ethanol as an internal standard in GC-MS quantitative analysis of alcoholic products was described and tested for the first time. An approach of throttling the ethanol signal was suggested and tested. It was shown that the ethanol response is linear in the range 1–100 % ABV. Analysis of biases, limits of quantification, relative standard deviation and determination coefficients demonstrated that "Ethanol as Internal Standard" method is robust and can be successfully employed in GC-MS measurements. Analogous to FID, the proposed method is simpler and more accurate than the traditional internal standard method. As expected, MS detector is much more sensitive than FID in the SIM mode. This difference suggests further favourable perspectives for use of the method in the analysis of alcoholic products and other materials.

Acknowledgments

This study was supported by the Belarusian Ministry of Education in the "Youth and policy" program and by the World Federation of Scientists in the National Scholarship program. The authors thank their scientific advisers Dr. Radomir Cabala from Faculty of Science of Charles University, Dr. S. Charapitsa, and Dr. S. Sytova from Institute for Nuclear Problems of Belarusian State University.

References

[1] *Commission Regulation (EC) No 2870/2000 laying down Community reference methods for the analysis of spirits drinks.*
[2] AOAC Official Method 972.10. *Alcohol (higher) and Ethyl Acetate in Distilled Liquors. Alternative Gas Chromatographic Method.*
[3] OIV method OIV-MA-BS-14: R2009. *Determination of the Principal Volatile Substances of Spirit Drinks of Viti-Vinicultural Origin.*
[4] Charapitsa S., Kavalenka A., Kulevich N., Makoed N., Mazanik A., Sytova S., Zayats N., Kotov Y.: Direct determination of volatile compounds in spirit drinks by gas chromatography. *J. Agric. Food Chem.* **61** (2013), 2950–2956.
[5] Charapitsa S., Sytova S., Korban A., Sobolenko L.: Single-laboratory validation of a gas chromatographic method of direct determination of volatile compounds in spirit drinks: Need for an improved interlaboratory study. *J. AOAC Int.* **102** (2019), 669–672.

Atomization of bismuthane in two flame atomizers for atomic fluorescence spectrometry

Barbora Štádlerová[a, b, *], Marta Kolrosová[a, b], Jiří Dědina[a], Stanislav Musil[a]

[a] *Institute of Analytical Chemistry of the Czech Academy of Sciences, Veveří 97, 602 00 Brno, Czech Republic* ✉ *stadlerova@iach.cz*
[b] *Department of Analytical Chemistry, Faculty of Science, Charles University, Hlavova 8, 128 43 Prague 2, Czech Republic*

Keywords
atomic fluorescence spectrometry
bismuth
hydride generation

Abstract
A method for bismuth determination by hydride generation coupled with atomic fluorescence spectrometry was developed. Bismuthane was generated by the reaction with $NaBH_4$ in HCl in a flow injection arrangement of the generator. An in-house assembled atomic fluorescence spectrometer was used for detection. A detailed optimization of atomization parameters in two flame atomizers – miniature diffusion flame and flame-in-gas-shield atomizer – was performed. An excellent repeatability and extremely low limits of detection were achieved, namely 2.3 ng l^{-1} with the miniature diffusion flame atomizer and 1.6 ng l^{-1} with the flame-in-gas-shield atomizer.

1. Introduction

Atomic fluorescence spectrometry coupled with hydride generation is a very sensitive analytical method for determination of several elements (As, Bi, Se, Sb, Te, Ge, Pb, Hg, and Cd). Its analytical performance can be comparable to that of ICP-MS with liquid nebulization but at significantly lower expenses. Atomic fluorescence spectrometry instruments can be also assembled in a laboratory from commercially available components [1]. The three main components are a radiation source, a photomultiplier tube used as a detector and an atomizer.

A miniature diffusion flame is usually employed in atomic fluorescence spectrometry instruments [1–3]. A design of the miniature diffusion flame atomizer is very simple (Fig. 1a). It consists of a vertical quartz tube which is supplied with argon and hydrogen together with the analyte hydride. The hydrogen-oxygen diffusion flame burns on the top of the vertical tube. Hydrogen radicals needed for atomization are formed in the outer zone of the flame and can then diffuse to the inner section, so the analyte is atomized in the whole observed volume of the flame [4]. Another type of the flame atomizer designed specifically for atomic fluorescence spectrometry is a flame-in-gas-shield atomizer [5]. The

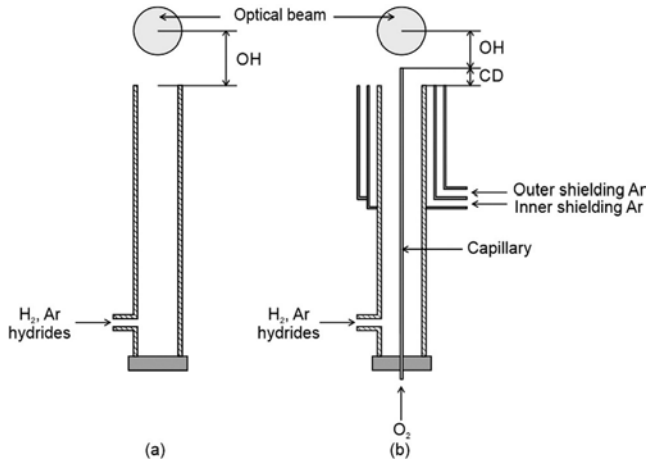

Fig. 1 Scheme of (a) miniature diffusion flame, and (b) and flame-in-gas-shield atomizers; OH – observation height, CD – capillary distance.

basic construction is the same as that of the miniature diffusion flame – a vertical quartz tube with a side inlet arm for hydrogen, argon and analyte hydride supply (Fig. 1b). The difference lies in the capillary that is inserted in the vertical axis of the vertical quartz tube through which a small amount of oxygen is introduced. A hydrogen-oxygen microflame burns on top of the capillary. The microflame is shielded from the ambient atmosphere by a flow of shielding argon which is introduced through a shielding unit fitted around the vertical tube [4–6].

The aim of this work was to optimize atomization conditions in both the miniature diffusion flame and flame-in-gas-shield atomizers and to compare their analytical characteristics for ultrasensitive determination of bismuth by atomic fluorescence spectrometry coupled with hydride generation.

2. Experimental

2.1 Reagents and chemicals

Deionized water (Ultrapur, Watrex, USA) was used for preparation of all solutions. A 0.5% (*m/v*) $NaBH_4$ in 0.4% (*m/v*) KOH was used as a reducing agent. A stock solution of 1 mol l^{-1} HCl was prepared from 37% HCl (Merck, Germany) and was used as a carrier and blank. Working 1 μg l^{-1} Bi solution was prepared fresh daily by dilution of 1000 μg l^{-1} Bi stock solution. The 1000 μg l^{-1} Bi stock solution was prepared by dilution of Bi standard solution (1000 mg l^{-1} Bi standard for AAS, Sigma-Aldrich, Germany) and was kept in a refrigerator.

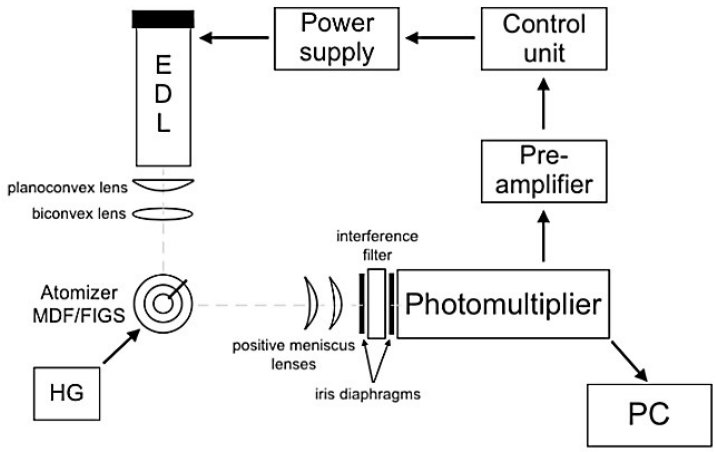

Fig. 2 Experimental setup of the atomic fluorescence spectrometer.

2.2 Instrumentation

2.2.1Atomic fluorescence spectrometer

An in-house assembled non-dispersive atomic fluorescence spectrometer constructed in our laboratory was used for Bi determination and is described in detail elsewhere [1]. This spectrometer of a simple design (Fig. 2) consists of three main components: radiation source, atomizer and photomultiplier tube. A Bi electrodeless discharge lamp (Perkin Elmer, System 2) was used as a radiation source with feeding power square-wave modulated at frequency of 40 Hz. The operating current for the electrodeless discharge lamp was 400 mA. The photomultiplier tube was placed perpendicular to the lamp to collect the fluorescence radiation emmited from the atomizer. The fluorescence radiation passed through an interference filter used for wavelength selection (222.63 nm, FWHM 10 nm, Melles Griot) and was then focused into the photomultiplier tube. A solar-blind photomultiplier tube (165–320 nm, Perkin Elmer, MH 1922) was employed as the detector. The output from the photomultiplier tube was then processed by a lock-in preamplifier. The preamplifier, control unit and a dedicated software were designed by DIRAM company (Czech Republic) specifically for this instrument.

2.2.2 Hydride generator and atomizers

A flow injection hydride generator was employed. The reducing agent ($NaBH_4$) (1.2 ml min^{-1}) and HCl (4 ml min^{-1}) were pumped by a peristaltic pump Reglo Digital (Ismatec, Switzerland). The manifold was constructed from PTFE tubing (1 mm i.d.). The sample was injected through a 1 ml sample loop into the flow of hydrochloric acid used as a carrier. The flow rate of hydrogen (H_2 generator) evolving from the reaction was around 15 ml min^{-1}. A glass gas-liquid separator

(volume of 5 ml) with forced waste removal was employed for separating the gas phase containing bismuthane, which was then carried to the atomizer by argon (Ar carrier). The miniature diffusion flame and flame-in-gas-shield atomizer, shown in Fig. 1, were used as the atomizers. The miniature diffusion flame consisted of a vertical quartz support tube with a side inlet arm through which argon (Ar flame), hydrogen (H_2 flame) and bismuthane were introduced. The basis of the flame-in-gas-shield atomizer is the same as that of the miniature diffusion flame, a quartz vertical tube with a side inlet arm. Moreover, a quartz capillary (0.53 mm i.d.) is situated in the axis of the vertical tube through which oxygen is introduced. A two-channel brass shielding unit [7] was fitted around the support tube and served for introduction of shielding argon. The observation height is defined as the distance from the top of the support tube (miniature diffusion flame) or top of the capillary (flame-in-gas-shield) to the center of the optical beam. Capillary distance is defined as the distance from top of the capillary to the top of the support tube (Fig. 1). All gas flow rates were controlled by mass flow controllers (Omega Engineering, USA and Cole-Parmer, USA).

2.3 Procedure and data evaluation

A 1 μg l^{-1} Bi standard solution in 1 mol l^{-1} hydrochloric acid was used for all optimization studies. The standard was injected 5 s after the start of recording the fluorescence signal had been switched on. The total time of recording was 60 s. The detector output provided signals in μV, the peak area was then interpreted in μV s. Peak area corrected to baseline and a signal to noise ratio were the parameters used to evaluate the data. Noise was calculated as an average standard deviation (μV) of three replicates of blank (each measured for 10 s representing 400 values). Signal to noise ratio was determined by dividing the peak height (signal) by an average standard deviation of blank (noise).

3. Results and discussion

The atomization conditions in the miniature diffusion flame and flame-in-gas-shield atomizers were optimized. The hydrogen fraction, total gas flow rate (argon and hydrogen) and observation height were the parameters optimized for both atomizers. Regarding the flame-in-gas-shield atomizer, more parameters needed to be optimized due to its more complex construction such as oxygen flow rate through the capillary, the capillary distance and the flow rates of shielding argon.

Hydrogen fraction was optimized in both atomizers (Fig. 3). The total gas flow rate was kept at 600 ml min^{-1} for both atomizers. The signal increases with decreasing hydrogen fraction in both cases. However, a hydrogen fraction sufficient for maintaining the flame stable had to be selected because at very low flow rates of hydrogen the flame was not stable and very often went out, especially

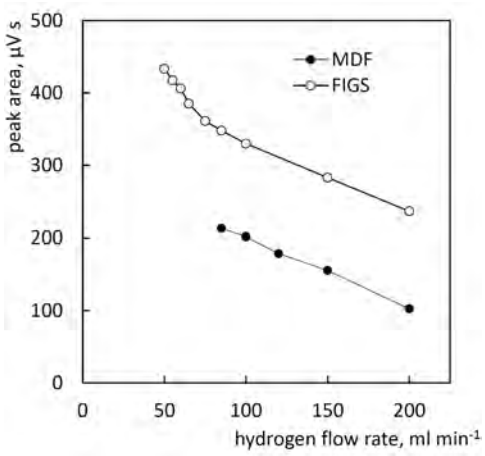

Fig. 3 Dependence of fluorescence signal on hydrogen flow rate for miniature diffusion flame (MDF, full circle) and flame-in-gas-shield (FIGS, empty circle); total gas flow rate 600 ml min^{-1}, 1 µg l^{-1} Bi, observation height of miniature flame-in-gas-shield atomizer diffusion flame 7 mm, observation height of flame-in-gas-shield 6 mm.

when the hydride generator was switched off. The optimum total hydrogen flow rate was chosen as 85 ml min^{-1} for miniature diffusion flame and 60 ml min^{-1} for flame-in-gas-shield atomizer. The highest signal to noise ratio is also obtained when a low hydrogen flow rate is employed because the background signal increases at higher hydrogen fractions.

The observation height has to be more than 5 mm for both atomizers. If the observation height is lower, the radiation from the lamp scatters on the top of the atomizer resulting in higher noise level. Since observation height needs to be higher, the total gas flow rate must be increased as well, so that the observed volume of flame is sufficiently large. The optimum observation height for miniature diffusion flame is 7 mm, for flame-in-gas-shield atomizer it is 6 mm.

Figure 4 shows the dependence of the fluorescence signal on the total gas flow rate. The higher the total gas flow rate, the higher the dilution of free analyte atoms, hence the lower signal. Low total gas flow rates in miniature diffusion flame result in a signal decrease due to insufficient volume of the flame at observation height of 7 mm. As for flame-in-gas-shield atomizer, the signal increases with lower total gas flow rates, but flow rates lower than 500 ml min^{-1} are not sufficient to maintain the flame stable. The optimum values were selected based on the highest peak area and highest signal to noise ratio obtained: 600 ml min^{-1} for miniature diffusion flame and 500 ml min^{-1} for flame-in-gas-shield.

The oxygen flow rate through the capillary was optimized for the flame-in-gas-shield atomizer. When lower flow rates of oxygen are employed the production of hydrogen radicals might not be sufficient for the analyte to be fully atomized. On the other hand, if higher flow rate is used the sensitivity decreases because of

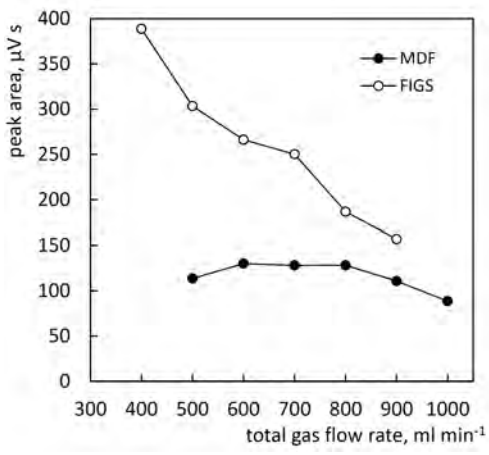

Fig. 4 Dependence of fluorescence signal on total gas flow rate for miniature diffusion flame (MDF, full circle) and flame-in-gas-shield (FIGS, empty circle); hydrogen fraction 1/5 for miniature diffusion flame and 1/8 for flame-in-gas-shield atomizer, 1 μg l^{-1} Bi, observation height of miniature diffusion flame 7 mm, observation height of flame-in-gas-shield 6 mm.

temperature expansion [8]. The oxygen flow rate of 7 ml min^{-1} was selected as the optimum value. Another important parameter is the capillary distance. The change of capillary distance did not influence peak area, though the highest signal to noise ratio was achieved with capillary distance 3 mm. The flow rates of shielding argon introduced through the two-channel shielding unit were optimized. Both the inner and outer optimum flow rates of shielding argon were 1500 ml min^{-1}. Under these conditions, the highest sensitivity and signal to noise ratio were achieved.

At optimized conditions the sensitivity with flame-in-gas-shield atomizer was approximately 2.4 times higher than with miniature diffusion flame. Limit of detection achieved for miniature diffusion flame and flame-in-gas-shield atomizers was 2.3 and 1.6 ng l^{-1}, respectively. The repeatability, expressed as relative standard deviation of peak area (n = 10), at 1 μg l^{-1} Bi was excellent using both atomizers, under 1%.

4. Conclusion

The atomization conditions for the miniature diffusion flame and the flame-in-gas-shield atomizer were optimized resulting in extremely low limits of detection for Bi determination. To compare the atomizers, the operation of the flame-in-gas-shield atomizer is more complicated due to its more complex construction and the gas supply required. As for the performance under optimized conditions, the miniature diffusion flame is probably more adequate for real samples analysis as it provides comparable limit of detection as the flame-in-gas-shield atomizer and excellent repeatability (under 1%). The developed methodology will be verified

on the analysis of certified reference materials. Interferences from other hydride forming elements are also yet to be investigated.

Acknowledgments

The support of the Grant Agency of the Czech Republic (17-04329S), Czech Academy of Sciences (Institutional support RVO: 68081715), and Charles University (project SVV260440) is gratefully acknowledged.

References

[1] Musil S., Matoušek T., Currier J.M., Stýblo M., Dědina J.: Speciation analysis of arsenic by selective hydride generation-cryotrapping-atomic fluorescence spectrometry with flame-in-gas-shield atomizer: achieving extremely low detection limits with inexpensive instrumentation. *Anal. Chem.* **86** (2014), 10422–10428.

[2] Kobayashi S., Nakahara T., Musha S.: Non-dispersive atomic fluorescence spectrometry of trace amounts of bismuth by introduction of its gaseous hydride into a premixed argon (entrained air)-hydrogen flame. *Talanta* **26** (1979), 951–957.

[3] Corns W.T., Stockwell P.B., Ebdon L., Hill S.J.: Development of an atomic fluorescence spectrometer for the hydride-forming elements. *J. Anal. At. Spectrom.* **8** (1993), 71–77.

[4] Dědina J.: Atomization of volatile compounds for atomic absorption and atomic fluorescence spectrometry: on the way towards the ideal atomizer. *Spectrochim. Acta, Part B* **62** (2007), 846–872.

[5] Dědina J., D'Ulivo A.: Argon shielded, highly fuel-rich, hydrogen–oxygen diffusion microflame: a new hydride atomizer. *Spectrochim. Acta, Part B* **52** (1997), 1737–1746.

[6] D'Ulivo A., Paolicchi I., Onor M., Zamboni R., Lampugnani L.: Flame-in-gas-shield miniature flame hydride atomizers for ultra trace element determination by chemical vapor generation atomic fluorescence spectrometry. *Spectrochim. Acta, Part B* **64** (2009), 48–55.

[7] CZ Pat 303957. Dědina, J., Musil S., D´Ulivo A.: *Dvoukanálová stínicí jednotka atomizátoru pro atomovou fluorescenční spektrometrii.* (In Czech.)

[8] Marschner K., Musil S., Dědina J.: Flame-in-gas-shield and miniature diffusion flame hydride atomizers for atomic fluorescence spectrometry: optimization and comparison. *Spectrochim. Acta, Part B* **109** (2015), 16–23.

Electrochemical detection of G-quadruplex by interaction with porphyrin ligand

Daniel Dobrovodský[a, b, *], Aleš Daňhel[a], Jana Malíková[a], Miroslav Fojta[a]

[a] *Institute of Biophysics of the Czech Academy of Sciences, Královopolská 135, 612 65 Brno, Czech Republic* ✉ *danield@ibp.cz*
[b] *Faculty of Science, Masaryk University, Kamenice 5, 625 00 Brno, Czech Republic*

Keywords
cyclic voltammetry
G-quadruplex
hanging mercury drop electrode
porphyrins

Abstract
Porphyrins are well-known binders of DNA and can also specifically target guanine quadruplexes (G4). Interaction of a selected porphyrin (Cu-TMPyPP) with oligonucleotide sequences either forming or not forming G4 was studied using cyclic voltammetry at hanging mercury drop electrode. The interaction is shown to be detectable by cyclic voltammetry as potential shift of a characteristic peak of Cu-TMPyPP which is observed for G4, single stranded as well as double stranded DNA. Nevertheless, further changes of this peak resulting from application of cyclic potential scans to the studied DNA before interaction with Cu-TMPyPP can be used to clearly distinguish G4 DNA, which can be applied as analytical tool for its detection.

1. Introduction

Outside of the well-known canonical double helix, DNA molecules can form alternative stable secondary structures under specific conditions, such as the guanine quadruplex (G-quadruplex, G4). This four-stranded helical structure can occur in nucleic acid sequences containing stretches of guanines. Guanine residues tend to self-associate via Hoogsteen hydrogen bonding to form G-tetrads, square planar structures (Fig. 1a) that stack on top of each other to produce the G4 [1, 2]. The central cavity of the quadruplex is occupied by cations (K^+, Na^+) that play a crucial role in G4 formation and stability [3]. G-quadruplexes exhibit a wide range of possible topologies. In addition to the number of associated DNA strands forming the G4 structure (one, two or four) and their relative orientation (parallel/antiparallel), the topology is also influenced by the number of stacked G-tetrads, *N*-glycosidic bond torsion angle, length and sequence of the loop regions connecting the guanine tracts as well as the type and concentration of cations [4]. Because G4 forming sequences can be often found in genomic DNA regions of high biological importance such as telomeres or gene promoters and are involved in essential biological processes [1], they may act as potential drug targets in anticancer therapy [5, 6]. Many types of G4 binding ligands have been

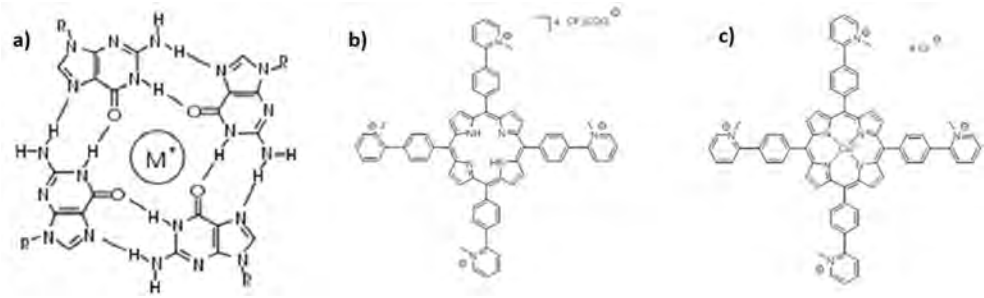

Fig. 1 Structure of (a) a G-tetrad with a monovalent cation M^+, and the studied G4 ligands (b) *meso*-5,10,15,20-tetrakis(4-(*N*-methyl-pyridinium-2-yl)phenyl)-porphyrin (H_2-TMPyPP), and (c) its copper complex (Cu-TMPyPP).

identified, among others selected cationic porphyrins. Their binding specificity towards G4 can be improved by various meso-substituents or by metal coordination [7].

Electrochemical methods have been established as useful tools of studying DNA structure and its changes [8]. In recent years, attempts have been made to apply these methods to study G4 structures as well [9, 10]. In this contribution, the possibility of using the specific interaction between a porphyrin G4 ligand and G4 DNA for electrochemical detection of these structures is investigated by studying the porphyrin interaction with different oligodeoxynucleotides (ODNs).

2. Experimental

2.1 Reagents and chemicals

Two selected porphyrin G4 ligands (Fig. 1 b, c), *meso*-5,10,15,20-tetrakis(4-(*N*-methyl-pyridinium-2-yl)phenyl)porphyrin (H_2-TMPyPP) and its copper complex (Cu-TMPyPP) were provided by Dr. Genevieve Pratviel (Toulouse, France). Following ODN sequences were used, supplied by Eurofins Genomics: human telomeric sequence hut-T2 ($d((AG_3T_2)_3AG_3)$) and its complementary sequence hut-com ($d((C_3TA_2)_3C_3T)$), telomeric sequence of the genus *Cestrum* ($d((AG_3T_6)_3AG_3)$), 4BAS-prim ($G_3TACG_2CG_3TAC$) and its complementary 4BAS-com ($d(GTAC_3GC_2GTAC_3)$), C30 (dC_{30}). Britton-Robinson (BR) buffer of various pH prepared from a mixture of acidic solution (0.04 mol l^{-1} H_3BO_3, 0.04 mol l^{-1} H_3PO_4, 0.04 mol l^{-1} CH_3COOH) and alkaline solution (0.2 mol l^{-1} NaOH) or 0.05 mol l^{-1} sodium phosphate buffer with 0.3 mol l^{-1} ammonium formate (AFP) pH = 6.9 were used as base electrolytes for electrochemical measurements. All chemicals were purchased from Sigma-Aldrich.

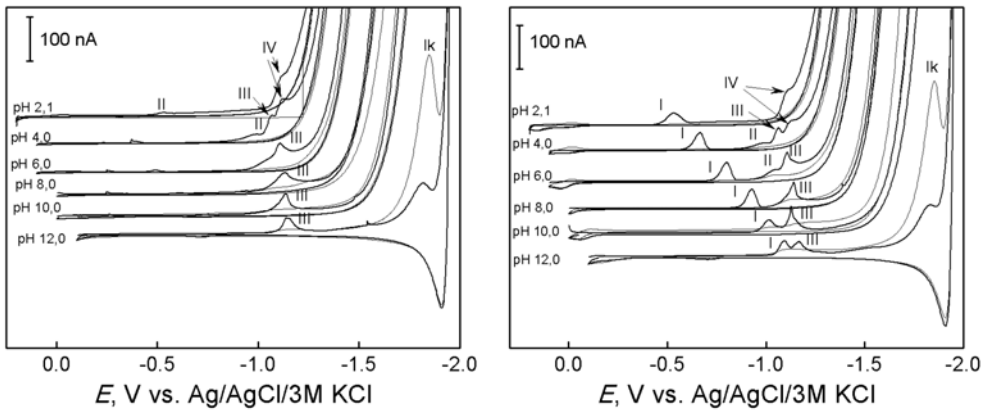

Fig. 2 Cyclic voltammograms of the G4 ligand H_2-TMPyPP (left) and Cu-TMPyPP (right), both 10 μmol l^{-1} at hanging mercury drop electrode in Britton-Robinson buffer pH = 2.1, 4.0, 6.0, 8.0, 10.0, and 12.0; scan rate 100 mV s^{-1}.

2.2 Instrumentation

For all electrochemical measurements potentiostat PGSTAT128N controlled by software Nova 2.1 (both Metrohm Autolab) was used, with standard three electrode system using hanging mercury drop electrode (HMDE) as working electrode, Ag/AgCl/3M KCl reference electrode and platinum auxiliary electrode.

2.3 Methods

The porphyrins were studied using cyclic voltammetry (CV) in BR buffer within the pH range 2–12 with scan rate 0.1 V s^{-1}. For the measurements of interaction between oligonucleotides and porphyrins, oligonucleotides were adsorbed on to the HMDE surface from 3 μl of 1 μmol l^{-1} solution to reach full surface coverage. Such modified HMDE was subsequently transferred into porphyrin solution in AFP buffer, where after an incubation period of 60 s, CV measurements were performed in the potential window (0.00 V; –1.85 V) at scan rate 1 V s^{-1}.

3. Results and discussion

Electrochemical analysis of the G4 ligands H2-TMPyPP and Cu-TMPyPP in dependence on pH of BR buffer (Fig. 2) revealed a series of three cathodic peaks obtained for both porphyrins (labelled II, III and IV) and a peak at highly negative potentials attributed to catalytic hydrogen evolution. Additionally, the porphyrin Cu-TMPyPP also offers a characteristic cathodic peak I. Because of this well-defined and easily analytically distinguishable peak, Cu-TMPyPP was selected for studies of interactions with oligonucleotides.

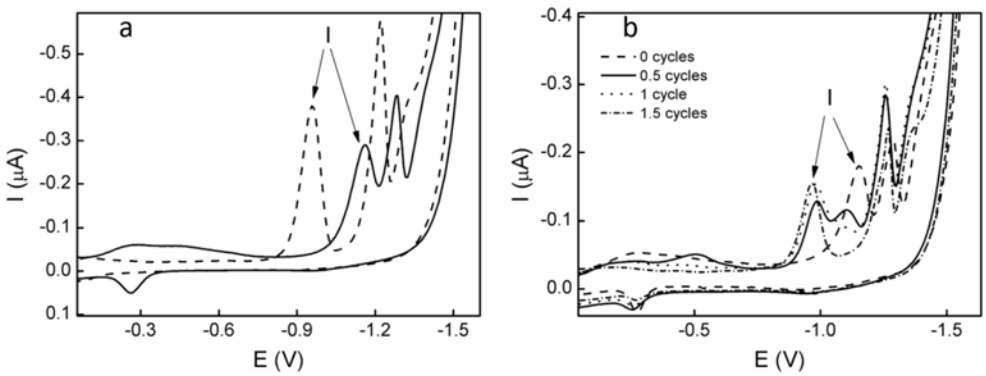

Fig. 3 Cyclic voltammograms of (a) 1 μmol l^{-1} Cu-TMPyPP alone (dash line) or in complex with hut-T2 (solid line), (b) 0.4 μmol l^{-1} Cu-TMPyPP in complex with hut-T2 subjected to 0.0–1.5 V cyclic scans prior to the interaction.

ODNs where G4 formation is either expected (hut-T2, 4BAS-prim, ces-T6) or not expected (hut-com, 4BAS-com, C30)) immobilised at HMDE were let to interact with Cu-TMPyPP from solution, resulting in distinct, concentration dependent CV peaks of the porphyrin together with signals of DNA. Apparently as a result of interaction between the ligand and ODNs, potential of the peak I of Cu-TMPyPP is shifted towards more negative potentials by approximately 0.2 V (Fig. 3a). While peak I height and its concentration dependency differ for each ODN, this potential shift is observed for all studied sequences, indicating that the DNA-ligand interaction is not structure specific for G4 but is present for single stranded DNA as well.

Reduction of guanine bases can disrupt the structure of G-quadruplex and alter its interaction properties. Therefore, in the next step, ODNs adsorbed on HMDE were reduced by a single linear voltammetric scan or reduced and re-oxidised by increasing number of cyclic scans in clean AFP buffer prior to being transferred to Cu-TMPyPP solution and measured by CV. For ODNs where G4 formation is expected, increasing number of cyclic scans applied leads to gradual splitting of peak I together with significant shift of its position to potentials corresponding to Cu-TMPyPP without the presence of ODNs (Fig. 3b). Conversely, only small changes of peak I shape and potential are present for single stranded ODNs. To further examine structural specificity of the observed effect, a double stranded ODN (hut-ds) was prepared by hybridization of the complementary ODNs hut-T2 and hut-com. As was the case with single stranded DNA, peak I of Cu-TMPyPP in complex with hut-ds showed no significant response to reduction or oxidation state of DNA. Therefore, current value at the potential of peak I of Cu-TMPyPP (without DNA) for G4 forming ODNs after the described procedure is significantly higher compared to other structures and can be used as an analytical parameter for G4 detection.

4. Conclusions

Selected G4 ligand Cu-TMPyPP as well as its interactions with ODNs with different secondary structure was studied by the means of CV at HMDE. The ligand was found to interact with G4, single stranded as well as double stranded DNA. However, changes of the peak I of Cu-TMPyPP observed when DNA is repeatedly reduced and oxidized prior to interaction with the ligand allow clear discrimination of G4 structures.

Acknowledgments

This work was supported by the project SYMBIT reg. no. CZ.02.1.01/0.0/0.0/15_003/0000477 funded from European Regional Development Fund (EFRD).

References

[1] Lipps H., Rhodes D.: G-quadruplex structures: in vivo evidence and function. *Trends Cell Biol.* **19** (2009), 414–422.
[2] Murat P., Balasubramanian S.: Existence and consequence of G-quadruplex structures in DNA. *Curr. Opin. Genet. Dev.* **22** (2014), 22–29.
[3] Bhattacharyya D., Arachchilage G. M., Basu S.: Metal caitons in G-quadruplex folding and stability. *Front. Chem.* **4** (2016), 38–51.
[4] Neidle S.: Structural diversity of G-quadruplex scaffolds. In: *Quadruplex Nucleic Acids.* Balasubramanian S. (edits.). Cambridge, RSC Biomolecular Sciences 2006, p. 81–99.
[5] Ou T., Lu Y., Tan J., Huang Z., Wong K., Gu L.: G-quadruplexes: Targets in anticancer drug design. *ChemMedChem* **3** (2008), 690–713.
[6] Neidle S.: Quadruplex nucleic acids as novel therapeutic targets. *J. Med. Chem.* **13** (2016), 5987–6011.
[7] Pratviel G.: Porphyrins in complex with DNA: Modes of interaction and oxidation reactions. *Coord. Chem. Rev.* **308** (2016), 460–477.
[8] Paleček E., Bartošík M.: Electrochemistry of nucleic acids. *Chem. Rev.* **112** (2012), 3427–3481.
[9] Vidláková P., Pivoňková H., Kejnovská I., Trnková L., Vorlíčková M., Fojta M., Havran L.: G-quadruplex-based structural transitions in 15-mer DNA oligonucleotides varying in lengths of internal oligo(dG) stretches detected by voltammetric techniques. *Anal. Bioanal. Chem.* **407** (2015), 5817–5826.
[10] Chiorcea-Paquim A., Oliviera-Brett A.: Redox behaviour of G-quadruplexes. *Electrochim. Acta.* **126** (2014), 162–170.

Method optimization for simultaneous separation of six triazole fungicides in HPLC

Ishak Kovač[a, b, d, *], Paula Martín Mián[c], Maria Del Sol Vega Alegre[c], Hana Dejmková[a], Jana Jaklová Dytrtová[b, d], Karolina Schwarzová[a]

[a] *Department of Analytical Chemistry, Faculty of Science, Charles University, Hlavova 8, 128 43 Prague 2, Czech Republic*
[b] *Institute of Organic Chemistry and Biochemistry of the Czech Academy of Sciences, Flemingovo nám. 542/2, 160 10 Prague 6, Czech Republic* ✉ *ishak.kovac@uochb.cas.cz*
[c] *Department of Analytical Chemistry, Faculty of Science, University of Valladolid, Ps. Belén, 47011 Valladolid, Spain*
[d] *Department of Physiology and Biochemistry, Faculty of Physical Education and Sport, Charles University, José Martího 269/31, 162 52 Prague 6, Czech Republic*

Keywords
capillary electrophoresis
HPLC
triazole pesticides

Abstract
Triazole pesticides are widely used in agriculture against fungi pathogens. Their application is not restricted on just one member of the group; more importantly, the application is usually carried out in a mixture of two or more triazoles. Hence, this work focuses on simultaneous separation and detection of six triazole fungicides: penconazole, tebuconazole, propiconazole, cyproconazole, fenbuconazole, and difenoconazole. Two different columns were tested with different parameters for isocratic and gradient elution in HPLC with UV detector. On Purospher Reverse Phase-18 column with gradient elution isomers of triazoles cyproconazole and propiconazole were successfully separated. However, on this column, there was an overlap of some triazoles. In contrast, the isocratic elution on Kromasil Eternity-5-PhenylHexyl column showed sufficient separation capabilities. In further research, chiral separation of triazoles will be considered using capillary electrophoresis.

1. Introduction

Triazole pesticides are a category of pesticides with antifungal and antimycotic properties [1]. Their structure is based on the 1,2,4-triazole ring, where N^1 binds to variable hydrophobic chains [2]. Regardless of their medical and agricultural application, they show some adverse effects on mammals. Triazole pesticides affect two enzymes of the cytochrome P450 superfamily involved in the steroid biosynthesis, aromatase and 14α-demethylase. Aromatase or (CYP19) is the enzyme that converts androgens to estrogens, thus it is important for the development of sexual organs and fertility. The second affected enzyme is 14α-demethylase or (CYP51) a key enzyme in the biosynthesis of meiosis-

activating sterol, which is applied as a modulator of the development of germ cells in both mammalian sexes. Therefore, the exposure to triazole pesticides has an adverse effect on steroid biosynthesis (of non-target species) resulting in impaired reproduction, alteration in differentiation (sexual), growth, and development of certain types of cancer [3–5].

There are several analytical methods in the literature dealing with the analysis of triazole compounds. The problem that every analytical method face is a sufficient separation of target compounds and the sensitivity of the method. Separation of triazole pesticides has been performed by different techniques, ranging from GC methods to HPLC which can be coupled with different detectors such as diode array detector, UV/Vis, fluorometric detector or mass-spectrometry. Those analytical methods are in many cases combined with classical cleanup procedures such as solid-phase or liquid-liquid extraction [6].

In recent years, more attention is given not only to the classical separation of compounds but also to a chiral separation in GC, HPLC, supercritical fluid chromatography or capillary electrophoresis. There is not much information concerning what role in fungicides plays chirality. Regarding the pesticide activity, there are many compounds which activity is associated with only one enantiomer. The chirality and chiral separation are also important from the biological aspect, different degradation pattern is observed in each enantiomer. The chiral separation in these methods has two different approaches, direct and indirect. Indirect approach prior separation needs derivatization step with a chiral agent, in contrast, direct approach separates chiral compounds without derivatization [7]. Emphasis on the chiral separation is a direct consequence of different behavior of the isomers. This contribution concentrates on HPLC separation of triazole mixtures with UV detection only.

2. Experimental

2.1 Reagents and chemicals

The standards of triazole pesticides (cyproconazole, penconazole, tebuconazole, difeconazole) were purchased from Sigma Aldrich (Germany), while propiconazole and fenbuconazole were purchased from Supelco (Germany). Stock solutions (1×10^{-4} mol L^{-1}) were prepared in methanol (HPLC grade, Sigma Aldrich), acetonitrile (HPLC grade, Sigma Aldrich) and deionized water (> 18.2 MΩ). Acetic acid, phosphoric acid and sodium hydroxide for buffer solution were purchased from Sigma Aldrich.

2.2 Instrumentation

HPLC analysis was carried out using an HPLC instrument consisting of a vacuum degasser, ternary pump enabling gradient elution (Ecom, CZ), manual injector,

ultraviolet detector with deuterium lamp Sapphire 600 (Ecom, CZ). Chromatographic software ECOMAC was used to control the HPLC system and record of chromatograms. For peak shape calculation, calibration, etc. Clarity software was used. The wavelength for UV detector on HPLC was optimized. The spectra of pesticides dissolved in methanol:water or acetonitrile:water solution were measured using Spectrophotometer Pye-Unicam PU 8800 (Philips-Unicam, England). The concentration of pesticides was 1×10^{-4} mol L^{-1}. To avoid interference of solvent and analyte [8] wavelength of 222 nm was chosen for HPLC measurement in contrast to 260 nm used by Gordien [9]. For HPLC separation two columns were chosen: Purospher RP-18; 5 μm, 4×125 mm (LiChroCART, Merck) and Kromasil Eternity-5-PhenylHexyl; 5 μm, 4.6×150 mm (Supelco, Merck).

The buffer combined with methanol or acetonitrile was used as mobile phase in HPLC. It was prepared of a mixture of 5×10^{-2} mol L^{-1} orthophosphoric acid and 5×10^{-2} mol L^{-1} acetic acid (or 5×10^{-2} mol L^{-1} orthophosphoric acid only) adjusting the buffer pH by addition of the necessary amount of 2×10^{-2} mol L^{-1} sodium hydroxide. For optimization of the chromatographic conditions 1×10^{-5} mol L^{-1} solutions of the individual pesticides and a multianalyte solution containing 1×10^{-5} mol L^{-1} of the six pesticides were used. Standards, stock solutions, and working solutions were stored at 4 °C.

3. Results and discussion

The first column which was used for separation was Purospher RP-18 column, using isocratic elution. For optimization of eluent composition, different ratios of methanol or acetonitrile (30–70%) and buffer (30–70%; pH = 2.5; 4.0; 6.0) was tested (Fig. 1). The optimal eluent composition was established to acetonitrile:5×10^{-2} mol L^{-1} phosphate and 5×10^{-2} mol L^{-1} acetate buffer pH = 6.0 (30:70, *v/v*) with isocratic elution for 7 minutes followed by gradient to 70:30, which allowed separation within thirteen minutes. The column was conditioned for 5 minutes for reequilibration after each measurement. In Fig. 1, there are visible two peaks for cyproconazole and two peaks for propiconazole. The explanation of these double peaks lies in the presence of both isomers of those azoles in a racemic mixture.

For optimization of separation with Kromasil Eternity-5-PhenylHexyl column, a similar procedure was used. Mobile phase consisted of a mixture of acetonitrile (40–60%) and acetate-phosphate buffer (40–60%). The pH of the buffer was changed from the 2.0 to 6.0. The best separation of triazoles on this column was achieved for the buffer of pH = 4.0. Nevertheless, instability of baseline was observed (Fig. 2), probably due to the presence of acetic acid in the used buffer. It absorbs at the same wavelength as detected triazoles, which results in a pulsing baseline. Hence, further experiments were performed in phosphate buffer to obtain stabilized baseline.

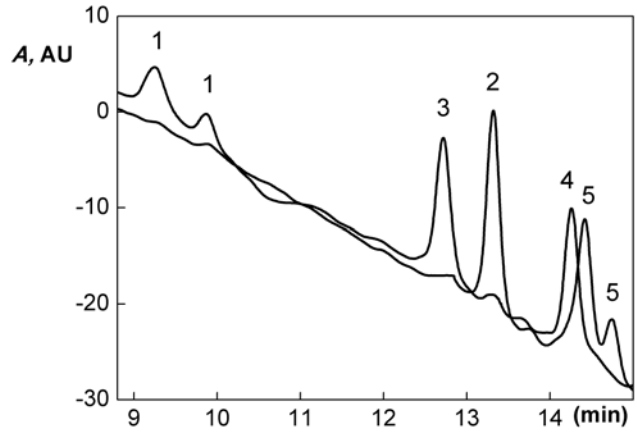

Fig. 1 Chromatogram of (1) cyproconazole, (2) fenbuconazole, (3) tebuconazole, (4) penconazole, and (5) and propiconazole (3×10^{-5} mol L^{-1} of each) on Purospher RP-18 column. Injection of two different solutions (one with cyproconazole, tebuconazole and penconazole, and the other one with fenbuconazole and propiconazole). Isocratic elution acetonitrile:5×10^{-2} mol L^{-1} acetate-phosphate buffer pH = 6.0 (30:70, *v/v*) for 7 min followed by gradient to 70:30 to 13 min. UV detection, λ = 222 nm, flow rate 0.5 mL min^{-1}.

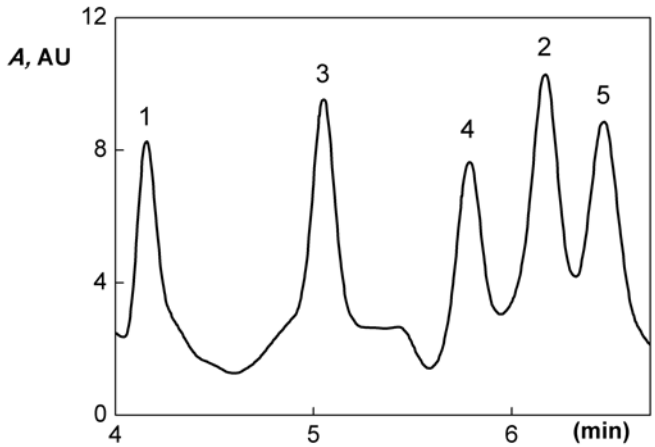

Fig. 2 Chromatogram of (1) cyproconazole, (2) tebuconazole, (3) penconazole, (4) fenbuconazole, and (5) propiconazole (1×10^{-5} mol L^{-1} of each) solution on Kromasil Eternity-5-PhenylHexyl column. Isocratic elution with acetonitrile:5×10^{-2} mol L^{-1} acetate-phosphate buffer pH = 4.0 (57:43, *v/v*). UV detection, λ = 222 nm, flow rate 1 mL min^{-1}.

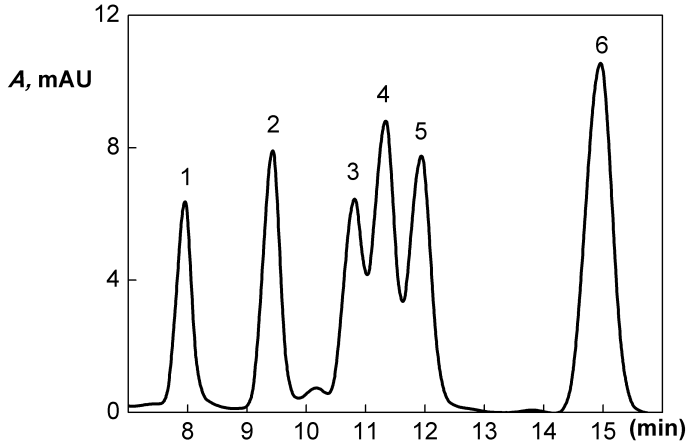

Fig. 3 Chromatogram of (1) cyproconazole, (2) tebuconazole, (3) fenbuconazole, (4) penconazole, (5) propiconazole, and (6) difeconazole (1×10^{-5} mol L^{-1}) solution on Kromasil Eternity-5-Phenyl-Hexyl column. Isocratic elution with acetonitrile:5×10^{-2} mol L^{-1} phosphate buffer pH = 6.8 (57:43, *v/v*). Flow rate 0.5 mL min^{-1}, V_{inj} = 20 µL, λ = 222 nm.

Table 1
Retention times and retention factors of the triazole pesticides (1×10^{-5} mol L^{-1}) using the optimized conditions: Kromasil Eternity-5-PhenylHexyl column; isocratic elution with acetonitrile:5×10^{-2}mol L^{-1} phosphate buffer pH = 6.8 (57:43, *v/v*). Flow rate 0.5 mL min^{-1}; V_{inj} = 20 µL; λ = 222 nm.

Triazole pesticide	t_r/min	*k*
Cyproconazole	7.98	2.61
Tebuconazole	9.49	3.11
Fenbuconazole	10.81	3.36
Penconazole	11.33	3.56
Propiconazole	11.93	3.75
Difeconazole	14.95	3.94

Maintaining the same ratio of acetonitrile:phosphate buffer (57:43, *v/v*), pH change from 4.0 to 6.8 does not make a significant impact on the retention time of pesticides (Fig. 3).

The optimized conditions and retention times and factors of all separated triazole pesticides are summarized in Table 1. Calibration dependences are linear in the range from 1×10^{-5} mol L^{-1} to 8×10^{-7} mol L^{-1}.

4. Conclusion

The HPLC separation method with UV detection using two different columns has been optimized for a mixture of six triazole pesticides. Gradient elution on Purospher RP-18, 4×125 mm (5 µm) column reveals the possibility of chiral

separation of two pesticides (cyproconazole and propiconazole), however, the chiral separation has not been the aim of the study. The best separation was achieved on the Kromasil Eternity-5-PhenylHexyl, 4.6×150 mm (5 μm) column. The developed HPLC-UV method for the detection of triazole pesticide is very fast and robust. Further research will be focused on the application of HPLC-UV method for determination of the studied pesticides in soil extracts and chiral separation of a mixture of triazole pesticides using capillary electrophoresis.

Acknowledgments

This work was supported by the Czech Science Foundation (18-01710S) and the Specific University Research (SVV 260440).

References

[1] Giavini E., Menegola E.: Are azole fungicides a teratogenic risk for human conceptus. *Toxicol. Lett.* **198** (2010), 106–111.

[2] Wu Y.S., Lee H.K., Li S.: High-performance chiral separation of fourteen triazole fungicides by sulfated β-cyclodextrin-mediated capillary electrophoresis. *J. Chromatogr. A* **913** (2001), 171–179.

[3] Sanderson J.T.: The steroid hormone biosynthesis pathway as a target for endocrine-disrupting chemicals. *Toxicol. Sci.* **94** (2006), 3–21.

[4] Kim K.H., Kabir E., Jahan S.A.: Exposure to pesticides and the associated human health effects. *Sci. Total Environ.* **575** (2017), 525–535.

[5] Van Maele-Fabry G., Lantin A.C., Hoet P., Lison D.: Residential exposure to pesticides and childhood leukemia: a systematic review and meta-analysis. Environ. Int. **37** (2011), 280–291.

[6] Locatelli M., Kabir A., Innosa D., Lopatriello T., Furton K.G.: A fabric phase sorptive extraction-High performance liquid chromatography-Photo diode array detection method for the determination of twelve azole antimicrobial drug residues in human plasma and urine. *J. Chromatogr. B* **1040** (2017), 192–198.

[7] Fernández V.P., García M.A., Marina M.L.: Chiral separation of agricultural fungicides. *J. Chromatogr. A* **1218** (2011), 6561–6582.

[8] Takala N., Sirén H., Jakl M., Dytrtová J. J.: Determination of important azoles in soil solution using CE. *Monatsh. Chem.* (2019), accepted for publication.

[9] Gordien J.B., Pigneux A., Vigouroux S., Tabrizi R., Accoceberry I., Bernadou J. M., Rouault A., Saux M.C., Breilh D.: Simultaneous determination of five systemic azoles in plasma by high-performance liquid chromatography with ultraviolet detection. *J. Pharm. Biomed. Anal.* **50** (2009), 932–938.

Fabrication, morphology and electrochemical properties of boron doped diamond microelectrodes on tungsten supports

Jana Vosáhlová[a,*], Mariola Brycht[a,b], Simona Baluchová[a], Jan Krůšek[c], Ivan Dittert[c], Vincent Mortet[d], Andrew Taylor[d], Ladislav Klimša[d], Jaromír Kopeček[d], Karolina Schwarzová[a]

[a] *Department of Analytical Chemistry, Faculty of Science, Charles University, Hlavova 8, 128 43 Prague 2, Czech Republic* ✉ *vosahloj@natur.cuni.cz*
[b] *Department of Inorganic and Analytical Chemistry, University of Lodz, Faculty of Chemistry, Tamka 12, 91 403 Lodz, Poland*
[c] *Institute of Physiology of the Czech Academy of Sciences, Vídeňská 1083, 142 20 Prague 4, Czech Republic*
[d] *Institute of Physics of the Czech Academy of Sciences, Na Slovance 1999/2, 182 00 Prague 8, Czech Republic*

Keywords
boron doped diamond
electrochemistry
fabrication
microelectrode
tungsten wire

Abstract
Two types of microelectrodes were prepared by insulating boron doped diamond-coated tungsten wires in glass capillary. During the deposition step using microwave plasma enhanced chemical vapour deposition process with linear antenna delivery, the wires were held in different positions. Raman spectroscopy and scanning electron microscopy were used for characterisation of the morphology of the boron doped diamond microelectrodes. Cyclic voltammetry was performed for electrochemical characterization using inner-sphere and outer-sphere redox markers and several supporting electrolytes in aqueous media. The uniformity of the boron doped diamond layer and its quality was assessed revealing a dependence on coverage according to the position during the deposition step.

1. Introduction

Boron doped diamond (BDD) possesses outstanding characteristics such as wide faradaic potential window in the region of positive potentials, low and stable background current, biocompatibility, and low proclivity to adsorption and fouling, thus its application in electroanalysis for a variety of organic analytes is favoured. Sensitive detection of neurochemicals, especially biogenic amines have been proven using BDD electrodes, revealing their perspectives in physiology and biology-related research fields. Thus, miniaturization of BDD electrodes is a

challenging task, especially for *in vitro* and *in vivo* sensing. Boron doped diamond microelectrodes can be prepared in various shapes on various types of substrates in the arrays [1, 2] or as single microelectrodes, most frequently using tungsten [3, 4] or platinum wires [5] as support.

In this contribution, microwave plasma enhanced chemical vapour deposition process with linear antenna delivery (MW-LA-PECVD) was used for deposition of BDD on tungsten wires. The wires were held in different positions in the deposition chamber and subsequently sealed in a glass capillary. The fabricated microelectrodes were characterized using spectral and electrochemical methods.

2. Experimental

2.1 Reagents and chemicals

Several supporting electrolytes (all p.a., Lachner, Czech Republic) were used for electrochemical characterisation, such as KCl (c = 1 mol l^{-1}), HNO_3 (c = 1 mol l^{-1}), H_2SO_4 (c = 0.5 mol l^{-1}), H_3PO_4 (c = 0.1 mol l^{-1}). Solutions of $[Ru(NH_3)_6]^{2+/3+}$, $[Fe(CN)_6]^{3-/4-}$ (c = 1 mmol l^{-1} for both, in 1 mol l^{-1} KCl) were used for electrochemical characterisation of boron doped diamond microelectrodes. Deionised water (Millipore Mili plus Q system, Billerica, USA) with resistance of not less than 18.2 MΩ was used for preparation of solutions in all experiments.

2.2 Instrumentation

A MW–LA–PECVD system (Fig. 1C) was used for the preparation of BDD microelectrodes, further details are reported in [6]. Tungsten wires with a diameter of 20 μm were used as substrates for BDD deposition. Prior to BDD growth wires were seeded with nano-diamond seeds suspended in a mixture of DMSO and PVA. Two sets of BDD microelectrodes, using the same growth conditions reported in [6], were produced. The difference between the two sets of the BDD microelectrodes was their orientation during BDD growth: BDDμE$_1$ samples were held vertically in the chamber, whereas BDDμE$_2$ were held horizontally. The BDD coated tungsten wires (Fig. 1A) were then subsequently embedded in glass micropipettes using UV light curable resin (Norland Optical Adhesive 68), and the uncoated ends of the tungsten wires were contacted to copper wires using conductive silver paint (Leitsilber, Degussa) (Fig. 1B). The surface morphology of deposited BDD layers was observed by scanning electron microscopy (SEM, Tescan FERA 3), and the layer thickness of samples was evaluated from cross section SEM observations of reference BDD coated Si samples, which were placed close to the W wires during growth. For assessment of composition and quality of the BDD layer Raman spectroscopy was carried out at room temperature using a Renishaw InVia Raman microscope at a wavelength of 488 nm and a laser power of 6 mW. For electrochemical characterisation cyclic

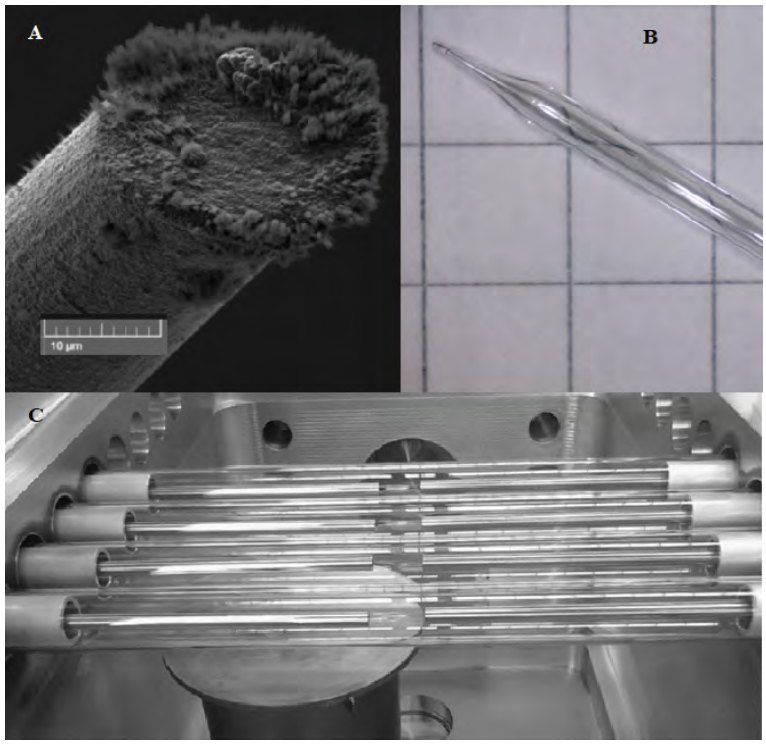

Fig. 1 (A) Scanning electron micrograph of BDDµE$_2$ (SEM HV: 5.0 kV), (B) whole BDD microelectrode sealed in glass capillary, (C) chamber of MW–LA–PECVD system.

voltammetry with bipotentiostat/bigalvanostat BP-300 (Bio-Logic Science Instruments, France) with EC–LAB software (version 11.20) was used. A classic three-electrode arrangement was used: BDD microelectrodes as working electrode, a silver chloride electrode (Ag | AgCl | 3 mol l^{-1} KCl) as reference electrode, and a platinum wire (both BASi, USA) as counter electrode. Digital pH meter 3510 with a combined glass electrode (Jenway, Essen, UK) was used for pH measurement. All electroanalytical experiments were carried out at laboratory temperature.

3. Results and discussion

SEM was used to compare the quality of the BDD coverage according to the different positioning during BDD growth: BDDµE$_1$ (vertical) and BDDµE$_2$ (horizontal). SEM revealed incomplete coverage of BDDµE$_1$, where bare tungsten wire and isolated BDD islands (circa 350 nm thick) with poorly developed sp^3 crystals were visible. The second set of microelectrodes, BDDµE$_2$, revealed a monolithic BDD layer (cca 420 nm thick) with a well-developed crystalline structure (Fig. 1A). Raman spectrum of the BDD coatings show characteristic features of highly boron doped diamond [7] with intense bands at circa 497 cm^{-1}

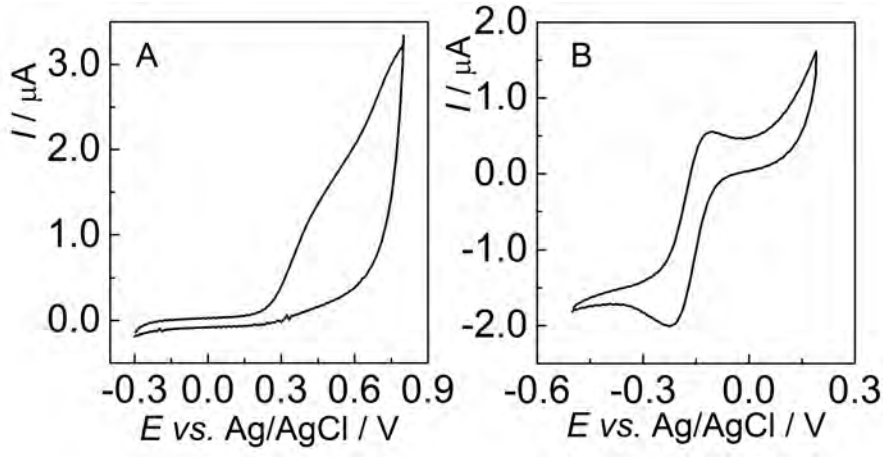

Fig. 2 Cyclic voltammograms (scan rate 100 mV s^{-1}) of redox markers (A) $[Fe(CN)_6]^{3-/4-}$ and (B) $[Ru(NH_3)_6]^{2+/3+}$ (both, c = 1 mmol l^{-1} in 1 mol l^{-1} KCl) measured on BDDμE_1.

Table 1
The widths of potential window in aqueous solutions of different supporting electrolytes for both sets of microelectrodes BDDμE_1 and BDDμE_2.

Supporting electrolyte	Potential window	
	BDDμE_1	BDDμE_2
KCl (c =1 mol l^{-1})	1.40 V; from −0.60 V to +0.80 V	2.00 V; from −0.65 V to +1.35 V
HNO_3 (c = 1 mol l^{-1})	0.90 V; from −0.30 V to +0.60 V	1.70 V; from −0.35 V to +1.35 V
H_2SO_4 (c = 0.5 mol l^{-1})	1.20 V; from −0.60 V to +0.60 V	2.00 V; from −0.45 V to +1.55 V
H_3PO_4 (c = 0.1 mol l^{-1})	1.35 V; from −0.65 V to +0.70 V	1.85 V; from −0.35 V to +1.50 V

and 1230 cm^{-1}, a red shifted (down to circa 1308 cm^{-1}) Fano shaped diamond Raman line and a contribution from non-diamond carbon phases at 1500 cm^{-1} and 1150 cm^{-1}. Based on the position of the boron related bands [8], the boron concentration in the BDD layers has been estimated to be ~ 8.0×10^{20} cm^{-3}. The reported Raman features match that of a reference BDD layer doped with 2000 ppm B/C in the gas phase.

For electrochemical characterization, cyclic voltammetry at a scan rate of 100 mV s^{-1} was performed in KCl (c = 1 mol l^{-1}), HNO_3 (c = 1 mol l^{-1}), H_2SO_4 (c = 0.5 mol l^{-1}), and H_3PO_4 (c = 0.1 mol l^{-1}). The width of the potential windows in all supporting electrolytes was 0.9 V and higher, depending on the type of microelectrode. BDDμE_1 had a narrower potential window than BDDμE_2 in each supporting electrolyte used, especially in the region of positive potentials as shown in Table 1. The inner-sphere $[Fe(CN)_6]^{3-/4-}$ and the outer-sphere $[Ru(NH_3)_6]^{3+/2+}$ redox markers were used for investigation of electrochemical response of both sets of BDD microelectrodes (Fig. 2). A quasireversible response

was obtained for $[Ru(NH_3)_6]^{3+/2+}$ on both types of microelectrodes; ΔE_p values were estimated to be 75 mV for $BDD\mu E_2$ and 130 mV for $BDD\mu E_1$. Limiting currents in cyclic voltammograms of $[Ru(NH_3)_6]^{3+/2+}$ redox marker recorded at $BDD\mu E_2$ approach steady state conditions. Redox peaks of inner-sphere marker $[Fe(CN)_6]^{3-/4-}$ were not observed on $BDD\mu E_1$ as a result of the incomplete coverage of tungsten wire. For both electrochemical characterisation regimes higher currents, in the μA range, were recorded for $BDD\mu E_1$, whereas the response for $BDD\mu E_2$ was in the nA range.

4. Conclusions

SEM and Raman characterization showed non-uniform coverage with the appearance of uncoated areas for the first set of BDD microelectrodes ($BDD\mu E_1$), which were held vertically in the deposition chamber. Fully coated BDD microelectrodes, which were held horizontally during deposition, ($BDD\mu E_2$), exhibited a wider potential window, up to +1.6 V in acidic media. We have shown that spectral and electrochemical methods can be used for characterization of BDD microelectrodes as well as for macro BDD electrodes [9, 10].

Acknowledgments

The financial support was provided by Czech Science Foundation (project 17–15319S) and Charles University (SVV 260440, GAUK 1390217).

References

[1] Argun A.A., Banks M.A., Gwendolynne M., Tempelman A.L., Becker F.M., Schuelke T., Dweik M.B.: Highly sensitive detection of urinary cadmium to assess personal exposure. *Anal. Chim. Acta* **773** (2013), 45–51.

[2] Pecková K., Barek J.: Boron doped diamond microelectrodes and microelectrode arrays in organic electrochemistry. *Curr. Org. Chem.* **17** (2011), 3014–3028.

[3] Oyobiki R., Kato T., Katayama M., Sugitani A., Watanabe T., Einaga Y., Matsumoto Y., Horisawa K., Doi N.: Toward high-throughput screening of NAD(P)-dependent oxidoreductases using boron-doped diamond microelectrodes and microfluidic devices. *Anal. Chem.* **86** (2014), 9570–9575.

[4] Arumugam P.U., Zeng H., Siddiqui S., Covey D.P., Carlisle J.A., Garris P.A.: Characterization of ultrananocrystalline diamond microsensors for in vivo dopamine detection. *Appl. Phys. Lett.* **102** (2013), 253107.

[5] Duran B., Brocenschi R.F., France M., Galligan J.J., Swain G.M.: Electrochemical activation of diamond microelectrodes: implications for the in vitro measurement of serotonin in the bowel. *Analyst* **139** (2014), 3160–3166.

[6] Taylor A., Ashcheulov P., Hubík P., Kopeček J., Remeš Z., Vlčková Živcová Z., Remezová M., Kavan L., Scheid E., Lorinčík J., Mortet V.: Precursor gas composition optimisation for large area boron doped nano-crystalline diamond growth by MW-LA-PECVD. *Carbon* **128** (2018), 164–171.

[7] Prawer S., Nemanich R.J.: Raman spectroscopy of diamond and doped diamond. *Philos. Trans. R. Soc. Lond. A* **362** (2004), 2537–2565.

[8] Mortet V., Vlčková Živcová Z., Taylor A., Frank O., Hubík P., Tremouilles D., Jomard F., Barjon J., Kavan L.: Insight into boron-doped diamond Raman spectra characteristic features. *Carbon* **115** (2017), 279–284.

[9] Schwarzová-Pecková K., Vosáhlová J., Barek J., Šloufová I., Pavlova E., Petrák V., Zavázalová J.: Influence of boron content on the morphological, spectral, and electroanalytical characteristics of anodically oxidized boron-doped diamond electrodes. Electrochim. Acta 243 (2017), 170–182.

[10] Vlčková Živcová Z., Frank O., Petrák V., Tarábková H., Vacík J., Nesládek M., Kavan L.: Electrochemistry and in situ Raman spectroelectrochemistry of low and high quality boron doped diamond layers in aqueous electrolyte solution. *Electrochim. Acta* **87** (2013), 518–525.

Study of synthetic oligonucleotides containing guanine by circular dichroism spectroscopy and voltammetry on a pyrolytic graphite electrode

Martina Outlá[a, *], Jan Špaček[b], Daniel Renčiuk[b], Miroslav Fojta[a, b]

[a] *Department of Biochemistry, Faculty of Science, Masaryk University, Kamenice 753/5, 625 00 Brno, Czech Republic* ✉ *394353@mail.muni.cz*
[b] *Institute of Biophysics of the Czech Academy of Science, v.v.i., Královopolská 135, 612 65, Brno, Czech Republic*

Keywords
circular dichroism spectroscopy
guanine
oxidation
voltammetry

Abstract
The possibility to study DNA quadruplex structures using voltammetric analysis of DNA hexamers was investigated using a pyrolytic graphite electrode in an acetate buffer (pH = 5.0). We have tested the influence of the hexamer sequence and DNA concentration their anodic oxidation. To verify the G quadruplex formation, or lack thereof, circular dichroism spectroscopy was used. Our results suggest that, on the pyrolytic graphite electrode, the guanine oxidation signals are not influenced by formation of G the quadruplex. Instead, the shape of the G oxidation multiple peak can be related to the primary structure of the oligonucleotide.

1. Introduction

Guanine rich strands of DNA which are naturally occurring in telomeres and promoter regions of some genes can undergo structural changes to form non-canonical DNA structure, namely G-quadruplexes, based on the environment including presence and kind of cations, pH, temperature, etc. [1, 2]. In G-quadruplexes there are four guanines assembled by Hoogsteen hydrogen bonds to form a guanine tetrad, which is strongly stacked to the other and stabilized by monovalent cations [1, 3, 4].

Electrochemical activity of nucleic acids has been known since the second half of the 1950s [5] and its anodic oxidation, as well as capability of strong and irreversible adsorption at carbon electrodes, was for the first time demonstrated in 1978 [6, 7]. The electrochemical behaviour of DNA is influenced by its structure because alternative secondary structures (such as G-quadruplex) or higher-order structures affect accessibility of the nucleobases, representing the redox-active moieties in the nucleic acids, to the electrode surface [8, 9] .

In this work we have studied influence of the primary and secondary structure of hexadeoxynucleotides dTGGGGT, dTG(8oxoG)GGT on their electrochemical behaviour using basal plane oriented pyrolytic graphite electrode. Our results suggest that the formation of G-quadruplex has no appreciable effect on anodic oxidation of guanine residues at a pyrolytic graphite electrode in aqueous solution. The only variables, which influenced the shape of multiple guanine oxidation peaks, were oligonucleotide concentrations on the electrode surface and particularly the sequence of the studied oligonucleotide.

2. Experimental

2.1 Reagents and chemicals

Oligodeoxynucleotides were purchased from Generi Biotech (Czech Republic). These were prior analysis thermally denatured (5 min at 90 °C) in 0.1 M sodium phosphate buffer (pH = 7.0). After that, potassium chloride was added to final concentration 0.2 M. Other chemicals were of analytical grade.

2.2 Circular dichroism spectroscopy

Circular dichroism measurements were performed by a JASCO J-815 zircular dichroism Spectrometer in 1 cm quartz Hellma cells placed in a thermostated holder (samples were preserved in that cells during whole experiments at laboratory temperature). Measurements were done from 210 nm to 330 nm with 4 accumulations in continual scan mode. The scan rate was 100 nm/min. Precise DNA concentrations were determined based on UV absorption at 260 nm measured in 0.1 M sodium phosphate buffer (pH = 7.0) at 90 °C and set to 70 μM nucleoside which corresponds to 20 ng μl^{-1}. Circular dichroism signals are expressed as the difference in the molar absorption ($\Delta\varepsilon$) of the left- and right-handed circularly polarized light (the molarity was related to nucleosides).

2.3 Linear sweep voltammetry

Voltammetric measurements were performed by a potenciostat PGSTAT302N (Methrom-Autolab) in 0.2 M sodium acetate buffer (pH = 5) using adsorptive transfer stripping linear sweep voltammetry using basal plane oriented pyrolytic graphite electrode as working electrode (DNA was adsorbed at freshly renewed surface of pyrolytic graphite electrode from 3 μl aliquot for 60 s, rinsed and measured in basic electrolyte).

A three electrode system with Ag/AgCl/3 M KCl reference electrode, with platinum wire counter electrode was used in all measurements.

Before each measurement the pyrolytic graphite electrode was pretreated by cycling potential between +2V and –2V, to remove/inactivate any adsorbed

residues, followed by electrode surface renewing by cleaving the surface using adhesion tape (Tesa).

3. Results and discussion

Guanine is the most easily oxidized canonical nucleobase which provides oxidation peak G^{ox} at about +1 V [6, 10]. It has been shown that under specific conditions guanine, as monomer [11] or in an oligonucleotide [12, 13] provides multiple oxidation peaks [13]. The origin of these signals has been attributed to involvement of radical intermediates of the guanine oxidation, undergoing oligo- or polymerization of these species [11, 14] . Alternative explanation for existence of the second oxidation peak has been attributed to the formation of G-quadruplex with mechanism based on worse accessibility of guanine oxidation sites in the quadruplex structure to the electrode surface [12]. In our studies we have observed formation of multiple signals in the region of peak G^{ox} using various G-containing oligonucleotides, which nevertheless did not form G-quadruplex. We thus decided to test if the above described mechanisms of worse guanine accessibility to the electrode surface can be generally applied to the secondary signals of guanine oxidation in dTGGGGT sequence [12]. As a control, we have chosen an oligonucleotide dTG(8-oxoG)GGT. In a G-quadruplex, guanines are forming tetrad through Hoogsteen bonding, in which N7 is an acceptor of hydrogen bond donated by amino group at C2 of neighbouring guanidine. However, N7 in 8-oxoG bears hydrogen atom and consequently it does not act as a hydrogen bond acceptor, which disfavours formation of the quadruplex structure in dTG(8-oxoG)GGT [15]. Since it is hypothesized that guanidine oxidation proceeds through 8-oxoG as an intermediate, presence of 8-oxoG in the control oligonucleotide should not cause major differences in the electrochemistry, compared to dTGGGGT oligonucleotide.

Due to the existence of characteristic circular dichroism spectrum for each G-quadruplex type, the circular dichroism spectroscopy is unique method for studying the G-quadruplex folding. Figure 1 shows circular dichroism spectra of dTGGGGT and dTG(8-oxoG)GGT measured in 0.1 M sodium phosphate buffer pH = 7.0 with 0.2 M potassium chloride measured immediately and 28 days after the salt addition to allow formation of the G-quadruplex. The spectrum of dTGGGGT, which was measured immediately after addition of potassium chloride, contained positive circular dichroism band at 255 nm and negative bands at 234 nm and 275 nm, The height of the positive band increased in time. Furthermore, we observed shifting of the maximum up to 265 nm and the first negative band shifted to 242 nm and the second negative band diminished. Such behaviour is characteristic for the parallel G-quadruplex. In contrast, with dTG(8-oxoG)GGT there were no significant spectral changes occurring within the 28 days after potassium addition (Fig. 1). Hence, under the same conditions under which dTGGGGT formed tetramolecular parallel quadruplex, dTG(8-oxoG)GGT did not.

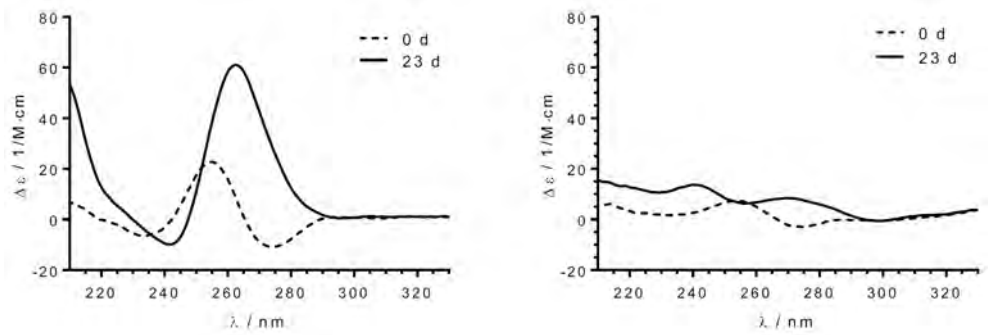

Fig. 1 Circular dichroism spectra of dTGGGGT on the left and dTG(8-oxoG)GGT on the right in 0.1 M phosphate buffer pH = 7.0 measured in 1 cm cells at 20 °C. Circular dichroism spectra were measured immediately (dashed line) and 23 days (full line) after addition of KCl.

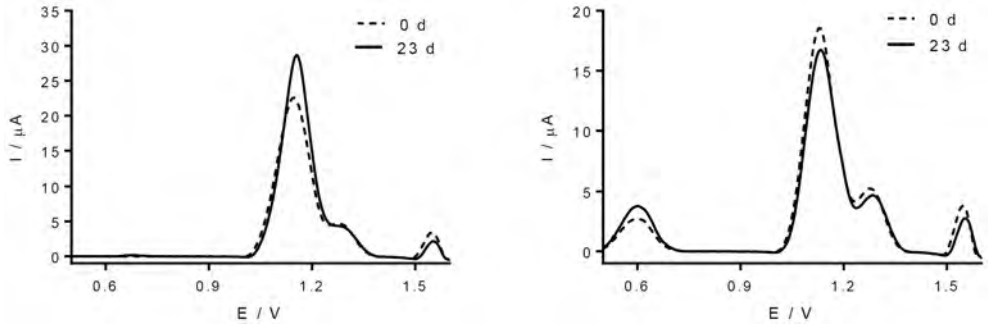

Fig. 2 Baseline corrected LSV voltammograms of dTGGGGT on the left and dTG(8-oxoG)GGT on the right in 0.2 M KCl measured in 0.2 M acetate buffer pH = 5.0 after preincubation in 0.2 M KCl for 0 days (dashed line) and 23 days (full line). Concentration of oligodeoxynucleotide during adsorption to pyrolytic graphite electrode was 20 ng μl^{-1}. DNA concentration during preincubation was 20 ng μl^{-1}.

The same samples, which were analysed using circular dichroism spectroscopy, were analysed in parallel by means of electrochemistry. Two separate peaks Gox were observed for both dTGGGGT and dTG(8-oxoG)GGT; the first at 1.15 V and the second one at 1.28 V (the third peak at 1.55 V corresponds to oxidation of thymine residues present in the oligonucleotides. The peak G^{ox} signal of dTG(8-oxoG)GGT was smaller than analogous signal of dTGGGGT, reflecting lower number of guanidine residues in the former. In addition, a peak at +0.6 V was detected, which corresponds to oxidation of 8-oxoG. Importantly, there were no significant differences observed in the shape of peak G^{ox} peaks on the LSV voltammograms (a) when comparing the two studied sequences dTGGGGT and dTG(8-oxoG)GGT under the same conditions, as well as (b) when comparing voltammograms recorded after different times after the salt addition in any of the sequences (Fig. 2). Thus, these results strongly suggest that on the surface of pyrolytic graphite electrode, the secondary (more positive) peak G^{ox} cannot be ascribed to the formation of G-quadruplex.

4. Conclusions

We have shown that there is no observable effect of the of G-quadruplex formation on anodic oxidation of guanine residues in oligodeoxynucleotides at pyrolytic graphite electrode in aqueous environment. The absence of the effect could be contributed to melting of the quadruplex structure on the surface of the pyrolytic graphite electrode, although this explanation is unlikely, since there has been observed G-quadruplex structures on highly oriented pyrolytic graphite using atomic force microscopy [12]. The presence of secondary peaks due to guanine oxidation in all studied sequences shows that this phenomenon cannot be ascribed to a worse accessibility of the guanine to the electrode surface due to Gq formation, but is much more likely caused by guanidine radical intra-chain oligomerization with neighbouring bases depending on the nucleotide sequence.

Acknowledgments

This research has been supported by a Czech Science Foundation project reg. no. 16-01625S and by the SYMBIT project reg. no. CZ.02.1.01./0.0/0.0/15_003/0000477 financed from the ERDF.

References

[1] Sen D., Gilbert W.: Formation of parallel four-stranded complexes by guanine-rich motifs in DNA and its implications for meiosis. *Nature* **334** (1988), 364–366.
[2] Phan A.T., Mergny J.L.: Human telomeric DNA: G-quadruplex, i-motif and watson-crick double helix. *Nucleic Acids Res.* **30** (2002), 4618–4625.
[3] Phillips K., Dauter Z., Murchie A.I.H., Lilley D.M.J., Luisi B.: The crystal structure of a parallel-stranded guanine tetraplex at 0.95 angstrom resolution. *J. Mol. Biol.* **273** (1997), 171–182.
[4] Lane A.N., Chaires J.B., Gray R.D, Trent J.O.: Stability and kinetics of G-quadruplex structures. *Nucleic Acids Res.* **36** (2008), 5482–5515.
[5] Palecek E.: Oszillographische Polarographie Der Nucleinsauren Und Ihrer Bestandteile. *Naturwissenschaften* **45** (1958), 186–187.
[6] Brabec V., Dryhurst G.: Electrochemical behavior of natural and biosynthetic polynucleotides at pyrolytic-graphite electrode a new probe for studies of polynucleotide structure and reactions. *J. Electroanal. Chem.* **89** (1978), 161–173.
[7] Brabec V., Dryhurst G.: Electrochemical oxidation of polyadenylic-acid at graphite electrodes. *J. Electroanal. Chem.* **91** (1978), 219–229.
[8] Palecek E., Bartosik M.: Electrochemistry of nucleic acids. *Chem. Rev.* **112** (2012), 3427–3481.
[9] Fojta M., Bowater R.P., Stankova V., Havran L., Lilley D.M.J., Palecek E.: Two superhelix density-dependent DNA transitions detected by changes in DNA adsorption/desorption behavior. *Biochemistry* **37** (1998), 4853–4862.
[10] Dryhurst G., Pace G.F.: Electrochemical oxidation of guanine at pyrolytic graphite electrode. *J. Electrochem. Soc.* **117** (1970), 1259–1264.
[11] Subramanian P., Dryhurst G.: Electrochemical oxidation of guanosine-formation of some novel guanine oligonucleosides. *J. Electroanal. Chem.* **224** (1987), 137–162.
[12] Pontinha A.D.R., Chiorcea-Paquim A.M., Eritja R., Oliveira-Brett A.M.: Quadruplex nanostructures of d(TGGGGT): Influence of sodium and potassium ions. *Anal. Chem.* **86** (2014), 5851–5857.
[13] Spacek J., Danhel A., Hason S., Fojta M.: Label-free detection of canonical DNA bases, uracil and 5-methylcytosine in DNA oligonucleotides using linear sweep voltammetry at a pyrolytic graphite electrode. *Electrochem. Com.* **82** (2017), 34–38.

[14] Li Q., Batchelor-McAuley C., Compton R.G.: Electrochemical oxidation of guanine: Electrode reaction mechanism and tailoring carbon electrode surfaces to switch between adsorptive and diffusional responses. *J. Phys. Chem. B* **114** (2010), 7423–7428.
[15] Fleming A.M., Burrows C.J.: G-Quadruplexes folds of the human telomere sequence alter the site reactivity and reaction pathway of guanine oxidation compared to duplex DNA. *Chem. Res. Tox.* **26** (2013), 593–607.

Continuous monitoring of anthraquinone-based anticancer drugs by amperometric technique

Štěpánka Skalová[a, b, *], Jan Fischer[a], Jiří Barek[a], Tomáš Navrátil[b], Jan Krejčí[c], Radka Kučerová[c], Vlastimil Vyskočil[a]

[a] *UNESCO Laboratory of Environmental Electrochemistry, Department of Analytical Chemistry, Faculty of Science, Charles University, Hlavova 8, 128 43, Prague 2, Czech Republic*
✉ *stepanka.skalova@natur.cuni.cz*
[b] *J. Heyrovský Institute of Physical Chemistry of the Czech Academy of Sciences, Dolejškova 3, 182 23, Prague 8, Czech Republic*
[c] *BVT Technologies, s.r.o., Hudcova 78c, 612 00, Brno, Czech Republic*

Keywords
amperometric detection
anthracyclines
anthraquinone-2-sulphonate
dual glassy carbon electrode
liquid-flow system

Abstract
This contribution is focused on the development of electroanalytical methods for the monitoring of anthraquinone-based anticancer drugs in physiological solution by combination of liquid-flow system and dialysis catheter, possibly inserted into blood circulation of patients. For this purpose, amperometric detection with dual glassy carbon electrode was developed and derivate of these drugs, anthraquinone-2-sulphonate, was used as a model compound. Two different flow rates of carrier solution (physiological solution) were tested (specifically, 1 and 5 μL min^{-1}) and the dependence of peak currents of anthraquinone-2-sulphonate on its concentration was verified

1. Introduction

Anthraquinone-based anticancer drugs (e.g., Doxorubicin, Daunorubicin, Zorubicin and Epirubicin) are widely used for treatment of different cancer types, such as leukaemia and solid tumours. However, effectiveness of these drugs is limited by various factors (adverse drug effects – main cytotoxicity, fixed doses or drug resistance). There are few ideas how to improve the treatment by these drugs and therapeutic drug monitoring is one of them as it can provide a powerful tool for assessing accurate dosages, which could potentially lead to the decreased cytotoxicity and to the increased effectiveness of treatment [1, 2].

For the development of such monitoring method, amperometric detection with a dual glassy carbon electrode (dualGCE) and anthraquinone-2-sulphonate as a model compound were used (Fig. 1). Anthraquinone-2-sulphonate is an easily available derivate of anthraquinone-based anticancer drugs containing anthraquinone moiety, which is electrochemically active. In addition, use of physiological

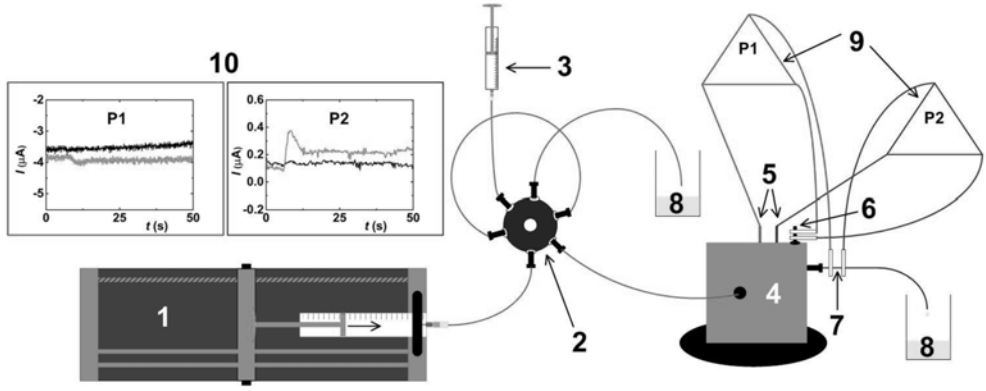

Fig. 1 Scheme of the measuring system consisting of: (1) injection pump with carrier solution (i.e, physiological solution), (2) 6/2-way valve, (3) syringe with sample, (4) electrochemical cell, (5) connections of working electrodes (dualGCE), (6) connection of reference electrode, (7) auxiliary electrode, (8) waste, (9) potentiostats P1 and P2, (10) amperometric signals (E(P1) = −800 mV, E(P2) = −400 mV; flow rate 500 μL min^{-1}; c(anthraquinone-2-sulphonate) = 1×10^{-5} mol L^{-1}), grey colour corresponds to physiological solution with a sample, black colour shows baseline.

solution (physiological solution, 154 mmol L^{-1} NaCl) as a carried solution was required.

2. Experimental

2.1 Reagents and chemicals

Physiological solution (physiological solution, 154 mmol L^{-1} NaCl) was prepared by dissolving of NaCl (Sigma-Aldrich) in deionized water (Millipore Mili plus Q system, USA) with resistance of not less than 18.2 MΩ). Subsequently, a weighted amount of anthraquinone-2-sulphonate (c = 1×10^{-3} mol L^{-1}, Merck, Germany) was dissolved in physiological solution. All solutions were stored in glass bottles in dark at laboratory temperature. The stability of anthraquinone-2-sulphonate in physiological solution was monitored for one month by UV/VIS spectrophotometry with no-changing value of absorbance.

2.2 Instrumentation

The used flow system (Fig. 1) consisted of a syringe pump (SyringePump NO. NE-510L, USA), an electrochemical cell (BASI®, USA) – with dualGCE working electrode, Ag/AgCl (3 mol L^{-1} KCl) reference electrode and a stainless capillary at the end of the cell as an auxiliary electrode. Measurements were carried out by PalmSens potentiostat/galvanostat (PalmSens, The Netherlands) equipped with a PSTrace software (version 4.2.2). The amperometric detection was performed under these conditions: flow rate of 5 μL min^{-1}, potential of GCE1

E(GCE1) = −1200 mV, potential of GCE2 E(GCE2) = −900 mV, syringe volume of 5 mL, and sample loop volume of 10 µL.

The dialysis apparatus consisted of a dialysis catheter (ProbeScientific, UK) inserted into the glass tube with a sample, and connected to a syringe pump (SyringePump NE-510L, USA). Flow rates of 1 and 5 µL min^{-1} were tested.

All measurements were carried out at laboratory temperature.

3. Results and discussion

Amperometric detection of anthraquinone-2-sulphonate in liquid-flow system was found to be a suitable technique for the determination of anthraquinone-2-sulphonate in the arrangement showed in the Fig. 1. pH of a carrier solution was not optimised due to the predetermined physiological solution composition. However, potentials of both GCEs of dual GCE had to be optimized. The best results in the terms of highest peak currents were obtained when following potentials were applied: E(GCE1) = −1200 mV and E(GCE) = −900 mV. Further, thickness (380 µm, 127 µm, and 51 µm) of Teflon cell gasket, inserted between dualGCE and a body of used electrochemical cell, and arrangement of auxiliary electrode were thoroughly studied. For further measurements, thickness of Teflon cell gasket of 127 µm and auxiliary electrode, a stainless capillary at the end of the body of electrochemical cell ended by rubber tube were found to be optimal. Calibration dependence was linear in the concentration range from 1×10^{-5} to 1×10^{-3} mol L^{-1} and the calculated limit of detection was 15 µmol L^{-1}.

Furthermore, use of dialysis catheter ended by dialysis membrane was tested. The recovery of dialysis process was investigated for two flow rates (1 and 5 µL min^{-1}). The recovery was circa 54% and 20% for the flow rates of 1 µL min^{-1} and 5 µL min^{-1}, respectively, in the range of concentrations from 1×10^{-3} to 1×10^{-5} mol L^{-1}.

4. Conclusions

In this research, we have verified the possibility of using dialysis catheter for dialysis of anthracycline-based anticancer drugs and its possible connection with amperometry in liquid-flow system. Amperometric detection was performed by employing dualGCE. As a carrier solution, physiological solution was used because of the potential future application of the developed method in hospitals. The concentration dependence was linear in the range from 1×10^{-3} to 1×10^{-5} mol L^{-1} with limit of detection of 15 µmol L^{-1} and dialysis recovery was approximately 20% for the higher flow rate of 5 µL min^{-1}.

Acknowledgments

This research was carried out within the framework of Specific University Research (SVV 260440). Š.S. thanks to the Grant Agency of Charles University (Project No. 243-250753) and the Czech

Science Foundation (GACR project No. 17-05387S), and T.N., J.B. and J.F. thank the Czech Science Foundation (GACR project No. 17-03868S) for providing financial support.

References

[1] Decosterd L.A., Widmer N., Zaman K., Cardoso E., Buclin T., Csajka Ch.: Therapeutic drug monitoring of targeted anticancer therapy. *Biomark. Med.* **9** (2015), 887–893.

[2] Herviou P., Thivat E., Richard D., Roche L., Dohou J., Pouget M., Eschalier A., Durando X., Authier N.: Therapeutic drug monitoring and tyrosine kinase inhibitors. *Oncol. Lett.* **12** (2016), 1223–1232.

Electrochemical characteristic of a novel bi-disc glassy carbon electrode

Justyna Lipińska*, Radosław Porada, Katarzyna Jedlińska, Bogusław Baś

Department of Analytical Chemistry, Faculty of Materials Science and Ceramics, AGH University of Science and Technology, A. Mickiewicza 30, 30-059 Kraków, Poland ✉ *justyna.lipinska@agh.edu.pl*

Keywords
cyclic voltammetry
electrochemical impedance spectroscopy
glassy carbon electrode
sensors

Abstract
This work deals with electrochemical characteristic of a novel type of the working electrode bi-disc glassy carbon electrode. The designed innovative electrode consists of two glassy carbon discs (d = 1.0 mm) placed symmetrically on the lateral surface on the silver rod which is covered with epoxy resin. Electrochemical characterization of the prepared electrode was made in the work. For this purpose, electrochemical impedance spectroscopy and cyclic voltammetry studies were performed. The results obtained during the characterization of the electrode were consistent with the reversible theory of reaction.

1. Introduction

One of the main trends of modern analytics is the search for new electrode materials and various geometries of working electrodes. The widely used group of materials for the construction of electrodes using electrochemistry is carbon materials. These materials are characterized by a wide window of useful potentials and chemical inertness. Particularly noteworthy is glassy carbon, which exhibits attractive physicochemical properties, thanks to which it has become one of the most frequently used electrode materials in voltammetry. The main advantages of the glassy carbon include: low price, no toxicity, good mechanical and electrical properties, a wide range of potential, high current density and low and stable background current [1–3].

Electrochemical impedance spectroscopy is an effective technique to study the properties of chemically modified electrodes and to understand the rate of electrochemical reactions, structure of electrical double layer and diffusive transport of the electroactive species. In this technique, the system's response to a sinusoidal disorder of small amplitude and different frequency is examined [1]. Cyclic voltammetry is the most commonly used technique used to obtain qualitative information about electrochemical reactions. The popularity of this technique stems from its ability to quickly provide information on the thermodynamics and kinetics of the redox processes of heterogeneous electron transfer reaction and the conjugated chemical reaction or adsorption processes [1, 4].

The aim of the work was to perform the electrochemical characteristics of a novel bi-disc glassy carbon electrode. For this purpose, cyclic voltammetry and electrochemical impedance spectroscopy measurements were made.

2. Experimental

2.1 Reagents and chemicals

The reagents, all of which were analytical reagent grade, were used: potassium chloride (POCH, Poland), potassium ferricyanide (POCH, Poland), MicroPolish Alumina 0.5 µm (Buechler, USA), distilled water.

2.2 Instrumentation

All voltammetric measurements were performed with the M161 electrochemical analyzer connected to the M164 electrodes stand (both mtm-anko, Poland) and equipped with software EALab 2.1.

Electrochemical impedance spectroscopy measurements were made with µAutolab III (EcoChemie, The Netherlands) with the FRA2 (Frequency Response Analyzer) module controlled by the Nova 2.0 Software in combination with the M164 electrode stand. The measurements were carried out in a three-electrode system containing: a working electrode, a reference electrode: silver chloride electrode (Ag/AgCl/3 mol L^{-1} KCl/2.5 mol L^{-1} KNO_3) and an auxiliary electrode: platinum wire.

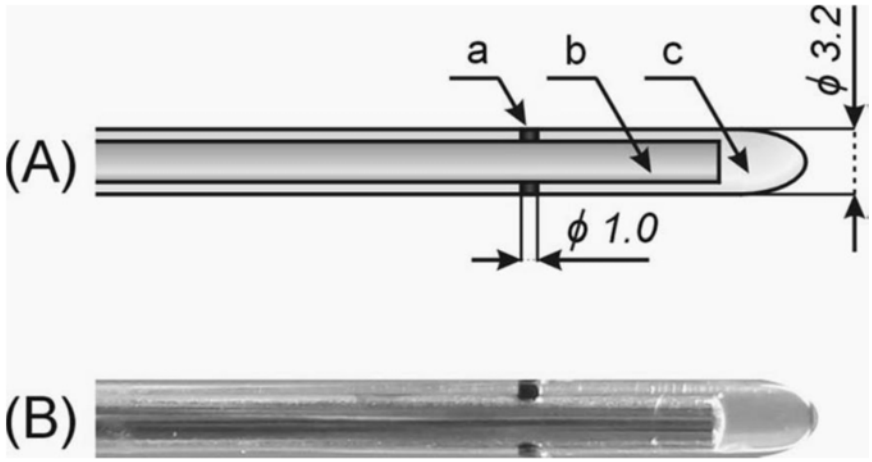

Fig. 1 Construction of the bi-disc glassy carbon electrode. (A) The electrode construction scheme: (a) a glassy carbon rod (d = 1.0 mm), (b) a silver rod (d = 2.5 mm), (c) epoxy resin. (B) Photography of the sensor [5].

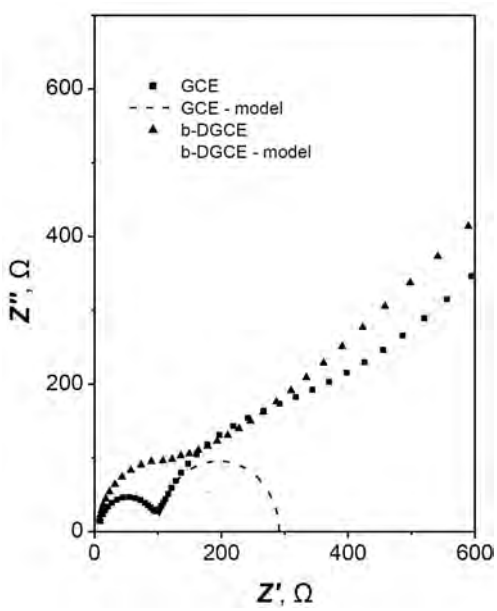

Fig. 2 Electrochemical impedance spectra: frequency range from 10 kHz to 10 mHz, applied sinusoidal signal of 10 mV amplitude at an open circuit potential.

2.3 Construction of bi-disc glassy carbon electrode

The proposed electrode is characterized by an easy and simple construction. The construction of the presented electrode is shown in Fig. 1. The bi-disc glassy carbon electrode was prepared from a glassy carbon rod of a diameter 1.0 mm (Alfa Aesar, Germany), silver rod of a diammeter 2.5 mm (Mint of Poland, Poland), and epoxy resin TRANSLUX D180 (AKSON, France) [5].

3. Results and discussion

The electrochemical properties of the prepared bi-disc glassy carbon electrode were examined by electrochemical impedance spectroscopy in an environment of 0.001 mol L^{-1} $[Fe(CN)_6]^{3-/4-}$ with 0.1 mol L^{-1} KCl. The experiments were carried out in the frequency range from 10 kHz to 10 mHz with a sinusoidal signal of 10 mV amplitude at the open circuit potential. Results obtained on the homemade bi-disc glassy carbon electrode were compared with commercially available glassy carbon electrode. To receive quantitative information about response of tested electrodes, the Randles equivalent circuit was adjust to the Nyquist plot (Fig. 2). The Randles model is presented Fig. 3. It consists of solution resistance, which is connected to a double-layer capacity expressed by a constant phase element parallel to the charge transfer resistance and Warburg impedance associated with diffusion of reagents.

In case of bi-disc glassy carbon electrode for the high and medium values of frequency a single, squeezed semicircle, associated with the charge transfer resistance of redox couple $[Fe(CN)_6]^{3-/4-}$ and the double layer capacity, was

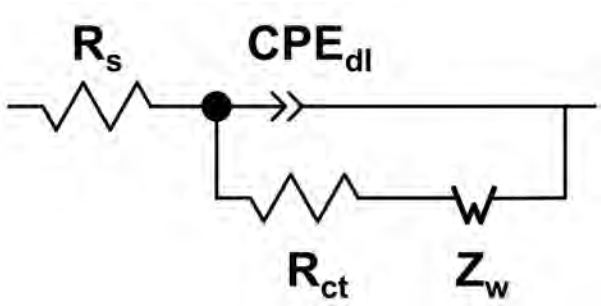

Fig. 3 The Randles equivalent circuit, where (R_s) solution resistance, (CPE_{dl}) constant phase element, (R_{ct}) the charge transfer resistance and (Z_w) Warburg impedance.

registered. The charge transfer resistance had a comparatively low value of 190 Ω, indicating the fast electron transfer through the bi-disc glassy carbon electrode–electrolyte boundary. For the commercially available glassy carbon electrode two semicircles were registered. The one on the right corresponded to the effects of electrical double layer and charge transfer, whose resistance was equaled to 187 Ω. The value of charge transfer resistance is inversely proportional to the product of electrode surface and rate constant of heterogenic reaction. Thus, although the charge transfer resistance is comparable for both electrodes, due to the smaller surface of bi-disc glassy carbon electrode its rate constant is bigger than that of commercial glassy carbon electrode. The inhibition of the charge transfer on the glassy carbon electrode could have been caused by an additional conductive layer on the electrode surface, whose resistance and capacitance can be determined from the semicircle on the left side of the Nyquist plot. In the low frequency range a straight line corresponding to the diffusion of the depolarizer was recorded for both tested electrodes. Based on the obtained results, it can be concluded that bi-disc glassy carbon electrode is characterized by faster and favorable electron transfer kinetics; therefore the studied reactions are more prone to be reversible.

In the next stage of the bi-disc glassy carbon electrode characteristic, a series of cyclic voltammetry measurements was carried out with different scan rates in the range from 0.025 to 1.0 V s^{-1}. Figure 4 shows the recorded voltammograms in a system containing 0.001 mol L^{-1} $[Fe(CN)_6]^{3-/4-}$ with 0.1 mol L^{-1} KCl. The presented voltammograms show well-shaped peaks in both directions (anodic and cathodic). The relationship between anodic and cathodic peak current and square root of scan rate was linear (Fig. 5). The electrochemical active surface area was calculated using the Randles-Sevcik equation

$$I_p = 0.4463 \left(\frac{F^3}{RT}\right)^{1/2} An^{3/2} D^{1/2} c_0 v^{1/2} \quad (1)$$

where I_p is peak current (A), $\boldsymbol{F}$ is Faraday constant (96 485 C mol^{-1}), $\boldsymbol{R}$ is the universal gas constant (8.314 J $mol^{-1}K^{-1}$), T is the absolute temperature (298 K),

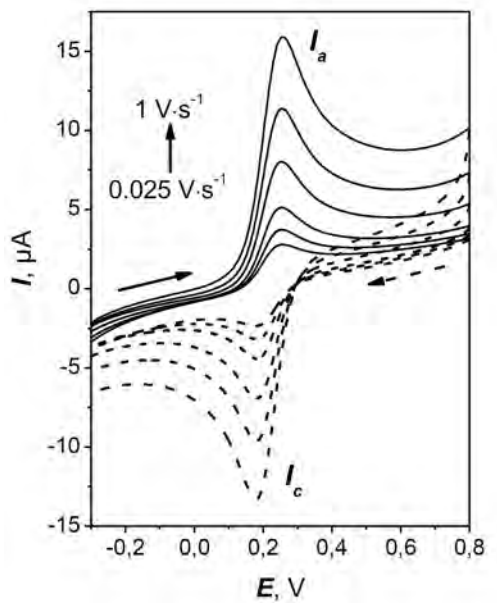

Fig. 4 Cyclic voltammograms of 0.001 mol L^{-1} $[Fe(CN)_6]^{3-/4-}$ with 0.1 mol L^{-1} KCl at bi-disc glassy carbon electrode (scan rate from 0.025 to 1.000 V s^{-1}).

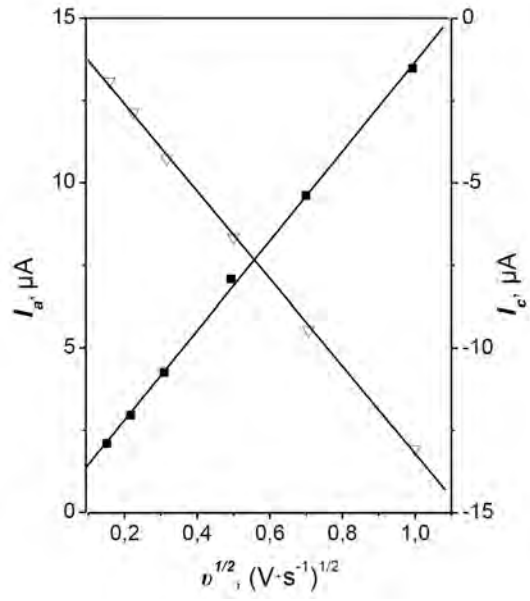

Fig. 5 Dependence between anodic peak current (■, $y = -0.429\,x - 0.003$, $r = 0.9995$) and cathodic peak current (∇, $y = -0.419\,x - 0.044$, $r = 0.9996$) and square root of the scan rates.

A is the electrode surface area (cm^2), n is the number of electrons involved in the redox reaction (for $[Fe(CN)_6]^{3-/4-}$ equal 1), D is diffusion coefficient of 7.2×10^{-6} cm^2s^{-1}, c_0 is the concentration of $K_3[Fe(CN)_6]$ (1.0×10^{-3} mol L^{-1}), and v is scan rate (V s^{-1}). In accordance with the obtained results the electroactive surface area was calculated. The values of 0.0185 cm^2 (based on anodic scan) and 0.0178 cm^2 (based on cathodic scan) was obtained while the geometric surface of the electrode was 0.0157 cm^2.

4. Conclusions

In the paper, a novel electrochemical sensor: bi-disc glassy carbon electrode was presented. The designed electrode is characterized by a unique construction, placement of working surfaces on the sides of the sensor. The advantages of the presented electrode are: simplicity of construction and easy surface preparation before measurements. The results of electrochemical impedance spectroscopy and cyclic voltammetry experiment shown that bi-disc glassy carbon electrode exhibits properties consistent with the theory of the reversible electrode processes. The proposed bi-disc glassy carbon electrode is fully compatible with the principles of green chemistry. The presented sensor ensures stable signals and can be used for voltammetric measurements in various environments.

Acknowledgments

JL and RP have been partly supported by the EU Project POWR.03.02-00-00-I004/16.

References

[1] Wang J.: *Analytical Electrochemistry.* 3rd ed. New York, Wiley-VCH 2006.
[2] Dekanski A., Stevanović J., Stevanović R., Nikolić B. Z., Jovanović V. M.: Glassy carbon electrodes: I. Characterization and electrochemical activation. *Carbon* **39** (2001), 1195–1205.
[3] Trouillon R., O'Hare D.: Comparison of glassy carbon and boron doped diamond electrodes: Resistance of biofouling. *Electrochim. Acta* **55** (2010), 6586–6595.
[4] Kisza A.: *Elektrochemia II. Elektrodyka*, Warszawa, Wyd. Naukowo-Techniczne 2001. (In Polish.)
[5] Jedlinska K., Lipińska J., Smarzewska S., Baś B.: The bi-disc glassy carbon electrode for determination of vitamin K2 (menaquinone) using stripping voltammetry. *J. Electrochem. Soc.* **166** (2019), 360–366.

Status quo of the arctic wastewater recipient – environment modification by chemical compounds including selected heavy metals (Longyearbyen, Svalbard)

Agnieszka Kalinowska[a,*], Małgorzata Szopińska[a], Stanisław Chmiel[b], Magdalena Kończak[b], Żaneta Polkowska[c], Katarzyna Jankowska[a], Aneta Łuczkiewicz[a]

[a] *Department of Water and Wastewater Technology, Faculty of Civil and Environmental Engineering, Gdansk University of Technology, 11/12 Narutowicza St., 80-233 Gdańsk, Poland*
✉ *agnieszka.kalinowska@pg.edu.pl*
[b] *Department of Hydrology and Climatology, Faculty of Earth Sciences and Spatial Management, Maria Curie-Sklodowska University, 2 cd Kraśnicka Ave., 20-718 Lublin, Poland*
[c] *Department of Analytical Chemistry, Faculty of Chemistry, Gdansk University of Technology, 11/12 Narutowicza St., 80-233 Gdańsk, Poland*

Keywords
Arctic contamination
Arctic marine environment
heavy metals
ICP-MS
wastewater discharge

Abstract
The largest human settlement on Svalbard archipelago, Longyearbyen, releases approximately 300 thousands m^3 of untreated wastewater annually to the nearby fiord, Adventfjorden. The environmental impact of this continuous discharge is unknown. For this reason, in this study raw wastewater was collected together with the sea water samples in Adventfjorden. Two surveys were carried out in summer and autumn season 2018, measuring physical, biological and chemical parameters at representative sites. In this study trace elements (V, Cr, Mn, Fe, Co, Ni, Cu, Zn, Hg, As, Cd, Pb, U), pH, electrolytic conductivity, total suspended solids and total organic carbon are reported. Results show that the raw wastewater introduces low concentrations of the heavy metals to the receiver.

1. Introduction

The Svalbard archipelago lays in the High Arctic, between 76.50–80.80 °N and 10–34 °E [1], with population density equal to 0.04/km^2, which places it amongst the most remote and least inhabited places in the world. Nevertheless, dramatic increase of tourism in the past decades contributed to major changes in polar regions, being subjected to climate shifts, atmospheric pollution deposition and other types of anthropogenic influence, including pollution from mining activity or release of untreated wastewater. Therefore a concern raises, whether Arctic can be considered as a pristine area any more. An interest in pollutants pathways and their fate in the Arctic environment are still rising.

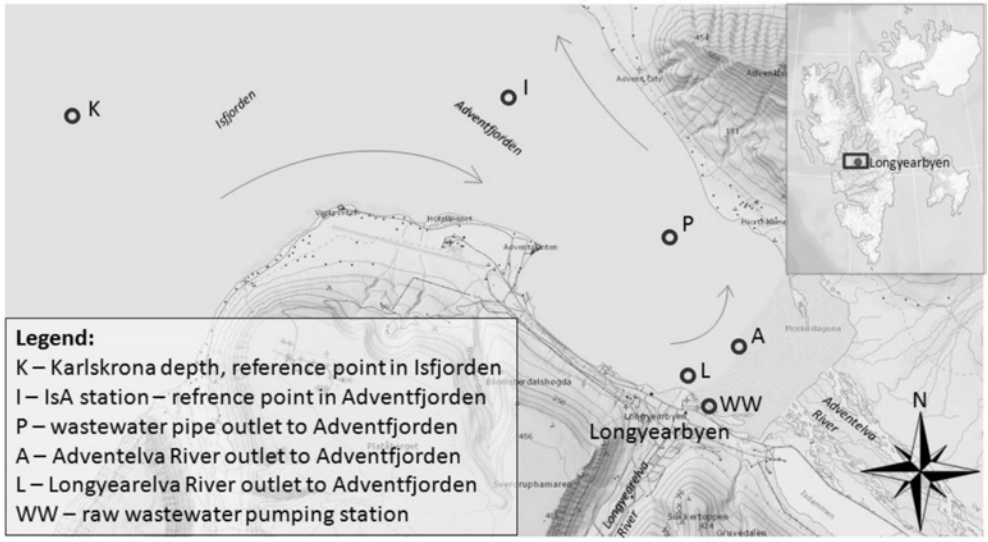

Fig. 1 Location of the study in Adventfjorden, Isfjorden. Circles represent sampling points, arrows represent general water current in Adventfjorden (modified from toposvalbard.no)

Wastewater is usually regarded as the source of excessive supply of nitrogen, phosphorus and organic compounds, as well as human related bacteria, leading to chemical and microbiological degradation of the receiving water body. Despite that, wastewater can contain heavy metals, which not only can have deteriorating effect on the food web, undergoing bioaccumulation and biomagnification in the food chain, but they may act as stress factors at the lower trophic level, inducing resistance among bacterial communities [1–3] and/or inhibit microbiological processes [4]. Considering all the above, the study aims to complete the knowledge about the impact of continuous discharge of raw wastewater on its recipient, Adventfjorden.

2. Experimental

2.1 Study area

The study area covered the central part of West Spitsbergen island (Svalbard archipelago) in the vicinity of the largest settlement on the island, Longyearbyen (Fig. 1). The city discharges untreated wastewater (about 300,000 m^3/yr) to the nearby marine wastewater recipient, Adventfjorden. Samples of raw wastewater were collected together with the marine water samples from Adventfjorden in order to determine (a) the influence of the wastewater on the receiver and (b) the spatial distribution of the pollutants. Importantly, the population of Longyearbyen is growing, similarly to the number of tourist, which has doubled over past 10 years, inevitably resulting in increased amount of the untreated wastewater being released to the fiord.

Adventfjorden is a part of the biggest fjord on the west coast of Spitsbergen, Isfjorden. Its wide and deep mouth facilitates the water exchange with central part of Isfjorden due to tidal pumping and wind-driven surface currents [5]. The fiord receives water from two glacial rivers: Adventelva and Longyearelva, which are the greatest contributors of sediment and freshwater and are fed by atmospheric precipitation, surface runoff, as well as snow and glacier melting. Both rivers carry large amounts of suspended solids (up to 826 mg L^{-1}) [6, 7]. In winter, when the rivers are frozen, water and sediment supply ceases.

Sampling points in Adventfjorden were located in order to reflect the inflow of the wastewater to the fiord (sampling point P, Fig. 1) and the impact of two glacial rivers: Adventelva (sampling point A) and Longyearelva (sampling point L). Also the reference points were sampled: station I (inside Adventfjorden) and K (Karlskrona depth located in the central part of Isfjorden). Untreated wastewater was collected from the pumping station (sampling point WW, Fig. 1).

2.2 Sampling

Samples were collected twice in various seasons: summer (July) and autumn (October) 2018. At the time preceding sampling, average daily temperatures varied around 5–10 °C in July and from –12 °C to to 5 °C in October, which might have had influenced rivers freezing and discharge. Precipitation did not exceed 0.4 mm/week prior to both the sampling campaigns.

Water samples from the recipient were collected at the surface and bottom of the water column by a 10 L Niskin bottle. To minimise the risk of sample contamination samples were collected using nitrile gloves and were rinsed with sampled water three times before filling. Bottles were filled completely without air bubbles. Simultaneously raw wastewater samples were collected. All the samples were kept frozen until further analysis.

2.3 Instrumentation

Total organic carbon concentration was determined by a TOC-VCSH/CSN Analyser (ShimadzU, Japan) using the catalytic combustion method with non-dispersive infrared detection (NDIR). Total suspended solids were determined in duplicates by membrane filtration method. The concentrations of metals in water samples were determined by inductively coupled plasma mass spectrometry, Thermo XSERIES 2 ICP-MS (Inductively Coupled Plasma Mass Spectrometer, Thermo Fischer Scientific, Germany). The trace element concentration coefficients of variation of the obtained triplicate results ranged from 0.5 to 3.0%. The selected validation parameters characterizing the analytical methods used are presented in Table 1.

To detect pair-wise relationships among the metals, total organic carbon and total suspended solids concentration in the investigated water samples, Pearson's

Table 1
Selected validation parameters characterizing the analytical methods used (LOD – limit of detection, LOQ – limit of quantification).

Analyte	Measurement range	*LOD*	*LOQ*	Unit
U, Cd	0.006–1	0.0020	0.0060	μg L^{-1}
Pb	0.01–1	0.0030	0.010	
V, Cr, Mn, Co, Ni, Cu, Zn, As	0.10–10			
	10–1000	0.030	0.10	
Fe	0.60–10			
	10–1000	0.30	0.60	
Total organic carbon	1–200	0.03	0.1	mg L^{-1}

correlation coefficients (r) were calculated using Excel 2010 (Microsoft Office, USA). Statistical significance of correlation coefficients was assessed at a significance level of $p < 0.05$. The statistical significance of correlations was verified using the *t*-Student test.

3. Results and discussion

In July total suspended solids concentration in the recipient was much higher than in October (average 133.63 mg L^{-1} and 6.36 mg L^{-1}, respectively) due to massive river water inflow. The highest values were noted in July in the immediate vicinity of the Adventelva River outlet (up to 835.11 mg L^{-1}). In terms of sediment input in summer, the river seems to impact mainly the surface water in the inner Adventfiorden basin (53.60–62.2 mg L^{-1} in the surface samples from points L and P compared to 16.1–29.5 mg L^{-1} in the bottom layer and 2.47–10.8 mg L^{-1} at outer stations K and I). Fresh water of the river origin stays on the surface of water column due to the higher temperature, lower salinity, and therefore different density than the marine water. Intense stratification of the water column in the summer restricts mixing of different water layers and therefore slows down the vertical migration of pollutants that are not bound to the solid particles and therefore not prone to settling. In October, when the river discharge into the fiord decreases, total suspended solids concentration did not exceed 12 mg L^{-1} (Fig. 2).

Organic matter concentration values (measured as total organic carbon) in wastewater were 40 times higher than in the recipient and equaled to 37.8 mg L^{-1} in October and 40.18 mg L^{-1} in July 2018. Total organic carbon values in Adventfjorden were more uniform in October, oscillating around 0.85±0.06 mg L^{-1}, compared to 0.95±0.28 mg L^{-1} in July (Fig. 2). The highest total organic carbon values were found in July at the mouth of Adventelva river, followed by surface sample at the wastewater discharge pipe (P). In October, the highest total organic carbon was noted at the outlet of Longyearelva (point L). No significant correlation was found between total suspended solids and total organic carbon in

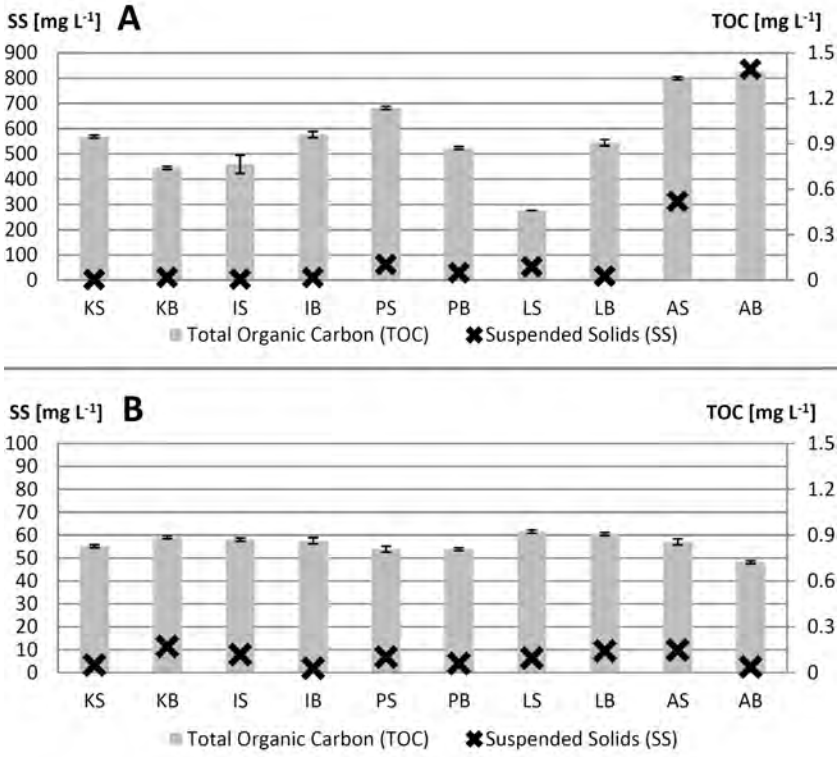

Fig. 2 Total organic carbon and suspended solids concentrations in the recipient in (A) July and (B) October. Labels on the *x*-axis refer to the name of the sampling station (K, I, P, L, A) and the depth: S for surface, B for bottom sample.

October, even though the correlations in July and for the whole set of data were strong (0.69 and 0.71, respectively).

In case of heavy metals, wastewater represented higher concentrations than the recipient in case of almost all the investigated heavy metals, despite U and Cd (Table 2). In domestic wastewater, heavy metals may originate from food, medicines, diet supplements, cosmetics, pigment in paints, metal cookware and pipes [7], toilet paper, sweat and dust [8]. Note, in Longyearbyen food leftovers are milled in sinks and directed to the sewer. This may increase not only the amount of total nitrogen and phosphorus or biological and chemical oxygen demand in wastewater, but also heavy metals concentrations.

In Adventfiorden basin, higher concentrations of heavy metals, particularly Mn, Fe, Co, Ni, Cd and U have been observed in July at the outlet of Adventelva, while at Longyearelva mouth higher Cu, Cr and Zn values were observed. Mean concentrations of V, Fe, Cu, Zn, Cd and Pb in the recipient were higher in October samples. Vanadium was almost two times higher in recipient in October than in July (mean 0.806 μg L^{-1} versus 0.449 μg L^{-1}). Also lead concentrations in marine

Table 2

Heatmap showing the concentrations of heavy metals and total organic carbon (TOC) in the recipient and wastewater (WW) samples. The darker the colour, the higher the concentration. S refers to surface. B to bottom water sample.

	Sample	Concentration/µg L^{-1}												TOC/mg L^{-1}
		V	Cr	Mn	Fe	Co	Ni	Cu	Zn	As	Cd	Pb	U	
August 2018	KS	0.45	0.2	0.95	0.94	0.1	0.39	0.36	1.38	1.46	0.01	<0.10	0.45	0.95
	KB	0.56	0.19	0.22	1.19	0.02	0.22	0.15	0.74	2.00	0.01	<0.10	0.43	0.74
	IS	0.61	0.18	1.59	1.51	0.14	0.36	0.29	1.15	1.62	0.01	<0.10	0.41	0.77
	IB	0.62	0.19	0.28	1.15	0.05	0.62	0.43	1.06	2.01	0.01	<0.10	0.42	0.96
	RS	0.31	0.21	3.88	1.55	0.08	0.56	0.4	0.86	0.98	0.02	<0.10	0.45	1.14
	RB	0.51	0.18	0.14	1.63	0.04	0.47	0.4	1.84	1.63	0.02	<0.10	0.42	0.87
	LS	0.34	0.24	2.81	2.47	0.08	0.36	0.98	3.35	1.01	0.02	<0.10	0.47	0.46
	LB	0.54	0.2	1.15	1.63	0.09	0.4	0.24	0.56	1.57	0.01	<0.10	0.42	0.91
	AS	0.25	0.1	3.47	4.37	0.3	1.01	0.35	0.69	0.42	0.04	<0.10	0.53	1.33
	AB	0.30	0.17	2.89	3.08	0.32	0.82	0.4	0.75	0.54	0.04	<0.10	0.49	1.38
	WW	1.47	1.48	132	282	1.59	12	2.73	12.26	2.55	0.03	1.49	0.10	40.2
October 2018	WW	2.61	1.51	220	170	1.55	13	1.69	3.94	1.57	0.02	0.74	0.12	37.8
	KS	0.69	0.16	0.69	1.21	0.06	0.21	0.24	0.81	1.25	0.02	0.11	0.5	0.83
	KB	0.85	0.22	0.91	1.32	0.03	0.06	0.35	1.86	1.49	0.02	0.11	0.45	0.89
	IS	0.79	0.18	1.07	4.12	0.07	0.26	1.58	2.9	1.29	0.03	0.13	0.44	0.87
	IB	0.88	0.17	0.4	1.74	0.04	0.12	0.17	1.4	1.33	0.02	0.09	0.4	0.86
	RS	0.67	0.15	1.55	2.42	0.07	0.23	0.46	2.01	0.95	0.02	0.11	0.45	0.81
	RB	0.88	0.16	0.41	1.33	0.04	0.37	0.29	1.54	1.14	0.02	0.12	0.46	0.81
	LS	0.78	0.13	0.72	1.73	0.06	0.38	0.4	1.69	1.36	0.01	0.11	0.32	0.92
	LB	0.73	0.40	1.01	4.86	0.06	0.27	0.41	2.21	0.87	0.02	0.10	0.42	0.91
	AS	0.88	0.13	0.78	1.67	0.05	0.18	0.25	1.46	1.09	0.02	0.10	0.42	0.86
	AB	0.91	0.15	0.43	1.78	0.04	0.13	0.17	0.74	1.08	0.03	0.10	0.42	0.72

Table 3
Values of Person correlation coefficient (r) for total concentrations of investigated elements (selected metals nonmetals and total organic carbon concentration). Strong and very strong correlations ($0.6 < |r| \leq 1.0$) are given in bold. Grey background emphasise very strong correlations ($0.8 < |r| \leq 1.0$). Values of Pearson's correlation coefficients in the range ($0.6 < |r| \leq 1.0$) are statistically significant at $p < 0.05$. Abrreviations: TSS – total suspended solids, TOC – total organic carbon.

	V	Cr	Mn	Fe	Co	Ni	Cu	Zn	As	Cd	Pb	U	TOC	TSS
V	1.000													
Cr	**0.832**	1.000												
Mn	**0.896**	**0.958**	1.000											
Fe	**0.721**	**0.955**	**0.870**	1.000										
Co	**0.774**	**0.968**	**0.950**	**0.957**	1.000									
Ni	**0.835**	**0.984**	**0.977**	**0.952**	**0.990**	1.000								
Cu	0.592	**0.833**	**0.744**	**0.876**	**0.827**	**0.820**	1.000							
Zn	0.504	**0.801**	**0.638**	**0.907**	**0.779**	**0.764**	**0.908**	1.000						
As	0.392	0.487	0.384	0.545	0.399	0.453	0.443	0.538	1.000					
Cd	0.006	0.173	0.145	0.273	0.311	0.218	0.349	0.296	−0.430	1.000				
Pb	**0.706**	**0.913**	**0.807**	**0.985**	**0.907**	**0.901**	**0.873**	**0.936**	0.544	0.296	1.000			
U	**−0.841**	**−0.914**	**−0.876**	**−0.897**	**−0.870**	**−0.905**	**−0.758**	**−0.767**	**−0.622**	0.021	**−0.878**	1.000		
TOC	**0.824**	**0.988**	**0.958**	**0.975**	**0.987**	**0.995**	**0.841**	**0.813**	0.494	0.223	**0.937**	**−0.919**	1.000	
TSS	−0.536	−0.154	0.541	0.361	**0.862**	**0.669**	−0.006	−0.270	−0.565	**0.671**	−0.334	0.457	**0.707**	1.000

water were lower in July (below the detection limit) than in October (0,10–0,13 μg L^{-1}). Mercury was below the detection level in all the samples analyzed.

In Adventfiorden, strong ($0.6 < |r| \leq 1.0$) and very strong ($0.8 < |r| \leq 1.0$) correlations have been observed in 67% of the pair-wise correlations between investigated heavy metals, but exclusively when wastewater has been taken into account. In the dataset excluding wastewater samples, strong and very strong correlations were observed in 23% of the pair-wise comparisons and very strong correlations were much less common. This suggests a relation between wastewater discharge and heavy metals concentrations.

Concentration of metals is known to depend on the presence of organic matter [9]. In the whole dataset, very strong correlations with total organic carbon were found for 9 out of 12 analyzed metals (V, Cr, Mn, Fe, Co, Ni, Cu, Zn, Pb) and very strong negative correlation with total organic carbon was found for U (Table 3). However, taking into account data from recipient only, none of metals is very strongly correlated with total organic carbon, and strong correlation was noted for Co and Ni only. All the above suggest that the wastewater is the main contributor of total organic carbon and heavy metals to the recipient, and suspended solids, which are mainly of the glacial river origin, does not contribute strongly to the heavy metals input to the fiord. The influence of the surface runoff or remobilization of heavy metals from the sediments has not however been studied.

4. Conclusions

In terms of heavy metals spatial distribution in the recipient, no clear pattern was found to be common for both summer and autumn season. The concentrations of heavy metals in the recipient at certain stations may by highly influenced by the water masses dynamics in the fiord, oceanic currents, river inflow and mixing. The fiord was noted to be under upwelling conditions in the autumn. In summer season water column is characterized by clear stratification due to the temperature and salinity difference, which restrain mixing and vertical transport of pollutants. Despite that the exact dispersion route of the pollutants is not easy to predict, we conclude that the raw wastewater from Longyearbyen introduces low concentrations of heavy metals in to the Arctic fiord, being its recipient. Further monitoring is recommended, especially taking into account that the release of heavy metals to the Arctic recipient via wastewater may increase in the following years, also due to growing number of visitors and inhabitants.

Acknowledgments

Authors thank the Research Council of Norway and Svalbard Science Forum for research funding for Arctic Field Grant "Influence of wastewater on the bacterioplankton community and its characteristics in Adventfjorden, Svalbard". Authors would also like to express gratitude to Longyearbyen Lokalstyre, (Mrs. Kjersti Olsen Ingerø) and University Centre in Svalbard staff: Arctic Biology Department (Anna Vader, Janne Søreide), Arctic Geophysics (Eva Falck, Ylva Ericson) and Logistics Department for help during the fieldwork campaign and data analysis.

References

[1] Levy S.B., Marshall B.: Antibacterial resistance worldwide: causes, challenges and responses. *Nat. Med.* **10** (2004), S122–S129.

[2] McConnell M:. *Abundance of Antibiotic Resistance Genes in Two Municipal Wastewater Treatment Plants and Receiving Water in Atlantic Canada.* Dalhousie University. Faculty of Graduate Studies. http://hdl.handle.net/10222/72778

[3] Rizzo L., Manaia C., Merlin C., Schwartz T., Dagot C., Ploy M.C., Michael I., Fatta-Kassinos D.: Urban wastewater treatment plants as hotspots for antibiotic resistant bacteria and genes spread into the environment: A review. *Sci. Tot. Envirom.* **447**, (2013), 345–360.

[4] Sandrin T.R., Maier R.M.: Impact of metals on the biodegradation of organic pollutants. *Environ. Health Persp.* **111** (2003), 1093–1101.

[5] Pawłowska J., Włodarska-Kowalczuk M., Zajączkowski M., Nygård H., Berge J.: Seasonal variability of meio-and macrobenthic standing stocks and diversity in an Arctic fjord (Adventfjorden, Spitsbergen). *Polar Biol.* **34** (2011), 833–845.

[6] Zajączkowski M., Włodarska-Kowalczuk M.: Dynamic sedimentary environments of an Arctic glacier-fed river estuary (Adventfjorden, Svalbard). I. Flux, deposition, and sediment dynamics. *Estuarine, Coastal Shelf Sci.* **74** (2007), 285–296.

[7] Szymańska N., Pawłowska J., Kucharska M., Kujawa A., Łącka M., Zajączkowski M.: Impact of shelf-transformed waters (STW) on foraminiferal assemblages in the outwash and glacial fjords of Adventfjorden and Hornsund, Svalbard. *Oceanologia* **59** (2017), 525–540.

[8] Moriyama K., Mori T., Arayashiki H., Saitot H., Chino M.: The amount of heavy metals derived from domestic wastewater. In: *Water Pollution Research and Control Brighton. Proceedings of the Fourteenth Biennial Conference of the International Association on Water Pollution Research and Control*. Brighton 1988, p. 1913–1916. DOI: 10.1016/B978-1-4832-8439-2.50219-4

[9] Szopińska M., Szumińska D., Bialik R.J., Chmiel S., Plenzler J., Polkowska Ż.: Impact of a newly-formed periglacial environment and other factors on fresh water chemistry at the western shore of Admiralty Bay in the summer of 2016 (King George Island, Maritime Antarctica). *Sci. Total Environ.* **613** (2018), 619–634.

Effect of metal sensitizers on photochemical vapor generation of bismuth for analytical atomic spectrometry

JAROMÍR VYHNANOVSKÝ[a, b, *], DILEK YILDIZ[c], STANISLAV MUSIL[a]

[a] *Department of Trace Element Analysis, Institute of Analytical Chemistry of the Czech Academy of Sciences, Veveří 97, 602 00 Brno, Czech Republic* ✉ *jaromir.vyhnanovsky@gmail.com*
[b] *Department of Analytical Chemistry, Faculty of Science, Charles University, Hlavova 8, 128 43 Prague, Czech Republic*
[c] *Department of Chemistry, Faculty of Science and Literature, Mugla University, 480 00 Mugla, Turkey*

Keywords
bismuth
high–resolution continuum source atomic absorption spectrometry
photochemical vapor generation
UV–radiation

Abstract
Conditions of photochemical vapor generation of bismuth were optimized in a flow–injection system with a standard mercury low-pressure tube lamp and a coiled reactor. A high-resolution continuum source atomic absorption spectrometer was used as a detector that was equipped with a miniature diffusion flame as an atomizer. The influence of flow rate of a carrier gas, irradiation time and composition of a reaction medium was investigated. Combination of 40% (*v/v*) acetic acid with 1.25% (*v/v*) formic acid was found optimal. Subsequently, the use of various metals as sensitizers was studied to achieve maximum generation efficiency. Except the already published positive effect of Fe^{2+}, three new sensitizers were found, with the enhancement effect in the following order: $Cu^{2+} < Cd^{2+} << Co^{2+}$. Interference from nitric acid which is commonly used for digestion of real samples was investigated. The limit of detection achieved with the optimal conditions was 5.9 μg L^{-1}.

1. Introduction

Photochemical vapor generation is an emerging sample introduction technique for analytical atomic spectrometry. This technique employs a source of UV–radiation for irradiation of a low molecular weight organic acid medium (most commonly formic acid, acetic acid, or their combinations) with the analyte. Produced highly reducing radicals and aquated electrons convert the analyte into a volatile species which is then transported into a detector [1]. In the recent years the use of photochemical vapor generation has been described for hydride-forming elements (As, Bi, Te, Sb, Pb, Se, Sn, and Tl) and mercury [1, 2], transition metals (Fe, Co, Ni, Cu, Mo, Cd, Ag, Au, Ir, Pd, Pt, Rh, and Os) [1, 3–5] and even non-metals (Br, I, Cl, and S) [1, 5, 6].

A first successful photochemical vapor generation of bismuth was described by Guo et al. in 2004 [5] which was followed by a more systematic study by Zheng et al. in 2010 [7]. However, the photochemical vapor generation efficiency was very low reaching around 1% [7]. To substantially increase the photochemical vapor generation efficiency, Yu et al. used Fe^{2+} ions as a sensitizer very recently [8].

In this work, we have studied the effect of various metal sensitizers in detail to enhance photochemical vapor generation of bismuth.

2. Experimental

2.1 Reagents and chemicals

Deionized water (< 0.2 μS cm^{-1}, Ultrapur, Watrex, USA) was used for the preparation of all solutions. Formic acid (98%, p.a., Lach-Ner, Czech Republic) and acetic acid (99.8%, p.a., Lach-ner, Czech Republic) were used for the preparation of the reaction medium. A stock solution 1000 mg L^{-1} Bi was purchased from Sigma-Aldrich (USA). Sensitizer stock solutions of various concentrations were prepared from: cadmium(II) acetate dihydrate (p.a., Lach-Ner, Czech Republic), cobalt(II) acetate tetrahydrate (p.a., Lach-Ner, Czech Republic), copper(II) acetate monohydrate (p.a., Merck, Germany), nickel(II) acetate tetrahydrate (p.a., Sigma-Aldrich, USA) and iron(II) sulphate heptahydrate (p.a., Lachema, Czech Republic). Nitric acid (65%, p.a., Lach-ner, Czech Republic) was used for an interference study.

2.2 Instrumentation

All the experiments were carried out with a high–resolution continuum source atomic absorption spectrometer (HR–CS–AAS) ContrAA 300 (Analytik Jena AG, Germany). Unless otherwise stated, 3 pixels of the detector were taken for evaluation of peak area. A commercial flame sample introduction system and a burner were replaced with an in–house made photochemical vapor generation system and with a miniature diffusion flame atomizer. A schematic diagram is shown in Fig. 1. Almost all tubing was made from PTFE (various internal (i.d.) and outer (o.d.) diameter, Vici Jour Research, Switzerland). A photoreactor consisted of a 15W low-pressure Hg germicidal lamp (Cole–Parmer, USA) which was wrapped around with 6 m of PTFE tubing (1 mm i.d., 1.59 mm o.d., Vici Jour Research, Switzerland; internal volume 4.71 mL). A steady flow of the reaction medium was supplied by a peristaltic pump (Reglo ICC, Ismatec, Switzerland) with tygon tubing (1.02 mm i.d., Ismatec, Germany) which was also used to evacuate a gas–liquid separator. Sample solutions were introduced into a stream of the reaction medium using an injection valve (V–451, IDEX Health and Science, USA; sample loop volume 0.5 mL). Effluent from the photoreactor was mixed with a flow of argon, and carried to the gas–liquid separator, where the volatile species

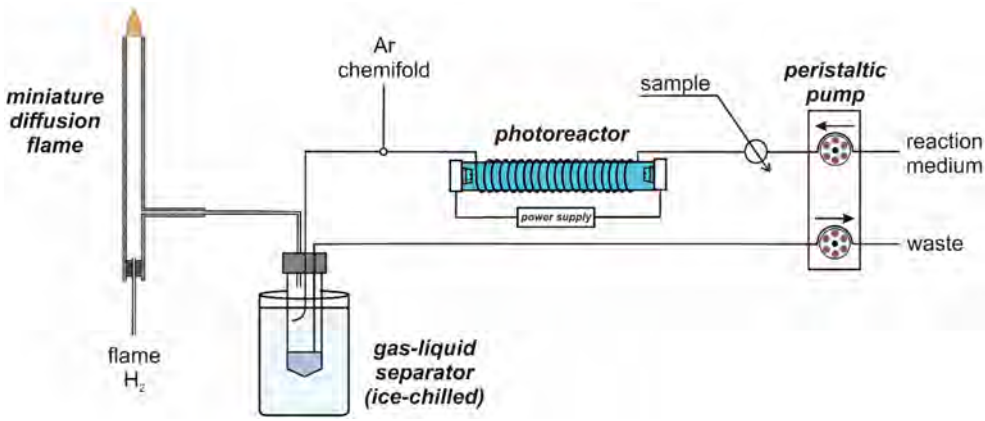

Fig. 1 Schematic diagram of a photochemical vapor generation system with a miniature diffusion flame atomizer.

were separated from the liquid waste. The gas–liquid separator was a modified polypropylene centrifuge vial with an internal volume of 50 mL and was immersed in an ice bath [3]. The gas–liquid separator was connected to an in-house made miniature diffusion flame atomizer by means of PTFE tubing (2 mm i.d., 4 mm o.d.). This atomizer consisted of a vertical quartz tube with 6 mm i.d. and it was supplied at the lower end with hydrogen that served as a fuel. The optical axis of the spectrometer, i.e. the axis of the radiation beam, intersected the (vertical) axis of the support tube of the atomizer. A more detailed description of the miniature diffusion flame atomizer is given elsewhere [9, 10]. The flow rates of argon (chemifold) and hydrogen (flame) were controlled by mass flow controllers (Omega Engineering, USA).

3. Results and discussion

The starting conditions were adopted from the work by Yu et al. [8]: composition of the reaction medium: 40% (*v*/*v*) acetic acid and 10% (*v*/*v*) formic acid, flow rate of the reaction medium 2 mL min^{-1}, addition of 50 mg L^{-1} of Fe^{2+} into the sample as a sensitizer. The flow rates of 100 mL min^{-1} for both argon (chemifold) and hydrogen (flame) were chosen on the basic of our previous experience with this type of the atomizer [9, 10].

The main aim of this work was to optimize the system to achieve the highest photochemical vapor generation efficiency. The first optimized parameter was the irradiation time, which was done by changing the flow rate of the reaction medium. The effect of the reaction medium flow rate is depicted in Fig. 2. The highest peak area was obtained for 3 mL min^{-1} corresponding to irradiation time of approximately 90 s.

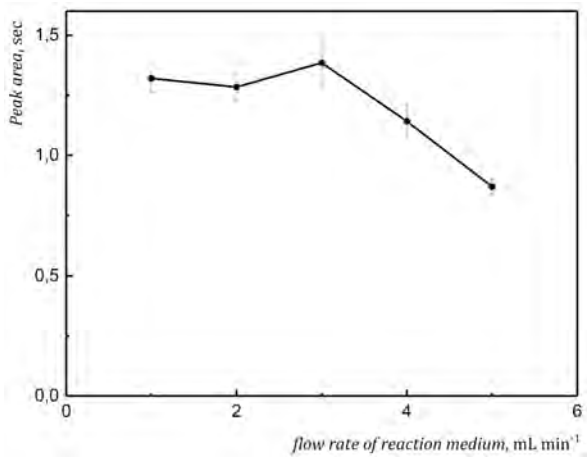

Fig. 2 Effect of reaction medium flow rate (irradiation time) on peak area; experimental conditions: 2 mg L^{-1} Bi, reaction medium 40% (*v/v*) acetic acid and 10% (*v/v*) formic acid, 50 mg L^{-1} Fe^{2+} as a sensitizer in the sample.

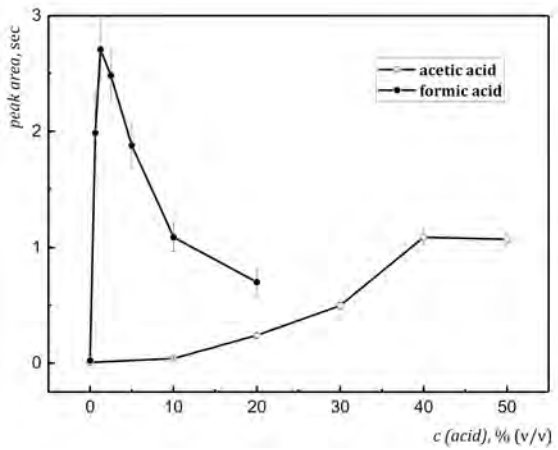

Fig. 3 Composition of reaction medium; experimental conditions: 2 mg L^{-1} Bi, reaction medium flow rate 3 mL min^{-1}, 50 mg L^{-1} Fe^{2+} as a sensitizer in the sample, 10% (*v/v*) formic acid for the optimization of acetic acid, 40% (*v/v*) acetic acid for the optimization of formic acid.

Afterwards the composition of the reaction medium was investigated. The highest generation efficiency was achieved with the reaction medium consisting of 40% (*v/v*) acetic acid and 1.25% (*v/v*) formic acid (Fig. 3).

Using this reaction medium, an effect of metal sensitizers other than Fe^{2+} was tested and compared to Fe^{2+}. In the absence of any sensitizer no signal response of bismuth could be detected. In order to compare the enhancement effect of various sensitizers, the signal measured with the addition of 5 mg L^{-1} Cu^{2+} was used as a reference value. Enhancement factors and optimum concentrations for Cd^{2+}, Fe^{2+},

Table 1
Comparison of relative enhancement effect of various metal sensitizers (relative to 5 mg L^{-1} Cu^{2+} in the sample).

Sensitizer	Tested concentration range/mg L^{-1}	Optimal concentration/ mg L^{-1}	Relative enhancement factor
Ni^{2+}	5–100	none	0
Cu^{2+}	1–100	5	1
Cd^{2+}	5–150	approx. 50	3–4
Fe^{2+}	50–500	≥ 500	at least 6.5
Co^{2+}	5–100	50	20

Co^{2+} and Ni^{2+} are shown in Table 1. The addition of Cd^{2+} led to an enhancement of the photochemical vapor generation but the repeatability of the measured signals was very poor, hence it was hard to draw conclusions about the exact enhancing ability of Cd^{2+}. In the case of Fe^{2+}, optimal concentration was not found, as the signal kept steadily increasing to very high concentrations (500 mg L^{-1}) which led to a decrease in repeatability due to the formation of iron deposits in the photoreactor and atomizer. No signal was observed with the addition of Ni^{2+} in the tested range of concentration 5–100 mg L^{-1}. The highest signal enhancement was observed for Co^{2+} in the range 20–100 mg L^{-1} and 50 mg L^{-1} Co^{2+} was chosen for further experiments.

Using optimal conditions, a calibration curve was linear in the range of 25–250 μg L^{-1} Bi. The limit of detection was determined by the measurements of 10 blanks and calculated as 5.9 μg L^{-1}. The repeatability of 10 consecutive measurements of 250 μg L^{-1} was 2.4%.

Interferences caused by nitric acid were also investigated. It was found that nitric acid is a serious interferent as a significant drop in sensitivity (by 13%) was observed even at concentration of 1 mmol L^{-1}.

4. Conclusions

The conditions of photochemical vapor generation of bismuth were optimized using AAS and miniature diffusion flame as the atomizer. Three new sensitizers with a significant effect on the photochemical vapor generation efficiency were described. Cobalt was found to be the most effective and led to a significant enhancement of the signal. Severe interferences from nitric acid were observed which is in line with the other works dealing with photochemical vapor generation [1]. Further experiments will follow dealing with the mechanism of the positive effect of transition metals on photochemical vapor generation and determination of the resultant generation efficiency using the metal sensitizers. To substantially decrease the limit of detection we plan to couple the system with an in-house built atomic fluorescence spectrometric detector [11] that should enable an ultratrace determination of bismuth in biological and environmental matrices.

Acknowledgments

The support of the Czech Science Foundation (Project No. 17–04329S and 19–17604Y), Czech Academy of Sciences (Institutional support RVO: 68081715) and Charles University (project SVV260440) is gratefully acknowledged.

References

[1] Sturgeon R.E.: Photochemical vapor generation: A radical approach to analyte introduction for atomic spectrometry. *J. Anal. At. Spectrom.* **32** (2017), 2319–2340.
[2] Xu T., Hu J., Chen H.: Transition metal ion Co(II)–assisted photochemical vapor generation of thallium for its sensitive determination by inductively coupled plasma mass spectrometry. *Microchem. J.* **149** (2019), 103972.
[3] Šoukal J., Sturgeon R.E., Musil S.: Efficient photochemical vapor generation of molybdenum for ICPMS detection. *Anal. Chem.* **90** (2018), 11688–11695.
[4] de Oliveira R.M., Borges D.L.: UV photochemical vapor generation of noble metals (Au, Ir, Pd, Pt and Rh): a feasibility study using inductively coupled plasma mass spectrometry and seawater as a test matrix. *J. Anal. At. Spectrom.* **33** (2018), 1700–1706.
[5] Guo X., Sturgeon R.E., Mester Z., Gardner G.J.: Vapor generation by UV irradiation for sample introduction with atomic spectrometry. *Anal. Chem.* **76** (2004), 2401–2405.
[6] Hu J., Sturgeon R.E., Nadeau K., Hou X., Zheng C., Yang L.: Copper ion assisted photochemical vapor generation of chlorine for its sensitive determination by sector field inductively coupled plasma mass spectrometry. *Anal. Chem.* **90** (2018), 4112–4118.
[7] Zheng C., Ma Q., Wu L., Hou X.,. Sturgeon R.E: UV photochemical vapor generation–atomic fluorescence spectrometric determination of conventional hydride generation elements. *Microchem. J.* **95** (2010), 32–37.
[8] Yu Y., Jia Y., Shi Z., Chen Y., Ni S., Wang R., Tang Y., Gao Y.: Enhanced photochemical vapor generation for determination of bismuth by inductively coupled plasma mass spectrometry. *Anal. Chem.* **90** (2018), 13557–13563.
[9] Vyhnanovský J., Kratzer J., Benada O., Matoušek T., Mester Z., Sturgeon R.E., Dědina J., Musil S.: Diethyldithiocarbamate enhanced chemical generation of volatile palladium species, their characterization by AAS, ICP–MS, TEM and DART–MS and proposed mechanism of action. *Anal. Chim. Acta* **1005** (2018), 16–26.
[10] Šoukal J., Benada O., Matoušek T., Dědina J., Musil S.: Chemical generation of volatile species of copper: Optimization, efficiency and investigation of volatile species nature. *Anal. Chim. Acta* **977** (2017), 10–19.
[11] Musil S., Matoušek T., Currier J.M., Stýblo M., Dědina J.: Speciation analysis of arsenic by selective hydride generation–cryotrapping–atomic fluorescence spectrometry with flame-in-gas-shield atomizer: achieving extremely low detection limits with inexpensive instrumentation. *Anal. Chem.* **86** (2014), 10422–10428.

Novel electrochemical DNA biosensor based on edge-plane pyrolytic graphite for DNA interaction studies

Michal Augustín*, Vlastimil Vyskočil

UNESCO Laboratory of Environmental Electrochemistry, Department of Analytical Chemistry, Faculty of Science, Charles University, Hlavova 8, 128 43 Prague 2, Czech Republic
✉ *michal.augustin@natur.cuni.cz*

Keywords
biosensor
DNA
graphite
voltammetry

Abstract
Carbon electrodes represent the most popular working electrodes used in electrochemical analysis of nucleic acids. Since the end of the 20th century, they have been frequently used for a lot of various applications in the field of electrochemical analysis of DNA, RNA, as well as synthetic mimics of nucleic acids such as PNA. Some of their remarkable properties enhanced their utilization as electrochemical transducers of sensors for DNA hybridization, DNA-drug interactions, or even monitoring DNA damage. The aim of the proposed study is the preparation, development, and subsequent testing of new electrochemical DNA biosensors based on relatively new type of carbon material "edge-plane" pyrolytic graphite (EPPG) and its subsequent utilization as a useful analytical tool.

1. Introduction

Pyrolytic graphite is a polycrystalline form of carbon with a high degree of orientation. The edge-plane form has attracted much attention because of its higher sensitivity to electron transfer compared with the basal-plane form [1]. The edge-plane surface has a higher degree of orientation than the basal-plane surface, enabling greater adsorption of chemical species and improving analytical determination [2].

The biosensor is an analytical device that converts the concentration of target substance (analyte) to an electrical signal through a combination of biological or from biology derived recognition system integrated in or in close contact with a suitable physico-chemical transducer [3]. Electrochemical biosensors for monitoring DNA damage generally consists of two parts: an electrode that represents an electrochemical transducer, and DNA as a biocomponent that is immobilized on the surface of a working electrode. The principle is the interaction between the immobilized DNA and the damaging agent, which is then converted through

changes in the electrochemical properties of the DNA recognition layer to a measurable electrical signal corresponding to the oxidation of purine bases [4].

The altered chemical, physico-chemical, or structural properties of damaged DNA are subsequently reflected in its redox behavior, which is used in many DNA damage detection techniques [5].

2. Experimental

2.1 Reagents and chemicals

Low molecular weight salmon sperm dsDNA was obtained from Sigma-Aldrich, Germany. Stock solutions (0.1 mg/ml) of dsDNA were prepared in a 0.1 mol/L phosphate buffer of pH = 7.4.

2.2 Apparatus

Voltammetric measurements were performed using the μAutolab III/FRA2 potentiostat/galvanostat (Eco Chemie, Netherlands) driven by a NOVA 1.11 software (Metrohm Autolab, Switzerland). All measurements were carried out in a three-electrode system using an "edge-plane" pyrolytic graphite working electrode (EPPGE) with an electroactive surface of 3 mm (BAS, Japan), a silver|silver chloride reference electrode (Ag|AgCl|sat. KCl), and a platinum counter electrode (Elektrochemické detektory, Czech Republic) in a 20 ml glass voltammetric cell at ambient temperature.

2.3 Preparation of the biosensor

Prior to the every measurement, surface of the EPPGE was mechanically cleaned by gentle wiping of the electrode on the soft polishing pad rinsed with distilled water. Afterwards, the electrode was rinsed with distilled water and placed in the phosphate buffer for the subsequent electrochemical activation. Electrochemical activation was performed in the phosphate buffer by applying potential of 1.5 V for 240 s without stirring. A potential pulse in working range of potentials (0.0–1.5 V) was then applied.

The electrochemical DNA biosensor based on the EPPGE (dsDNA/EPPGE biosensor) was prepared by the adsorption of dsDNA on the EPPGE. Default parameters of the dsDNA adsorption were: a concentration of dsDNA of 0.1 mg/ml in the phosphate buffer (cg(dsDNA)), a deposition potential (Edep) of 0.3 V, and an adsorption time of 5 min (tads) with no solution stirring.

Square-wave voltammetry (SWV) was used as a direct electrochemical method for monitoring the oxidation of dsDNA bases. For the preparation of the dsDNA/EPPGE biosensor to be applied with SWV, optimum adsorption parameters were: c_g(dsDNA) = 0.06 mg/ml, E_{dep} = 0.7 V, and t_{ads} = 5 min with no

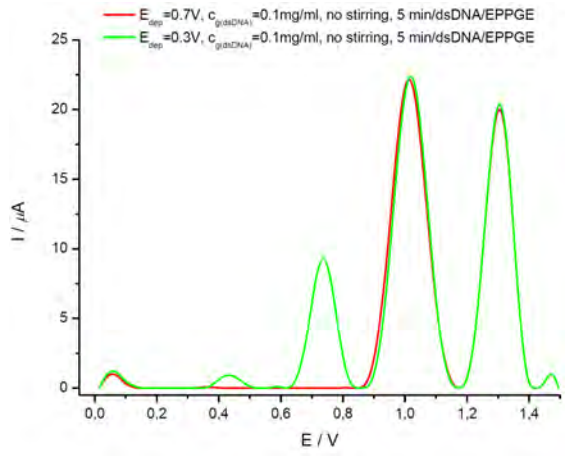

Fig. 1 Baseline-corrected SWV responses of dsDNA bases at the dsDNA/EPPGE biosensor recorded in the phosphate buffer corresponding to the different values of E_{dep} = 0.3 V, resp. 0.7 V.

solution stirring. After that, the prepared dsDNA/EPPGE biosensor was placed in the phosphate buffer for 5, 35, or 60 min in order to achieve the equilibrium state, and the recordings of SWV were obtained.

2.4 Procedures

The experimental parameters were as follows: SWV in the phosphate buffer (pH = 7.4) with a pulse amplitude of 20 mV, a frequency of 50 Hz, a scan rate of 750 mV/s, and a potential step of 15 mV. All curves were measured three times.

3. Results and discussion

Since EPPG represents a practically new type of carbon-based electrode material, particularly in the preparation of electrochemical DNA biosensors, its practical application had to be preceded by careful optimization, with some important parameters being addressed such as deposition potential associated with the accumulation of DNA on the electroactive surface of the EPPGE (E_{dep}), the time range in terms of the application of the deposition potential (t_{dep}), as well as the optimal concentration of the DNA solution associated with the complete coverage of the electroactive surface of the EPPGE (c_g(satur)).

The first parameter, which has represented an important basis for the whole optimization, was E_{dep} (Fig. 1). Parameters such as c_g(dsDNA) (1 mg/ml vs. 0.1 mg/ml), as well as the parameter of the stirring of the DNA solution during the DNA deposition were simultaneously optimized. In this case, results showed that the signals corresponding to the electroactivity of DNA are higher in the case of lower DNA concentration and more stable in solutions without stirring.

Most of the scientific researches related to the preparation of electrochemical DNA biosensors utilize the E_{dep} of 0.5 V [6]. However, it should be noted that the electrode material used in these studies was mainly glassy carbon, or its various modifications. In our case, we have decided to shift the E_{dep} towards more negative potentials (0.3 V), which should be sufficiently distant from the voltammetric peaks corresponding to the electroactivity of dsDNA. In this case, it is possible to observe the occurrence of four voltammetric peaks (Fig. 1): peaks at the potential of 1.01 V and 1.30 V corresponds to the electrooxidation of guanine (dGua) and adenine (dAde) moieties, respectively; the peak recorded at the more negative potential (0.73 V) probably corresponds to free guanine bases, which are present in the DNA solution.

Note: The voltammetric peak with potential of 0.43 V, which does not provide an analytically valuable signal, probably corresponds to the electrooxidation of these free guanine bases or some of their derivatives.

Since electrochemical DNA biosensors for detection of DNA damage are primarily based on monitoring changes in the signals of dGua resp. dAde, and since with the alternation of potential towards more positive values these signals remain stable and practically the same, 0.7 V was chosen as the optimal value of the E_{dep} [7].

The next step of optimization involved finding the optimal value of the c_g(satur). This parameter is an important criterion for assessing possible interactions of different chemical compounds with dsDNA. As mentioned above, comparison of high and low DNA concentrations did not yield any significant difference in current responses corresponding to the DNA electroactivity, suggesting that the electrode surface is already saturated by DNA. Because of this, attention has been dragged towards lower DNA concentrations (0.10–0.01 mg/ml).

In the case of three upper concentrations (0.10, 0.08, and 0.06 mg/ml), the current responses are practically the same (Fig. 2). With a shift towards lower DNA concentrations, it is possible to observe a decrease in the current responses together with a small potential shift towards negative potentials, the size of which is proportional to decreasing DNA concentration. Based on the above-mentioned observations, a concentration of 0.06 mg/ml was chosen as the optimal value of c_g(satur).

Perhaps the most important parameter of optimization was a time stability of the prepared biosensor. In this regard, the prepared biosensor was immersed in the phosphate buffer solution for selected periods of time (5, 35, and 60 min) (Fig. 3).

Since the observed changes in DNA signals do not show the same course for both bases, we decided to discuss them separately. In the case of the signal corresponding to the dGua, a significant decrease together with a small shift of potential towards negative values can be observed already at 5 min. With a further incubation time (35 min), this decrease deepens while, at the same time, it is reaching a maximum, since with the additional incubation time (60 min), the observed oxidation signal remains practically the same.

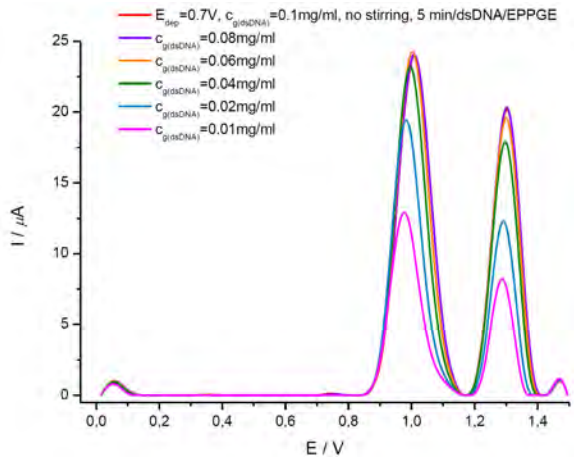

Fig. 2 Baseline-corrected SWV responses of dsDNA bases at the dsDNA/EPPGE biosensor recorded in the phosphate buffer corresponding to the different concentrations of dsDNA (0.1–0.01 mg/ml).

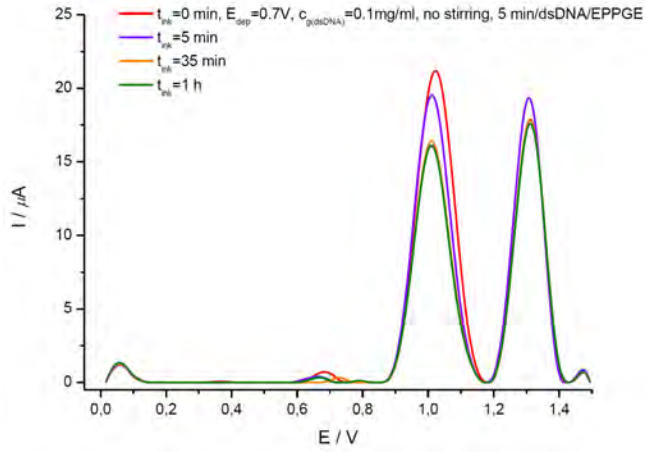

Fig. 3 Baseline-corrected SWV responses of dsDNA bases at the dsDNA/EPPGE biosensor recorded in the phosphate buffer after its incubation for a different time periods in the phosphate buffer (5, 35, and 60 min).

In the case of a signal corresponding to the dAde, a different course can be observed. With an initial incubation time (5 min), a slight increase in the oxidation signal was observed, which is likely to be related to the slight opening of the DNA molecule, where exposure of the bases occurs. With an additional incubation time (35 min), this signal returns to its initial value, which is retained within the final incubation time (60 min).

Although the temporal changes, which have been recorded within the signals corresponding to the dGua, suggest that DNA may be desorbed from the EPPGE, rather different phenomenon is likely to occur. The first reason is that changes in

signals have a distinctly different (almost reversed) pattern for each base. The second reason is that the decrease in the dGua signal reaches its maximum at 60 min, when its further decline was no longer noted. This suggests that there is no desorption of DNA from the electrode surface, but the DNA itself undergoes some conformational changes associated with achieving equilibrium at the EPPGE. For this reason, the prepared biosensor had to be submerged in the phosphate buffer within a given period of time (t_{stab} = 35 min) to achieve stabilization of the dsDNA surface activity prior to each measurement with the dsDNA/EPPGE biosensor.

4. Conclusions

In this contribution, we present a new electrochemical dsDNA biosensor based on EPPG that provides sufficiently satisfying current responses corresponding to the electroactivity of DNA which are in good correlation with some of the previous carbon-based electrode materials (e.g. glassy carbon) [8,9]. Important parameters, such as E_{dep}, c_g(satur), or t_{stab} were optimized and helped in the way of understanding the biosensor working principles. Further research should be devoted to investigation of the biosensor functionality towards some of the most notable chemical substances which has been previously studied in connection with electrochemical DNA biosensors.

Acknowledgments

This research was supported by the Specific University Research (SVV260440).

References

[1] Banks C.E., Compton R.G.: New electrodes for old: from carbon nanotubes to edge plane pyrolytic graphite. *Analyst* **131** (2006), 15–21.
[2] Saberi R.-S., Shahrokhian S.: Highly sensitive voltammetric determination of amotrigine at highly oriented pyrolytic graphite electrode. *Bioelectrochemistry* **84** (2012), 38–43.
[3] Lowe C.R., Goldfinch M.J.: Novel electrochemical sensors for clinical analysis. *Biochem. Soc. Trans.* **11** (1983), 448–451.
[4] Diculescu V.C., Chiorcea-Paquim A.-M., Oliveira-Brett A.-M.: Applications of a DNA-electrochemical biosensor. *TrAC Trends Anal. Chem.* **79** (2016), 23–36.
[5] Paleček E., Fojta M., Tomschik M., Wang J.: Electrochemical biosensors for DNA hybridization and DNA damage. *Biosens. Bioelectron.* **13** (1998), 621–628.
[6] Wang J., Rivas G., Cai X., Chicharro M., Dontha N., Luo D., Palecek E., Nielsen P.: Adsorption and detection of peptide nucleic acids at carbon paste electrodes. *Electroanalysis* **9** (1997), 120–124.
[7] Brabec V., Dryhurst G.: Electrochemical behavior of natural and biosynthetic polynucleotides at the pyrolytic graphite electrode – a new probe for studies of polynucleotide structure and reactions. *J. Electroanal. Chem. Interfacial Electrochem.* **89** (1978), 161–173.
[8] Hájková A., Barek J., Vyskočil V.: Voltammetric determination of 2-aminofluoren-9-one and investigation of its interaction with DNA on a glassy carbon electrode. *Electroanalysis* **27** (2015), 101–110.
[9] Hájková A., Barek J., Vyskočil V.: Electrochemical DNA biosensor for detection of DNA damage induced by hydroxyl radicals. *Bioelectrochemistry* **116** (2017), 1–9.

Structural characterization of fatty acids with triple bond and unusual double bond positions by HPLC/APCI-MS^2

PETRA HORKÁ[a, b, *], VLADIMÍR VRKOSLAV[b], JOSEF CVAČKA[a, b]

[a] *Department of Analytical Chemistry, Faculty of Science, Charles University, Hlavova 2030/8,128 43 Prague 2, Czech Republic*
[b] *Institute of Organic Chemistry and Biochemistry of the Czech Academy of Science, Flemingovo náměstí 542/2, 166 10 Prague 6, Czech Republic* ✉ *petra.horka@uochb.cas.cz*

Keywords
acetonitrile-related adducts
acetylenic lipids
multiple bond localization
mass spectrometry

Abstract
Fatty acid methyl esters (FAMEs) were analyzed by reversed-phase HPLC coupled to atmospheric pressure chemical ionization (APCI) mass spectrometry. Acetonitrile was used as mobile phase. The gas-phase reactions of acetonitrile and unsaturated FAMEs in the APCI source provided $[M + C_3H_5N]^{+\bullet}$ adducts. Subsequent MS/MS analysis of these ions gave diagnostic fragments. The formation and fragmentation of the acetonitrile-related adducts were utilized for the structural characterization of FAME with isolated double bonds in (*Z*)-9,19-hexacosadienoic acid methyl ester, FAME with conjugated double bonds in (*Z*)-9,11-octadecadienoic acid methyl ester and FAME with a triple bond in 9-octadecynoic acid methyl ester.

1. Introduction

A number of unusual unsaturated fatty acids with isolated double bonds, conjugated double bonds or a triple bond exist in nature. For instance, (*Z*)-9,19-hexacosadienoic acid has been discovered in the fat body of the early bumblebee (*Bombus pratorum*) [1] and in various marine sponges like *Microciona prolifera* [2]. Fatty acids with conjugated double bonds can be found in pomegranate seeds (*Punica granatum*), for instance, puninic acid (9*Z*,11*E*,13*Z*-octadecatrienoic acid) [3].

More than 700 compounds containing one or more triple bonds are distributed throughout the flora and fauna. They are found in plants, fungi, microorganisms, and invertebrates [4, 5]. Although the above-mentioned lipids are a relatively common part of the lipidome of many organisms, analytical tools for determining the position(s) of such multiple bonds need to be developed. GC/MS with dimethyl disulfide derivatization [6, 7] is most commonly used for structural characterization of unsaturated fatty acid methyl esters (FAMEs), but other techniques like Ag-HPLC, MSn, CID, CACI, OzESI, OzIDcan also be applied [8]. Liquid

chromatographic analytical approaches are more versatile than GC, offering an analysis of FAMEs regardless of their chain length, degree of unsaturation and the need for derivatization. Double bonds in lipids can be localized by reacting the analyte with acetonitrile-related ions in the gas phase [9–11]. Acetonitrile is commonly used in HPLC mobile phases and the reaction takes place directly in common APCI sources without any modification. So far this approach has been used to localize double bonds in various unsaturated neutral lipids including wax esters [12], monounsaturated FAMEs and FAMEs with the methylene-interrupted arrangement of double bonds [13], and diol diesters and triacylglycerols from vernix caseosa [14, 15]. The aim of this work is to demonstrate that the same approach is also applicable for FAMEs with isolated or conjugated double bonds and with a triple bond.

2. Experimental

2.1. Chemicals and lipid standards

Acetonitrile and methanol mass spectrometry grade (Sigma-Aldrich, USA) were used as received. The other solvents (chloroform, hexane, diethyl ether) were distilled in glass from analytical-grade solvents (Penta, Czech Republic). The standards of the FAMEs (purity: 99%) were purchased from Cayman Europe (Estonia) or Larodan (Sweden). These standards were dissolved in methanol:chloroform (3:2, *v/v*) at the concentrations of 1–20 mg/mL.

2.2. Transesterification of triacylglycerols

FAMEs were obtained by transesterification of triacylglycerols isolated from the peripheral fat body of three specimens of bumblebee *Bombus pratorum*. The fat samples were extracted in chloroform (500 µl for each) and triacylglycerols were isolated from the extract by semipreparative TLC on pre-cleaned silica-gel plates using hexane:diethyl ether:acetic acid (80:20:1, *v/v/v*) mobile phase. The zone corresponding to triacylglycerols was scraped off the plate, extracted with diethyl ether and the solvent was evaporated to dryness. Triacylglycerols were dissolved in methanol:chloroform (3:2, *v/v*, 250 µl) and transesterified according to [16].

2.3. HPLC/APCI-MS

The liquid chromatograph consisted of a Rheos Allegro UHPLC pump, Accela autosampler with an integrated column oven and an LCQ Fleet ion-trap mass spectrometer; the system was controlled by Xcalibur software (all Thermo Fisher Scientific, USA). Develosil RP-Aqueous C30 (250×4.6 mm, particle size: 5 µm; Nomura Chemical, Japan) stainless-steel column and isocratic elution with acetonitrile at 1 ml/min flow rate, the column temperature 10 °C or 40 °C were

used. The injected volume of samples was 10 or 20 μL. The FAME standards dissolved in chloroform:methanol (3:2, *v/v*) were also directly injected by a loop (10 μL) into the mobile phase flow. The APCI vaporizer and heated capillary temperatures were set to 380 °C and 180 °C, respectively; the corona discharge current was 2 μA. Nitrogen served both as the sheath and auxiliary gas at a flow rate of 60 and 45 arbitrary units, respectively. The MS spectra of positively charged ions were recorded in the *m/z* 180–500 range. The CID MS^2 spectra of $[M + 55]^{+\bullet}$ were collected using a data-dependent analysis with an isolation width of 2-3 Da and normalized collision energy of 28–32%. The masses of the acetonitrile adducts for fragmentation were calculated as higher partners of the base peaks (*m/z* $[M + H]^+ + 54$ Da).

2.4. The FAME abbreviations and nomenclature

An abbreviated nomenclature for the FAMEs was used. For instance, the abbreviation FAME 26:2n−7,17 is used for (*Z*)-9,19-hexacosadienoic acid methyl ester. The diagnostic ions in the MS/MS spectra of $[M + 55]^{+\bullet}$ are denoted as α - containing an ester moiety and ω - carry the terminal-carbon end [11].

3. Results and discussion

In agreement with the previous study [13], the formation of $[M + C_3H_5N]^{+\bullet}$ was observed in the APCI source. The MS/MS (CID) spectra of the $[M + C_3H_5N]^{+\bullet}$ adducts provided α and ω fragments indicating unsaturated carbon-carbon bond positions. Fragments corresponding to a neutral loss of hydrogen, CH_3OH or alkene were observed in the FAME spectra as well.

3.1 FAME with two isolated double bonds

The chromatogram of FAMEs from *Bombus pratorum* is shown in Fig. 1. FAME 26:2n-7, 17 ((*Z*)-9,19-hexacosadienoic acid methyl ester) elutes with retention time 36,98 min. Fig. 2 shows the MS/MS spectrum of FAME 26:2n-7, 17 ((*Z*)-9,19-hexacosadienoic acid methyl ester) from *Bombus pratorum*. The fragments α and ω indicating the position of double bonds were clearly visible and formed very abundant peaks in the spectra. Peaks *m/z* 376 and *m/z* 238 indicated fragments α n-7 and α n-17 and peaks *m/z* 304 and *m/z* 166 indicated fragments ω n-17 and ω n-7, respectively. The most abundant fragments were formed by cleaving of C-C bonds next to the first and last double bonds, α n-7 and ω n-17. The double bond positions were in agreement with previous results [13]. Less intense fragments composing a series of ions separated by 14 Da were formed by neutral losses of alkene. Peak *m/z* 460 and *m/z* 429 correspond to a loss of hydrogen and CH_3OH, respectively.

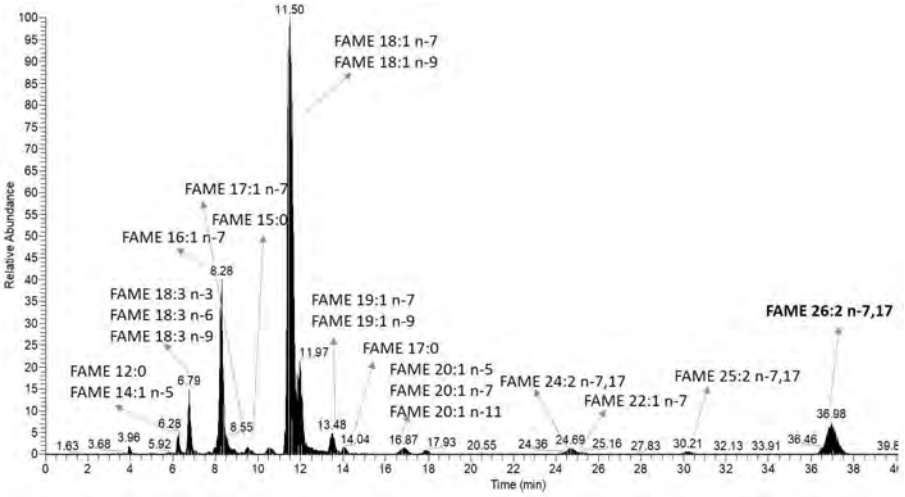

Fig. 1 Chromatogram of FAMEs from the fat body of *Bombus pratorum*. FAME 26:2n-7, 17 ((*Z*)-9,19-hexacosadienoic acid methyl ester) elutes with retention time 36.98 min.

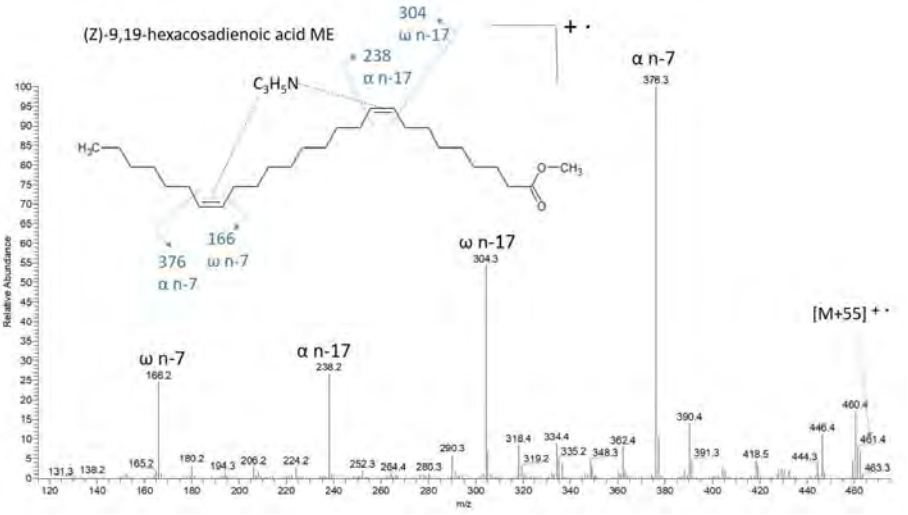

Fig. 2 The APCI MS/MS spectrum of the $[M + 55]^{+\bullet}$ adduct of FAME 26:2n-7,17.

3.2 FAME with two conjugated double bonds

The MS/MS spectrum of acetonitrile adduct of FAME 18:2n-7,9 ((*Z*)-9,11-octadecadienoic acid methyl ester) is in Fig. 3. The abundant ions corresponding to double bond positions were as follows: α n-7 peak at *m/z* 264, α n-9 peak at *m/z* 238, ω n-7 peak at *m/z* 166 and ω n-9 peak at *m/z* 192. The most abundant peaks were formed by cleaving C-C bonds next to the first and last double bonds, i.e., α n-7 and ω n-9. With the increasing number of double bonds and their closer

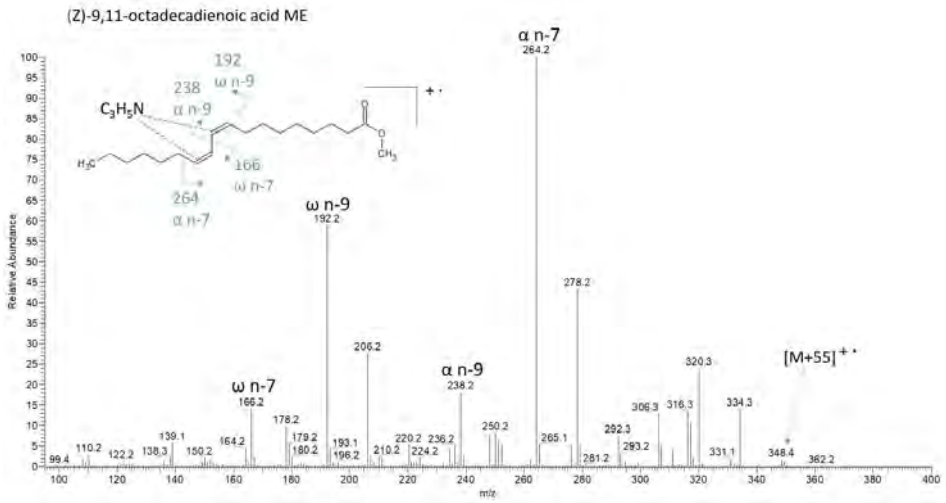

Fig. 3 The APCI MS/MS spectrum of the $[M + 55]^{+\bullet}$ adduct of FAME 18:2n-7,9.

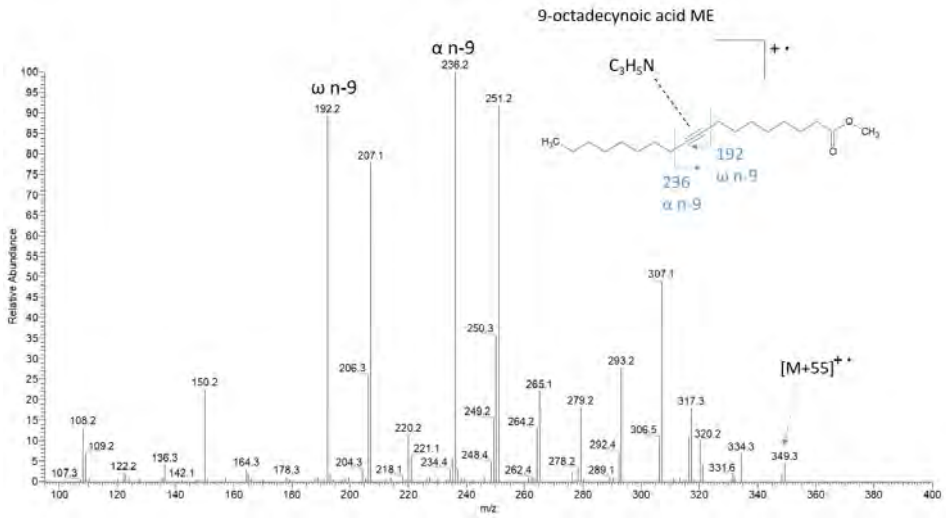

Fig. 4 The APCI MS/MS spectrum of the $[M + 55]^{+\bullet}$ adduct of 9-octadecynoic acid methyl ester.

position, the satellite fragments differing from α and ω ions by 14 mass units became more intense [13]. This is especially evident for fragments formed by cleaving C-C bonds next to the first and last double bond +14 mass units. Despite the existence of satellite fragments, the spectrum provided clear evidence of the conjugated double bonds in FAME 18:2n-7, 9. Less intense fragments composing a series of ions separated by 14 Da were formed by neutral losses of alkene. The peaks *m/z* 316 corresponded to the loss of CH_3OH and the *m/z* 348 was consistent with loss of hydrogen.

3.3 FAME with one triple bond

Figure 4 shows 9-octadecynoic acid methyl ester and MS/MS spectrum of its $[M + 55]^{+\bullet}$ adduct (*m/z* 349). The spectrum contained α and ω ions (*m/z* 236 and *m/z* 192), which indicated the position of the triple bond. Unlike FAMEs with double bonds, the satellite fragments differed by 15 mass units. This difference can be used to identify FAMEs with a combination of double and triple bonds. The satellite fragments differing from α and ω ions by + 15 mass units reached almost the same intensity as α and ω fragments. Less abundant fragments composing a series of ions separated by 14 Da were formed by neutral losses of alkene. The peak *m/z* 317 corresponded to the loss of CH_3OH. Hydrogen loss was not as abundant as in the case of FAMEs with double bonds.

4. Conclusions

The experiments showed that acetonitrile-related adducts formed in the APCI source can be used for localizing isolated and conjugated double bonds, as well as a triple bond in FAMEs. The satellite ions in the MS/MS spectra make it possible to differentiate between one triple bond from two double bonds. The advantage of this method is based on simplicity and speed of analysis, where lipid separation by HPLC with acetonitrile as a mobile phase is used.

Acknowledgments

This work was financially supported by Grant Agency of Charles University in Prague (Project No. 10119) and Charles University in Prague (Project SVV260440).

References

[1] Cvačka J., Kofroňová E., Vašíčková S., Stránský K., Jiroš P., Hovorka O., Kindl J., Valterová I.: Unusual fatty acids in the fat body of the early nesting bumblebee, *Bombus pratorum*. *Lipids* **43** (2008), 441–450.

[2] Morales R.W., Litchfield C.: Incorporation of 1–^{14}C-acetate into C26 fatty acids of the marine sponge *Microciona prolifera*. *Lipids* **12** (1977), 570–576.

[3] Topkafa M., Kara H., Sherazi S.T.H.: Evaluation of the triglyceride composition of pomegranate seed oil by RP-HPLC followed by GC-MS. *J. Am. Oil Chem. Soc.* **92** (2015), 791–800.

[4] Bohlmann F., Burkhardt T., Zdero C.: *Naturally Occurring Acetylenes.* New York, Academic Press 1973.

[5] Dembitsky V.M., Rezanka T.: Distribution of acetylenic acids and polar lipids in some aquatic bryophytes. *Phytochemistry* **40** (1995), 93–97.

[6] Dunkelblum E., Tan S.H., Sikl P.J.: Double-bond location in monounsaturated fatty acids by dimethyl disulfide derivatisation and mass spectrometry: application to analysis of fatty acids in pheromone glands of four Lepidoptera. *J. Chem. Ecol.* **11** (1985), 265–277.

[7] Christie W.W., Han X.: *Lipid Analysis: Isolation, Separation, Identification and Lipidomic Analysis.* Bridgwater, The Oily Press 2010.

[8] Mitchell T.W., Pha H., Thomas M.C., Blanksby S.J.: Identification of double bond position in lipids: From GC to OzID. *J. Chromatogr. B* **877** (2009), 2722–2735.

[9] Lawrence P., Brenna J.T.: Acetonitrile Covalent adduct chemical ionization mass spectrometry for double bond localization in non-methylene-interrupted polyene fatty acid methyl esters. *Anal. Chem.* **78** (2006), 1312–1317.

[10] Michaud A.L., Yurawecz M.P., Delmonte P., Corl B.A., Bauman D.E., Brenna J.T.: Identification and characterization of conjugated fatty acid methyl esters of mixed double bond geometry by acetonitrile chemical ionization tandem mass spectrometry. *Anal. Chem.* **75** (2003), 4925–4930.
[11] Van Pelt C.K., Brenna J.T.: Acetonitrile chemical ionization tandem mass spectrometry to locate double bonds in polyunsaturated fatty acid methyl esters. *Anal. Chem.* **71** (1999), 1981–1989.
[12] Vrkoslav V., Háková M., Pecková K., Urbanová K., Cvačka J.: Localization of double bonds in wax esters by high-performance liquid chromatography/atmospheric pressure chemical ionization mass spectrometry utilizing the fragmentation of acetonitrile-related adducts. *Anal. Chem.* **83** (2011), 2978–2986.
[13] Vrkoslav V., Cvačka J.: Identification of the double-bond position in fatty acid methyl esters by liquid chromatography/atmospheric pressure chemical ionisation mass spectrometry. *J. Chromatogr. A* **1259** (2012), 244–250.
[14] Háková E., Vrkoslav V., Míková R., Schwarzová-Pecková K., Bosáková Z., Cvačka J.: Localization of double bonds in triacylglycerols using high-performance liquid chromatography/atmospheric pressure chemical ionization ion-trap mass spectrometry. *Anal. Bioanal. Chem.* **407** (2015), 5175–5188.
[15] Šubčíková L., Hoskovec M., Vrkoslav V., Čmelíková T., Háková E., Míková R., Coufal P., Doležal A., Plavka R., Cvačka J.: Analysis of 1,2-diol diesters in vernix caseosa by high-performance liquid chromatography—atmospheric pressure chemical ionization mass spectrometry. *J. Chromatogr. A* **1378** (2015), 8–18.
[16] Stránský K., Jursik T.: Simple quantitative transesterification of lipids 1. Introduction. *Lipid/Fett* **98** (1996), 65–71.

A novel version of a silver solid amalgam electode for the combination of hollow fiber supported membrane extraction and voltammetric determination of acidic substances

VÍT NOVOTNÝ*, KAROLÍNA SCHWARZOVÁ, JIŘÍ BAREK

UNESCO Laboratory of Environmental Electrochemistry, Department of Analytical Chemistry, Faculty of Science, Charles University, Hlavova 8, 128 43 Prague 2, Czech Republic
✉ *novotnvt@gmail.com*

Keywords
Aclonifen
2,4-dinitrosalicylic acid
hollow fiber supported liquid membrane extraction
meniscus modified silver solid amalgam electrode
voltammetry

Abstract
An electrode capable of voltammetric measurements inside a polypropylene hollow fiber with an octanol supported liquid membrane has been developed. The intended application is determination of the herbicide Aclonifen in environmental matrices after hollow fiber supported liquid membrane extraction. As a proof of concept calibration dependencies were measured for 2,4-dinitrosalicylic acid in the concentration range 1×10^{-3} mol L^{-1} to 2×10^{-4} mol L^{-1} and they are linear for both a bare electrode and an electrode inside the hollow fiber. Results of optimization studies of the extraction of 2,4-dinitrosalicylic acid and Aclonifen combined with voltammetric determination will be presented.

1. Introduction

Hollow fiber supported liquid membrane extraction is a well-established technique of sample preconcentration and cleanup [1, 2]. Two modes of hollow fiber supported liquid membrane extraction exist: one using partitioning between aqueous phase on the outside of a hollow fiber and an organic solvent inside, and one using partitioning of species that can undergo protonation or deprotonation between aqueous phases with different pH separated by an organic solvent trapped in the pores of the hollow fiber. Both have been coupled to many mainstream analytical techniques such as GC and HPLC. The combination with electrochemical detection is however still not well studied. The work of Hrdlička et al. [3] attempts to combine the two sequentially, but the approach of this work is much more straightforward and integrated. It aims to combine the techniques by placing a meniscus modified silver solid amalgam electrode (m-AgSAE) designed

for this purpose into the lumen of a polypropylene hollow fiber infused with octanol. The m-AgSAE is suited very well for this application, as mercury dropping electrode cannot be used for obvious reasons and m-AgSAE has the advantage of atomically smooth mercury amalgam that does not suffer from passivation as much as solid electrode materials [4]. The diphenyl ether herbicide Aclonifen is our target analyte, but determination of 2,4-dinitrosalicylic acid is developed first as a proof of concept due to its lower cost. Aclonifen was chosen because most other diphenyl ether herbicides do not undergo protonization or deprotonization at reasonable pH values. Aclonifen has been well studied from the electrochemical point of view [5–7], so it is suitable to showcase the use of the newly developed extraction/determination method on an environmentally relevant analyte.

2. Experimental

2.1 Chemicals

Sodium hydroxide (g. r. Penta, Czech Republic), potassium chloride, ferric chloride hexahydrate, hydrochloric acid 35% (all g. r. Lachner, Czech Republic), methanol (HPLC, Avantor, Poland), acetonitrile (Honeywell, USA) 2,4-dinitrosalicylic acid (Sigma-Aldrich, USA) and *n*-octanol (for synthesis, Merck, Germany) were used. The stock solution of 2,4-dinitrosalicylic acid (c = 1×10^{-3} mol L^{-1}) has been prepared by dissolving 0,0228 g of 2,4-dinitrosalicylic acid in 100 mL of deionized water.

2.2 Apparatus

Measurements of pH were performed on a XS Instuments pH 50 pH-meter with a CHS Polymer Green glass electrode (type CHS-5670-N1B). The electrode was calibrated by standard buffer solutions in water. Accurel polypropylene hollow fibres(600 μm i.d., 200 μm wall thickness, and 0.2 μm pore size) purchased from Membrana (Germany) were used. Palmsens Electrochemical Sensor Interface (Palm Instruments, The Netherlands) and the PalmsensPC software were used for all voltammetric measurements. Pulses of width of 100 ms and height of –50 mV were used while performing DPV. A polarization rate of 20 mV s^{-1}, and potential resolution of 5 mV were used. All measurements were performed using a three electrode system. A silver chloride electrode (1 mol L^{-1} KCl) type RAE 113, (Monokrystaly, Czech Republic), a platinum wire auxiliary electrode and an m-AgSAE were used. The AgSAE was made of a 380 μm isolated copper wire etched by ferric chloride staffed by silver powder and amalgamated. The wire was then pushed through a 22 gauge flat tip syringe needle so that the wire protruded approximately 1 mm. The electrode could then be used either bare or covered in a hollow fiber filled with the acceptor phase. If the hollow fiber was used a 5 mm section of gauge 22 stainless tube with soldered on isolated copper wire inserted

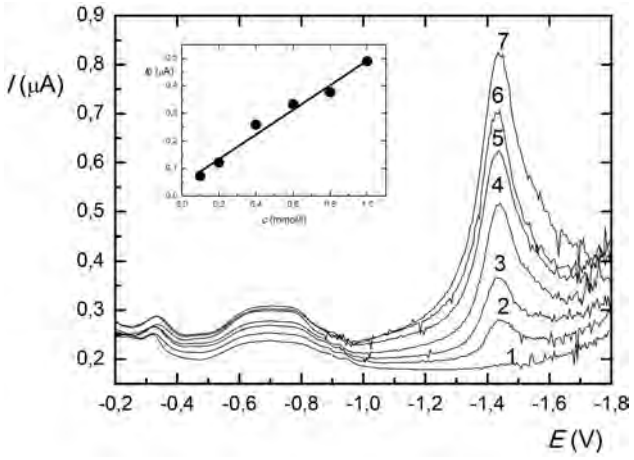

Fig. 1 DP Voltammograms of 2,4-dinitrosalicylic acid at a m-AgSAE made of etched copper wire filled with silver powder and amalgamated. Concentration of 2,4-dinitrosalicylic acid: (1) 0.0, (2) 0.1, (3) 0.2, (4) 0.4, (5) 0.6, (6) 0.8, and (7) 1.0 mmol L^{-1}. The corresponding calibration straight line is in the inset.

into the opposite end of the hollow fiber than the working electrode was used as the auxiliary electrode.

2.3 Procedures

The measurements inside fiber were performed using 0.1 mol L^{-1} NaOH with 0.1 mol L^{-1} KCl as both the donor phase and as the acceptor phase. The KCl was used to improve conductivity and decrease the liquid junction potential between the donor and acceptor phase. The hollow fibers were cut to a length of 1 cm, degreased in methanol, let to dry and immersed in *n*-octanol to create the supported liquid membrane. The fibers were capped by the working electrode on one end and a stainless steel counter electrode on the opposite end.

3. Results and discussion

At first the bare electrode was tested by measuring a calibration dependence of 2,4-dinitrosalicylic acid under basic conditions. The voltammograms of 2,4-dinitrosalicylic acid in 0.1 mol L^{-1} NaOH can be found in Fig. 1. The calibration dependence of 2,4-dinitrosalicylic acid in the concentration range from 1×10^{-3} to 2×10^{-4} mol L^{-1} is in the inset. The calibration dependence is linear. To establish that the electrode is capable of performing measurements inside the fiber a calibration dependence of 2,4-dinitrosalicylic acid was measured with the electrode covered with the fiber infused with *n*-octanol with a solution of 2,4-dinitrosalicylic acid in NaOH as both the donor and acceptor solution. The same concentration range was covered as with the bare electrode and the

Table 1
Parameters of the calibration dependencies of 2,4-dinitrosalicylic acid measured on a bare electrode and inside the holow fiber.

Electrode	Slope/mA mol^{-1} L	Intercept/μA	*R*
Bare	0.960137	0.030077	0.953262
Hollow fiber	0.55411	–0.02512	0.940044

calibration dependence was also linear, but the sensitivity decreased slightly. The parameters of the resulting calibration dependencies can be seen in Table 1.

4. Conclusions

A new type of m-AgSAE electrode capable of measurements inside a hollow polypropylene fiber has been developed. Its function was tested by measuring a calibration dependence of 2,4-dinitrosalicylic acid under basic conditions with a bare electrode in the concentration range 2–10×10^{-4} mol L^{-1}. To show the capability of the electrode to measure inside the hollow fiber calibration dependence was also measured with the electrode inside the hollow fiber. The electrode proved to be functional but slightly less sensitive. Results of extraction efficiency optimization of 2,4-dinitrosalicylic acid from acidic donor solution with regards to relevant parameters (time, donor solution pH, etc.) will be presented and compared to HFSLE/HPLC with UV detection determination. The application of the electrode for Aclonifen extraction and determination will also be included.

Acknowledgments

FFinancial support of this work by the Czech Science Foundation, Project GAČR No. 17-03868S, is gratefully acknowledged.

References

[1] Thordarson E., Pálmarsdóttir S., Mathiasson L., Jönsson.J.Å.: Sample preparation using a miniaturized supported liquid membrane device connected on-line to packed capillary liquid chromatography. *Anal. Chem.* **68** (1996), 2559–2563.
[2] Jönsson J.Å., Mathiasson L.: Membrane-based techniques for sample enrichment. *J. Chromatogr. A* **902** (2000), 205–225.
[3] Hrdlička V., Navrátil T., Barek J..: Application of hollow fibre based microextraction for voltammetric determination of vanillylmandelic acid in human urine. *J. Electroanal Chem.* **835** (2019), 130–136.
[4] Yosypchuk B., Šestáková I..: Working electrodes from amalgam paste for electrochemical measurements. *Electroanalysis* **20** (2008), 426–433.
[5] Rupp E.B., Zuman P., Sestakova I., Horak V.: Polarographic determination of some pesticides. Application to a study of their adsorption on lignin. *J. Agric. Food Chem.* **40** (1992), 2016–2021.
[6] Orr G.L., Elliott C.M., Hogan M.E.: Determination of redox behavior in vitro of nitrodiphenyl ether herbicides using cyclic voltammetry. *J. Agric. Food Chem.* **31** (1983), 1192–1195.
[7] Novotný V., Barek J.: Voltametrické stanovení acifluorfenu, nitrofenu a oxyfluorfenu na stříbrné tuhé amalgámové elektrodě. *Chem. Listy* **103** (2009), 217–223. (In Czech.)

Author Index

Keyword Index

Proceedings of the 15th International Students Conference "Modern Analytical Chemistry"

Edited by Karel Nesměrák.
Published by Charles University, Faculty of Science.
Prague 2019.
1st edition – viii, 285 pages

ISBN 978-80-7444-068-7

ISBN 978-80-7444-068-7